DOCTOR OF SCIENCES

Phenotypic adaptation and regulatory response to copper stress in Cupriavidus metallidurans

Maertens, Laurens

Award date:
2021

Awarding institution:
University of Namur

UNIVERSITÉ DE NAMUR

sck cen
Exploring
a better tomorrow

Phenotypic adaptation and regulatory response to copper stress in *Cupriavidus metallidurans*

Laurens Maertens

Promoter: Prof. Dr. Jean-Yves Matroule

Co-promoter: Dr. Ir. Rob Van Houdt

Dissertation presented in partial fulfillment of the requirements of the degree of Doctor in Sciences

2021

October 2021 Laurens Maertens

Phenotypic adaptation and regulatory response to copper stress in *Cupriavidus metallidurans*

Laurens Maertens was financially supported by by the European Space Agency (ESA-PRODEX) and the Belgian Science Policy (Belspo) through the BIOFILMS project (C4000129318), as well as a Fonds Spécial de la Recherche of UNamur.

Jury members

Prof. Dr. Jean-Yves Matroule (Promoter)
Unité de Recherché en Biologie des Micro-organismes (URBM)
Namur Research Institute for Life Sciences (Narilis)
UNamur, Namur, Belgium

Dr. Ir. Rob Van Houdt (Co-Promoter)
Microbiology Unit
Interdisciplinary Biosciences
Institute for Environment, Health, and Safety
Belgian Nuclear Research Centre (SCK CEN), Mol, Belgium

Prof. Dr. Xavier De Bolle (Chairman)
Unité de Recherché en Biologie des Micro-organismes (URBM)
Namur Research Institute for Life Sciences (Narilis)
UNamur, Namur, Belgium

Dr. Kristel Mijnendonckx
Microbiology Unit
Interdisciplinary Biosciences
Institute for Environment, Health, and Safety
Belgian Nuclear Research Centre (SCK CEN), Mol, Belgium

Prof. Dr. Ralf Möller
Radiation Biology
Institute of Aerospace Medicine
German Aerospace Center (DLR), Cologne, Germany

Prof. Dr. Dirk Springael
Bodem- en Waterbeheer
Departement Aard- en Omgevingswetenschappen
KULeuven, Louvain, Belgium

Dr. Andrea Sass
Laboratory of Pharmaceutical Microbiology (LPM)
UGent, Ghent, Belgium

Acknowledgements

This PhD project has finally come to an end. In the last four years, I have been challenged like never before, learned more and more independently than ever, and was at many points confronted by my own limits in expected and unexpected ways. In short, I would gladly do it all over again. Looking back, it is easy to pinpoint decisions I could have made differently, opportunities I could have handled better or exploited more, additional resources and contacts I could have capitalized on etc. However, I am firmly convinced of the quality of the work I was able to build. Likewise, many of the skills I developed will serve me well in professional (and less professional) situations alike. I want to stress that the achieved results, as described below, could not have been brought about without the extensive and valued help of many people.

First of all I want to express my gratitude to my mentor at SCK CEN, **Rob Van Houdt**. Essentially everything I was able to achieve and build in the last 4 years was in some way influenced by your guidance, help, and insights. From your daily support with practical issues in the lab, over your invaluable feedback during experimental design sessions, to the streamlining of the publication process, I hope to have picked up at least a little from your pragmatic, result-focused approach. Somehow you were able to strike a perfect balance between letting me develop research skills on my own, and preventing me from sidetracking too much. Most of all, I want to thank you for the genuine ease and low barrier of communication, during stressful moments as well as during the many good times.

I also want to sincerely thank **Jean Yves Matroule**, my promoter at UNamur. The way you remained directly approachable and closely involved with the daily goings-on of the project (despite the physical distance) was truly remarkable. Your knowledge and experience were crucial and, at the same time, always at hand. Simultaneously, the high standards and critical eye imposed by your supervision posed a challenge I gladly strived towards. I also want to thank you for the warm welcome I received at

the URBM laboratory at UNamur, enabling me to spend a couple of very pleasant months among very pleasant colleagues.

I am grateful for the insights and valuable feedback of my PhD committee members, **Kristel Mijnendonckx** and **Dirk Springael**. Kristel, you were always available for help with laboratory practicalities, and to give supportive (as well as humorous) comments during formal and informal presentation sessions. Dirk, when I had to pick an additional PhD committee member four years ago, you were an obvious first pick. Your guidance during my years at KU Leuven, and especially during my Master's thesis, was crucial to prepare me for the challenges during my PhD project. Throughout the project itself you could always be counted on to emphasize the biology of it all, making me circle back from getting lost in technicalities. Thank you for everything.

In the same vein I want to extend my thanks to **Ralf Möller**, **Andrea Sass**, and **Xavier De Bolle**. Ralf, I really enjoyed our cooperation and the state-of-the-art insights into spaceflight research, as well as the opportunity to present my work in the DLR virtual seminars. Andrea, thank you for helping me out with the RNA-Seq and RACE experimental background, and for providing a contact point to discuss all the sRNA details. Xavier, thanks for the friendly welcome at UNamur, and for serving as president of the jury.

Thanks a lot to all my fellow PhD students at SCK CEN. **Tom, Charlotte, and Gleb**, this PhD project would not have been the same without you guys. We went through so many ups and downs together, and have (almost!) brought our projects to successful ends together. Tom, I will always think back fondly on the innumerable good times inside and outside of the lab. You could always be counted on for good advice, listening to the best and the worst music, and exchanging jokes of dubious quality. Team Cupri forever! Charlotte, your insatiable drive for good results was something to admire and work towards, and at the same time you were always there to share laughs and celebrations. Gleb, your (initially) unexpectedly dry commentaries on all and everything were the source of quite some memorable moments. Thanks a lot for all the help with the mathematical and computational aspects of my PhD project, too. **Noami**, thank you for brightening the atmosphere in our office every day, for all the help when I was just starting out, for all the daily chatter… We learned and shared a lot together, thanks for everything! Thanks a lot to all my other PhD colleagues as well: **Francisco, Ali, Emma, Shari, Tom, Jana, Valérie, Magy, Auchi, Kai, Niels, Nathalie, Lorain, Eline,** and **Meryem**, for all of the laughs, complaints, deep sighs,

wisdom, help, anecdotes, and on and on. I'm looking forward to seeing you all soon, hopefully over a cold beer. Best of luck with bringing your projects to a successful end!

This PhD project could not have been finalized without the support of the technicians and senior staff at SCK CEN. **Ilse** and **Ann**, thank you for the many, many hours spent helping me out in the laboratory. You taught me so much about all aspects of applied microbiology, cloning, extractions, lab maintenance etc. Despite my numerous mistakes and clumsy moments in the lab, you were always there to help me out with a smile (or 5000 agar plates). **Carla, Wietse, Amelie, Ann, Lotte, Mieke, Randy**, you all deserve a lot of gratitude too, for helping me out throughout my project. Thank you! I also want to thank the senior scientists, always available for feedback and valuable criticism, practical knowledge, and collaborations: **Natalie, Max, Hugo, Felice, Paul, Jürgen, Pieter, Mohamed, and Surya**.

My various stays in UNamur were made brighter by the diverse but invariably helpful PhD students and postdocs at the URBM laboratory. **Gwen** and **Sébastien**, thank you for introducing me to the practical side of working with *Caulobacter*, the microscopy, synchronizations, and for always being available to answer my questions. Special thanks to **Pauline**, for all the help with the various RNA-Seq experiments, for the cooperation towards our publication, and everything else already mentioned! Finally, a big thank you to **Francesco, Françoise, Régis**, and **Angy**.

I had ample opportunity to supervise bachelor and master students doing their internships or working on their theses. Managing your projects, responding to dire situations and requests, and being able to teach you a thing or two in the lab always felt very rewarding to me, and I consider many of those moments personal highlights. **Michelle, Michael, Valerie, Andra, Julie,** and **Nissem**, thank you for all the hard work, the patience, the ambition, and the willingness to work together towards successful ends.

Mams, Paps, Sander, and **Sybrand**, and **Rebecca** and **Els**, thank you for all the support over the last 2-27 years. There is a lot I'm used to taking for granted, which I am discovering more and more are things to be truly grateful for, and humbled by. I hope I will have plenty of opportunity to reciprocate all of that.

Liesbet, thank you for everything. Let's build something worthwhile together.

Summary

Microbes are becoming more resistant to commonly used antimicrobials. This trend became noticeable soon after the introduction of mass scale production and use of novel antibiotics early in the 20th century, and is predicted to continue with devastating implications for sectors like healthcare and agriculture. Therefore, there is a need for the development of novel, alternative antimicrobials. For instance, the potent antimicrobial properties of metallic copper (Cu) have been investigated for use in biocontrol applications. Other than the aforementioned sectors, Cu-based antimicrobials could also be of interest for spaceflight operations, where decontamination protocols are presently insufficient. Consequently, there is a risk for the health of spacecraft crew, as well as for structural degradation of equipment. The ESA BIOFILMS project aims to study the bacterial response to metallic Cu aboard the International Space Station. This thesis was conceived in the context of ESA BIOFILMS, to provide new insights into the interaction of bacteria with metallic Cu, and to investigate the regulatory response to Cu exposure.

First, we evaluated the inactivation kinetics of *Cupriavidus metallidurans* CH34, a model organism for metal resistance, in wet contact with metallic Cu. Viability and membrane permeability were examined for 9 days with viable counts and flow cytometry. After an initial drop in viable counts, a significant recovery was observed starting after 48 hours. This behavior could be explained by either a recovery from an injured/viable-but-non-culturable state or regrowth of surviving cells by metabolizing lysed cells. Either hypothesis would necessitate an induction of Cu resistance mechanisms, since no recovery was seen in a CH34 derivative lacking metal resistance mechanisms, while being more pronounced when Cu resistance mechanisms were pre-induced. Interestingly, no biofilms were formed on the Cu surface, while extensive biofilm formation was observed on the stainless steel control plates. When CH34 cells in mineral water were exposed to $CuSO_4$, a similar initial decrease in viable counts was observed, but cells recovered fully after 7 days. In conclusion, we showed that long-term bacterial survival in the presence of a Cu surface is possible upon the induction of metal resistance mechanisms. This

observation may have important consequences in the context of the increasing use of Cu as an antimicrobial surface, especially in light of potential co-selection for metal and antimicrobial resistance.

In a second study, we performed a thorough analysis of the transcriptome of *C. metallidurans* CH34 acutely exposed to Cu by tagRNA-sequencing. Several metabolic pathways were impacted by Cu exposure, and a broad spectrum of metal resistance mechanisms, not limited to Cu-specific clusters, was overexpressed. In addition, several gene clusters involved in the oxidative stress response and the cysteine-sulfur metabolism were induced. In total, 7500 transcription start sites (TSSs) were annotated and classified with respect to their location relative to coding sequences (CDSs). Predicted TSSs were used to re-annotate 182 CDSs. The TSSs of 2422 CDSs were detected, and consensus promoter logos were derived. Interestingly, many leaderless messenger RNAs (mRNAs) were found and many mRNAs were transcribed from multiple alternative TSSs. We observed pervasive intragenic TSSs both in sense and antisense to CDSs. Antisense transcripts were enriched near the 5' end of mRNAs, indicating a functional role in post-transcriptional regulation. In total, 578 TSSs were detected in intergenic regions, of which 35 were identified as putative small regulatory RNAs. Finally, we provided a detailed analysis of the main Cu resistance clusters in CH34, which were found to include many intragenic and antisense transcripts. These results clearly highlight the ubiquity of noncoding transcripts in the CH34 transcriptome, many of which are putatively involved in the regulation of metal resistance.

Third, we investigated the role of several newly detected putative sRNAs in *C. metallidurans* CH34 as regulators for Cu resistance. The presence and transcription start sites of these sRNAs was confirmed via 5'RACE, and their expression in several conditions was confirmed via *luxCDABE*-based promoter probe experiments. On the antisense strand of the *silDCBA* cluster, which encodes a tripartite efflux pump conveying copper and silver resistance, a previously unknown transcript was detected. The regulatory capacity of this transcript, dubbed *silY*, was confirmed by assaying its effect on translation of the polycistronic *silDCBA* mRNA. In addition, repression of SilDCBA translation by *silY* induced a Cu-sensitive phenotype, both in Cu tolerance and resistance. The biological importance of the *silY* sRNA requires further confirmation, with questions regarding its regulation and the precise mechanism of repression, but nevertheless our study has provided novel insights into the regulation of the *silDCBA* cluster.

In a final study, we examined the role of the environment in the bacterial response to Cu ion exposure. We employed a tagRNA-seq approach to elucidate the disparate responses of two morphotypes of *Caulobacter crescentus* NA1000 to moderate Cu stress in a complex rich (PYE) medium and a defined poor (M2G) medium. The study of the less metal-resistant *C. crescentus* allows for a comparison to *C. metallidurans*, while retaining relevance to oligotrophic environments such as those related to the ESA BIOFILMS project. Indeed, much like *Cupriavidus* strains, *Caulobacter* strains have been isolated from spacecraft environments. The transcriptome of *C. crescentus* NA1000 was more responsive to Cu exposure in M2G, where we observed an extensive oxidative stress response and reconfiguration of the proteome, as well as the induction of metal resistance clusters. In PYE, little evidence was found for an oxidative stress response, but several transport systems were differentially expressed, and an increased need for histidine was apparent. These results show that the response to Cu exposure is strongly dependent on the cellular environment. In addition, induction of the extracytoplasmic function sigma factor SigF and its regulon was shared by the Cu stress responses in both media, and its central role was confirmed by the phenotypic screening of a *sigF::*Tn*5* mutant. In both media, stalked cells were more responsive to Cu stress than swarmer cells, and a stronger basal expression of several cell protection systems was noted in the latter, indicating that the swarmer cell is inherently more Cu resistant. Our approach also allowed for detecting several new transcription start sites, indicating small regulatory RNAs and additional levels of Cu-responsive regulation.

In conclusion, we have provided novel insights into the phenotypic and regulatory responses of bacteria to Cu exposure. Our results can be used to optimize Cu-based antimicrobials in a broad context. For instance, it has become clear that the use of viable counts for quantification of microbial load might lead to a strong underestimation. In addition, the hazard of bacterial Cu resistance mechanisms has been charted, with additional research to be performed on the horizontal transfer of these mechanisms. We have detailed the transcriptome of Cu-exposed cells of both *C. metallidurans* CH34 and *C. crescentus* NA1000 (the latter in disparate environments), which has enabled the search for novel regulatory features. As a result, the newly detected *silY* transcript has emerged as a putative regulator of the *silDCBA* cluster.

Résumé

La résistance aux agents antimicrobiens couramment utilisés accroit de jour en jour. Cette tendance est apparue au début du 20ème siècle avec le début de la production en masse ainsi que l'utilisation de nouveaux antibiotiques. Des prédictions mettent en évidence des conséquences dramatiques pour, notamment, les secteurs de la santé et de l'agriculture. Il est urgent de développer de nouvelles alternatives antimicrobiennes. À la lumière de son potentiel antimicrobien, le cuivre (Cu) métallique a été étudié dans le cadre de traitements de biocontrôle. En plus des secteurs précédemment cités, des antimicrobiens contenant du Cu pourraient être intéressants dans le cadre de vols spatiaux, opérations pour lesquelles les protocoles de décontamination sont pour le moment insuffisants. Cela engendre un risque pour la santé du personnel spatial ainsi qu'une potentielle dégradation du matériel. Le projet ESA BIOFILMS cherche à investiguer la réponse bactérienne au Cu métallique à bord de la Station Spatiale Internationale. Cette thèse s'inscrit dans le contexte de ESA BIOFILMS, pour fournir de nouvelles connaissances à propos de l'interaction entre bactéries et Cu métallique, ainsi que d'étudier la réponse régulatoire suite à une exposition au Cu.

Dans un premier temps, nous avons évalué la cinétique d'inactivation de *Cupriavidus metallidurans* CH34, l'organisme modèle pour la résistance aux métaux, lors d'un contact humide avec du Cu métallique. La viabilité et la perméabilité membranaire ont été observées pendant 9 jours, via le nombre de bactéries viables et de la cytométrie de flux. Après une baisse initiale de la viabilité, un rétablissement significatif a été observé après 48h. Ce comportement pourrait être expliqué par un rétablissement d'un état endommagé/*viable-but-non-culturable*, ou par une croissance des bactéries survivantes métabolisant les cellules lysées. Chaque hypothèse nécessiterait une induction des mécanismes de résistance au Cu, puisque aucun rétablissement n'a été observé dans un dérivé de CH34 déficient pour la résistance aux métaux. D'un autre côté, le rétablissement est plus important lorsque ces mécanismes de résistance sont pré-induits. De façon intéressante, aucun biofilm ne s'est formé sur les surfaces de Cu, tandis que de nombreux biofilms ont été

observés sur les plaques contrôles composées d'acier inoxydable. Après avoir supplémenté des cellules CH34 dans de l'eau avec du $CuSO_4$, une diminution initiale similaire a été observée, avec un rétablissement complet après 7 jours. En conclusion, nous avons montré que la survie bactérienne à long terme en présence d'une surface cuivrée est possible après induction des mécanismes de résistance aux métaux. Cette observation pourrait avoir de sérieuses conséquences dans le contexte d'une utilisation croissante du Cu comme surface antimicrobienne, en particulier à la lumière d'une potentielle co-sélection de résistances aux métaux et aux composés antimicrobiens.

Ensuite, nous avons réalisé une analyse approfondie du transcriptome de *C. metallidurans* CH34 intensivement exposé au Cu, par *tagRNA-sequencing*. Plusieurs voies métaboliques ont été impactées par l'exposition au Cu, et un large spectre de mécanismes de résistance aux métaux, non limités aux groupes spécifiques au Cu, étaient surexprimés. De plus, plusieurs groupes de gènes impliqués dans la réponse au stress oxydatif et dans le métabolisme cystéine-souffre, étaient induits. Au total, 7500 sites de départ de la transcription (*transcription start site*, TSS) ont été annotés et classés en fonction de leur localisation relative à la séquence codante (*coding sequence*, CDS). Les TSSs prédits ont été utilisés pour réannoter 182 CDSs. Le TSS de 2422 CDSs ont été détectés, et des séquences promotrices consensus en ont dérivé. Curieusement, de nombreux ARN messagers (ARNm) *leaderless* ont été identifiés et de nombreux ARNm étaient transcrits à partir de plusieurs TSSs alternatifs. Nous avons observé de manière récurrente des TSSs intra-géniques dans le sens et dans l'antisens des CDSs. Les transcrits antisens étaient enrichis près de l'extrémité 5' des ARNm, indiquant un rôle fonctionnel dans la régulation post-transcriptionnelle. Au total, 578 TSSs ont détectés dans des régions intergéniques, desquels 35 ont été identifiés comme des petits ARN régulateurs putatifs. Finalement, nous avons fourni une analyse détaillée des groupes principaux de résistance au Cu chez CH34, lesquels incluent de nombreux transcrits antisens et de régions intergéniques. Ces résultats soulignent clairement l'ubiquité des transcrits non-codants dans le transcriptome de CH34, parmi lesquels de nombreux seraient impliqués dans la régulation de la résistance aux métaux.

Dans un 3ème temps, nous avons investigué le rôle de plusieurs ARNnc précédemment prédits chez *C. metallidurans* CH34 en tant que régulateurs de la résistance au Cu. La présence et le TSS de ces ARNnc ont été confirmé par 5'RACE, tandis que le niveau d'expression dans différentes conditions a été confirmé via

l'utilisation de la sonde basée sur le promoteur de *luxCDABE*. Sur le brin antisens de l'opéron *silDCBA*, encodant une pompe à efflux tripartite impliquée dans la résistance au Cu et à l'argent, un transcrit inconnu a été identifié. La capacité régulatrice de ce transcrit, nommé *silY*, a été confirmé en mesurant son effet sur la traduction de l'ARNm polycistronique *silDCBA*. En outre, la répression de la traduction de SilDCBA par *silY* induit une hypersensibilité au Cu, aussi bien pour la tolérance que pour la résistance. L'importance biologique de l'ARNs *silY* requiert de plus amples investigations, en adressant la question de sa régulation ainsi que le mécanisme exact de répression. Néanmoins, notre étude démontre de nouvelles connaissances concernant la régulation de l'opéron *silDCBA*.

Finalement, nous avons examiné le rôle de l'environnement dans la réponse bactérienne suite à une exposition au Cu. Nous avons utilisé comme approche le *tagRNA-sequencing* pour comprendre la réponse hétérogène des deux morphotypes de *Caulobacter crescentus*. La souche NA1000 a été exposé à un stress moyen en milieu complexe et riche (PYE) ainsi que dans un milieu défini et pauvre (M2G). L'étude d'une bactérie moins résistante aux métaux, *C. crescentus*, permet la comparaison avec *C. metallidurans*, tout en restant pertinent au regarde des environnements oligotrophes liés au projet ESA BIOFILMS. En effet, tout comme *C. metallidurans*, des souches de *Caulobacter* ont été isolées à partir d'engins spatiaux. En M2G, le transcriptome de *C. crescentus* NA1000 était plus réactif puisque nous avons observé une vaste réponse au stress oxydatif et une reconfiguration du protéome, ainsi qu'une induction des systèmes de résistance aux métaux. Cependant, en PYE, peu de résultats ont été mis en évidence pour la réponse au stress oxydatif, alors que plusieurs systèmes de transport étaient différemment exprimés et une augmentation de la demande pour de l'histidine est apparue. Ces résultats montrent que la réponse à l'exposition au Cu est fortement dépendante de l'environnement cellulaire. En outre, l'induction du facteur sigma extracytoplasmique SigF et son régulon est commune aux deux milieux. Son rôle-clé a été démontré grâce aux différents phénotypes du mutant *sigF*::Tn*5*. Dans chacun des milieux, les cellules pédonculées étaient plus réactives au stress en Cu que les cellules flagellées. Une plus forte expression basale de plusieurs systèmes de protection cellulaire a été observée, indiquant que les cellules flagellées sont intrinsèquement plus résistance au Cu. Notre approche nous a également permis de détecter la présence de plusieurs nouveaux sites d'initiation de la transcription,

supposément une indication pour de petits ARN régulatoires et de niveaux additionnels de la régulation de la réponse au Cu.

Pour conclure, nous avons fourni une plus grande compréhension des réponses phénotypique et régulatoire des bactéries suite à une exposition au Cu. De manière générale, nos résultats peuvent être utilisés dans l'optimisation d'antimicrobiens contenant du Cu. Par exemple, il est devenu clair que l'utilisation d'un comptage de viabilité pour la quantification de la charge bactérienne peut mener à une importante sous-estimation. De plus, le danger lié aux mécanismes bactériens de résistance au Cu a été retracé, avec de plus amples recherches sur le transfert horizontal de ces systèmes de résistance. Nous avons détaillé le transcriptome des cellules exposées au Cu de *C. metallidurans* CH34 et de *C. crescentus* NA1000 (dans différents environnements pour cette souche), ce qui a mené à la recherche de nouvelles fonctions régulatoires. De ce fait, le transcrit nouvellement détecté, *silY*, est apparu comme un régulateur potentiel de l'opéron *silDCBA*.

List of abbreviations

AMR	Antimicrobial Resistance
ABC	ATP-Binding Cassette
AOC	Assimilable Organic Carbon
asRNA	antisense RNA (cis-encoded)
CDS	CoDing Sequence
CFU	Colony Forming Units
CHASRI	Copper Homeostasis and Silver Resistance Island
COG	Cluster of Orthologous Groups
CRM	Cu Resistance Mechanism
CuNP	Cu NanoParticle
DDTC	sodium DiethylDithioCarbamate
ECF	ExtraCytoplasmic Function
EDTA	EthyleneDiamineTetraAcetic acid
eggNOG	evolutionary genealogy of genes: Non-supervised Orthologous Grouping
EMSA	Electrophoretic Mobility Shift Assay
EPS	Extracellular Polymeric Substances
ESA	European Space Agency
FDR	False Discovery Rate
HAI	Healthcare-Associated Infection
HME	Heavy Metal Efflux
HMR	Heavy Metal Resistance
ICP-MS	Inductively Coupled Plasma-Mass Spectrometry
IGR	InterGenic Region
ISS	International Space Station
MCS	Multiple Cloning Site
MFP	Membrane Fusion Protein
MIC	Minimal Inhibitory Concentration
M-MLV	Moloney-Murine Leukemia Virus
mRNA	messenger RNA

NCBI	National Center for Biotechnology Information
OMP	Outer Membrane Protein
ORF	Open Reading Frame
pasRNA	putative antisense RNA
PBS	Phosphate-Buffered Saline
PCA	Principal Component Analysis
PI	Propidium Iodide
PSS	Processing Start Site
qRT-PCR	quantitative Real Time-Polymerase Chain Reaction
RACE	Rapid Amplification of cDNA Ends
RBS	Ribosome Binding Site
RIN	RNA Integrity Number
RLU	Relative Luminescence Units
RND	Resistance-Nodulation-cell Division
ROS	Reactive Oxygen Species
SRA	Sequence Read Archive
sRNA	small regulatory RNA
ST	STalked morphotype
SW	SWarmer morphotype
TEX	Terminator EXonuclease
TSS	Transcription Start Site
UTR	UnTranslated Region
UV-C	deep UltraViolet light (λ = 100-280 nm)
VBNC	Viable-But-Non-Culturable

Table of contents

CHAPTER 1 Introduction*

1.1 Cu as antimicrobial agent

The rise of antimicrobial resistance (AMR) poses a worldwide threat to the treatment of infectious diseases and precludes the effective control of bacterial contamination [1]. Even in ancient civilizations, humans were exposed to organic antimicrobials, as evidenced by the traces of tetracyclines found in Sudanese Nubian and Egyptian skeletons [2, 3]. However, the active, industrial-scale development and application of organic antimicrobials only began in earnest at the onset of the 20th century. The landmark discovery of the antimicrobial potential of arsfenamine, and later penicillin, paved the way for the 'golden era of discovery of novel antibiotics' between ca. 1950-1970 [4]. However, no new antibiotic classes have been discovered since, and (pathogenic) bacteria have developed mechanisms for AMR relatively quickly. Indeed, the mortality attributable to multidrug-resistant bacteria is high and increasing [5, 6]. It is estimated that by 2050, 10 million people will die every year from AMR complications if proceeding with existing policies, which is comparable to the current cancer mortality [7].

It is clear that novel antimicrobials are needed to help relieve the growing burden of AMR. Alternative strategies such as newly developed antimicrobial vaccines [8], phage therapy [9] and even the resurrection of medieval medicinal concoctions [10] have attracted interest. Another class of antimicrobials is that of metals with biocidal activity, such as copper (Cu) and silver (Ag), as well as cobalt (Co), zinc (Zn), and lead (Pb). Some of these metals also exert a considerable toxicity on multicellular organisms, and are consequently poor one-on-one substitutes for therapeutic use [11]. At the same time, metals such as Cu and Ag usually do not induce harmful

* Part of this chapter is based on the following publications: Maertens, L., Matroule, J.Y., and Van Houdt, R. (2021). Characteristics of the copper-induced viable-but-non-culturable state in bacteria. World J Microbiol Biotechnol 37(3): 37 and Siems, K., Müller, D., Maertens, L. et al. (2021). Designing the spaceflight experiment BIOFILMS: testing laser-patterned metal surfaces for prevention of bacterial biofilm formation in microgravity. *In preparation*.

effects on e.g. humans, since they possess potent homeostatic pathways for metal uptake and excretion. For this reason, Cu and Ag-containing medical instruments such as dental and intrauterine devices do not often pose health problems [12, 13]. Nonetheless, some aggravating predispositions exist, such as Menkes syndrome and Wilson's disease [13, 14]. It is clear that antimicrobial metals possess a number of key advantages in the control of (environmental) microbial contaminations. Here, we will focus on Cu, which is of special interest due to its strong antimicrobial potency and its relatively low cost.

The first evidence of the antimicrobial use of Cu goes back to the ancient Egyptians at least 4000 years ago, with a hieroglyphic description of a mixture containing the $CuCO_3$ mineral malachite ("green pigment") to treat inflamed wounds [15]. In fact, Cu-based antimicrobial therapies were widespread throughout history, being used by ancient Greeks, Romans, Persians and Aztecs [16]. Disparate sources mention such therapies throughout the Middle Ages and Cu began to be actively implicated in epidemiological studies from the 19th century onwards. However, the rise of organic antimicrobials in the 20th century largely outshone the development of (Cu) metal antimicrobials. In the present day, a niche for Cu as a clinical antimicrobial has reopened due to the threat of AMR. In addition, its biocidal properties are exploited in numerous industries, such as agriculture, woodworking, and food and drinking water production [17].

Cu antimicrobials come in distinct designs, tailored to specific use cases. For instance, Cu salts and organic complexes are used as fungicides [18] and algicides [19], and Cu-doped zeolites are being investigated to simultaneously disinfect and remove metals from wastewater [20]. Cu salt-based formulations can be applied topically to combat infections, e.g. herpes [21, 22] and vaginitis [23]. Several other Cu salt-based therapies have been developed in recent years [21, 24]. In parallel, a surging contribution of Cu nanoparticle (CuNP) formulations, which are intrinsically of interest due to their high surface to volume ratio, has been noted, again often in healthcare settings. CuNPs can be incorporated into polymeric matrices such as textiles, glass and polypropylene, as reviewed by Tamayo *et al.* [25] and Borkow [26]. These CuNP-infused matrices convey several key advantages, among which the controlled release of Cu ions and the increased surface area of the antimicrobial material. Such materials can be used for food packaging, water disinfection and medical applications. For example, CuNP-containing cotton and bamboo rayon clothing is toxic towards *Staphylococcus aureus*, which is associated with many

healthcare-associated infections (HAIs) [27-29]. Another formulation of Cu antimicrobials comes in the shape of solid surfaces of Cu metal and its alloys. Metallic Cu is extremely efficient in killing microbes in atmospherically dry conditions, e.g. by pipetting droplets of a bacterial suspension on a metallic Cu surface and letting them air dry, with near-complete inactivation in minutes to hours [30]. Important parameters influencing the killing rate are ambient temperature and Cu concentration in the alloy [31, 32]. Interestingly, in wet applications, e.g. by submerging a metallic Cu surface in a bacterial suspension, the antimicrobial effects of Cu surfaces are diminished, with inactivation times of several hours [33, 34]. The potential antimicrobial applications of Cu surfaces have been reviewed by Vincent *et al.* [35], who emphasized their utility in hospital environments owing to their ability to efficiently inactivate HAI-associated strains such as methicillin-resistant *S. aureus* and vancomycin-resistant enterococci. The biocidal efficacy of Cu surfaces can also be enhanced chemically via modifying surface wettability, and physically by etching µm-scale patterns into the surface [36].

The question remains how these antimicrobial formulations precisely impart their biocidal effects. It is important to point out that, while highly toxic at excess amounts, Cu ions function as a micronutrient and intracellular Cu ion concentrations must consequently be carefully regulated to achieve viable homeostasis. Cu ions can cycle between their borderline hard/soft cupric (Cu^{2+}) and soft cuprous (Cu^{+}) forms at biologically relevant redox potentials, and both forms are readily complexed by cellular ligands [37, 38]. For example, in more aerobic cellular compartments such as the periplasm, the (less toxic) cupric ion is more prevalent, while there is a bias towards the cuprous form in the cytoplasm [39]. This ability to change oxidation state makes the Cu ion an interesting cofactor for enzymes such as superoxide dismutases [40, 41], but uncontrolled cycling between cupric and cuprous ions leads to considerable toxic effects. In bacteria, Cu ion toxicity has been shown to act via multiple modes of action, which has been expertly reviewed both by Lemire *et al.* [42] and Giachino and Waldron [38]. The cell envelope represents an important target since Cu can inhibit the correct enzymatic maturation of lipoproteins by binding to catalytic cysteine residues. This leads to an increased level of toxic intermediates in the inner membrane, in turn activating the envelope stress response [43]. In a similar manner, Cu can impede peptidoglycan crosslinking and its binding to membrane lipoproteins, thus weakening the cell envelope [44]. Lastly,

Cu can oxidize thiol residues involved in the maturation of periplasmic polypeptides, again leading to the buildup of misfolded intermediates [45].

For CuNPs and Cu surfaces, the direct contact with bacterial cells seems to be an essential facet of toxicity, next to the release of Cu ions [30]. This phenomenon is termed 'contact killing', and has been elegantly demonstrated by Mathews *et al.* [46], by comparing killing rates of naked Cu surfaces to Cu surfaces covered with an inert polymeric grid, inhibiting contact killing but not the release of ions. Membrane lipid peroxidation has been proposed as a key process in contact killing [47, 48], but the exact mechanism remains unclear.

Finally, another general mechanism of Cu toxicity is the generation of reactive oxygen species (ROS), such as hydroxyl and hydroperoxyl radicals, which can damage cellular components. Since it remains difficult to identify intracellular ROS directly, due to their high reactivity, evidence for this toxicity mechanism has been mostly circumstantial [49]. Consequently, the exact contribution of ROS generation to overall Cu toxicity is ambiguous. However, Macomber *et al.* [50] have shown that Cu catalyzes hydroxyl radical formation in the periplasm *in vivo*, and Cu-catalyzed ROS generation via a Fenton-like process has been demonstrated *in vitro* [51, 52]. In addition, the high affinity of the cuprous ion for thiol groups can lead to the depletion of antioxidants like glutathione and the destruction of redox-active Fe-S clusters [53, 54].

1.1.1 Applications beyond Earth?

Perhaps unexpectedly, Cu-based antimicrobials are also studied in the context of human space exploration. An enduring human presence in space is required to achieve the primary goals of space programs worldwide, and as longer manned missions, e.g. to Mars, are being planned for the foreseeable future, the optimization of isolated self-sustaining habitats is of prime importance. One key aspect in this regard is extensive microbial control. The ubiquity of microbes in manned spacecraft such as the International Space Station (ISS) poses several critical risks to astronauts as well as to structural spacecraft materials. In addition, planetary protection protocols rely on restricting forward and backward contamination of extraterrestrial systems. Besides possible negative consequences, microbes have also been shown to provide unparalleled potential for regenerative life support systems, such as MELiSSA, which has been designed to enable long-term manned missions in space [55].

Microbiological studies have shown the pervasive presence of microbes aboard the ISS associated with dust particles [56, 57], filter debris [58, 59], air vents [60], walls and panels [61], as well as touch surfaces such as laptop keyboards and handrails [60]. The microbial population described in these studies is mostly composed of human-associated strains, but environmental organisms are also present. Several bacterial and fungal strains have been characterized in detail, often with specific attention towards AMR and stress responses [62-64]. The prevalence of AMR genes in the ISS microbiome was examined in a longitudinal study, indicating multiple multidrug-resistant organisms [65]. A similar study showed the persistence of several opportunistic pathogens, such as *Klebsiella pneumoniae* and *Staphylococcus aureus* [66]. In the same study, an increase in AMR genes and virulence was observed over the duration of the study. These results are worrying in light of a decreased immune function of astronauts [67-69]. However, it has also been proposed that these health concerns are unjustified, and that the risks accompanying unchecked microbial contamination are associated with degradation of equipment integrity rather than human health-related [70]. This hypothesis finds validation in the low number of observed health issues and infections of crew members [71].

Monitoring and controlling microbial contamination on the ISS has been reviewed by Van Houdt *et al.* [72]. While air and surface contamination levels were generally within acceptable levels, onboard potable water sources were found to be unsuited for human consumption in 60% of cases [73], leading to increased costs and wasted crew time. Despite repeated decontamination attempts, e.g. with silver, microbial counts rapidly increased again above acceptable levels. These results were explained by the possible prevalence of silver resistance mechanisms in contaminating cells [64], as well as adaptation to the oligotrophic environment by entering a viable but non-culturable (VBNC) cell state [74, 75], which could be more resistant to extant biocides. Lastly, the formation of biofilms on equipment surfaces could impair the correct functioning of biocidal applications.

Biofilms have been defined as aggregated cell communities enveloped in extracellular polymeric substances (EPS), often associated with surfaces [76]. Biofilm cells are often more resistant to antimicrobial agents, because of a decreased permeation of these agents into the biofilm [77], and a high cellular heterogeneity including dormant cells with increased stress resistance [78]. Biofilm formation on spacecraft materials has been observed in the ISS [79, 80], as well as in the Mir space station [81, 82]. The presence of biofilms is known to cause damage to structural

equipment via polymer deterioration, metal corrosion and biofouling. Microbial cells in space, in the planktonic phase as well as in biofilms, are not subjected to the same net gravitational field as on Earth, which leads to a decreased mixing rate by convection. Consequently, mass transfer between the cell and its immediate environment is limited to diffusion [83]. This can lead to depletion of nutrients and accumulation of metabolites in the immediate extracellular environment, which can elicit a biological response in the cell. In order to study the effects of spaceflight on biofilm formation several experiments have been conducted, as reviewed by Zea *et al.* [84]. In *Pseudomonas aeruginosa*, an increased propensity for biofilm formation was observed in space, dependent on nutrient availability and, curiously, cell motility [85]. This effect of motility on mixing rates in the fluid surrounding the cell has been hypothesized to (partially) negate the effects of microgravity and decreased convective phenomena [83]. However, this hypothesis was criticized by Santomartino *et al.* [86]. In *Escherichia coli*, cells in liquid medium clustered together rather than being homogeneously distributed in the medium, indicating enhanced biofilm formation in space [87]. Lastly, it must be noted that the function of quorum sensing mechanisms, which depend on small signaling molecules, can be impacted in microgravity. Cell-cell communication via quorum sensing plays a role in e.g. biofilm formation and adaptation to a changing environment, but also bacterial virulence [88]. An increased concentration of N-acyl-homoserine lactones, which function as signaling compounds, was shown in *Rhodospirillum rubrum* in simulated microgravity, while cell density was unaltered [89].

The prevalence of multispecies biofilms and their possible effects on human health and equipment integrity, in combination with the frequent problems with bacterial contamination of drinking water, illustrates the need for advanced, integrated decontamination systems [72]. The biocidal effects of biofilm exposure to colloidal silver and hydrogen peroxide were tested in a setup seeded with bacterial isolates previously isolated from the ISS, and resulted in the complete eradication of pre-grown biofilms [90]. Another promising alternative for existing antimicrobial strategies is the use of copper (Cu) surfaces, as described in the sections above. The functionality of Cu antimicrobials aboard the ISS is being investigated as part of the ESA-backed BIOFILMS project.

1.1.2 The model organism *Cupriavidus metallidurans* CH34

Bacteria have evolved several distinct metal resistance mechanisms, and these are especially widespread in species associated with metal-enriched environmental

niches [91]. A model strain for bacterial metal resistance is *Cupriavidus metallidurans* CH34 (free translation: *copper-hungry metal-tolerant*). Originally isolated in 1976 from a zinc decantation basin in a non-ferrous metallurgical facility near Engis, Belgium, CH34 was quickly shown to encode a wide variety of metal resistance determinants (often plasmid-bound) [92, 93]. To illustrate, the water in this basin contained millimolar concentrations of Zn^{2+} and Cu^{2+}, as well as high micromolar concentrations of Cd^{2+} [93]. Indeed, CH34 is able to tolerate high concentrations of toxic metals in its environment and encodes resistance mechanisms not only to Zn and Cu, but also to Ni, Co, Cd, Cr, Pb, Ag, Au, As, Hg, Cs, Bi, Tl, Se, and Sr [94]. These metal resistance mechanisms are usually organized into gene clusters, and are located mostly on CH34's megaplasmids (pMOL28 and pMOL30). In addition, the gene clusters on these megaplasmids are sometimes mirrored in (partially) homologous clusters on the chromosome and the chromid. An overview of the genomic content has been given by Janssen et al., 2010 [94], while the metal resistance mechanisms of CH34 have been described in detail by Mergeay and Van Houdt [91, 95]. Metal resistance in bacteria can be achieved on several levels, as postulated by Bruins *et al.* [96]. Of the five mechanisms described (Figure 1-1), several examples of active efflux, metal sequestration and enzymatic detoxification can be found in CH34 [91]. In the next section, we will describe the extant resistance mechanisms for Cu, with a focus on active efflux and enzymatic conversion.

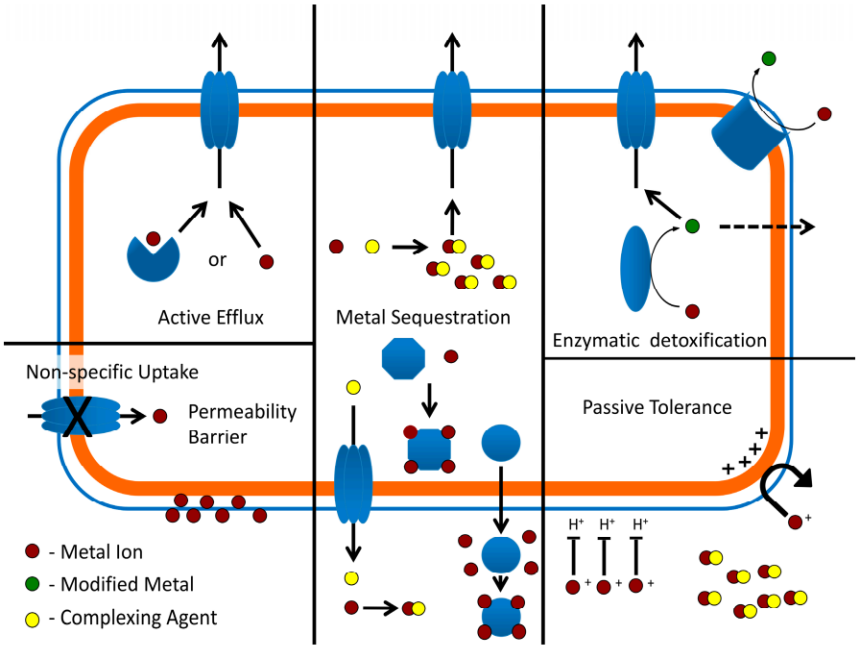

Figure 1-1. Overview of bacterial metal resistance mechanisms. Active efflux systems can either directly bind cytoplasmic and periplasmic metal ions, or they can be shuttled via metal-binding chaperones. Metal sequestration can occur via chaperones or small molecules such as phosphate anions, both of which can then interact with export systems. Enzymatic detoxification can chemically modify metal ions, often reducing them to a less toxic valence state. The orange barrier represents the cell wall and membrane(s). The external blue barrier represents a permeability barrier such as an S-layer or a biofilm. These external barriers can be modified to enhance metal-binding properties, which can decrease metal stress on the cell itself. Acidophilic bacteria, in contrast to neutrophiles, maintain a positively charged transmembrane potential, inhibiting passage of metal cations across the membrane. This figure was adapted from Wheaton *et al.* [97].

1.1.3 Cu tolerance and resistance mechanisms

The cellular toxicity derived from Cu antimicrobials depends on many factors, such as the magnitude and timing of the Cu dose received by the cell, the chemical makeup of the cell's environment, and its own Cu resistance mechanisms (CRM). A distinction can be made between Cu tolerance and resistance, although these terms are often interchanged. Cu tolerance describes the ability of a population to survive Cu exposure, and is often linked to the toxic effects of Cu to cellular metabolism,

membrane and DNA integrity. These toxic effects have been briefly described above, and the curious case of the Cu-induced VBNC state will be discussed in section 1.2.4. For further reading, we refer to the recent paper by Brauner *et al.* [98]. Cu resistance depicts the ability of a population to grow under Cu stress conditions, usually characterized by the minimal inhibitory concentration (MIC). This growth is often only possibly upon the induction of CRMs.

Bacteria can ward off Cu toxicity at different levels, e.g. controlling Cu import, oxidizing cuprous ions to their cupric form, sequestering Cu ions in the cytoplasm and the periplasm, and removing Cu ions from the cellular interior and membranes. Fairly little is known about Cu import [38, 99], so we will focus on the three latter mechanisms. Basic Cu homeostasis mechanisms are partially conserved in essentially all Proteobacteria, with a prime example found in the P-type ATPase CopA, which removes Cu^{+} from the cytoplasm [100]. CRM have been studied extensively in *E. coli*, where CopA is supplemented by the tripartite Heavy Metal Efflux Resistance-Nodulation-Cell Division (HME-RND) efflux system CusCBA [101]. HME-RND pumps consist of three parts: an inner membrane protein (RND family), a periplasmic adaptor protein (Membrane Fusion Protein family, MFP), and an outer membrane fusion protein (Outer Membrane Protein family, OMP) [102]. The CusF protein, part of the *cusCFBA* cluster, likely sequesters periplasmic Cu [103, 104]. The third CRM active in *E. coli* is the CueO protein, a multicopper oxidase which oxidizes periplasmic Cu^{+} to Cu^{2+} [105]. Curiously, the *cus*/*sil* and *cop*/*pco* systems are quite often detected adjacent to one another, indicating some level of co-selection and cross-regulation [106]. This co-occurrence of CRMs has been dubbed CHASRI (Cu Homeostasis And Silver Resistance Island). CHASRI likely evolved from the combination of pre-existing gene modules, and has since spread via horizontal gene transfer, possibly under evolutionary pressure of (historical) anthropogenic Cu emissions [107]. Finally, Cu homeostasis can be achieved in part by periplasmic chelation by Cu-binding proteins, such as the CueP protein in *Salmonella enterica* [108] (Figure 1-2).

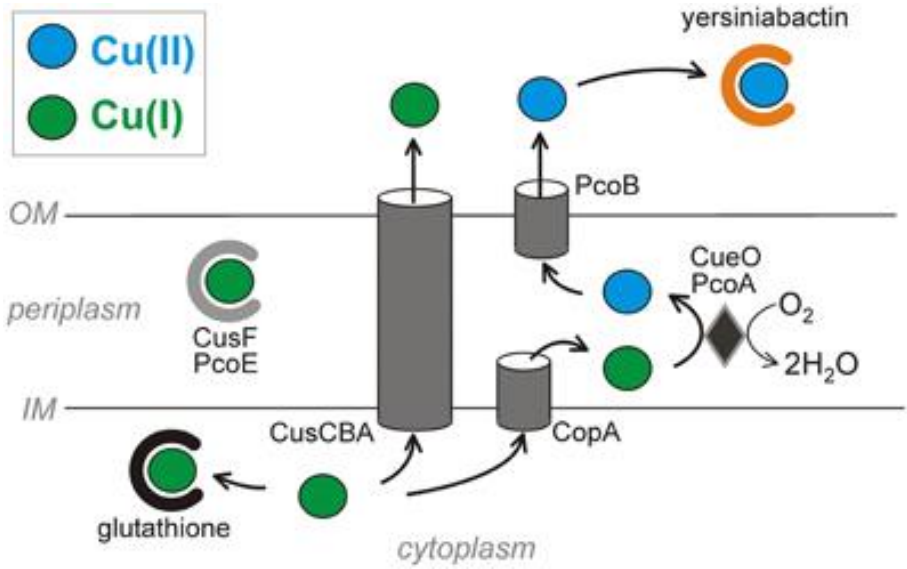

Figure 1-2. Copper resistance strategies across membranes of pathogenic *E. coli*. The virulence-associated siderophore yersiniabactin sequesters Cu^{2+} outside the cell and prevents its reduction to the more toxic Cu^{+}. Copper ions that reach the cytosol are subject to chelation by glutathione and export by two ATPases. The CusCBA HME-RND complex exports Cu^{+} from both the cytoplasm and the periplasm (via CusF) to the extracellular space. Alternatively, the CopA ATPase exports cytoplasmic copper across the inner membrane. Periplasmic Cu^{+} can bind the CusF and PcoE proteins or be oxidized by the copper oxidases CueO or PcoA to less toxic Cu^{2+}. PcoB has a putative function of exporting Cu^{2+} across the outer membrane. Figure adapted from Chaturvedi and Henderson [109].

Strains isolated from Cu-enriched environments often carry additional CRM. For example, the *pcoABCDRSE* cluster was detected in both *E. coli* and *S. enterica* isolated from faeces of swine fed with Cu-supplemented feed. This cluster encodes an additional multicopper oxidase (PcoA) as well as the Cu chelators PcoC and PcoE, all under the control of the Cu-sensing two-component system PcoSR [110-113]. CRM can be acquired easily via horizontal gene transfer, as is the case for many *Pseudomonas syringae* pv. *actinidae* strains. This again highlights the evolutionary drift imposed on strains exposed to (anthropogenically) elevated Cu concentrations in the environment [114]. Another such strain isolated from a metal-contaminated environments is *C. metallidurans* CH34, as discussed above. CRM in CH34 have been associated with the 21-gene *cop*$_1$ cluster on pMOL30, as well as the neighboring *silDCBA* cluster. In addition, homologous *cusDCBAF*, *cupRAC* and *copS*$_2$*R*$_2$*A*$_2$*B*$_2$*C*$_2$*D*$_2$ clusters exist on the chromosome and chromid (Table 1-1). While essentially all

genes in these clusters are upregulated upon Cu exposure, the exact function of many of them remains unknown [115, 116]. Despite these uncertainties, Cu resistance in CH34 has mostly been attributed to three mechanisms working in parallel. First, the periplasmic Cu detoxification cluster *copABCD* is homologous to the *pcoABCDRSE* cluster found, in part, in *E. coli* and *Caulobacter crescentus*. This cluster likely encodes a multicopper oxidase as well as a Cu transport system [39, 110, 117]. Cu export is also achieved by the *silCBA* system, encoding an HME-RND type export pump. Lastly, the P_{IB1}-type ATPase encoded by the *copF* gene serves as an additional Cu efflux system. In order to avoid any confusion over gene or phenotypic designations, Table 1-1 compares the CRMs of *C. metallidurans* with those identified in other bacteria extensively studied for Cu resistance (e.g. *E. coli*, *P. syringae* and *Enterococcus hirae*.

Table 1-1. Homologous of *C. metallidurans* CH34 copper resistance mechanisms.

Function	*C. metallidurans*	*E. coli*	*P. syringae*	*E. hirae*
Periplasmic detoxification	*copA*$_1$*B*$_1$*C*$_1$*D*$_1$[a]	*pcoABCD*	*copABCD*	
	copA$_2$*B*$_2$*C*$_2$*D*$_2$[c]			
Multicopper oxidase	*copA*$_1$[a]	*pcoA*	*copA*	
	copA$_2$[c]	*cueO*		
Efflux P_{IB1}-type ATPase	*copF*[a]	*copA*	*copA*	*copA*
	cupA[b]			*copB*
HME-RND-driven efflux	*silDCBA*[a]			
	cusCBA[c]	*cusCBA*		

Located on [a]pMOL30; [b]chromosome or [c]chromid.

To round out this section, we provide here a small overview of CRM in *C. crescentus* NA1000, an α-Proteobacterium which will be further discussed in Chapter 5. *C. crescentus* NA1000 has been intensively studied for its distinct cell cycle [118-120]. Interestingly, Cu homeostasis in NA1000 was found to differ between its swarmer and stalked cell morphotype [117]. The stalked cell type relies mostly on the constitutively expressed PcoAB system, which consists of a multicopper oxidase PcoA and a periplasmic Cu efflux pump PcoB. Conversely, the swarmer cell type, which is equipped with a polar flagellum for efficient motility, employs negative chemotaxis to flee from local Cu contaminations. Its genome contains additional CRM homologues, but deletion of these genes did not confer Cu-sensitivity.

1.1.4 Regulation of bacterial metal resistance

Canonical regulation of gene expression relies on (de-)repression and activation by regulatory proteins, which interact with recognition sequences on the genome, with each other, and with RNA polymerase. Famously originally proposed by Jacob and Monod in 1961 [121], the model still represents the main level of gene expression regulation in bacteria [122]. This paradigm can be extended to cover metal resistance regulation (in *C. metallidurans* CH34), which relies on regulatory proteins of several classes. Cytoplasmic regulators such as MerR and ArsR alter transcription of their cognate regulon upon interacting with metal ions [123, 124]. Two-component systems, like CzcRS, consist of a sensor protein that can detect metal ions in the periplasm, which subsequently activates a regulator in the cytoplasm that in turn directs transcription of target genes [125]. Finally, some sigma factors, many with extracytoplasmic function (ECF), are (in)directly involved in metal resistance [126]. Noteworthy, the homeostasis of trace metals (e.g. Fe, Zn, Cu) requires a finely tuned regulation, since a relatively constant intracellular availability must be achieved both under conditions of metal starvation and of (potentially toxic) excess. In contrast, regulation of purely toxic metals (e.g. As, Cd, Ag) is more straightforward, as there is essentially always a benefit in removal of these metals from the cell [127].

More specifically, Cu is a micronutrient that constitutes a necessary component of, among else, cytochrome and multicopper oxidases, and no resistance mechanism can evolve that results in removal of all Cu ions from the cell [128]. In *C. metallidurans* CH34, regulation of the *cop* cluster on pMOL30, harboring many CRMs, is commonly associated with the CopRS two-component system [129]. However, it is unclear whether all genes in this cluster are (solely) regulated by CopRS, and not much at all is known about the regulation of the neighboring *sil* cluster. High-resolution transcriptomics have indicated the existence of antisense RNAs in this region [116], and it has been shown that *cop* genes can also be induced by metals other than Cu [115].

Since roughly the turn of the millennium, regulation via small regulatory RNAs (sRNAs) have been reported in essentially every bacterium studied. sRNAs of many variable lengths have been found and the specified length range differs from review to review, but overall it seems fair to define them as roughly 50-500 nt in length [130-132]. Some sRNA genes are located between CDSs, in intergenic regions, or are derived from processing of (sometimes polycistronic) mRNAs (Figure 1-3, panels B-G) [133, 134]. These sRNAs interact with mRNAs transcribed from other genomic

regions, so they are denoted trans-encoded sRNAs. Trans-encoded sRNAs usually display imperfect base pairing with their target mRNA, and often rely on proteins to catalyze sRNA-mRNA interaction, such as Hfq and ProQ [135-138]. Because of this imperfect matching, trans-encoded sRNAs can modulate several target mRNAs, and in this way foment a broad physiological response [139]. Another class of sRNAs are transcribed from the antisense strand opposite of their target mRNA (Figure 1-3, panel A). These cis-encoded sRNAs interact with only a single cognate mRNA, and interaction with this mRNA is not mediated by chaperones like Hfq [140].

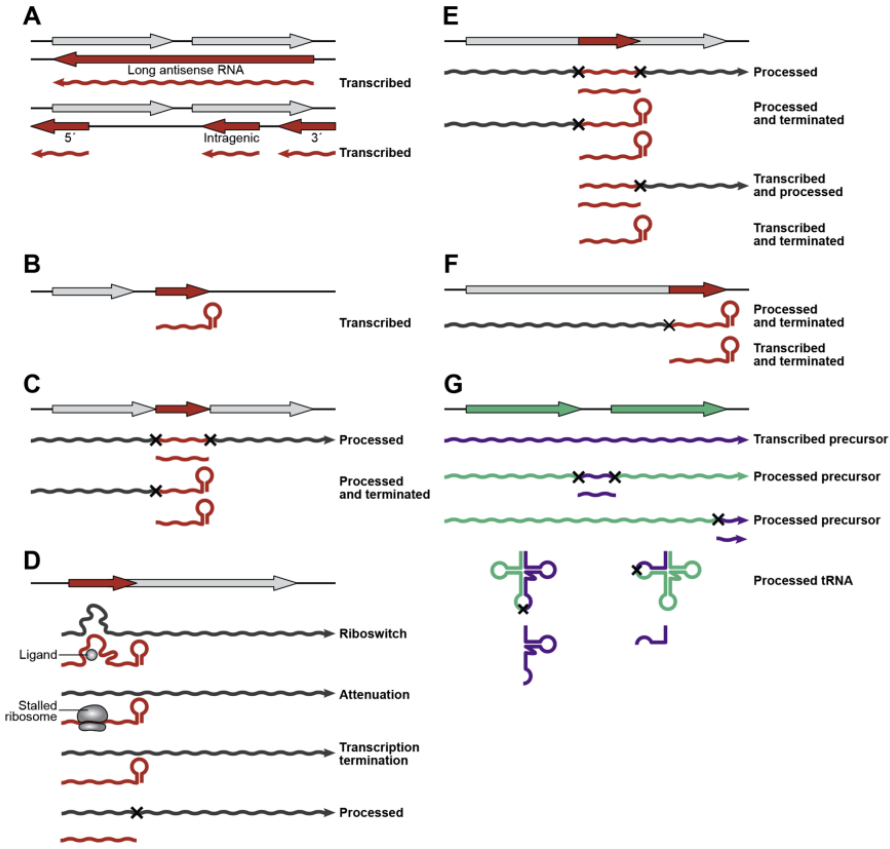

Figure 1-3. Origin of sRNAs form diverse genomic loci. (A) antisense (B) intergenic (C) operon-derived (D) 5'-derived (E) intragenic (F) 3'-derived (G) tRNA-derived. Coding sequences are shown in gray, sRNA sequences in red, tRNA sequences in green, and regulatory tRNA sequences in purple. Processing cleavage sites are indicated with an 'X'. Instances of known transcription termination are indicated by a hairpin. 3' ends corresponding to known processed RNAs are blunt. An arrow is used if the mechanism of

3’ end generation is unknown. Figure adapted from Adams and Storz [141]. Permission for reproduction granted by Elsevier.

Generally, sRNAs modulate gene expression on a post-transcriptional level by directly interacting with mRNAs [142]. A simplified overview of sRNA-mRNA interaction is shown in Figure 1-4. However, we must mention that a continuously expanding variety of regulatory mechanisms is being discovered, such as direct interaction with proteins like the carbon storage regulator CsrB [143, 144]. In the following, we will focus on cis-encoded sRNAs, also named antisense RNAs (asRNAs).

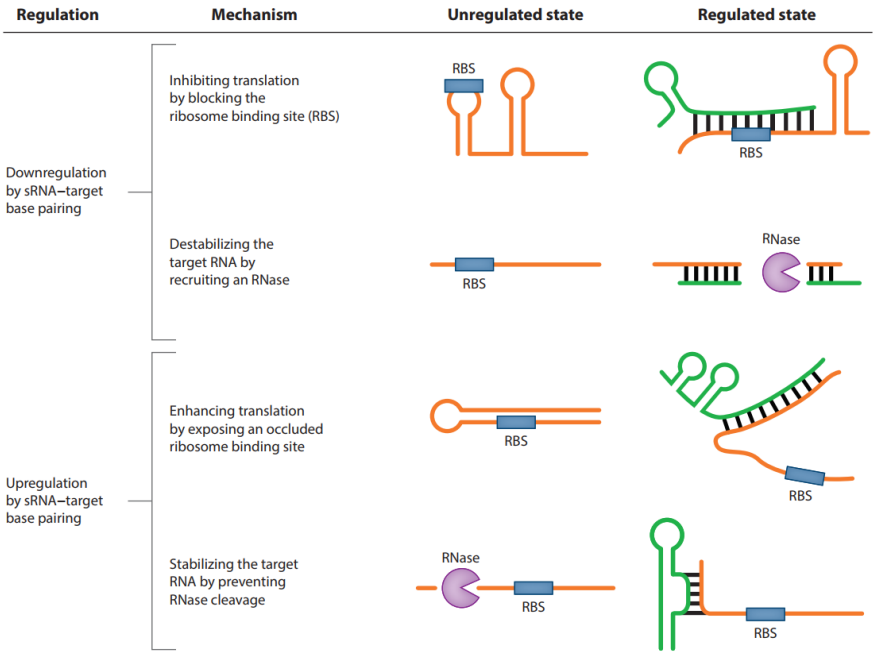

Figure 1-4. Mechanisms of sRNA-based regulation, on a post-transcriptional level. Interaction between sRNAs (green) and mRNAs (orange) is shown. Adapted from Nitzan *et al.* [145]. Permission for reproduction acquired from Annual Reviews, Inc.

Antisense RNAs have been detected in many strand-specific RNA-seq-based studies, and regulation by such sRNAs seems promising as a novel tool for biotechnological applications [146-148]. They have been encountered across many domains of life, including prokaryotes [146], eukaryotes [149] and archaea [150, 151]. A surprising proportion of the genome displays antisense transcription, reaching ca. 66% in *Bacillus anthracis* [152], 50% in *Helicobacter pylori* [153], 29% in *Methanolobus*

psychrophilus [150] and 10% in *C. metallidurans* [116]. Transcription of cis-encoded sRNAs is often controlled by sigma factors with defined regulatory motifs [148, 154]. asRNAs can also be under the control of other regulators, responding to changing environmental conditions [155, 156]. Experimental validation of their biological function often lags behind standard genome-wide detection studies, and consequently, we must be wary of an overrepresentation of cis-encoded sRNAs due to spurious transcription initiation and methodological biases, such as exceedingly deep sequencing [148, 157, 158].

Regulation by asRNAs can proceed in various ways, as thoroughly described by Georg and Hess [147] in 2011. First, interaction between asRNA and target mRNA can lead to RNase-mediated co-degradation, as in *Synechocystis* PCC6803, where the relative abundances of the IsiA mRNA and its cis-encoded sRNA IsrR regulate the organization of photosynthesis [159, 160]. However, direct interaction between asRNA and its target mRNA can in some cases stabilize the mRNA, e.g. by protecting it from degradation by RNase E [161, 162]. Second, asRNAs can occlude the ribosome binding site (RBS), and in this way inhibit translation of the mRNA [163]. Nevertheless, translation can be positively and negatively impacted by asRNAs without necessarily interacting directly with the RBS [164-166]. Third, rather than acting at a post-transcriptional level, asRNAs can interfere with mRNA transcription itself. Several mechanisms exist, relying on transcription attenuation by premature termination after forming a terminator hairpin [167, 168], or via collision and blocking of sense and antisense RNA polymerase complexes [169-171]. Additional mechanisms of asRNA-mediated regulation and its applications, can be found in e.g. Saberi *et al.* [172], Bordoy and Chatterjee [173], Villegas and Zaphiropoulos [174], and Brophy and Voigt [146].

sRNA-mediated gene regulation has as number of advantages compared to protein-mediated gene regulation, mostly hypothesized for trans-acting sRNAs but largely valid for cis-encoded sRNAs as well. Beisel and Storz [175] noted that sRNAs have the advantage of being metabolically inexpensive, as they are often short and do not require translation into (regulatory) proteins. However, as sRNAs often act at the post-transcriptional level, the metabolic cost of target mRNA transcription has already been expended, before sRNA regulation comes into play. There is also the aspect of the regulatory dynamics: Shimoni *et al.* [176] showed that sRNA-based regulation can respond faster to sudden stress conditions, where regulatory proteins often have to be newly synthesized. Another advantage, specifically for asRNAs, is

the potential for additional regulation without the need to expand the genome, since the regulator is inherently present on the opposite strand of the mRNA. Small changes in codon usage of the sense mRNA could then result in an altered asRNA promoter, resulting in differential regulation [153].

sRNAs are involved in the regulation of many distinct cellular processes, but especially in response to stress [177]. However, relatively few studies have focused on the role of sRNAs in the regulation of metal resistance. One well-studied example is that of RyhB in *E. coli*, which is part of the Fur regulon, controlling the Fe metabolism [178]. Likewise, in *S. aureus*, the RsaC sRNA aids in Mn starvation [179]. While essential under starvation conditions, these examples tell us little about the stress of excess metal concentrations. Post-transcriptional regulation of the Cu stress response was noted in *Xanthomonas citri* subsp. *citri*, where the CohL sRNA likely interacts with CopAB [180]. Lastly, sRNAs have been implicated in the indirect response to metal toxicity, for example in the response to oxidative stress that plays a large part of e.g. Cu toxicity, as well as the envelope stress response [181-185]. A well-known example is that of the sRNA OxyS, which indirectly blocks translation of the RpoS mRNA, thus favoring the use of the household sigma factor RpoD. RpoD in turn allows for the expression of OxyR, an important regulator of the oxidative stress response [182]. As a side note, the Hfq protein, an important catalyst for sRNA-based regulation, has been shown to play a crucial role in the adaptive response to spaceflight conditions [186, 187].

1.2 The viable-but-non-culturable cell state: a result of damage accumulation

1.2.1 Copper toxicity induces the VBNC state

It is clear that elevated Cu concentrations are highly toxic to bacteria. In order to understand the bacterial response to this toxicity, it is relevant to study the effects of sub-lethal Cu concentrations. A curious observation in this regard is the apparent loss of culturability of Cu-exposed bacterial cells. At the same time, these cells often retain characteristics of viability such as intact cell membranes and metabolic activity. An overview of tested strains exhibiting this behavior is provided in Table 1-2. The latter includes human as well as plant pathogens, reflecting the medical and agricultural use of Cu antimicrobials.

The question arises whether these observations are merely a consequence of sustained cell damage, which we will denote as 'sublethal injury', or whether it concerns the active induction of a regulated cellular state as a response to the perceived Cu stress. This cellular state is often denoted as the 'viable-but-non-culturable' (VBNC) state. An excellent review on the phenotypic characteristics and the mechanisms of identification has been written by Pinto *et al.* [188]. VBNC cells cannot be cultured on standard laboratory media, but retain membrane integrity, and low but measurable levels of metabolism and gene expression [74, 75]. They are formed under harsh conditions like starvation and in the presence of various chemical and physical stressors. The VBNC state displays similar traits to the so-called 'cellular quiescence', a noted survival strategy of *Mycobacterium tuberculosis*, but no in-depth comparison of these states has been performed [189, 190]. It is often difficult to verify experimentally whether a cell population is sub-lethally injured or in the VBNC state, or both, since many measurable properties are shared by both cell states. One key distinction is the inability of sub-lethally injured cells to grow on selective media, while colony growth would be observed on non-selective media, as claimed by Bogosian and Bourneuf [191]. However, it is abundantly clear that no extant culture medium is entirely non-selective. Thus, this definition of sub-lethal injury seems untenable, especially when comparing species over multiple clades, each with their own optimal growth conditions. Consequently, many researchers do not make the above distinction and term both cell states under the VBNC denomination. Furthermore, the evolutionary conservation of entering a VBNC state in response to a range of stress conditions and the growing body of evidence elucidating its molecular mechanisms indicates that it is a cell-programmed phenomenon. Finally, there exists an ongoing discussion about the similarities between VBNC cells and persister cells. Persister cells are slow-growing, antibiotic-tolerant cells that represent a subpopulation of actively dividing cultures. This phenotypic heterogeneity allows for rapid recolonization of habitats after transient stress conditions [192]. The VBNC state shares characteristics with persister cells, such as morphology and resuscitation characteristics. Based on these similarities, Kim *et al.* [193] suggested that VBNC cells and persister cells are one and the same. However, this conclusion was refuted by Ayrapetyan *et al.* [194].

A fraction of the VBNC cell population can often be manipulated in order to make them regain culturability. This process is called resuscitation. The ability to show resuscitation is essential when arguing in favor of a programmed VBNC state, and

has become a mainstay of VBNC studies [188, 191]. Multiple resuscitation stimuli have been listed by Pinto *et al.* [188], but it is difficult to distill information about putative molecular mechanisms considering the large number of experimental conditions and the phylogenetic distance of the tested strains. A note must be made that resuscitation is often difficult to distinguish from regrowth of the remaining culturable population. Protocols such as the analysis of dilution series exist to minimize the likelihood of mistaking regrowth for resuscitation, but they are not consistently used in practice [195]. Consequently, this distinction must be approached with caution.

Table 1-2: Overview of bacterial species with Cu-induced VBNC state.

Bacteria		Induction conditions			Max ind. efficiency	VBNC state characteristics	Resuscitation conditions
Species	**Strains**	**Medium**	**CFU/mL**	**[Cu^{2+}] µM**			
E. coli	ES80, K-12 (C600), O157:O7 (EDL933), O104:H4 (RKI 01-09591)	S	10^6-10^8	500	No CFU in 7 days; no CFU in 5 days	IM; IM, decreased cell size	Washing with EDTA, resuspending in saline solution; identical
P. aeruginosa	PA14, AdS, DSM 50071, PAO1	PBS; H_2O	10^6-10^7	4 - 10	6 log in 2 h; no CFU in 10 h	IM; IM, intact rRNA, not cytotoxic	Adding DDTC to medium; identical
R. solanacearum	AS108, SL341	S; PBS	10^8	5 - 500	3.5 log in 9 days at 5 µM; no CFU in 24 h	IM, KP; intact membrane, strong aggregation, lower PHB content, lower RNA content, various proteome changes, increased H_2O_2 content	Attempted but not achieved; spontaneous at low $CuSO_4$, not observed at higher concentration
C. metallidurans	CH34, AE104	H_2O	10^8	10	4 log in 3 h for CH34, no CFU in 1 h for AE104	IM	Spontaneous for CH34, not observed for AE104
E. amylovora	CFBP1430, IVIA1892-1	MM	10^7	5 - 50	No CFU in 30 days at 5 µM	IM, CP, reduced pathogenicity,	Addition of equimolar (to Cu^{2+}) EDTA, asparagine, citric acid,

Bacteria		Induction conditions			Max ind. efficiency	VBNC state characteristics	Resuscitation conditions
Species	**Strains**	**Medium**	**CFU/mL**	**[Cu^{2+}] µM**			
						increased cell size and envelope thickness	fresh immature pear juice, King's Broth
A. citrulli	AAC00-1	MM	10^7	0.5 - 50	2 log in 10 days at 0.5 µM	IM, not pathogenic	Resuspension in LB broth, cell-free supernatant, AB medium + casein hydrolysate, or washing with EDTA
X. axonopodis	49b	H_2O	10^6	45 - 225	3 log in 30 mins at 45 µM	CP, reduced pathogenicity	Addition of EDTA
A. tumefaciens	At493	H_2O	10^8	50 - 5000	No CFU in 1 day	IM, KP	Spontaneous at low $CuSO_4$ but not observed at higher concentrations
R. leguminosarum	F6	H_2O	10^8	5 - 500	No CFU in 1 day	IM, KP	Spontaneous at low$CuSO_4$ but not observed at higher concentrations
C. michiganensis	BT0505	S	10^7	0.05 - 50	No CFU in 37 days at 0.05 µM	IM	*In planta*, resuspension in LB

IM: Intact membrane as per LIVE/DEAD staining; KP: positive test in Kogure assay; CP: positive test in respiratory activity assay with CTC. References: Grey and Steck [196], Aurass *et al.* [197], Bedard *et al.* [198]; Dwidjosiswojo *et al.* [33], Grey and Steck [199]; Um *et al.* [200], Maertens *et al.* [34], Ordax *et al.* [201], Alexander *et al.* [202], Alexander *et al.* [202], Jiang *et al.* [203], Kan *et al.* [204], del Campo *et al.* [205].

1.2.2 Mechanisms behind the Cu-induced VBNC state

Evidently, Cu is not the only stress capable of inducing the VBNC state. Common stressors in this regard include starvation, desiccation, low temperature, pH extremes and oxidative compounds like hypochlorous acid [188, 206]. It seems unlikely that a direct regulatory pathway exists between the sensing of each separate stressor and the induction of a general VBNC state. More plausible would be VBNC induction triggered by one or more common consequences elicited by these distinct stressors. Therefore, we may derive insights from the interpolation of these mechanisms.

Oxidative stress can induce the VBNC state in different bacterial species [207, 208]. In addition, Li *et al.* [209] suggested that the oxidative stress regulator OxyR is involved in the regulation of VBNC state induction, based on work of Longkumer *et al.* [210], Abe *et al.* [211] and Wang *et al.* [212]. Oxidative stress is an important component of many conditions able to induce the VBNC state, such as desiccation [213], starvation [214] and exposure to common disinfectants like hypochlorous acid [215]. As mentioned before, it is also a substantial component of Cu toxicity. Kan *et al.* [216] showed increased levels of superoxide dismutase and alkyl hydroperoxide reductase proteins in Cu-induced *Acidovorax citrulli* VBNC cells as well as during the early stages of resuscitation. In addition, an increased H_2O_2 content was detected in Cu-induced *Ralstonia solanacearum* VBNC cells [200]. Thus, we conclude that oxidative stress elicited by Cu is an important facet of the Cu-induced VBNC state.

The rapid response required for the detoxification of VBNC state-inducing stressors can put a strain on the cellular energy reserves. For instance, Cu-exposed cells have a lower ATP content, and a decreased electron transport and dehydrogenase activity [217, 218]. In addition, this decreased ATP content has been used to define toxic CuNP levels [219]. While metabolic activity is by definition maintained in VBNC cells, it is often diminished. ATP levels are often, but not always, lower in VBNC cells [208, 220, 221]. However, ATP content is not a straightforward indicator of general metabolic activity [222] and ATP content in Cu-induced VBNC cells is still to be evaluated. All the while, many proteins involved in central metabolic processes were downregulated in Cu-induced VBNC *Acidovorax citrulli* cells [216]. In addition, PHB content, which functions as a cellular energy reserve, is reduced in Cu-induced VBNC *Ralstonia solanacearum* cells [200]. Consequently, the decrease of metabolic activity due to Cu stress appears to be another vital facet of the Cu-induced VBNC state.

Degradation of the proteome can derive both directly from the interaction of proteins with Cu ions, and from the destructive action of ROS. In addition, the proteome needs some measure of reconfiguration to cope with the imposed stresses, by repairing degraded peptides and synthesizing stress defense mechanisms. Proteome adaptations are common in VBNC cells [206, 223] and in cells undergoing Cu stress [129, 224]. However, to date we could find only a single study investigating the proteomic composition of Cu-induced VBNC cells. In Kan *et al.* [216], 3 of the 5 COG classes with the most changes in VBNC and resuscitating cells correspond to some aspect of proteome reconfiguration (posttranslational modification, protein turnover, and chaperones; amino acid and transport; translation, ribosomal structure, and biogenesis). It remains unclear to what extent these changes are due to direct changes as a result of Cu toxicity, or to the adaptive response of the cell to this toxicity. Evidence for the latter was found in the upregulation of a Cu-translocating ATPase and superoxide dismutase enzyme.

Overall, it remains clear that more research is needed to characterize Cu-induced VBNC cells. Additional whole-cell proteome, transcriptome, and metabolome studies would provide valuable insights into the complex but similar behavior exhibited by these phenotypically distinct cells. Likewise, it would be interesting to study the heterogeneity of this behavior via single-cell techniques.

1.2.3 Copper resistance mechanisms and their role in entry into the VBNC state

Higher Cu concentrations lead to a higher proportion of the initial cell population entering the VBNC state [199, 201, 203, 205] and CRMs limit the entry in the VBNC state upon exposure to sub-lethal Cu concentrations [34]. These observations corroborate that Cu ions are inducing the VBNC state and that CRMs play an important role in the Cu-induced VBNC state by preventing the buildup of excessive amounts of Cu in the cytoplasm.

While it is clear that CRM activity protects the cell against Cu stress, this protection is not sufficient to maintain culturability under increased Cu concentrations. Culturability can often be regained upon chelation of excess Cu ions by EDTA, DDTC, or complex media such as LB. In the case of resuspension in growth media, we cannot rule out effects other than direct chelation of Cu ions. Conversely, spontaneous resuscitation, without the addition of chelating agents, has been observed in *Cupriavidus*, *Ralstonia*, *Agrobacterium*, and *Rhizobium* (Table 1-2). This behavior

occurs only upon low Cu toxicity. In *Cupriavidus*, spontaneous resuscitation was only observed in strains containing the pMOL30 megaplasmid, highlighting the necessity of CRM in this process. While it would be interesting to compare the extent of VBNC state induction to the activity and complexity of CRM further, the multiplicity of the experimental conditions largely prohibits this analysis. Indeed, retesting these strains in more standardized conditions could provide essential results in this regard. While the role of CRM in (spontaneous) resuscitation requires further study, the risk for VBNC cells escaping common detection strategies while retaining the potential for resuscitation has been emphasized previously [225]. An additional risk factor is the spread of metal resistance genes within and between bacterial populations repeatedly exposed to metal stress, which could exacerbate this effect. While the Cu-induced VBNC state has been described in (opportunistic) pathogens such as *E. coli* O104:H4 and *P. aeruginosa* PAO1, no *in vivo* studies have been undertaken to determine the generation of difficult-to-detect VBNC cells by existing Cu-based therapies. However, such studies could provide interesting and relevant data for the medical field.

1.2.4 The VBNC state: towards a general model?

Recent years have seen the curious observation of a Cu-induced VBNC state in many phylogenetically distinct bacterial species. Here we summarized these observations and investigated the mechanisms of VBNC state induction by Cu toxicity (Figure 1-5). While more research into this matter is needed, we argue that the VBNC state induced by Cu is the result of an adaptive response to this stressor. Sub-lethal Cu concentrations bring about cellular damage, rendering the cell unable to multiply. In response, it will redirect its metabolism to enable reparation of sustained damage and synthesis of CRM. This response is likely under the control of alternative sigma factors. In this sense, the Cu-induced VBNC state is a programmed phenomenon. However, many different stresses can result in non-culturability, so VBNC states seem to be a common consequence of stress rather than a programmed behavior with a single and discrete set of regulators. This is evident from the observation that different stressors capable of inducing a VBNC state, such as starvation, hypochlorous acid, low temperatures and Cu, prompt the bacterial cell to activate resistance mechanisms to each of these stressors separately [188]. Thus, it seems counterintuitive to search for common regulators controlling the VBNC state induced by distinct stressors with distinct mechanisms of toxicity. Rather, we could view the VBNC state as the phenotypical result of a damaged cell opting for survival over

multiplication, governed by stressor-specific regulatory mechanisms. Whatever the case, it is certain that understanding the particularities of the VBNC state is a crucial task in ensuring satisfactory biosafety and biocontrol. Several uncertainties remain at many levels, from the initial interaction of the cell with Cu ions over the type, site, and extent of damage accrued, to the molecular mechanisms governing the cellular response. Since, in most cases, only a certain fraction of the initial population can be converted to and resuscitated from the VBNC state, one research question in particular concerns the cellular heterogeneity of these processes. In this sense, single cell-oriented techniques may provide much-needed information. Overall, it is clear that these studies would benefit from a standardized multifaceted experimental approach, integrating whole-cell analyses of copper chemistry, single cell proteomics and metabolomics in order to pinpoint the metabolic status of VBNC cells and the sensory system facilitating resuscitation.

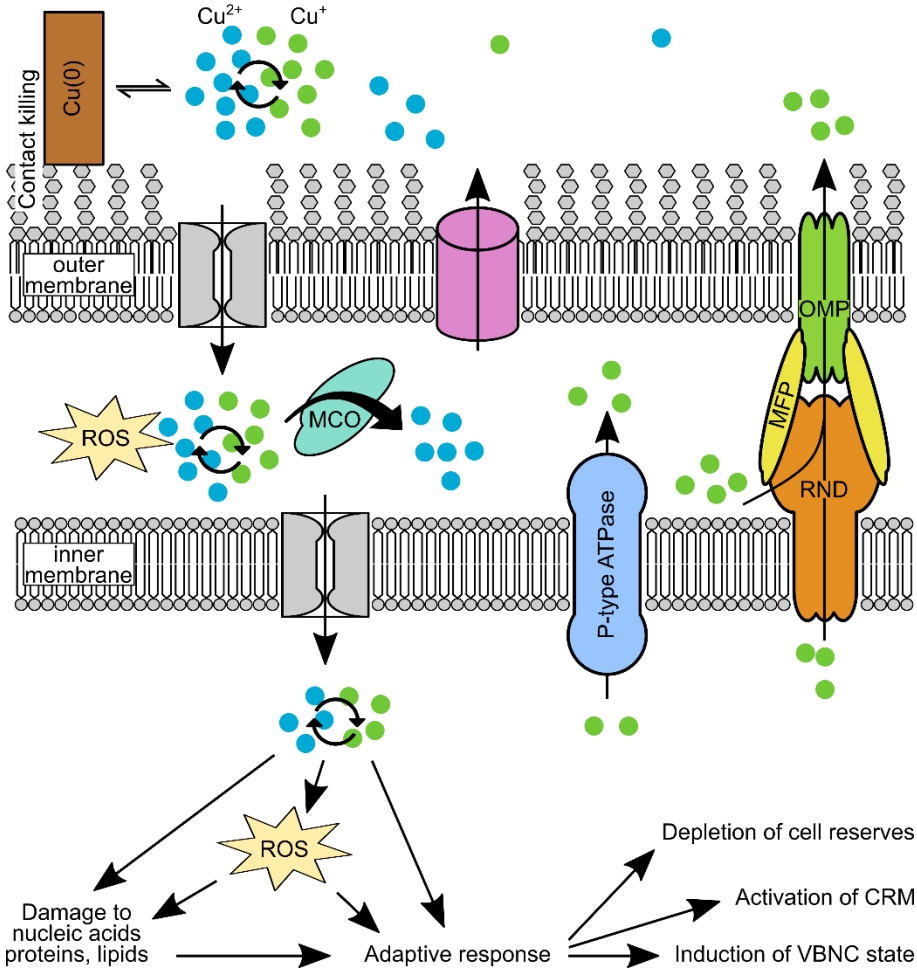

Figure 1-5. Overview of pathways from Cu exposure to induction of the VBNC state.

Scope of the work

As explored in **Chapter 1**, antimicrobial resistance is an issue of growing concern worldwide. This is leading to the development of novel antimicrobials and the rediscovery of antimicrobial therapies predating the golden era of antibiotics. Therefore, recent years have seen a renewed interest in metals, such as solid Cu, as antimicrobials. However, much like resistance to common antibiotics has evolved and spread between bacterial populations, Cu resistance mechanisms have the potential to decrease the efficacy of Cu antimicrobials strongly. In addition, supposedly lethal Cu toxicity can lead to the conversion of bacterial populations to the VBNC state. Such VBNC cells are difficult to detect with standard culture-based detection methods, and can regain culturability and virulence in favorable conditions. Consequently, there is a need for the thorough validation of Cu antimicrobials, and a thorough examination of the bacterial response to Cu stress. Interestingly, this renewed interest into Cu antimicrobials has also been picked up by space agencies in order to control persistent microbial contamination during spaceflight, which could impact crew health and equipment integrity. *C. metallidurans* CH34 was selected as a model organism for its impressive arsenal of well-described metal resistance mechanisms, and the fact that several strains of *Cupriavidus* and the closely related genus *Ralstonia* have been isolated from the ISS, the Mir space station, the Shuttle, and several spacecraft assembly and servicing facilities [226-231]. In addition, CH34 has been the focus of several studies onboard the ISS [232-235], and is part of the ESA BIOFILMS project, planned to be conducted onboard the ISS in 2021.

Our first aim **(Chapter 2)** was to investigate the phenotypic response of *Cupriavidus metallidurans* CH34 to solid Cu surfaces in wet conditions (i.e. drinking water), specifically paying attention to the development of the viable-but-non-culturable cell state. In addition, we studied the role of Cu resistance mechanisms on the conversion to the VBNC state and the subsequent recovery. Finally, biofilm formation on Cu and stainless steel surfaces were assessed.

Next, we aimed to form a global picture of gene regulation in Cu-stressed *C. metallidurans* CH34 cells **(Chapter 3)**. Therefore, the transcriptome and transcription start sites were studied. As sRNA-based regulation had not been studied in *C. metallidurans* before, we paid close attention to the annotation of noncoding RNAs. Interestingly, it has been shown that sRNA-based regulation is an important regulation level of the behavior of bacteria under space conditions. By opting for an acute but moderate Cu stress via the supplementation of a defined concentration of $CuSO_4$, we attempted to mimic the initial contact of cells with a solid Cu surface with concomitant release of Cu ions, while retaining a practically controllable experimental setup. Finally, we focused on putative regulatory regions of the *cop* and *sil* clusters.

Subsequently, analysis of the biological function of selected noncoding RNAs was pursued in **Chapter 4**. The transcription start site and expression levels of these sRNAs were evaluated, after which we focused on a newly detected transcript (*silY*) located antisense of the *silDCBA* cluster. The latter encodes a HME-RND efflux pump with a role in copper and silver resistance. We investigated the regulatory function of this antisense transcript by studying its effect on translation of the polycistronic SilDCBA mRNA, and the consequences on the Cu resistance phenotype. The study of *silY* was undertaken to provide new insights into the regulation of *silDCBA*, which was previously unclear due to the absence of a co-localized regulator.

Finally, in **Chapter 5**, we aimed to evaluate the role of the environment on the Cu stress response, with the model α-Proteobacterium *Caulobacter crescentus* as a case study. Similar to *C. metallidurans, C. crescentus* strains are commonly associated with oligotrophic environments, including those aboard the ISS [66, 236]. The analysis of Cu-stressed *C. crescentus* provides a valuable comparison of the Cu-tolerant *C. crescentus* to the Cu-resistant *C. metallidurans*. The transcriptomes of Cu-stressed *C. crescentus* morphotypes were analyzed in a complex and a defined medium. The chemical environment of the cell is an often underappreciated factor in metal toxicity studies, but in the end of vital importance.

CHAPTER 2 Copper resistance mediates long-term survival of *Cupriavidus metallidurans* in wet contact with metallic copper [*]

2.1 Introduction

The historical use of copper (Cu) for sterilization of drinking water and the treatment of various illnesses dates back to the third millennium B.C. Indeed, ancient civilizations ranging from Egyptian over Greek to Aztec utilized Cu in different formulations to combat bacterial proliferation in diverse conditions [16]. Recently, the widespread use of antibiotics and concomitant development of antibiotic resistance mechanisms has brought renewed interest in the antimicrobial properties of Cu [48].

Copper metal, which is routinely used for plumbing works, can impart bactericidal effects on waterborne microorganisms via the leaching of Cu ions. The solubility of Cu in water depends on chemical parameters such as pH, concentration of dissolved oxygen and free Cl^- ions [237], and the presence of chelating agents [238]. For many bacterial species, relatively low concentrations of ionic Cu are sufficient for inactivation, e.g. *Legionella pneumophila* in drinking water shows a 6-log_{10} decrease in CFU/ml within three hours after the addition of 100 µg/l (0.74 µM) $CuCl_2$ [239], more than 99.9% of *Pseudomonas aeruginosa* cells in deionized water are inactivated within 24 hours by adding 1 µM (160 µg/l) $CuSO_4$ [33], and hospital isolates as well as control strains showed near-complete killing after 48 hours storage in a Cu vessel containing a saline solution or water [240]. In addition to the

[*] This chapter is based on the following publication: Maertens, L., Coninx, I., Claesen, J., Leys, N., Matroule, J.Y., and Van Houdt, R. (2020). Copper Resistance Mediates Long-Term Survival of *Cupriavidus metallidurans* in Wet Contact With Metallic Copper. Frontiers in Microbiology 11: 1208.

toxic effects of ions present in the medium, the direct interaction of bacterial cells with the metal surface can lead to a strongly enhanced killing effect [46], coined as contact killing and recently reviewed by Vincent *et al.* [30]. This enhanced toxicity was demonstrated by covering the copper surface with an inert polymeric grid, which prevented direct bacterial attachment but not the release of Cu ions in the medium, resulting in a drastic decrease of toxicity. Contact killing rates depend on, among else, copper content, temperature and humidity [241, 242], and medium composition [243]. The mechanisms of Cu toxicity to bacterial cells have been under increasing scrutiny [30, 42]. Several modes of action have been put forward, although their sequence and interactions remain unclear. The production of reactive oxygen species can be catalyzed by Cu via a Fenton-like reaction *in vitro*, but contrasting data have been reported regarding its role in DNA degradation *in vivo* [50, 244-247]. The inactivation of Fe-S proteins by competition of Cu with Fe in an oxygen-independent manner has been reported [53, 54], as well as membrane damage via lipid peroxidation [47, 248, 249]. In addition, the induction of a viable but non-culturable (VBNC) cell state after exposure to Cu has been observed in multiple studies. This state is defined as cells with low metabolic activity that maintain membrane integrity and a low level of gene expression, but which do not form CFUs on culture media [74, 75]. The VBNC state is thought to enable an increased resistance to many environmental stresses, including antibiotics [250], oxidative stress and metals such as copper [251]. Many questions still surround the VBNC state, but it is clear that VBNC cells can still pose problems since resuscitation and subsequent toxicity of bacteria from drinking water have been reported [33, 209, 252-254].

While the inactivation of bacteria by low Cu concentrations might imply the absence of a Cu requirement for bacterial metabolism and growth, this is clearly not the case. In fact, bacteria must carefully regulate intracellular concentrations of this micronutrient and have evolved a multitude of mechanisms devoted to this task. In contrast to export systems, import of Cu to the cytoplasm is poorly understood, with early research indicating the importance of outer membrane porins in *E. coli* [255]. In more recent studies, putative roles for major facilitator superfamily [256] and TonB-dependent transport systems [257] have been identified. Free Cu in the cytoplasm is quickly bound by chaperones and delivered to export systems, such as P_{IB1}-type ATPases and HME-RND systems [54]. Multicopper oxidases with various functions provide an extra layer of defense. Some bacteria harbor multiple CRM that

can interact to a high level of complexity and lead to the ability to withstand millimolar concentrations. The *Cupriavidus metallidurans* species, isolated on many occasions from harsh metal-contaminated, oligotrophic industrial environments, provides a striking example. Type strain *C. metallidurans* CH34, which has become a model strain for studying metal resistance, was isolated in 1978 from a decantation basin in a non-ferrous metallurgical plant [93]. Its *cop* cluster, located on the megaplasmid pMOL30 and conferring high resistance to Cu ions, consists of 21 genes among which several chaperones, a P_{IB1}-type ATPase, a HME-RND system and a multicopper oxidase. Almost all are upregulated after exposure to Cu^{2+} [125, 129]. Remarkably, this species has been repeatedly found to contaminate the International Space Station, including on dust and in cooling and drinking water reservoirs [57, 226, 228].

The importance of CRM in relation to contact killing has only been poorly studied, especially in conditions relevant to drinking water treatment and in timeframes longer than several hours. In dry and semi-dry conditions, the deletion of copper resistance determinants leads to a slightly faster inactivation of *E. coli* [258], *P. aeruginosa* [259], and *Enterococcus hirae* [48]. In this chapter, we investigated the inactivation kinetics of *C. metallidurans* CH34 in contact with metallic copper in drinking water and evaluated the role of its CRM.

2.2 Materials and methods

2.2.1 Bacterial strains, media and culture conditions

Cupriavidus metallidurans CH34 [93], AE104 (plasmidless derivative of CH34) [92] and *Cupriavidus campinensis* AE1239 (derivative of DS185 carrying a Cu-responsive *lux*-fusion in pMOL90::Tn*4431*) [260] were routinely grown in Tris-buffered mineral medium (MM284) [92] supplemented with 2 g/l gluconate, on an orbital shaker at 180 rpm in the dark at 30 °C. MM284 agar plates were prepared by adding 2% agar (Thermo Scientific, Oxoid, Hampshire, UK) to the liquid medium. Ionic Cu was added to the medium as $CuSO_4$ (Sigma-Aldrich, Overijse, Belgium). Phosphate-buffered saline solution (PBS) was prepared by dissolving a PBS tablet (Gibco™) in Milli-Q water (Merck Millipore, Belgium), achieving final concentrations of 10 mM sodium phosphates (to attain a pH of 7.4), 2.68 mM KCl and 140 mM NaCl.

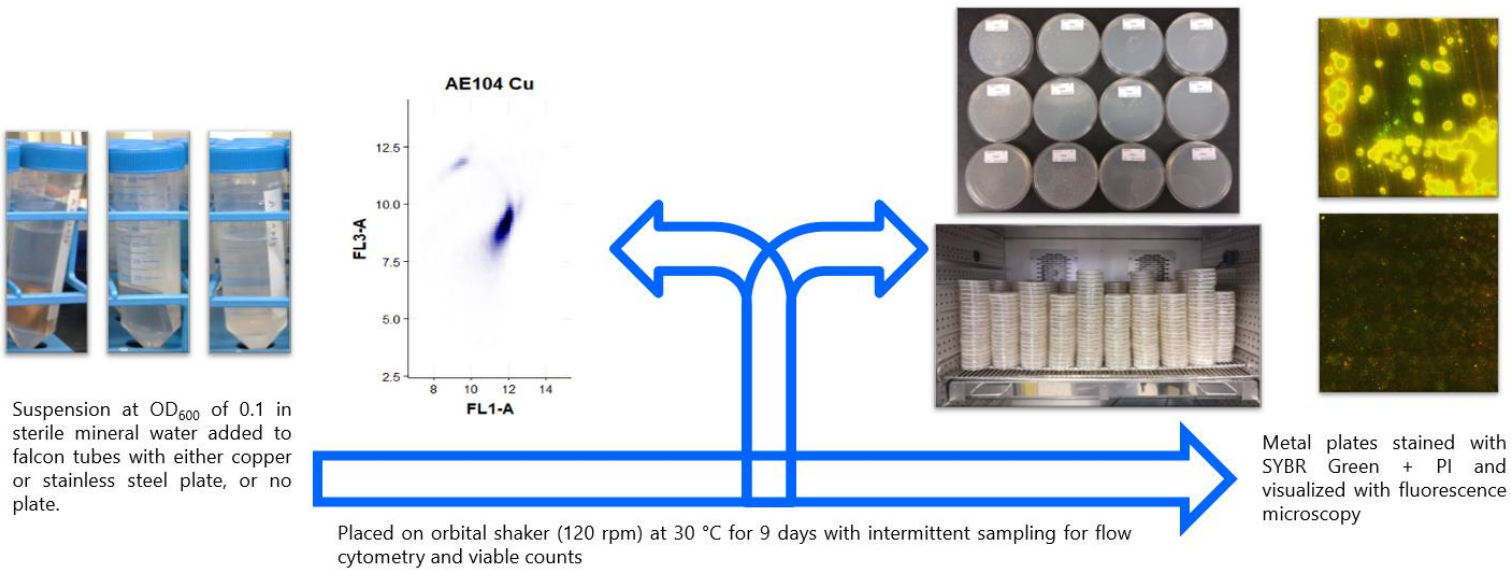

Figure 2-1. Generalized overview of survival experiments with metal plates.

2.2.2 Preparation and setup of survival experiments

Copper (99,99%) and stainless steel (AISI 304) plates were prepared by submerging them in a 70% ethanol solution for 10 minutes to inactivate possible contaminants and to solubilize organic components on the plate surface. After this step the plates were sonicated at 130 kHz in a TI-H-5 (Elma Schmidbauer GmbH, Germany) in deionized water for 10 minutes to remove contamination and to dissolve any extant salts. Plates were then sterilized at 121 °C for 20 minutes to kill any remaining cells, dried at 60 °C and stored in sterile containers at room temperature. Bacterial cultures of *C. metallidurans* CH34 and AE104 were grown in MM284 for 72 hours. While the stationary phase is reached in about 36 hours, cells were cultured for an additional 36 hours to induce a starvation response. This step was introduced to reflect natural environments and to diminish the confounding effects of sudden nutrient depletion in the main experiment. This approach did not affect the initial number of CFUs. Pre-induced *C. metallidurans* CH34 cultures were prepared by adding 300 µM $CuSO_4$. Cultures were washed twice in filter-sterilized mineral water (Ordal, Ranst, Belgium) and subsequently resuspended in this mineral water (final OD_{600} of 0.1). The prepared Cu and stainless steel plates were separately inserted into a 50 ml conical centrifuge tube with vent cap until stuck against the conical tube bottom. No plates were inserted in the control condition tube. Forty ml of prepared bacterial suspension was added to each tube and all tubes were placed upright on an orbital shaker at 150 rpm in the dark at 30 °C. A generalized overview of this setup can be found in Figure 2-1. In a separate experiment, cultures were prepared identically, but instead of inserting a Cu plate, 10 µM $CuSO_4$ was added. An equivalent volume of Milli-Q water was added to the control condition. All survival experiments were performed in biological triplicate.

2.2.3 Viable counts and flow cytometry

Samples for viable counts and flow cytometry were taken at 0, 1, 3, 5, 24, 48, 72, 96, 144, 168 and 192 hours after the start of the experiment. For each sample, 20 µl of bacterial suspension was taken from ca. 1 cm below the water level. Cell enumeration by total viable count was performed by spreading 100 µl of a serial ten-fold dilution in sterile PBS on MM284 agar and counting colonies after a minimum of 4 days at 30 °C. Cell enumeration by flow cytometry was performed by diluting 20 µl of bacterial suspension 100- and 1000-fold in filter-sterilized (0.2 µm) mineral water (Evian). Next, SYBR Green (Life Technologies) and propidium iodide (PI, Merck) were

added to a final concentration of 1X (starting from a 10,000X commercial stock solution) and 200 µM, respectively. Suspensions were incubated in the dark at 37 °C for 20 minutes to allow complete binding of the dyes. Stained bacterial suspensions were analyzed on an Accuri C6 (BD, Erembodegem) with a blue (488 nm, 20 mW) laser, which was calibrated according to the manufacturer's recommendation. Standard optical filters included FL-1 (530/30) and FL-3 (670 nm LP). SYBR Green was detected with FL-1, PI with FL-3. Samples were analyzed using the BD Accuri C6 software version 1.0.264.21, and gating and counting of events was performed using the PhenoFlow package for R [261].

2.2.4 Biofilm visualization

After 9 days of incubation, the copper and stainless steel plates were placed in a 6-well plate and immediately stained with 100 µl SYBR Green (1X) and propidium iodide (200 µM) solution. The plates were incubated in the dark at 37 °C for 20 minutes. Unattached bacterial cells and excess dye were gently rinsed off the plates with 1 ml of PBS.

An automated inverted fluorescence microscope (TE2000-E; Nikon, Tokyo, Japan) equipped with a motorized XYZ stage, emission and excitation filter wheels, shutters and a triple dichroic mirror (436/514/604) was used for the image acquisition of the surface of the stainless steel and Cu plates. Images were acquired with a 20X objective and an Andor iXon EMCCD camera (Andor Technology, South Windsor, CT, USA). For each sample, at least five sets of 25 pictures in a 5x5 grid, each containing one field of view, were computationally stitched together with 15% overlap using NIS-elements AR 5.11.01 (Nikon).

2.2.5 ICP-MS

At 0, 5, 48, and 216 hours after the start of the experiment samples were taken for ICP-MS measurement to determine the concentrations of Cu, Ni and Zn in the aqueous phase. Two milliliters were centrifuged at 10,000 g for 2 minutes, and the supernatant was stored at -20 °C until further processing. Samples were acidified to a final concentration of 2% HNO_3 and metal concentrations were measured with an ICP-MS X-Series II (Thermo Fisher Scientific).

2.2.6 Biosensor experiments

The response of the Cu biosensor AE1239 was quantified using a multimode microplate reader (CLARIOstar®, BMG Labtech). This strain has a reported detection

limit of 1 µM [262]. AE1239 cultures were prepared by growing them in MM284 for 72 hours at 30 °C, subsequently washing them twice with filter-sterilized mineral water (Ordal) and resuspending them in either filter-sterilized mineral water or MM284. The response on metal plates was measured by pipetting 200 µL of cell suspension on top of each plate placed in a 6-well plate. Focal height was optimized to 7.5 mm, and a maximal gain of 4095 was used. Measurements were performed approximately every 5 minutes without intermittent shaking of the plate. The response to ionic Cu was measured by adding 200 µL to a 96-well plate. Focal height was optimized to 11 mm, again with maximal gain. For these experiments, intermittent shaking occurred at 150 rpm and the optical density at 600 nm was measured in addition immediately before the luminescence measurement.

2.2.7 Statistics

For statistical analysis, the lmerTest and emmeans-packages in R 3.6.1 were used to fit linear mixed models (lmer), followed by a pairwise comparison and Bonferroni's procedure for multiple testing (pairs(emmeans())). Adjusted p-values below 0.05 were considered statistically significant.

2.3 Results and discussion

2.3.1 Survival of *C. metallidurans* CH34 in wet contact with metallic Cu

In a first setup, we tested the survival of *C. metallidurans* CH34 in sterilized drinking water in contact with either a submerged Cu plate, a stainless steel plate or no plate. The Cu condition showed a clear and significant drop in viable counts of more than 4 $\log_{10}$ within 3 hours after the start of the experiment (Figure 2-2a). This decrease in viable count was confirmed but not exacerbated after 5 hours. Between 5 and 48 hours, the viable count remained stable, after which it increased significantly with 2.7 $\log_{10}$ until 144 hours after the start of the experiment. After 144 hours, viable counts decreased again, but this process was concomitant to the decrease observed in the stainless steel and the control condition, where some loss of viability was measured over the course of the experiment (Figure 2-2a). The results evoke the question whether the decrease in viable counts is due to cell death, sublethal injury or a rapid conversion to a VBNC state. Since our experimental setup cannot discriminate between sublethally injured and VBNC cells, all cells with a non-permeable membrane (as per flow cytometric analysis) that do not form CFUs are

regarded as VBNC cells. In case of an initial killing of cells, the surviving 0.01% of cells could utilize the scarce assimilable organic carbon (AOC) in the drinking water and the contents of permeabilized cells to mount a defense against the toxic effects of Cu, after which regrowth could be possible. In the second case, VBNC cells could use AOC, as well as intracellular stored nutrient reserves such as polyhydroxybutyrate, to repair cellular damage and activate Cu resistance mechanisms, after which a gradual resuscitation to a culturable state is achieved without any change in cell number due to regrowth. It is conceivable that both scenarios occur in parallel.

In addition to viable count data, cell viability was assessed via SYBR Green + PI staining and flow cytometry. SYBR Green was used to stain all cells as it can enter cells independent of their physiological state. The total number of all events per ml did not significantly vary between conditions and over time (Figure 2-3a), indicating that no considerable cell disintegration or sedimentation occurred and that VBNC cells could be detected by the flow cytometry approach. Over the course of several days, recorded events in the Cu condition showed a decrease in their SYBR signal strength, while the PI signal became stronger (Figure 2-2b, Figure 2-3b and c, and Figure 2-4). Thus, as visualized in FL3 vs. FL1 plots (Figure 2-4), events migrated from the original zone of non-permeable cells to a zone that contained permeable (likely non-viable) cells, which coincided with the positive control of heat-killed cells. The latter represented the gradual decay of the cell envelope, allowing more PI to enter the cells. As a result, the number of events corresponding to non-permeable cells decreased with 2 $\log_{10}$ after 48 h after which they remained fairly stable around 5×10^6 events per ml (Figure 2) and this trend was inversely proportional to the number of events corresponding to permeable cells. Finally, VBNC cells accounted for the majority of the viable cells after 24 to 48 h (roughly 99.9 and 99 %, respectively) and gradually decrease to roughly 75 % at 144 h.

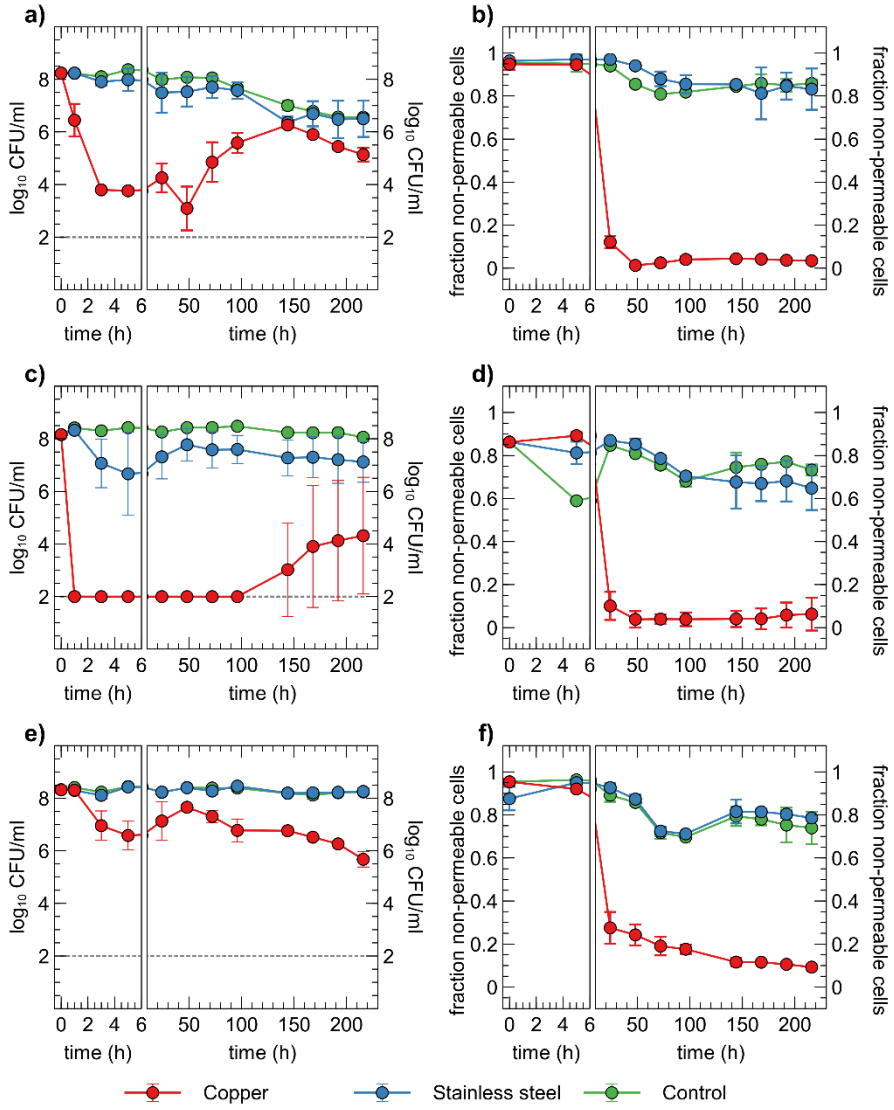

Figure 2-2. Viable counts (a, c and e) and fraction of non-permeable cells (b, d and f) of *C. metallidurans* CH34 (a and b), *C. metallidurans* AE104, lacking metal resistance mechanisms (c and d) and *C. metallidurans* CH34 pre-induced with 300 µM CuSO4 (e and f) in the presence of metallic Cu (red), stainless steel (blue) and control condition (green). All experiments were independently performed with n = 3.

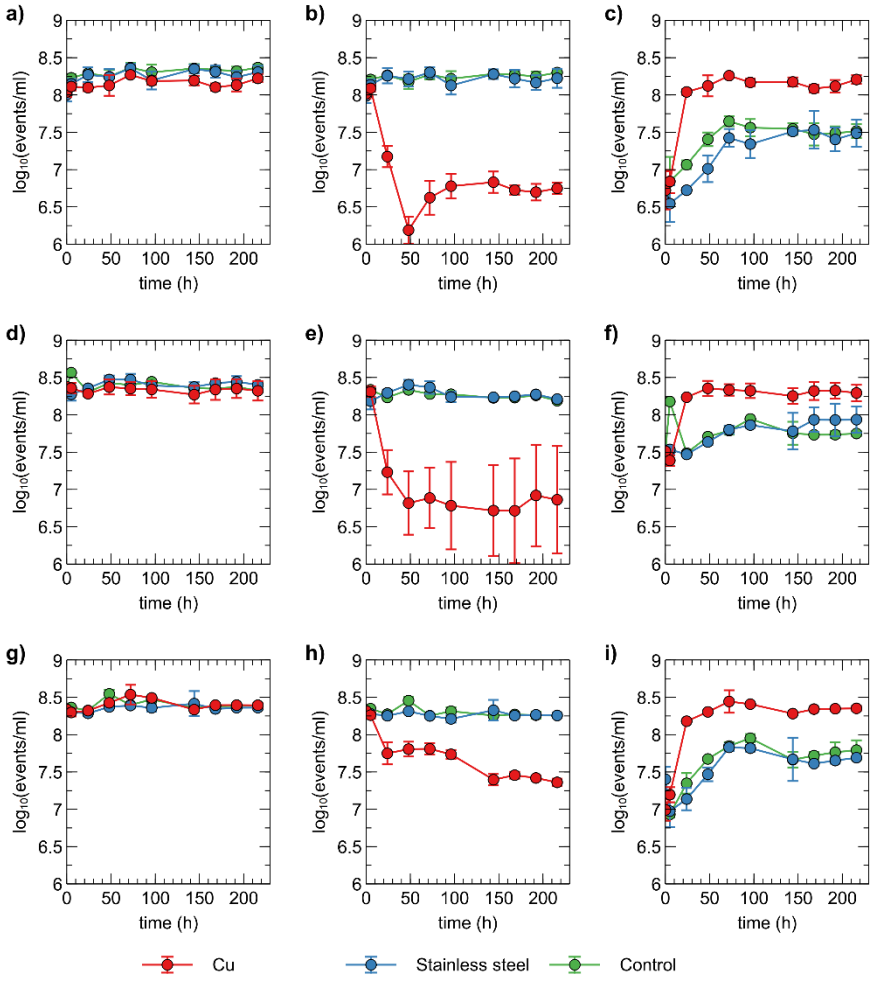

Figure 2-3. Concentration of total events (a, d, g), events corresponding to non-permeable cells (b, e, h) and events corresponding to permeable events (c, f, i) recorded for *C. metallidurans* CH34 (a, b, c), *C. metallidurans* AE104 (d, e, f) and *C. metallidurans* CH34 pre-induced with 300 µM $CuSO_4$ (g, h, i) in the presence of metallic Cu (red), stainless steel (blue) and control condition (green). All experiments were independently performed with n = 3.

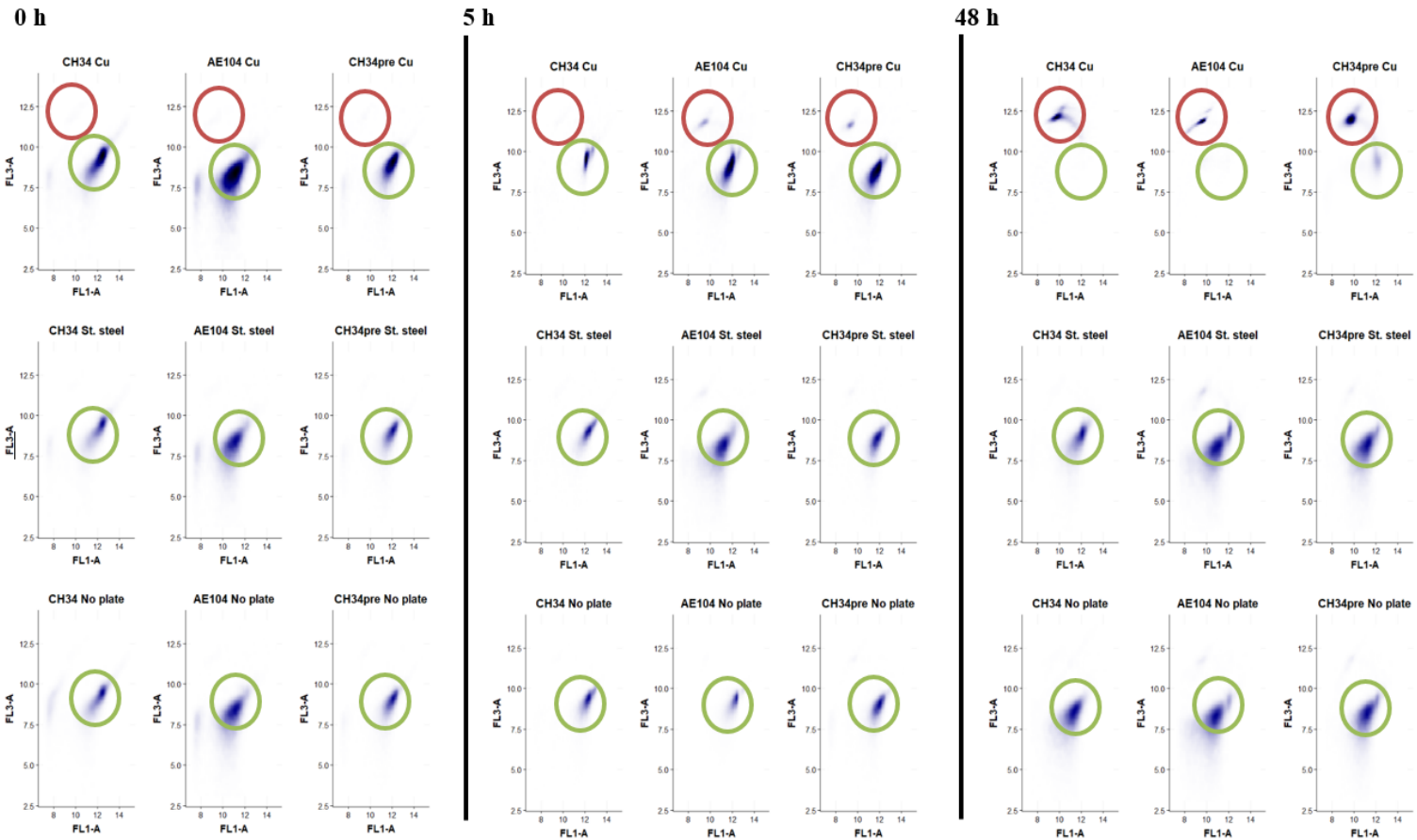
0 h
5 h
48 h
CH34 Cu
AE104 Cu
CH34pre Cu
CH34 St. steel
AE104 St. steel
CH34pre St. steel
CH34 No plate
AE104 No plate
CH34pre No plate
FL1-A
FL3-A

Figure 2-4 (previous page). Flow cytometric profiles (FL3-A ~ FL1-A, representing propidium iodide signal vs. SYBR Green signal) of cells in different conditions on three time points: 0 h (left), 5 h (middle), and 48 h (right). Within each time point: copper condition (top row), stainless steel condition (middle row), no plate control condition (bottom), *C. metallidurans* CH34 (left column), *C. metallidurans* AE104, lacking metal resistance mechanisms (middle column), *C. metallidurans* CH34 pre-induced with 300 µM of $CuSO_4$ (right column). Green and red circles represent events corresponding to non-permeable and permeable cells, respectively.

The discrepancies between the viable and flow cytometry counts merit in-depth discussion. The lag of several hours between the initial decrease in cell culturability and the decrease of events in the non-permeable zone could be due to purely physicochemical processes in which several hours are needed before the cell envelope of killed/injured cells is sufficiently permeable to PI. Alternatively, it could be due to a rapid conversion to a VBNC state in which cells are not permeable to PI since their envelope is still intact. As such, culturable cells cannot be distinguished from VBNC cells by our flow cytometry analysis. Second, no clear increase of events corresponding to non-permeable cells was observed, which indicates that cells were recovering from a metabolic state that could only be measured via culturing, instead of regrowth of the population after an initial killing. Therefore, we hypothesize that within 48 hours, ca. 5% of the initial population is converted to a VBNC cell state, while the remaining 95% of the population is permeabilized and thus killed. Almost 25% of these VBNC cells recover to a culturable state after 144 h. Finally, although PI is an indicator for cell viability and should only stain cells with damaged or permeable membranes [263], several studies have reported contrasting data regarding the use of PI for viability staining, e.g. when applied in the early exponential phase [264]. For instance, ostensibly PI-permeable *Shewanella decolorationis* S12 cells, supposedly in a VBNC state, have been observed to repair membrane damage and lose PI signal strength upon switching of their respiratory metabolism [265]. This complex relation between PI staining and the presence of intermediate cell states has been reported for several other bacterial species [266]. Nonetheless, we opted for a SYBR Green + PI staining procedure as it is routinely used in viability testing. To summarize, we conclude that *C. metallidurans* CH34 is indeed being killed by the presence of the Cu plate, but to a much lesser extent than indicated by the viable count as the Cu plate induces a VBNC cell state in part of the population.

2.3.2 Copper resistance mechanisms provide a defense against metallic copper

We hypothesized that the induction of CRM allowed for either growth or resuscitation of copper-stressed cells. To test this hypothesis, two additional experiments were performed. In the first one, a similar setup was used with strain *C. metallidurans* AE104. This latter is derived from CH34 by curing of its megaplasmids pMOL28 and pMOL30 that encode most functional copies of its metal resistance mechanisms, including the main copper resistance determinants on pMOL30, as detailed in the introduction. Consequently, its minimum inhibitory concentration (MIC) is much lower than that of CH34 for most metal ions (for Cu^{2+}: 600 µM vs. 3000 µM). Immediately apparent was the significant 6-$\log_{10}$ decrease in viable counts after only 1 hour in the Cu condition, which further decreased to the detection limit after 3 hours (Figure 2-2c). It is evident that the lack of metal resistance mechanisms on pMOL30 resulted in a much greater sensitivity to the Cu stress. However, viable counts increased again after 144 hours. This increase appeared at different levels and only in two out of the three replicates (Figure 2-5).

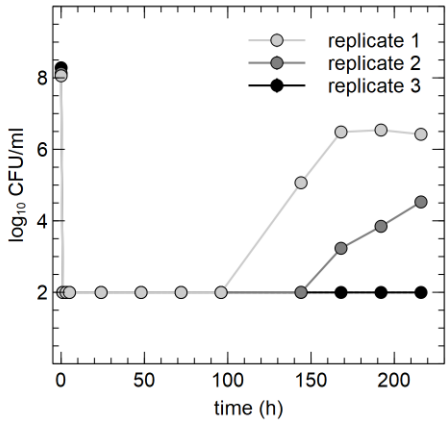

Figure 2-5. Viable counts of *C. metallidurans* AE104, lacking metal resistance mechanisms, incubated in drinking water containing a copper metal plate.

It is possible that mutations or genomic rearrangements occurred in these replicates that relieved the Cu stress, as this has previously been shown for zinc stress [267], but this was not further examined by retesting or genome sequencing. In the presence of stainless steel, there is a small but non-significant decrease in viable

counts. However, this decrease is far less drastic than that seen in the Cu condition. In the no-plate control condition, only a small decrease in viable counts was observed over the course of the experiment, which could again be ascribed to starvation and a slow conversion to the VBNC state. We did observe significant differences between the control conditions of the survival experiments with CH34 and AE104, starting after 96 hours. Nevertheless, it is clear by the differences in viable counts of CH34 in the control of the Cu plate and ions experiments (see 2.3.5, $p < 0.05$ after 168 hours), which could be seen as biological replicates, that variation not related to the tested conditions is observed (Figure 2-2a and Figure 2-8). Flow cytometry showed a significant decrease in the non-permeable cell fraction only in the presence of Cu from 24 hours onwards (Figure 2-2d). These results were comparable with those from strain CH34 (Figure 2-2c and d).

In a second experiment, the *C. metallidurans* CH34 cells were pre-induced with a non-lethal concentration of Cu^{2+} (300 µM). This concentration was previously shown to induce the cellular production of Cu resistance mechanisms [129]. Viable counts showed an initial small decrease after 5 hours in the Cu condition (Figure 2-2e). Interestingly, viable counts recovered completely after 48 hours. It is clear that the initial stress imposed by the Cu plate on the pre-induced cell population elicited a smaller effect than that on the non-induced population. The decrease in viable counts for the pre-induced cells could putatively be ascribed to a difference in the Cu concentration experienced by the bacterial cells, combined with the difference in medium, from MM284 to mineral water, and the decrease in cell density, from 10^9 CFU/ml to 10^8 CFU/ml. While the Cu ion is predominantly present in its cupric form in both MM284 and mineral water [268], the concentrations of most anionic ligands are decreased in the latter, which could lead to a difference in the Cu-ligand species apparent to the bacterial cells. Though the initial viable counts were never reached again, the pre-induced *C. metallidurans* CH34 cells were better equipped to deal with the presence of the Cu plate. Interestingly, after 48 hours the viable counts decreased again, reaching a number similar to the non-induced *C. metallidurans* CH34 cells at the end of the experiment. We hypothesize that the metabolic burden posed by the constant necessity for functional Cu resistance mechanisms could not be sustained on longer terms by either stored energy reserves or the limited AOC present in the medium. In the stainless steel condition and control condition, no noticeable decrease was observed (Figure 2-2e). Flow cytometry data corresponded well with viable counts and the number of events in the non-permeable zone in the

Cu condition was consistently and significantly higher than in either non-induced *C. metallidurans* CH34 or AE104 (Figure 2-3 (b, e, h); $p < 0.05$ for all samples between 48 h and 96 h).

2.3.3 Biofilm formation on metallic Cu and stainless steel

At the end of the experiment (216 hours after start), biofilms were visualized using fluorescence microscopy. Extensive biofilms were formed by all strains on stainless steel plates (Figure 2-6). In contrast, in none of the experiments with either non-induced *C. metallidurans* CH34, AE104, or pre-induced *C. metallidurans* CH34 cells, biofilms could be detected on the Cu plates. Some single cells were found on the surface of some plates, but these could be artefacts of an insufficient rinsing procedure. This result again showed the high toxicity of metallic Cu, even to the highly metal-resistant *C. metallidurans*. Since the toxicity of metallic copper also relies on the release of copper ions from the surface [243], it is plausible that the CRM of CH34 play a role in survival both in the bulk liquid phase and in close proximity to the metal surface. Our results do not refute the capacity of CH34 to form biofilms on the copper surface after longer incubation times and continued activation of its CRM. Biofilm formation on copper pipes after long incubation times has already been observed, even for less metal-resistant bacterial species [269-272].

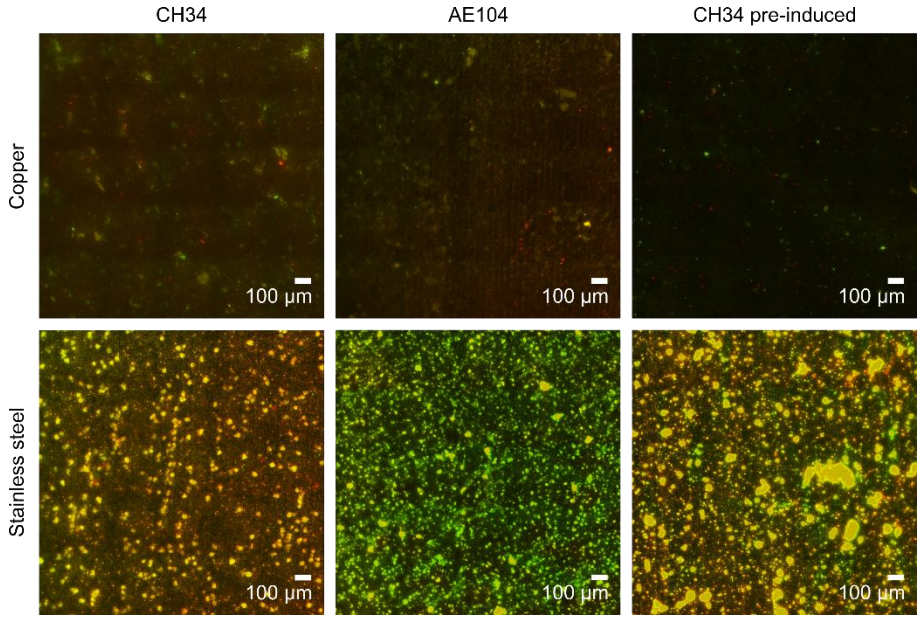

Figure 2-6. Biofilm formation of *C. metallidurans* CH34 (left column), *C. metallidurans* AE104, lacking metal resistance mechanisms (middle column), and *C. metallidurans* CH34 pre-induced with 300 µM $CuSO_4$ (right column) on copper (top row) and stainless steel (bottom row). Cells were stained with SYBR Green and propidium iodide, and visualized by fluorescence microscopy.

2.3.4 Cu concentrations in the liquid phase

Copper concentrations were measured in the liquid phase by ICP-MS at several time points. In the copper condition with CH34, pre-induced CH34 and AE104 the copper concentration gradually increased, reaching ca. 400 µg/l (6.3 µM) at the end of the experiment (Figure 2-7). The observed Cu concentrations were below the solubility of 1300 µg/l in mineral water at comparable pH [268] and far below the MIC of 3 mM in MM284 [115]. However, values were comparable to those applied in the previously mentioned studies, i.e. 1.6 µM, where a similar rapid decrease in viable counts was observed. Therefore, we hypothesize that in our experiments the toxic effects of Cu in the liquid phase play an important role, next to the possible contribution of contact killing, in the observed decrease in viable counts. We propose that there could be a net transport of Cu ions from the metal plate surface to the bacterial cells and that there is likely a high level of Cu sequestration by the cells, even considering the relatively low Cu concentrations in the liquid phase, because of the homogenization of concentration boundary layers by continuously shaking and a favorable association between Cu ions and bacterial cells [249]. This cellular Cu sequestration may result in considerable stress for the bacteria. The Cu concentration in the abiotic control condition (i.e. without the addition of bacterial cells) is on average lower than in the three biotic conditions, although this difference is not statistically significant. Therefore, the perceptible enhanced release of Cu ions from the copper plate by bacterial interactions is not statistically justified. It has been previously shown that the presence of bacteria does not result in a higher rate of Cu ion dissolution from metal surfaces [46]. In the stainless steel and no plate conditions, very little Cu was present in the medium, approaching the detection limit of the measuring device (2 µg/l – 0.03 µM). The presence of Cr and Ni, the main non-iron constituents in stainless steel, was not detected in any of the stainless steel samples.

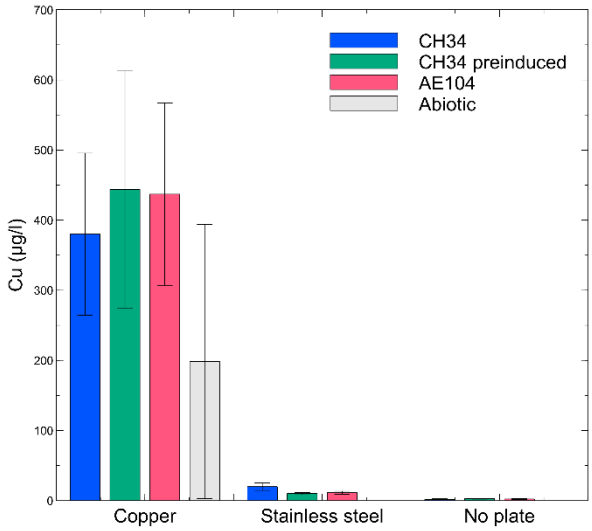

Figure 2-7. Liquid phase Cu concentrations for *C. metallidurans* CH34 (blue), *C. metallidurans* AE104, lacking metal resistance mechanisms (red), *C. metallidurans* CH34 pre-induced with 300 µM CuSO4 (green), and an abiotic control (gray) incubated for 9 days in the presence of Cu, stainless steel or no metal (control).

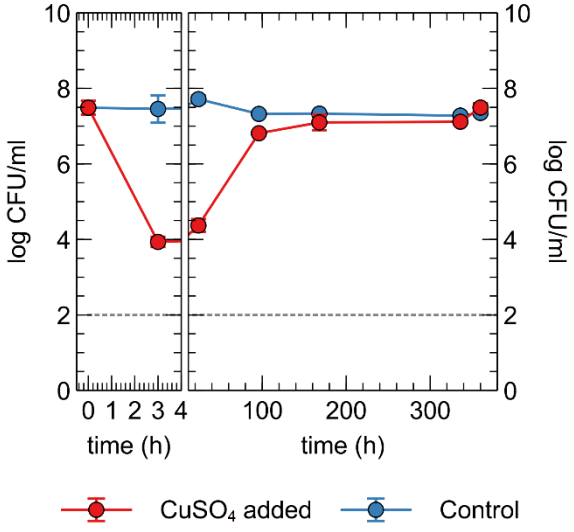

Figure 2-8. Viable counts of *C. metallidurans* CH34 in drinking water supplied with or without 10 µM $CuSO_4$.

2.3.5 Effect of Cu ions on viable counts

Next, we tested whether the observed decrease in viable counts in the Cu plate condition was due to a toxic effect of Cu ions in the liquid phase or close association with the Cu plate surface itself, via so-called 'contact killing'. A CH34 suspension was prepared similarly to the first metal plate experiment, without pre-induction of Cu resistance mechanisms. Copper sulfate was added to the drinking water, to a final concentration of 10 µM (in range with the concentration observed in the liquid phase of the Cu plate experiments). Viable counts were measured at several time points for 15 days (Figure 2-8). Immediately apparent was the approximate 3-log decrease in viable counts after 3 hours in the Cu condition, which could not be seen in the control condition. By 96 hours, viable counts in the Cu condition were almost completely restored to control levels. While a similar rapid decrease in viable counts after the addition of Cu ions is seen in many bacterial species, the subsequent recovery or regrowth without addition of a chelating agent is not [33, 203, 204]. When comparing this data to the Cu plate experiment data, it seems that the induction of Cu resistance mechanisms plays an important role in this setup as well, allowing for a full return to control condition levels. In contrast, the gradual decrease in viable counts observed in the Cu plate experiment after 144 hours was not seen here, indicating a toxic effect either via contact killing or the gradual release of Cu ions from the metal plate as the closed system strives towards a chemical equilibrium.

2.3.6 Influence of medium composition on the induction of Cu resistance mechanisms

As demonstrated above, the presence of Cu resistance mechanisms plays a prominent role in the survival of bacterial cells when in wet contact with metallic Cu. However, despite the induction of these resistance mechanisms, cells are still being killed or inactivated as shown by the viable counts and flow cytometry. Therefore, we hypothesize that this induction is hampered by the low amount of nutrients and energy sources available.

To test this hypothesis the Cu biosensor strain *C. campinensis* AE1239, which is closely related to *C. metallidurans* CH34, was used. It emits a bioluminescent signal upon induction of Cu resistance genes. In a first experiment, we measured the bioluminescence of an AE1239 suspension on Cu and stainless steel plates. Since Cu ions dissolved rapidly and massively when the Cu plates were placed in MM284

growth medium, this could not be used as a positive control. Therefore, the setup was first optimized on a stainless steel plate using a cell suspension in MM284 with $CuSO_4$ added to a final concentration of 100 µM. This clearly yielded an induction with a maximal intensity reached around 220 minutes after the start of the induction. Without $CuSO_4$, no induction was measured. When washed *C. campinensis* AE1239 cells were resuspended in sterile mineral water and pipetted onto a stainless steel plate, no induction was measured with $CuSO_4$ concentrations of 0, 10, or 100 µM. When a cell suspension in sterile mineral water was pipetted onto a Cu plate surface, again no induction was measured within the 4 hours of measurement time.

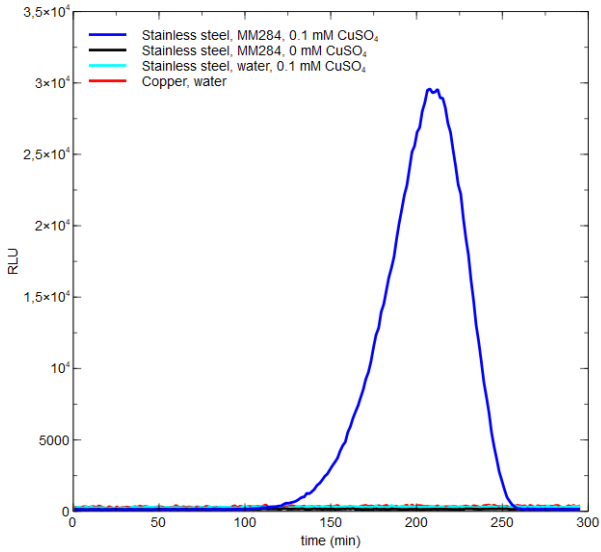

Figure 2-9. Bioavailable Cu^{2+} concentration, measured by biosensor *C. campinensis* AE1239, in MM284 medium containing a stainless steel plate (black) supplemented with 0.1 mM $CuSO_4$ (blue), in water containing a stainless steel plate and 0.1 mM CuSO4, and in water containing a copper plate. The bioluminence output of the reporter was recorded for 300 min and shown as relative light units (RLU).

In a second setup we tested the effect of different $CuSO_4$ concentrations on the induction of Cu resistance mechanisms in MM284 and sterile mineral water supplemented with varying levels of gluconate and Na_2HPO_4 (Figure 2-10). A clear response to the Cu stress was visible in MM284 with 10 and 100 µM $CuSO_4$, with a maximum induction at 150 minutes after Cu addition. Interestingly, irrespective of the addition of $CuSO_4$, gluconate or Na_2HPO_4, no induction was observed in mineral

water. It seems that additional nutrients are necessary to generate a measurable response to Cu stress, other than a source of cellular energy.

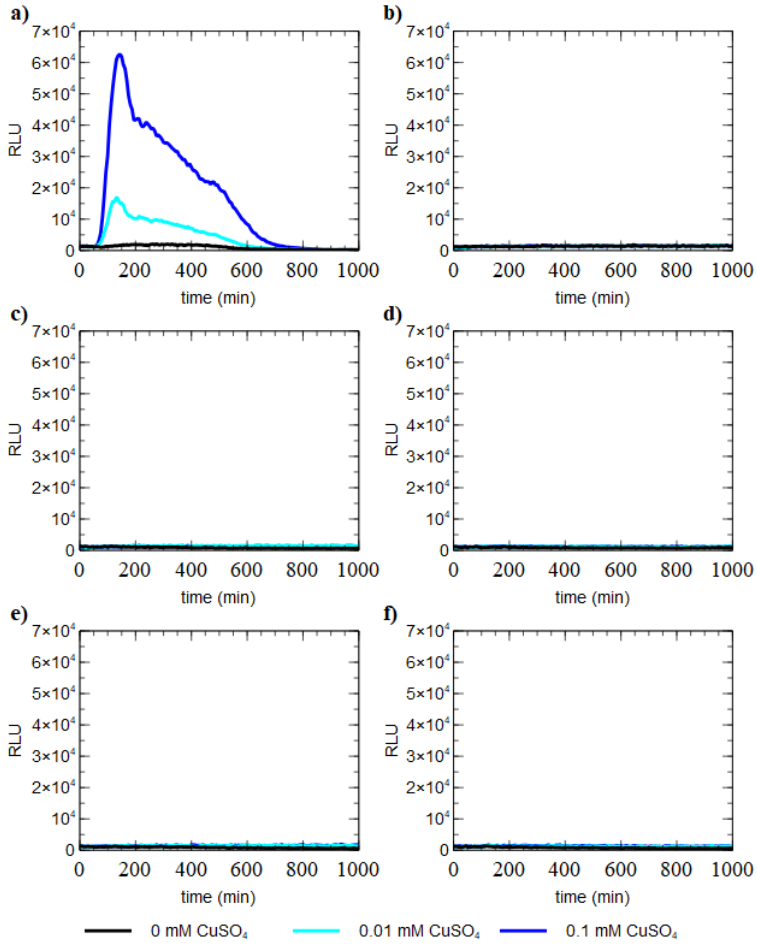

Figure 2-10. Bioavailable Cu^{2+} concentration, measured by biosensor *C. campinensis* AE1239 in liquid media in 6 conditions: MM284 (a) filter sterilized drinking water (b) drinking water supplemented with 0.2 g/l Na-gluconate added (c) drinking water supplemented with 0.2 g/l Na_gluconate and 40 mg/l Na_2HPO_4 added (d) drinking water supplemented with 2 g/l Na-gluconate (e) drinking water supplemented with 2 g/l Na-gluconate and 40 mg/l Na_2HPO_4 (f). The bioluminence output of the reporter was recorded for 1000 min and shown as relative light units (RLU) normalized by cell density (OD_{600}).

2.4 Conclusions

We evaluated the inactivation kinetics of *C. metallidurans* CH34 in contact with metallic Cu in drinking water. While a rapid decrease in viable counts was observed within several hours, this is likely the result of a conversion to an injured or VBNC state. After several days, viable counts returned to the control level, an observation that has not been made in other bacterial species. This is likely due to a slow induction of Cu resistance mechanisms, as shown by the lack of recovery/regrowth of the AE104 strain (cured from most Cu resistance determinants) and the rapid recovery/regrowth of a CH34 culture with pre-induced resistance mechanisms. Based on similar inactivation kinetics in a setup supplemented with ionic Cu, we surmise that the toxic effect of Cu ions in the liquid phase plays a more important role than so-called 'contact killing'. These results warrant caution in interpreting the growing body of evidence highlighting the antimicrobial properties of metallic Cu, especially in the context of drinking water production and storage [35]. Since the induction of Cu resistance provides a clear advantage in surviving on or near metallic Cu, it raises the question to what extent resistance determinants can be transferred to or protect other bacterial species. In addition, co-selection between metal resistance and antibiotic resistance has often been reported [273-276]. One way to amplify the killing efficiency of Cu metal could be to limit the extant AOC levels, that the bacteria need to synthesize and energize those resistance determinants. A final question that needs further research, here as well as in many similar publications [reviewed in 191], is in what ways the resuscitation of sublethally injured and VBNC cells is distinct from the regrowth of a small fraction of survivor cells.

Metal resistant bacterial strains, many among the genus *Cupriavidus*, have been isolated from water sources on many occasions [277-279]. During space missions, where the antimicrobial properties of metallic Cu are being evaluated to allow long-term inactivation of persistent microbial contamination, *Cupriavidus metallidurans* strains have been isolated from drinking water in several sampling campaigns [226-228]. This study has focused on the efficiency of Cu antimicrobials in wet conditions, more specifically in drinking water. However, the chemical composition of the liquid phase has an impact on metallic Cu toxicity [243]. Additional research is needed to accommodate this factor, and in the framework of the ESA BIOFILMS project the additional variable of microgravity. In the following chapter, we will aim our attention at the regulation of Cu exposure in CH34, on a transcriptomic level.

CHAPTER 3 The transcriptomic landscape of *Cupriavidus metallidurans* CH34 acutely exposed to copper*

3.1 Introduction

Environmental pollution with toxic metals due to anthropogenic activities is an internationally growing concern [280-282]. The exposure and the risk of elevated concentrations of these pollutants in the environment can lead to bioaccumulation and harmful effects [283-285], which are facilitated by the high toxicity and recalcitrance of some metals [275, 286]. Consequently, monitoring tools for metal accumulation in natural environments such as soils and water bodies are needed. Physicochemical analysis techniques, while accurate and sensitive, often fail to chart the bioavailability and the toxicity of the polluting components [287-289]. At the same time, microorganisms show great promise as biosensors to quantify the bioavailable fraction of heavy metals such as copper [290], an essential trace element that is highly toxic when overly abundant [128]. In addition, microorganisms can be used to combat environmental contamination with heavy metals in a process called bioremediation [282, 286, 291, 292]. Bioremediation has been the focus of extensive research in recent years as a clean and efficient alternative to conventional strategies (reviewed in Tabak et al., 2005 [293] and Akcil et al., 2015 [294]).

Cupriavidus metallidurans strains are exemplary β-proteobacteria in metal-contaminated industrial environments [91]. Type strain CH34 was first isolated from a decantation basin in a zinc factory near Engis, Belgium, in 1976 [93, 128]. It was quickly shown to encode resistance mechanisms to a wide range of metals [92] and has become a model organism to study heavy metal resistance (HMR) in bacteria

* This chapter is based on the following publication: Maertens, L., Leys, N., Matroule, J.Y., and Van Houdt, R. (2020). The Transcriptomic Landscape of *Cupriavidus metallidurans* CH34 Acutely Exposed to Copper. Genes 11: 9.

[91]. Copper resistance in strain CH34 is mediated by multiple cooperating Cu detoxification systems; *copF* and *copA₁B₁C₁D₁* encode a Cu efflux P-type ATPase and a periplasmic detoxification system, respectively, and are part of the extensive 21-gene *cop* cluster. The neighboring *silDCB*A cluster encodes a heavy metal efflux-resistance nodulation division (HME-RND) driven system. These gene clusters are encoded on the pMOL30 megaplasmid, and homologous systems can be found on its chromosome and chromid (Table 1-1). In addition, many more accessory genes may play a role in Cu resistance. The integration of these systems brings about a minimum inhibitory concentration of 3 mM Cu^{2+}, three times higher than that of *E. coli* K38 [115, 295]. A detailed description of Cu resistance in strain CH34 can be found in Chapter 1 and Mergeay and Van Houdt [91].

In a previous study, biosensors for metals such as Pb^{2+}, Zn^{2+}, and Cu^{2+} have been developed based on *Cupriavidus* strains [260, 296]. These biosensors function via a transcriptional fusion of metal-specific promoter regions to a *luxCDABE* luciferase gene cluster, which allows for the emission of a measurable bioluminescent signal upon translation (BIOMET® system). The strength of this signal is proportional to the biologically available fraction of a specific metal. *Cupriavidus*-based biosensors have been used for the characterization of bioavailable metal fractions in soil, sediments, mineral wastes, etc. [297-299]. In addition, the bioremediation potential of CH34, owing to its capacity for metal solubilization and biocrystallization, has been demonstrated in several experimental setups [296, 300]. For instance, the deposition of $ZnCO_3$ and $CdCO_3$ crystals around the cell surface, both biologically catalyzed and via abiotic processes, can lead to efficient depletion of these toxic metal ions from the environment. *Cupriavidus* strains are especially interesting in the case of mixed pollution with metals and recalcitrant organic compounds, since they are often able to degrade a broad array of aromatic compounds [94, 301]. However, the construction of bacterial strains able to efficiently cope with mixed pollutions remains challenging [302].

In order to understand, optimize, and control the molecular processes underlying the above mentioned applications, it is vital to understand their regulation. Indeed, an elaborate network of sigma factors [126, 303] and transcriptional regulators [54, 304] has been found to play an important role in CH34. However, new paradigms in bacterial gene regulation highlight the role of small regulatory RNAs (sRNAs), acting at a (post-)transcriptional level in disparate stress responses [177, 305, 306]. For instance, sRNAs are involved in a plethora of biological processes, including virulence

[186, 307-313], antibiotic resistance [314-317] and mobile genetic elements [318] as well as oxidative and metal stress [178-181, 183, 319, 320] and the degradation of organic compounds [321].

Thus, in order to fully understand the intricate response of *C. metallidurans* CH34 to Cu stress, a highly detailed map of its transcriptome is a basic necessity. Although its genome is fully sequenced and annotated [94], and transcriptome data in response to metal stress are available [115, 126], these data do not allow analyzing pertinent features such as transcription start sites (TSSs), 5' untranslated regions (5' UTRs), RNA processing sites (PSSs) and regulatory RNAs. Therefore, we used a tagRNA-sequencing (tagRNA-seq) approach, a modified RNA-seq method that is based on the differential labeling of 5' RNA ends and that enables whole transcriptome sequencing with the discrimination of primary from processed 5' RNA ends [322, 323]. The ability of tagRNA-seq to annotate TSSs has been well established in recent years, and is commonly exploited in research on regulatory features of the bacterial transcriptome.

3.2 Materials and methods

3.2.1 Bacterial strains, media, and culture conditions

C. metallidurans CH34 [93] was routinely grown in Tris-buffered mineral medium (MM284) [92] supplemented with 2 g/L gluconate on an orbital shaker at 180 rpm in the dark at 30 °C. MM284 agar plates were prepared by adding 2% agar (Thermo Scientific, Oxoid, Hampshire, UK) to the liquid medium.

3.2.2 RNA extraction

Bacterial cultures were prepared in triplicate by inoculating pre-warmed MM284 medium with several *C. metallidurans* CH34 colonies and growing the cells at 30 °C on an orbital shaker at 120 rpm. After 48 h, cultures were diluted with pre-warmed MM284 medium to an OD_{600} of 0.1 and grown to an OD_{600} of 0.4. At this point, either $CuSO_4$ was added to a final concentration of 400 µM (copper condition) or a corresponding volume of H_2O (control) was added. After 10 minutes of exposure, cultures were put on ice and washed twice with a chilled 10 mM $MgSO_4$ solution at 4 °C. After washing, bacterial pellets were flash frozen and stored at -80 °C until RNA extraction. RNA extraction was performed with the *mir*Vana™ miRNA Isolation kit (Invitrogen™, Carlsbad, California, USA). Lysis was performed by resuspending the bacterial pellet in 50 µL of a 3 mg/ml lysozyme solution (Sigma Aldrich, Saint Louis,

Missouri, USA) and incubating it at room temperature for 15 minutes. After lysis, a volume of 500 µL Lysis/Binding buffer was added. The protocol for total RNA extraction was followed without enrichment for small RNAs. Total RNA quality was measured by Agilent 2100 Bioanalyzer using Nano chips. Only samples with a RIN value above 9 were accepted for sequencing.

3.2.3 tagRNA-sequencing protocol

A tagRNA-seq protocol [324-326] was performed by Vertis Biotechnologie AG (Freising, Germany) (Figure 3-1). The complementary DNA (cDNA) libraries were constructed in the following manner: the 5' Illumina TruSeq sequencing adapter with a CTGAAGCT tag was ligated to the 5' monophosphate groups of rRNA-depleted RNA samples. Subsequently, samples were treated with Terminator Exonuclease (TEX, Lucigen, Middleton, Wisconsin, USA) to remove RNAs with non-ligated 5' monophosphate ends. Then, RNA 5'-polyphosphatase (5'PP, Lucigen) was used to convert 5' triphosphate groups into 5' monophosphate groups, and the 5' Illumina TruSeq sequencing adapter with TAATGCGC was ligated to the newly formed 5' monophosphate groups. RNA samples were then fragmented, and a 3' sequencing adapter was ligated to the RNA fragments' 3' ends. First-strand cDNA synthesis was performed using M-MLV reverse transcriptase and the 3' adapter as primer. The resulting cDNA was purified, ligated with a 5' sequencing adapter, and PCR amplified using a proofreading enzyme. The cDNA was then purified using the Agencourt AMPure XP kit (Beckman Coulter Genomics, Chaska, Minnesota, USA) and analyzed by capillary electrophoresis. The size fraction of 160–500 bp was eluted and sequenced on an Illumina NextSeq 500 system using 75 bp read length. The different sequencing adapters in combination with RNA fragmentation resulted in three read libraries for each sample: reads originating from the 5' end of 5'-monophosphate (5'-P) RNA molecules (processed start sites, PSS reads), reads originating from the 5' end of 5'-triphosphate (5'-PPP) RNA molecules (transcription start sites, TSS reads), and reads originating from non-tagged RNA fragments enabling coverage over the entire transcript. For each sample, ca. 20 million reads were generated. Adapter sequences were trimmed from all read libraries using Trimmomatic version 0.36 [327], and raw read quality was assessed using FastQC version 0.10.0 (https://www.bioinformatics.babraham.ac.uk/projects/fastqc/). Reads were aligned to the *C. metallidurans* CH34 reference genome (National Center for Biotechnology Information (NCBI) accession numbers NC_007971.1, NC_007972.1, NC_007973.1, and NC_007974.1) with bowtie2 [328] using default parameters. Within each

biological replicate and condition, coverage values were similar over all four replicons. The RNA-seq datasets generated and analyzed for this study are available from the NCBI Sequence Read Archive (SRA) under accession number PRJNA639913.

3.2.4 Differential gene expression calculation and functional enrichment analysis

Differential gene expression was calculated by merging PSS, TSS, and unassigned libraries of each sample using samtools merge [329]. Coverage of annotated genes of the resulting bam files was performed with the featureCounts function of the Rsubread package [330] for R version 3.6.1. Options –isStrandSpecific and –fraction were set to TRUE, and option –countMultiMappingReads was set to FALSE. Differential gene expression of the resulting count matrix was accomplished using edgeR [331, 332] and limma [333], using a Benjamini–Hochberg [334] approach to control for Type 1 statistical errors. Functional enrichment analysis was performed using the eggNOG [335] classification of annotated genes, as found on the MaGe platform [336], and the MLP package for R, version 1.34.0, was used for *p*-value calculation.

3.2.5 Transcriptional start site profiling

TSSs were detected using an in-house Python script (Python version 2.7, TSS_res_finder.py in Supplementary data*) [116]. The 5' most base of all reads in the TSS read library was selected using bedtools (version 2.19.1) [337], and subsequent analyses were performed on the single base position to which the read was reduced. Reads of triplicate TSS libraries from the same condition were combined into a single library for further analysis. The PSS and the unassigned libraries were not used for TSS profiling. Coverage values of a sliding window with an arbitrary width of 5 nt were calculated for all nucleotide positions. If the coverage value of a sliding window exceeded 50 reads relative to a read library size of two million reads, the coverage-weighted average TSS position within this sliding window was calculated.

*Supplementary data can be found at the following url: https://www.mdpi.com/2073-4425/11/9/1049.

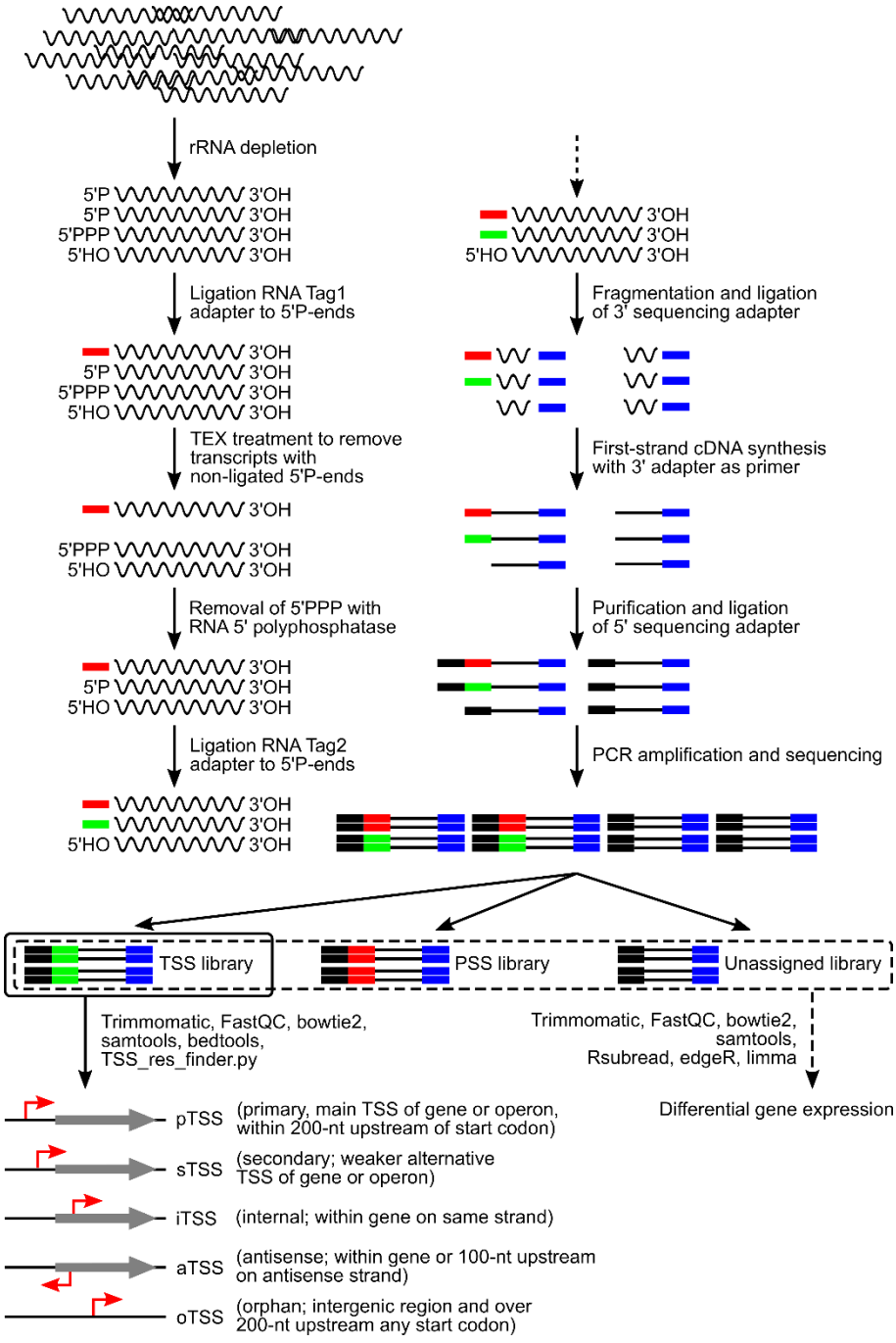

Figure 3-1. General overview of the tagRNA-seq workflow and analysis.

Table 3-1. Primers used for 5'and 3' RACE experiments.

Primer	Sequence	TSS position	Replicon	Genomic context
copA_5'RACE_GSP1	GATTACGCCAAGCTTGCCAAACCTTGTACGAAACGGCG	191243	pMOL30	pTSS of Rmet_6112
copA_5'RACE_NGSP1	GATTACGCCAAGCTTTGGCAGGTTGGGCAGCAAG	191243	pMOL30	pTSS of Rmet_6112
pasRNA1_5'RACE_GSP1	GATTACGCCAAGCTTCAGCGACAAAAATGGATGCGGGT	2045559	CHR2	aTSS of Rmet_5332
pasRNA1_5'RACE_NGSP1	GATTACGCCAAGCTTCTGCTTAACCTTGTGTTGGATATCGAC	2045559	CHR2	aTSS of Rmet_5332
pasRNA2_5'RACE_GSP1	GATTACGCCAAGCTTCTTCTGAGCAGTCCTGGAAAGCCTACG	1951037	CHR2	aTSS of Rmet_5250 5'UTR
pasRNA2_5'RACE_NGSP1	GATTACGCCAAGCTTGAAAGCCTACGAGCACCCCG	1951037	CHR2	aTSS of Rmet_5250 5'UTR
pasRNA3_5'RACE_GSP1	GATTACGCCAAGCTTACCTTCAACCTGCACCTGAACACCGA	2102508	CHR2	aTSS of Rmet_5375
pasRNA3_5'RACE_NGSP1	GATTACGCCAAGCTTCCGAGGCGGTGGCGTCA	2102508	CHR2	aTSS of Rmet_5375
pasRNA4_5'RACE_GSP1	GATTACGCCAAGCTTGGCTGTGGGCCGAGCTCAATTTC	168587	pMOL30	aTSS of Rmet_6135
pasRNA4_5'RACE_NGSP1	GATTACGCCAAGCTTCAATTTCCTGATGCCGCTTGCGA	168587	pMOL30	aTSS of Rmet_6135
pasRNA5_5'RACE_GSP1	GATTACGCCAAGCTTGAAGTAAGACTCCCACTCCTCCCAAGC	73395	pMOL30	aTSS of Rmet_6376
pasRNA5_5'RACE_NGSP1	GATTACGCCAAGCTTGCCACGTGCAGCGCGAA	73395	pMOL30	aTSS of Rmet_6376
pasRNA6_5'RACE_GSP1	GATTACGCCAAGCTTATGTCGGCTTCGTATGCTTTGGAAATG	84813	pMOL30	aTSS of 3' end of Rmet_5977
pasRNA6_5'RACE_NGSP1	GATTACGCCAAGCTTCGGGCGTGCCTGCGTC	84813	pMOL30	aTSS of 3' end of Rmet_5977
3492_o_5'_RACE_GSP1	GATTACGCCAAGCTTCGGGTTCGGTCCAGGCTACTCTTACA	3784021	CHR1	oTSSs 5' of Rmet_3492
3492_o_5'_RACE_NGSP1	GATTACGCCAAGCTTCGCATCGGAGTGTTCTCTCCGCAACT	3784021	CHR1	oTSSs 5' of Rmet_3492
3492_o_3'_RACE_GSP1	GATTACGCCAAGCTTCCCCGCCGCTAAAGCATTGAAAA	3784021	CHR1	oTSSs 5' of Rmet_3492

Table 3-1. Primers used for 5'and 3' RACE experiments.

Primer	Sequence	TSS position	Replicon	Genomic context
3492_o_3'_RACE_NGSP1	GATTACGCCAAGCTTGCGCTGAAGAAAGCCCCTCAGGTA	3784021	CHR1	oTSSs 5' of Rmet_3492
3492_o_3'_RACE_GSP2	GATTACGCCAAGCTTGGACCAACCCAGCAGACGTTGCA	3784104	CHR1	oTSSs 5' of Rmet_3492
3492_o_3'_RACE_NGSP2	GATTACGCCAAGCTTCAGGTTGATCCGGAAAACCAGGAAGAC	3784104	CHR1	oTSSs 5' of Rmet_3492
3493_o_5'_RACE_GSP1	GATTACGCCAAGCTTGTAGCCTGGACCGAACCCGTTCCTT	3784309	CHR1	oTSSs 5' of Rmet_3492
3493_o_5'_RACE_NGSP1	GATTACGCCAAGCTTTCGAATTGACCCCTCGAAGGGATTTT	3784309	CHR1	oTSSs 5' of Rmet_3492
3493_o_3'_RACE_GSP1	GATTACGCCAAGCTTGCGCGGACGGGAAAATCCCTT	3784309	CHR1	oTSSs 5' of Rmet_3492
3493_o_3'_RACE_NGSP1	GATTACGCCAAGCTTGGGTCAATTCGAAGGAACGGGTT	3784309	CHR1	oTSSs 5' of Rmet_3492
copL_as_5'_RACE_GSP1	GATTACGCCAAGCTTCCCGATATTTACGAGAACGCCGACAA	181548	pMOL30	aTSS of Rmet_6120
copL_as_5'_RACE_NGSP1	GATTACGCCAAGCTTACCAGCGTGCGTTCGCAAGGTTGCTTCA	181548	pMOL30	aTSS of Rmet_6120
copL_as_3'_RACE_GSP1	GATTACGCCAAGCTTCTTTGATCCCCACGCCGCTCAGT	181548	pMOL30	aTSS of Rmet_6120
copL_as_3'_RACE_NGSP1	GATTACGCCAAGCTTGGATCGCGGTGAGCATCTCTGCTT	181548	pMOL30	aTSS of Rmet_6120
3616_o_5'_RACE_GSP1	GATTACGCCAAGCTTCTGCCAGGCAACGTTGCCGACCTAGTA	147562	CHR2	oTSS 5' of Rmet_5941
3616_o_5'_RACE_NGSP1	GATTACGCCAAGCTTGGGCAGGGTGATGACGAAGGGGAAGAAT	147562	CHR2	oTSS 5' of Rmet_5941
3616_o_3'_RACE_GSP1	GATTACGCCAAGCTTCACGCCCGAGTCAGCAAATGGGTT	147562	CHR2	oTSS 5' of Rmet_5941
3616_o_3'_RACE_NGSP1	GATTACGCCAAGCTTGACACTTCCCGTGTCCGGCCTTT	147562	CHR2	oTSS 5' of Rmet_5941
silB_as_3'_RACE_GSP1	GATTACGCCAAGCTTGCGATTGCGGTCGTTTTCATGGT	168587	pMOL30	aTSS of Rmet_6367
silB_as_3'_RACE_NGSP1	GATTACGCCAAGCTTGGTTGATCCCCTTGCGTGGATG	168587	pMOL30	aTSS of Rmet_6367

3.2.6 5’ and 3’ RACE protocol

The 5’ and the 3’ rapid amplification of cDNA ends (5’/3’ RACE) was performed using the SMARTer® 5’/3’ RACE kit (Takara Bio, Saint-Germain-en-Laye, France) using the standard protocol. Total RNA was obtained as described in the section "RNA extraction”. A list of primers can be found in Table 3-1 (first 14 primers). Random primers were used for 5’-first-strand cDNA synthesis. In a second round of RACE experiments, RNA was poly(A)-tailed for 20 minutes using poly(A)-polymerase (Invitrogen™, Carlsbad, California, USA) before proceeding with 5’ and 3’ RACE protocol. Primer sequences can be found in Table 3-1 (last 20 primers).

3.2.7 Statistics

The functional enrichment of eggNOG classes with disparate TSS classes was calculated using Fischer’s exact test with subsequent Benjamini–Hochberg correction for multiple testing [334]. R version 3.6.1 was used for all statistical analyses. Adjusted *p*-values below 0.05 were considered statistically significant.

3.3 Results and discussion

3.3.1 Differential gene expression analysis

First, the transcriptomic response to acute non-lethal Cu^{2+} exposure was analyzed. This yielded 352 coding sequences (CDSs) that were significantly up- (155) or downregulated (197) in the presence of Cu^{2+}, amounting to 5.15% of the total number of CDSs. Thirty-two and nine of these were located on pMOL30 and pMOL28, respectively. CDSs with false discovery rate (FDR) values lower than 0.05 and logFC values higher than 1 or lower than -1 were considered differentially expressed. In comparison with the previous microarray analysis (403 up and 373 down), the overlap was limited with 40 up- and 25 downregulated CDSs shared between both analyses. However, it is important to acknowledge the difference in dose (100 vs. 400 µM) and exposure time (30 min vs. 10 min), as both factors may have strongly influenced the transcriptomic response measured [22].

The functional relevance of differentially expressed CDSs was explored using functional categories from the eggNOG classification system and the MLP package. Classes P (inorganic transport and metabolism), E (amino acid transport and metabolism), and O (posttranslational modification, protein turnover, and chaperones) were significantly enriched (Table 3-2). In the previous microarray

analysis [115], eggNOG classes P and M (cell wall/membrane/envelope biogenesis) were significantly overrepresented. This observation again underlines the adjustability of the copper-exposed transcriptome as a response to differences in dose and response time. The strong enrichment of class P was mostly because of the upregulation of many HMR systems (Figure 3-2). As mentioned previously, the three main Cu detoxification systems are encoded by the *cop*$_1$ and the *sil* clusters on the pMOL30 plasmid. With respect to the Cu resistance gene clusters (Table 1-1), the whole *cop*$_1$ cluster was upregulated, except *copE* (unknown function) and *copL* (cys-rich cytosolic protein) (Figure 3-2). The neighboring *ubiE* (Rmet_6137) and *ubiE*$_2$ (Rmet_6131) genes, encoding methyltransferases, were also upregulated. Interestingly, no differential expression was observed for the *silDCBA* cluster (Rmet_6133-6136). The latter is mainly induced by Ag^+, but *silA*, *silC* and *silD* have been reported to be induced by Cu^{2+} after 30 minutes of exposure [91]. As indicated above, each of the main Cu detoxification systems has a homologous system on the chromosome or the chromid (Table 1-1). All of them, P-type ATPase (*cupRAC*; Rmet_3523-3525), periplasmic detoxification system (*copD*$_2$*C*$_2$*B*$_2$*A*$_2$*R*$_2$*S*$_2$; Rmet_5668-5672), and HME-RND-driven system (*cusDCBAF*; Rmet_5030-5034), were completely upregulated, with the exception of *cusD*. This observation was surprising, since it has been hypothesized that the *cop*$_2$ cluster on the chromid is involved in a late response to relatively low Cu^{2+} concentrations [129]. Our results clearly show a prompt response of these clusters to acute Cu stress.

Table 3-2. MLP output for functional enrichment analysis.

eggNOG class and description		#*	*p*-value
P	Inorganic transport and metabolism	353	$7.65*10^{-22}$
E	Amino acid transport and metabolism	383	0.00276
O	Posttranslational modification, protein turnover, chaperones	197	0.00331
T	Signal transduction mechanisms	279	0.180
K	Transcription	497	0.187
V	Defense mechanisms	64	0.600
G	Carbohydrate transport and metabolism	201	0.739
Q	Secondary metabolites biosynthesis, transport and catabolism	192	0.813
M	Cell wall/membrane/envelope biogenesis	305	0.826
C	Energy production and conversion	434	0.835
H	Coenzyme transport and metabolism	142	0.845
J	Translation, ribosomal structure and biogenesis	181	0.879
F	Nucleotide transport and metabolism	93	0.919
U	Intracellular trafficking, secretion, and vesicular transport	146	0.921
N	Cell motility	77	0.928
I	Lipid transport and metabolism	287	0.934
D	Cell cycle control, cell division, chromosome partitioning	35	0.945
L	Replication, recombination and repair	334	1.000

*Number of genes in class

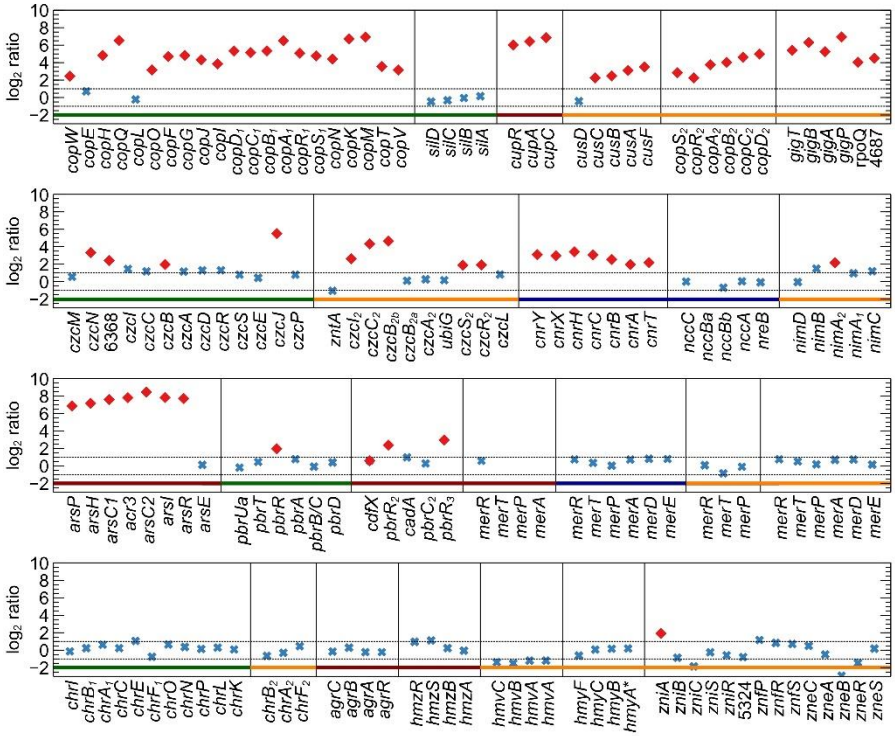

Figure 3-2. Differential gene expression of metal resistance genes from *C. metallidurans* CH34 exposed for 10 min to 400 µM Cu^{2+}. Significant (red diamond; $p < 0.05$) and non-significant (blue cross) $\log_2$ ratios are shown for known metal resistance genes located on the chromosome (red line under graph), chromid (orange), pMOL28 (blue), and pMOL30 (green). Dotted lines correspond to -1 and 1, respectively.

Cross-regulatory interactions, i.e., the induction of other HMR mechanisms by Cu, were observed for at least six clusters. The 8-gene *ars* cluster on the chromosome (Rmet_0327-0334), encoding resistance mechanisms against As, was completely upregulated (except *arsE*). It has previously been shown that the *ars* cluster is upregulated after exposure to As^{3+}, Pb^{2+}, Zn^{2+}, Co^{2+}, Cd^{2+}, and Se^{6+} [115], but a link with Cu exposure has thus far not been found. However, it has been shown that the regulator ArsR can bind Cu^{2+} [124]. Cross-regulation with resistance mechanisms against Cd^{2+}, Zn^{2+}, and Co^{2+} toxicity was also observed via the upregulation of *czcB₁*, *czcJ₁*, and *czcN₁*, with *czcJ₁* also shown to be upregulated after 30 min Cu exposure [115]. The chromid-borne *czc₂* cluster (Rmet_4464-4469, Rmet_4595-4597) was partly upregulated (Figure 3-2). The response regulators $CopR_1$ and $CopR_2$ are fairly similar to $CzcR_1$ and $CzcR_2$ (roughly 60% amino acid identity), which could elicit cross-

regulation. Furthermore, the regulon of response regulators could be broader than their co-localized targets [338-340]. Enhanced transcription of the CzcRS two-component system after Cu exposure was also noted in *Pseudomonas aeruginosa* [341]. Induction of several genes involved in Pb^{2+} resistance was also detected, with three copies of the *pbrR* gene encoding a MerR-type regulator being upregulated. Two copies are located on the chromosome (Rmet_2302, Rmet_3456), but lead resistance is mainly attributed to the *pbrUTRABCD* cluster on pMOL30 (Rmet_5944-5949). However, none of the other genes in this cluster were overexpressed. Additional cross-regulation was observed in the complete upregulation of the *cnr* cluster on pMOL28 (Rmet_6205-6211), which encodes resistance against Ni^{2+} and Co^{2+}. It has previously been observed that the transcriptomic responses of CH34 to Cu^{2+}, Co^{2+}, and Ni^{2+} overlap considerably [115]. Finally, the *gig* cluster on the chromid (Rmet_4682-4687) was completely and strongly induced. This cluster was found to be upregulated by Au^{3+} [342] and Ag^{+} [115] in a previous study and is controlled by the extracytoplasmic function (ECF) RpoQ sigma factor [342], which is also overexpressed after acute Cu stress. RpoQ has also been implicated in the resistance to Cd^{2+} and in the regulation of thiol/sulfide metabolism in CH34 [126].

A second eggNOG class enriched upon Cu exposure was class O, comprising posttranslational modification, protein turnover, and chaperones, which can be associated with the production of reactive oxygen species and antioxidant depletion elicited by Cu toxicity [42]. In agreement with previous studies [343], even after 10 minutes of Cu exposure, considerable changes were observed in the expression of genes involved in redox cycling and their regulatory mechanisms. Redox sensors *oxyR* [344] and *soxR* [345] were both upregulated. Curiously, CH34 lacks the homologs of their regulatory counterparts *oxyS* and *soxS*, thus the exact mechanisms of transcriptional regulation are unknown and may differ from canonical mechanisms in, e.g., *E. coli* [94]. In addition to *oxyR* and *soxR*, several peroxidase genes, such as *katA, aphC,* and *aphD* but not *sodB* and *sodC*, genes involved in thioredoxin and glutaredoxin metabolism and Fe-S cluster assembly as well as *ohrR* (coding for a transcriptional regulator of organic hydroperoxide resistance [346, 347]) and *dpsA* (encoding a DNA-binding protein associated with oxidative stress protection), were upregulated (Supplementary Table S3, Sheet "DGE" [*]) [116]. Antioxidants such as glutathione as well as Fe-S cluster-containing proteins with

[*]Supplementary data can be found at the following url: https://www.mdpi.com/2073-4425/11/9/1049.

roles as transcriptional regulators, catalytic enzymes, or oxidative stress sensors have been shown to play an important role in relieving oxidative stress [348-354]. Interestingly, this response to oxidative stress was not observed in a previous experiment with a longer exposure time (30 min) at a lower concentration (100 µM) [115], suggesting that oxidative stress is only elicited at higher Cu concentration or is rapidly counteracted. Several genes related to protein turnover and protein chaperoning were differentially expressed, which, together with the overrepresentation of class E (amino acid transport and metabolism), indicates the need to reconfigure the proteome in order to protect the cell from Cu toxicity. One of two copies of the chaperone *clpB* [355] was upregulated, as were *dnaK* [356], the *hslUV* operon (encoding a bipartite ATP-dependent protease [357]), *mucD* (periplasmic endopeptidase) [358], *prlC* (oligopeptidase) [359], and *ftshH* (metalloprotease) [360, 361] (Supplementary Table S3, sheet "DGE"*) [116]. The importance of protein turnover, both as a direct result of and as an active response to Cu stress, has been well established [362, 363]. In addition, several upregulated pathways are associated with amino acid metabolism (Supplementary Table S3, sheet "DGE"*) [116]. For instance, the two *cys* clusters involved in cysteine metabolism were almost completely upregulated [364]. The importance of the cysteine metabolism, which is intimately linked to the use of cellular S pools, has been implied in Cu resistance in other studies [343, 365-368]. A prime example is the need for L-cysteine in the biosynthesis of glutathione, of which the anabolic pathways were upregulated in the copper condition. Next to changes in S-metabolism, the transcriptome governing the metabolism of several other amino acids was also altered by exposure to Cu (Supplementary Table S3, sheet "DGE"*) [116].

3.3.2 Transcriptional start site profiling

3.3.2.1 General Characteristics of Detected TSSs

In a next step, the tagRNA-seq data were used to identify and probe the type of the 5' ends of RNAs in order to obtain a global snapshot of the transcriptional organization in *C. metallidurans* CH34 and to scrutinize the impact of Cu stress on the RNA landscape. The transcription start site (TSS) detection algorithm, as described in Materials and Methods, was fine-tuned to annotate the 7500 most

*Supplementary data can be found at the following url: https://www.mdpi.com/2073-4425/11/9/1049.

highly expressed TSSs in both the control and the copper condition. This number was roughly based on the number of annotated genes and pseudogenes in CH34 (6514). These TSSs were divided into primary, secondary, internal, antisense, and orphan TSS according to their location, similar to previous publications [369] with minor modifications (Figure 3-1). A primary TSS (pTSS) is the main TSS of a gene or operon and is located within 200 bp upstream of a start codon. It is expressed at least twice as strongly as the second most highly expressed TSS within those 200 bps. The remaining TSSs in this region were classified as secondary TSSs (sTSSs). An internal TSS (iTSS) is located within and on the coding strand, while an antisense TSSs (aTSS) is located on the non-coding strand of a CDS or within 100 bp upstream of its start codon. The orphan TSSs (oTSSs) are not associated with CDSs. An overview of this classification for every replicon is shown in Table 3-3. As TSS classification was prioritized via the following cascade: pTSS > sTSS > iTSS > aTSS > oTSS; there is no overlap between the different classes. In addition, the tagRNA-seq data was verified with 5' and 3' RACE of selected transcripts, including *copA*$_1$ mRNA and several antisense and orphan transcripts (see below) (Supplementary Figure S3[*]) [116]. Similarly, the previously identified TSSs of *cnrC*, *czcI,* and *pbrA* were also detected and confirmed by the tagRNA-seq results [267, 370, 371], all of which corroborate the validity of the TSS identification with the tagRNA-seq procedure.

[*]Supplementary data can be found at the following url: https://www.mdpi.com/2073-4425/11/9/1049.

Table 3-3. Number and overlap of detected transcription start sites (TSSs) in each replicon [1].

	pTSS			sTSS			iTSS			aTSS			oTSS		
	CT	**Cu**	∩	**CT**	**Cu**	∩	**CT**	**Cu**	∩	**CT**	**Cu**	∩	**CT**	**Cu**	∩
CHR1	1490	1382	1231	729	734	483	1294	1390	916	1015	934	723	278	248	216
CHR2	741	674	586	187	166	102	497	526	359	499	446	348	161	155	134
pMOL28	45	43	38	19	19	13	89	83	74	97	92	77	21	22	18
pMOL30	86	108	78	17	42	11	100	150	76	129	132	101	53	54	46
Genome	2362	2207	1933	952	961	609	1980	2149	1425	1740	1638	1249	513	479	414

[1] For each replicon and the full genome, the number of TSSs detected in the control (CT) and Cu condition, as well as the intersection (∩), are shown per TSS category (primary (pTSS), secondary (sTSS), internal (iTSS), antisense (aTSS) and orphan (oTSS)).

3.3.2.2 Primary TSSs

Primary TSSs were detected for 2422 CDSs, amounting to 35.8% of all annotated CDSs. In a first step, this information was combined with the output of the recently developed GeneMarkS-2 gene prediction tool [372]. CDSs for which no pTSS was detected and that contained an iTSS between the original start codon and the newly predicted one, being preceded by a predicted ribosome-binding site (RBS), were scrutinized. This resulted in the putative reannotation of 182 CDSs. In addition, the consensus RBS and the spacer length were derived (Figure 3-3).

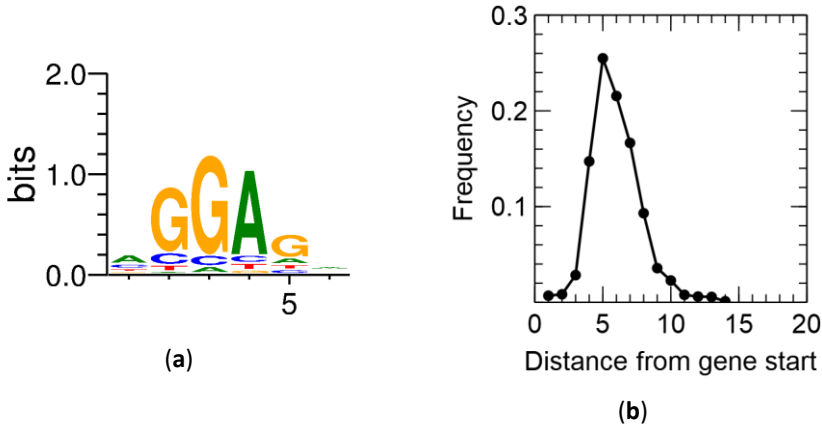

Figure 3-3. Ribosome-binding site sequence motif (**a**) and spacer length distribution (**b**) of *C. metallidurans* CH34.

Four cases were related to metal resistance. First, related to copper, *copM* encoding a 136 aa uncharacterized pre-protein was putatively re-annotated to be 114 aa. The cleavage site was similar for both, i.e., the processed proteins were identical, but the signal peptide prediction was much better for the newly annotated CDS (0.82 vs. 0.66; SignalP-5.0) (Figure 3-4 and Figure 3-5). In addition, *cupC* encoding 133 aa Cu chaperone was putatively reannotated to be 66 aa (Figure 3-4 and Figure 3-6). Related to the *czc* cluster involved in cadmium, zinc, and cobalt resistance, *czcN* (273 aa; 30.1 kDa predicted molecular weight) encoding a membrane-bound isoprenylcysteine carboxyl methyltransferase was putatively reannotated to be 216 aa (23.7 kDa predicted molecular weight) (Figure 3-4 and Figure 3-7). CzcN is homologous to NccN of *Alcaligenes xylosoxidans* 31 (reclassified as *C. metallidurans*), which was found to be a 23.5 kDA protein [373]. Finally, the *pbrD* gene coding for a Pb^{2+}-binding protein [370] could be putatively reannotated based on both TSS

identification and GeneMarkS-2 prediction (CDS and RBS) (Figure 3-8). However, the new CDS is not in frame and codes for a 150 aa protein unrelated to PbrD. These results merit further study of its function and sequence, since *pbrD* appears not to be necessary for Pb^{2+} resistance and is absent in all other known lead-resistant bacteria [374]. Moreover, although it is heterologously expressed in *E. coli,* it does show Pb^{2+} absorption [375].

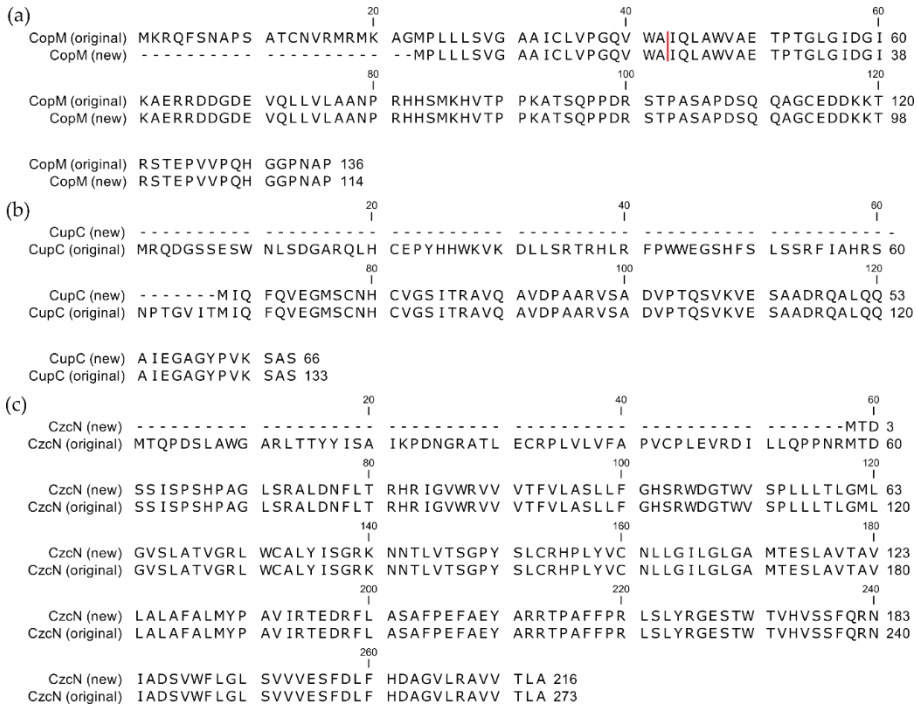

Figure 3-4. Alignment of original and newly annotated CDSs related to gene clusters involved in metal resistance.

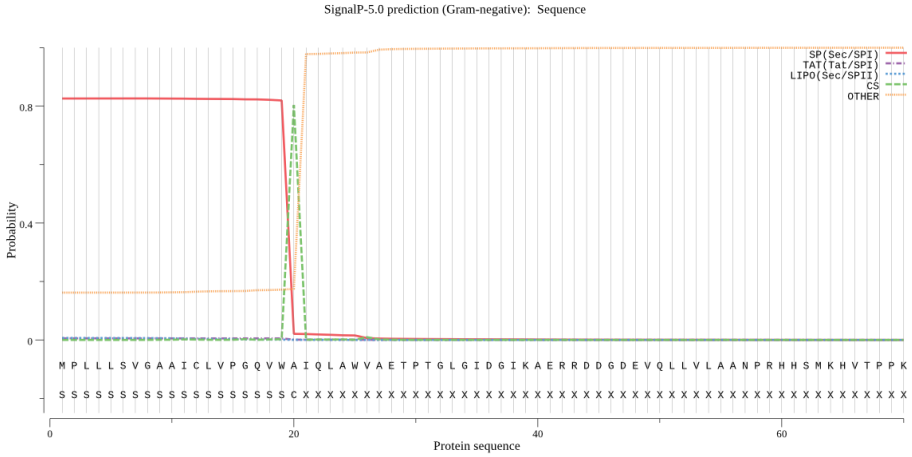

Figure 3-5. SignalP-5.0 output of signal peptide prediction for the reannotated CopM.

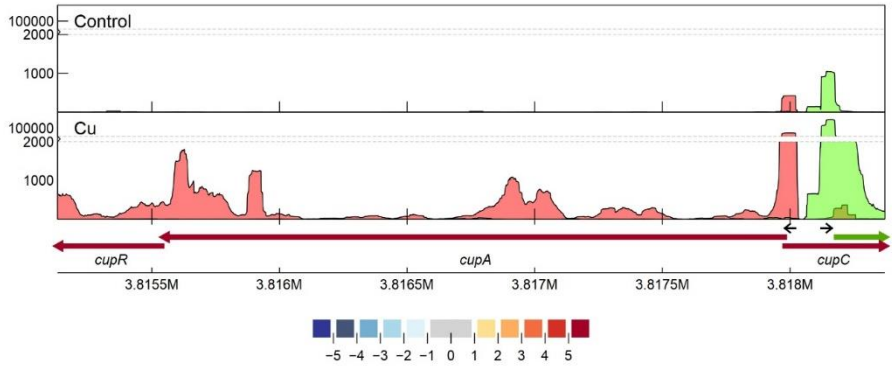

Figure 3-6. Transcription profile analysis of the *cupRAC* cluster from *C. metallidurans* CH34 when exposed to copper. Combined TSS read counts of the three biological replicates for control (upper) and Cu condition (lower) are shown for the positive (green) and negative (red) strand, with the y-axis containing a break pair (2000-50000) represented as striped grey lines. CDSs related to the *cupRAC* cluster (coordinates for the chromosome region shown at the bottom) are colored based on their $\log_2$ fold change. The small black arrows indicate clearly identified primary and internal TSSs. The green arrow represents a re-annotated CDS.

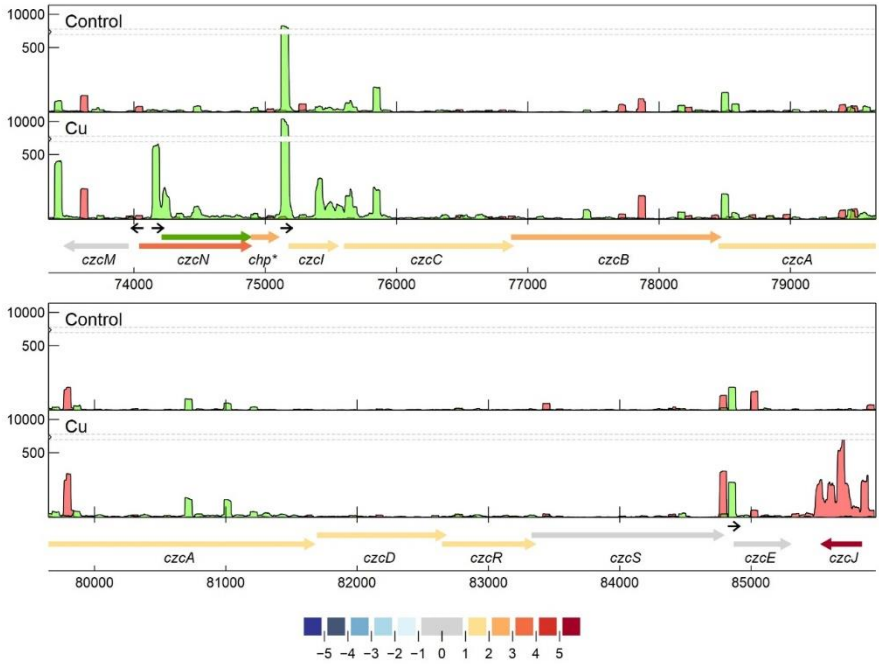

Figure 3-7. Transcription profile analysis of the *czc* cluster from *C. metallidurans* CH34 when exposed to copper. Combined TSS read counts of the three biological replicates for control (upper) and Cu condition (lower) are shown for the positive (green) and negative (red) strand, with the y-axis containing a break pair (600-2000) represented as striped grey lines. CDSs related to the *czc* cluster (coordinates for the pMOL30 region shown at the bottom) are colored based on their $\log_2$ fold change. The small black arrows indicate clearly identified primary and internal TSSs. The green arrow represents a re-annotated CDS.

Next, the 5' untranslated region (5' UTR) lengths and their distribution were calculated (Figure 3-9), which showed a peak at a length of 26 nt, after which it tapered off. No difference was noted between the control and the Cu condition, indicating that Cu exposure does not entail a global measurable bias in the 5' UTR length of expressed genes. A curious observation was the high number of leaderless mRNA (4.67% of all pTSSs), defined as those mRNAs with a 5' UTR length shorter than 5 nt. Because of the lack of a 5' UTR, these transcripts are translated via non-canonical mechanisms. Similar observations have been made in *Burkholderia cenocepacia* [376], *Streptomyces coelicor* [377], *S. enterica* [378], *C. crescentus* [119, 379], and *Helicobacter pylori* [153, 380]. A functional enrichment analysis showed that leaderless mRNAs was significantly enriched in eggNOG class K (transcription), which has already been observed in many bacterial species [381], and class L

(replication, recombination, and repair). Several leaderless mRNAs coding for transcriptional regulators were also differentially expressed in the presence of Cu^{2+}, including *arsR*, *ompR*, *ohrR,* and *zniR*. In addition, *copJ*, *merP*, *rpoN,* and *czcI₂* were transcribed into leaderless mRNAs. The prevalence of leaderless mRNAs has been shown to be higher in organisms with an earlier evolutionary age, and has been linked to extreme habitats [381, 382].

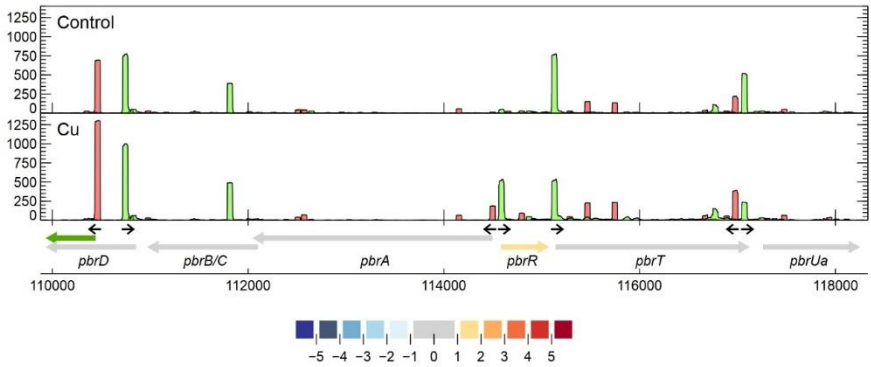

Figure 3-8. Transcription profile analysis of the *pbr* cluster from *C. metallidurans* CH34 when exposed to copper. Combined TSS read counts of the three biological replicates for control (upper) and Cu condition (lower) are shown for the positive (green) and negative (red) strand. CDSs related to the *pbr* cluster (coordinates for the pMOL30 region shown at the bottom) are colored based on their $\log_2$ fold change. The small black arrows indicate clearly identified primary and internal TSSs. The green arrow represents a re-annotated CDS.

Finally, to complete the promoter information, the consensus sequence in a region of 100 nt around each pTSS was identified with Improbizer [383], which allowed us to weigh the location of detected motifs. On the chromosome, the chromid, and the megaplasmid pMOL30, a TAnAAT consensus motif was detected around the -10 position, generally flanked by GC-rich stretches (Figure 3-10). At the -35 position, a TTGACA-like motif with higher variability was detected, again flanked by short GC-rich stretches (Figure 3-10). It is possible that CDSs preceded by these consensus motifs, which are similar in location and sequence to those found in *E. coli*, are under transcriptional control of the two housekeeping σ^{70}-factors *rpoD₁* (Rmet_2606) and *rpoD₂* (Rmet_4661) [94]. Interestingly, although pMOL28 and pMOL30 do not contain essential housekeeping genes, TAnAAT consensus motifs were found on pMOL30 but not pMOL28, indicating a difference in sigma factor recruitment for the initiation of pMOL28 and pMOL30 gene transcription. Noteworthy, in contrast with

pMOL30, which does not encode any sigma factors, pMOL28 encodes the ECF sigma factor CnrH. However, it is only involved in transcription of the *cnr* locus [267]. In addition, it has been shown that none of the remaining 10 ECF sigma factors, which are encoded on the chromosome (6) and the chromid (4), are necessary for the upregulation of any of the operons responding to metal shock [126]. Nevertheless, the involvement of non-plasmidic sigma factors in the transcription of plasmidic genes is not unexpected. On pMOL30, most CDSs preceded by a TAnAAT motif have an unknown function, but some genes involved in metal resistance are preceded by a TAnAAT-like pattern (*czcE*, *pbrT*, *ubiE,* and *copM*). Further determination of the functions of the remaining hypothetical proteins on both pMOL28 and pMOL30 may provide conclusive insights in this matter.

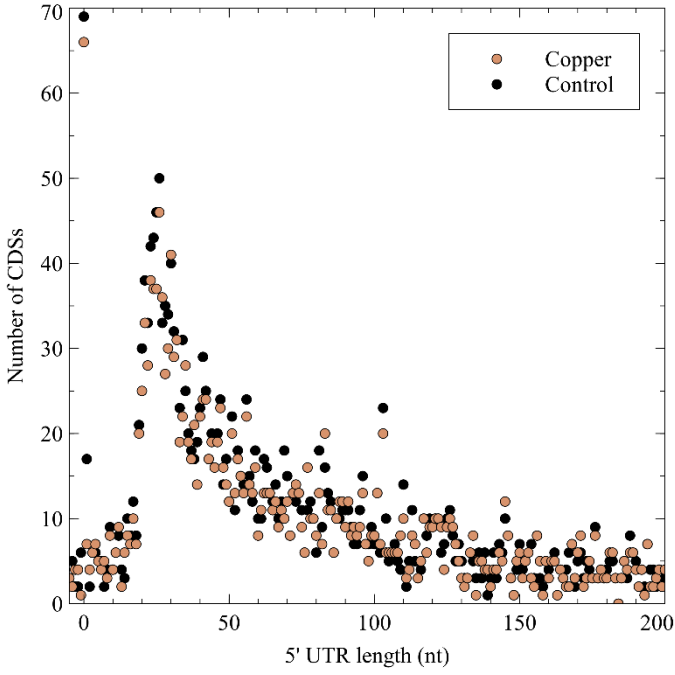

Figure 3-9. The 5’ untranslated region (UTR) length distribution in the *C. metallidurans* transcriptomes. CDS: coding sequence.

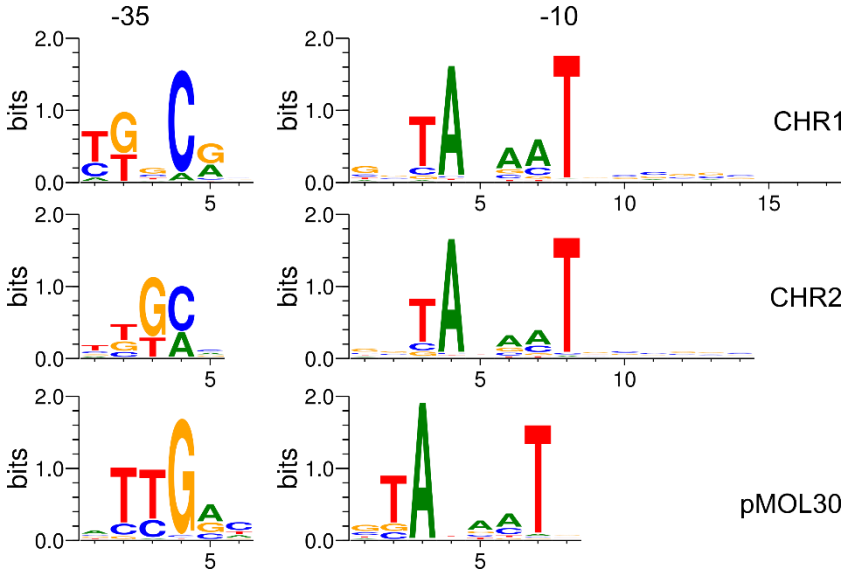

Figure 3-10. Consensus motifs (-35 and -10) in *C. metallidurans* CH34 promoters on the chromosome (CHR1), chromid (CHR2) and pMOL30.

3.3.2.3 Secondary TSSs

Alternative mRNAs deriving from secondary TSSs were detected for 623 CDSs. Among the genes differentially expressed under Cu stress, a high number of regulatory proteins was readily apparent, including the main regulators of pMOL30-based (*copR*$_1$) and chromid-based periplasmic (*copR*$_2$) Cu detoxification systems as well as *ohrR* (Rmet_3619), *zniS* (Rmet_5322), *bzdR* (Rmet_1223), *iscR*, *rpoH,* and *czcR*$_2$. In addition, several genes involved in HMR and stress responses were transcribed from alternative TSSs (Supplementary Table S3, Sheet "sTSS"*) [116]. Alternative TSSs have been reported in several bacterial and archaeal species [150, 384, 385] and have been linked to differences in translational efficiency and mRNA stability [386]. Longer 5' UTRs enable more extensive post-transcriptional regulation, e.g., via sRNAs, and can contain riboswitches that respond to various environmental cues [387]. Interestingly, many mRNAs coding for sigma factors showed multiple TSSs, including *rpoA, rpoD*$_1$*, rpoE, rpoH*, *rpoI, rpoK,* and *rpoM* (Figure 3-11), which could have an impact on the transcription of genes associated with a particular sigma factor.

*Supplementary data can be found at the following url: https://www.mdpi.com/2073-4425/11/9/1049.

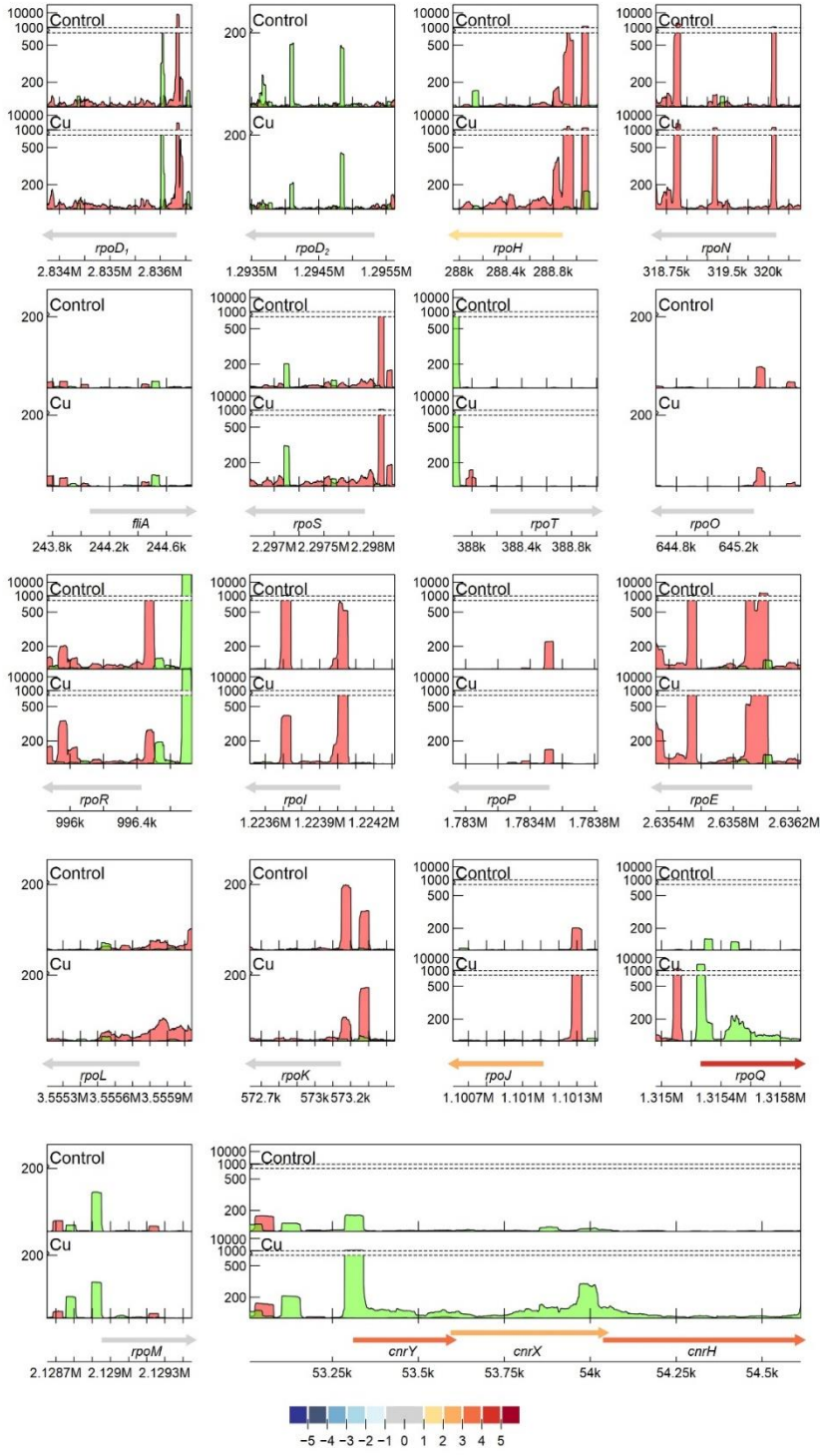
Control
Cu
rpoD1
2.834M 2.835M 2.836M
rpoD2
1.2935M 1.2945M 1.2955M
rpoH
288k 288.4k 288.8k
rpoN
318.75k 319.5k 320k
fliA
243.8k 244.2k 244.6k
rpoS
2.297M 2.2975M 2.298M
rpoT
388k 388.4k 388.8k
rpoO
644.8k 645.2k
rpoR
996k 996.4k
rpoI
1.2236M 1.2239M 1.2242M
rpoP
1.783M 1.7834M 1.7838M
rpoE
2.6354M 2.6358M 2.6362M
rpoL
3.5553M 3.5556M 3.5559M
rpoK
572.7k 573k 573.2k
rpoJ
1.1007M 1.101M 1.1013M
rpoQ
1.315M 1.3154M 1.3158M
rpoM
2.1287M 2.129M 2.1293M
cnrY
cnrX
cnrH
53.25k 53.5k 53.75k 54k 54.25k 54.5k
−5 −4 −3 −2 −1 0 1 2 3 4 5

Figure 3-11. Transcription profile analysis of sigma factors from *C. metallidurans* CH34 when exposed to copper. Combined TSS read counts of the three biological replicates for control (upper) and Cu condition (lower) are shown for the positive (green) and negative (red) strand. CDSs are colored based on their $\log_2$ fold change (*previous page*).

3.3.2.4 Intragenic TSSs

The second most abundant TSS class after the pTSSs was that of the iTSSs. As all TSSs were derived from primary 5'-PPP-RNA, these iTSSs are unlikely to be the result of RNA degradation, e.g., by 5'-exonucleases, although some could be pTSSs or sTSSs due to misannotated CDSs, or transcriptional noise from spurious promoters. More importantly, iTSSs can also mark the start site of noncoding RNAs.

Even though the roles of the detected iTSSs are unclear, they are pervasive in the CH34 transcriptome. Functional enrichment analysis showed that, in the copper condition, eggNOG classes C, F, J, M, O, P, and T were enriched in iTSSs. In total, 55 of the 167 genes involved in metal resistance contained at least 1 iTSS, e.g. almost all *cop₁* genes (Supplementary Table S3, sheet "iTSS"*) [116] and follow-up functional analyses could provide more insights into their specific role in metal resistance. The iTSSs related to the Cu resistance mechanisms (*cop₁* and *sil* clusters on pMOL30) are provided and discussed in detail below.

In both the control and the Cu condition, iTSSs were significantly enriched in the first 10% of the encompassing CDS, and were significantly depleted in the last 10% (pairwise comparison with Poisson modelling, $p < 0.05$ for control condition and $p < 0.1$ for Cu condition, Figure 3-12). This observation lends credibility to the hypothesis that many detected iTSSs are pTSSs or sTSSs to misannotated CDSs. However, these were not included in our re-annotation, as the current approach does not allow discriminating between the original and the putative new start codon. Of course, these uncertainties could be addressed with additional protein-based experiments such as proteome profiling (though not straightforward, as the absence of a longer protein over the presence of a shorter one needs to be shown), but this is out of the scope of this study. Since there is currently no evidence that iTSSs in the first percentile are linked more to coding RNAs than in other percentiles, we conclude that many iTSSs either mark the start site of noncoding RNA or are the result of transcriptional noise.

*Supplementary data can be found at the following url: https://www.mdpi.com/2073-4425/11/9/1049.

3.3.2.5 Antisense TSSs

Similar to intergenic TSSs, antisense TSSs are ubiquitously found in the CH34 transcriptome. In total, 2129 aTSSs were associated with 692 CDSs, indicating that many mRNAs can putatively be complexed by multiple antisense transcripts. Of all aTSSs, 408 showed a logFC smaller than -1 or greater than 1, indicating differential expression. Six differentially expressed aTSSs were validated by 5' RACE experiments (Table 3-1 and Figure 3-13). It is generally assumed that aTSSs mark the start of noncoding transcripts, however, whether a detected antisense transcript has a (regulatory) function or is the result of transcriptional noise [157] needs to be determined case-by-case. Since antisense transcripts can obscure regulatory features of the sense transcript by perfect base pairing [388], the location of aTSSs relative to the 5' and 3' ends of the sense transcript was scrutinized (Figure 3-13b). There is an apparent enrichment of aTSSs near the 5' end of the sense CDS, with a less prominent enrichment near the 3' end, indicating a putative regulatory role of the antisense transcripts. However, neither were statistically significant.

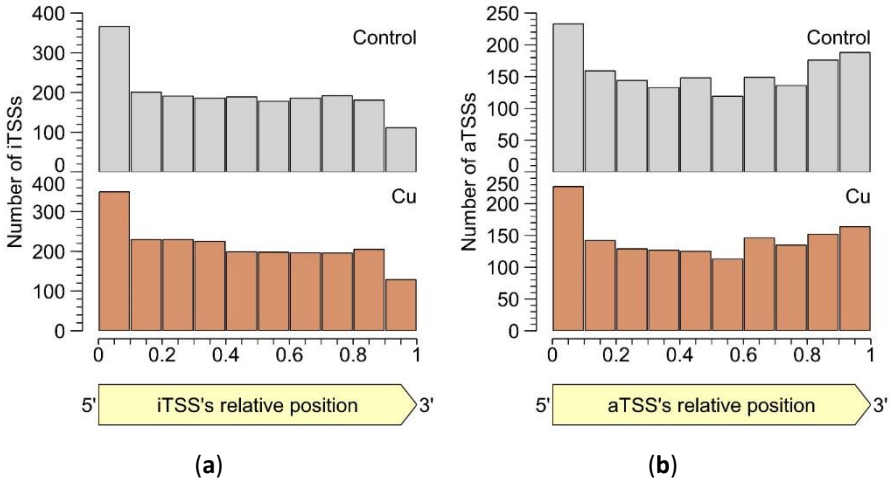

Figure 3-12. Percentile-wise distribution of iTSSs (**a**) and aTSSs (**b**) positions relative to the cognate CDS.

Specifically related to copper resistance, aTSSs were found in *silB*, *copA*$_1$, *copF*, *copG*, *copH*, *copL,* and *copM* (Figure 3-14 and Figure 3-15). The aTSSs in *silB* (nt position 168,587 on pMOL30, *silY*) and *copL* (nt position 181,548 on pMOL30, *copY*) were further selected for 3' RACE validation (detailed in 3.3.2.7), indicating rough

transcript lengths of approximately 700 and 500 bp, respectively (Figure 3-13). In addition, an aTSS was found in *czcA*$_1$ (Figure 3-7).

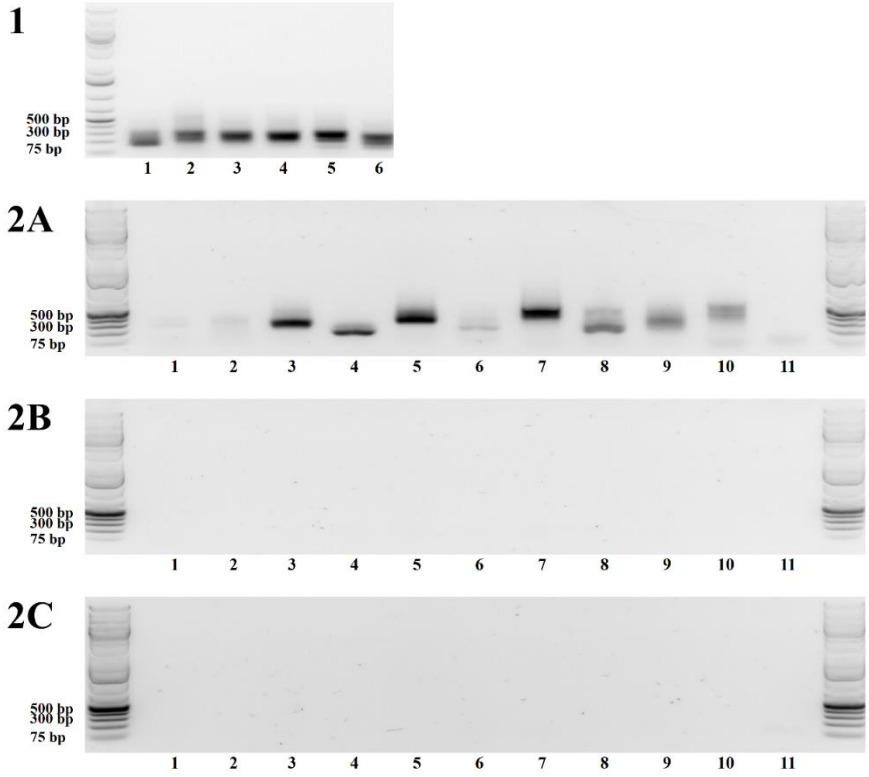

Figure 3-13. Agarose gel images of RACE experiments. Ladder used in all images is GeneRuler 1 kb Plus (Thermo Fischer Scientific). Primers used are Universal Primer Short (all reactions) and nested gene-specific primers (compare to Table 3-1). 5'RACE results for pasRNA1 (1.1), pasRNA2 (1.2), pasRNA3 (1.3), SilY (1.4), pasRNA5 (1.5), pasRNA6 (1.6). 2A) Additional nested PCR reactions. Primers used are Universal Primer Short (all reactions) and nested gene-specific primers and Rmet_101 (5') (2A.1), Rmet_101 (3') (2A.2), Rmet_1021 (alternative 3') (2A.3), Rmet_102 (5') (2A.4), Rmet_102 (3') (2A.5), CopY (5') (2A.6), CopY (3') (2A.7), Rmet_103 (5') (2A.8), Rmet_103 (3') (2A.9), SilY (5') (2A.10), SilY (3') (2A.11). 2B) Control reactions for 5' and 3' RACE reactions in (2A), omitting gene-specific primers from the reaction mixture. 2C) Control reactions for 5' and 3' RACE reactions in (2A), omitting Universal Primer Short from the reaction mixture. See also Table 4-3.

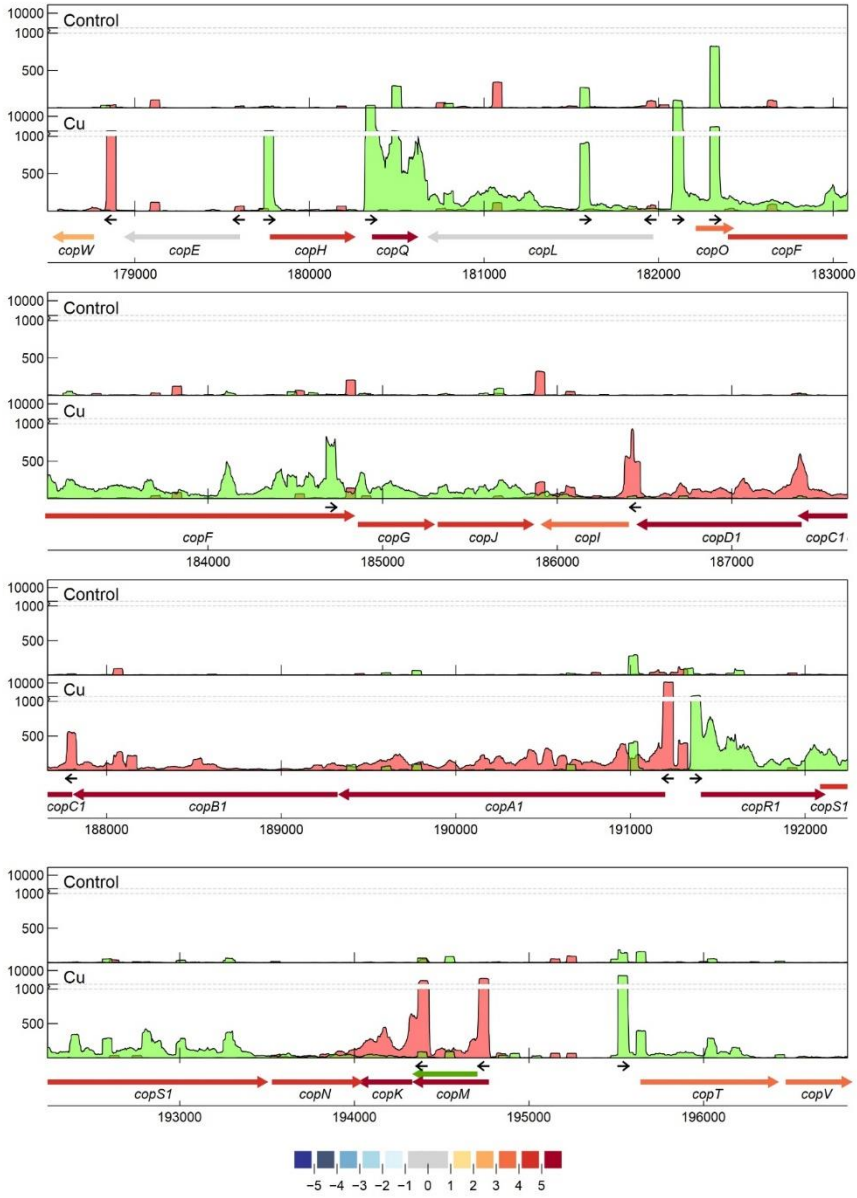

Figure 3-14. Transcription profile analysis of the *cop* cluster from *C. metallidurans* CH34 when exposed to copper. Combined TSS read counts of the three biological replicates for control (upper) and Cu condition (lower) are shown for positive (green) and negative (red) strands, with the *y*-axis containing a break pair (1000–1200) represented as striped grey lines. CDSs related to the *cop* cluster (coordinates for the pMOL30 region shown at the bottom) are colored based on their $\log_2$ fold change. The small black arrows indicate clearly identified primary and internal TSSs. The green arrow represents a re-annotated CDS.

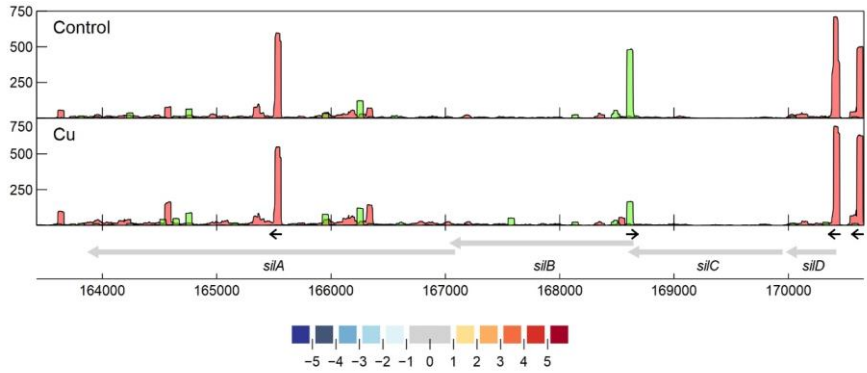

Figure 3-15. Transcription profile analysis of the *sil* cluster from *C. metallidurans* CH34 when exposed to copper. Combined TSS read counts of the three biological replicates for control (upper) and Cu condition (lower) are shown for positive (green) and negative (red) strands. CDSs related to the *sil* cluster (coordinates for the pMOL30 region shown at the bottom) are colored based on their $\log_2$ fold change. The small black arrows indicate clearly identified primary and internal TSSs.

Antisense TSSs were enriched in CDSs belonging to eggNOG classes L (replication, recombination, and repair), M (cell wall/membrane/envelope biogenesis), and T (signal transduction mechanisms) in the control condition, and classes J (translation, ribosomal structure and biogenesis), L, and M in the copper condition. Class T was only significantly overrepresented in the control condition, which could indicate that repression of translation via antisense transcription is common for CDSs related to signal transduction and partially relieved under copper stress. Many sigma factors, such as *rpoB* (Rmet_3334), *rpoD₁* (Rmet_2606), *rpoN*, *rpoB,* and *rpoS* (Rmet_2115), showed antisense transcription to a high extent (Figure 3-11). The role of alternative sigma factors in the initiation of antisense transcription has been described before [156, 389, 390]; inversely, an interesting case of the regulation of the sigma factor RpoS itself by antisense and anti-antisense RNAs has been shown in *E. coli* [166].

3.3.2.6 Orphan TSSs

In total, 578 TSSs were detected in intergenic regions unassociated with CDSs. These orphan TSSs could mark the start of transcripts resulting from the 5' of mRNAs with exceptionally long 5' UTRs, unidentified CDSs, often coding for short peptides [391], and trans-acting sRNAs [392], or they could result from transcription by spurious promoters.

First, the prevalence of long 5' UTRs was investigated. A 200–300 nt region upstream of known start codons was scrutinized for oTSSs, and uninterrupted coverage from the oTSS to the start codon was manually verified. In this way, 126 oTSSs marked the 5' of putative long 5' UTRs. Interestingly, *hfq*, coding for a small RNA-binding protein that stabilizes sRNAs and modulates RNA–RNA interactions [393] showed a long 5' UTR (209 bp) next to two other mRNA isoforms with 5' UTRs of 25 and 137 bp. Relative expressions of these three isoforms (25, 137, and 209 nt 5' UTR) were 6.1%, 81.1%, and 12.8% and 15.0%, 74.7%, and 10.3% for control and copper conditions, respectively. These disparate 5' UTRs might have given rise to differences in post-transcriptional regulation of the *hfq* mRNA. While the relative coverage of each alternative TSS was quite similar in control and copper conditions, it is possible that stronger selection of differential TSSs exists in other (stress) conditions.

In a subsequent analysis, the existence of putative open reading frames (ORFs) downstream of oTSSs was studied. In total, 417 oTSSs were located upstream an ORF with ATG, GTG, or TTG as start codons and either with a minimum length of 150 nt or with homology to proteins in the non-redundant protein database. A list of these proteins with their inferred function, among which several transporters, can be found in Supplementary Table S3, sheet "oTSS ORF BLAST"* [116].

Consequently, the remaining 35 oTSS were neither located within 300 nt upstream of known CDSs nor associated with putative ORFs. These oTSSs were assumed to mark the 5' end of noncoding RNAs. Eleven oTSSs showed a $\log_2$ fold change above 1 or below -1. As the expression of these oTSSs is affected by Cu stress, they are especially interesting as candidates for sRNAs with regulatory functions in the response to metal exposure. Three of them, based on interesting locations relative to known HMR genes, were experimentally validated by 5' RACE (Table 3-1 and Figure 3-13). Two of these differentially expressed orphan transcripts (Figure 3-16) were also experimentally validated by 3' RACE (one at CHR1 nt position 3,784,309 and one at CHR2 nt position 147562), indicating lengths of roughly 550 bp and 450 bp (Figure 3-13). It must be mentioned that 3' ends of coding and non-coding RNAs cannot be accurately inferred from tagRNA-seq coverage, hence the need for additional experimental validation (via 3' RACE or other techniques).

*Supplementary data can be found at the following url: https://www.mdpi.com/2073-4425/11/9/1049.

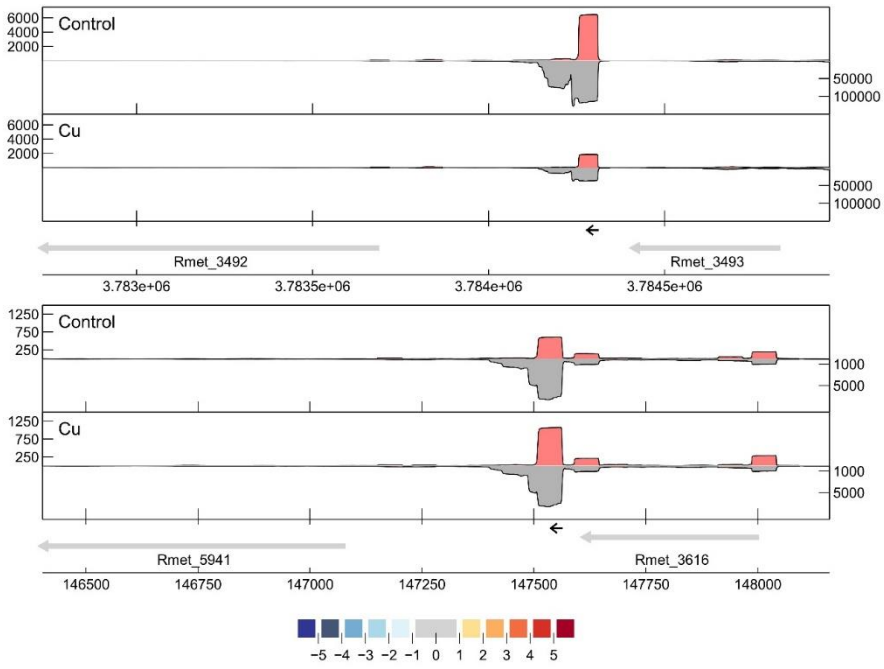

Figure 3-16. Transcription profile analysis of 2 identified oTSSs (small black arrows; top figure: located on the negative strand of CHR1 at nt 3784309; bottom figure: located on the minus strand of CHR2 at nt 147562) from *C. metallidurans* CH34 when exposed to copper. Combined TSS read counts (red) and combined TSS, PSS and unassigned read counts (grey, mirrored) of the three biological replicates for control (upper) and Cu condition (lower) are shown for the negative strand. Neighboring CDSs are colored based on their $\log_2$ fold change.

3.3.2.7 Detailed Analysis of cop and sil Clusters on pMOL30

As mentioned earlier, the *copVTKMNS$_1$R$_1$A$_1$B$_1$C$_1$D$_1$IJGFOLQHEW* cluster on pMOL30 harbors two of the three main Cu resistance systems. It is aided by the neighboring clusters *silDCBA*, *gtrM$_2$A$_2$B$_2$*, *ompP$_2$*, *ubiE,* and *ubiE$_2$*. Homologous but less extensive combinations of Cu/Ag resistance mechanisms are widespread and are often associated with mobile genetic elements [107]. Although the *cop* cluster was almost completely induced by Cu^{2+}, not all genes were induced to the same extent (Figure 3-2 and Figure 3-14). It has previously been shown that the transcriptomic response of some *cop* genes to Cu^{2+} stress is time-dependent [129], which indicates an additional level of regulatory complexity. Based on expression levels and TSS data,

pTSSs were identified for *copW, copE, copH, copQ, copL, copO, copF, copGJ, copI, copC, copA, copR₁S₁N, copK, copM,* and *copTV*. The *copA* pTSS was validated with 5' RACE. We investigated whether regulatory motifs could be found upstream of these pTSSs. Results using MEME [394] showed a 37 bp conserved motif around 50 bp upstream of all pTSSs, except *copG*, *copK,* and *copO* (Figure 3-17). In repeating this analysis with Improbizer, a 10 bp consensus motif was detected for all detected pTSSs, ca. 60 upstream for most and ca. 70 bp upstream for *copE*, *copL*, *copC*, and *copK*. Palindromic or direct-repeat chromosomal binding sites have been demonstrated for many response regulators of OmpR, NarL, LytR, and PrrA families [395] as well as autoregulation (motif in promoter region of *copR₁*). Consequently, this could be a putative $CopR_1$ binding site. Interestingly, we observed considerable variation in the expression levels of *cop₁* genes with similar consensus motifs. This could indicate that these small variations of the operator sequence have large effects on their interaction with regulatory proteins (e.g. $CopR_1$), as was shown for binding of response regulator AgrR in *C. metallidurans* NA4 [396], or that additional regulatory factors are involved. In addition, this motif was also detected upstream of the pTSSs of *cusA*, *cupA*, *cupC,* and *copB₂* (FIMO; $p < 0.001$ [397]). This discovery implies similarities in the regulation of different Cu-responsive clusters on the chromosome, the chromid, and the pMOL30. Evidently, this putative cross-regulation needs to be validated further.

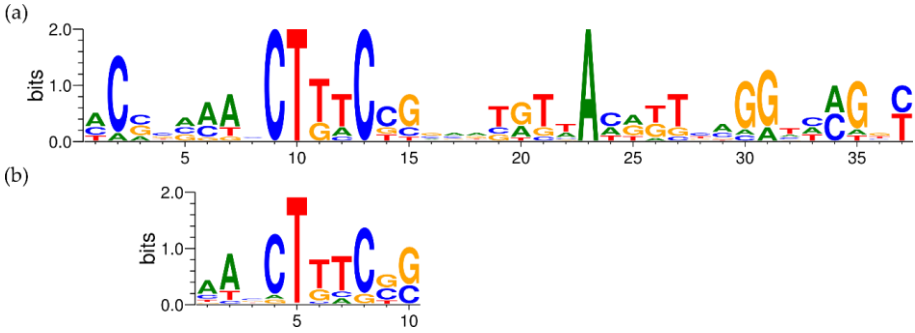

Figure 3-17. Conserved motifs 5' of the *cop* cluster pTSSs according to MEME (a) and Improbizer (b).

Several other TSSs were detected in the *cop* cluster. Secondary TSSs were found for *copA₁*, *copT,* and possibly *copR₁*. The sTSS at position 191326, likely related to *copA₁*, was detected in both conditions, but the much stronger pTSS at position 191,243 was only detected in the Cu condition. This observation provides a good example of a Cu-inducible promoter region with a strong signal-to-noise ratio, which can be

exploited, e.g., for the construction of optimal Cu-responsive biosensors. Intragenic TSSs were found in 13 of the 21 *cop* genes. Interestingly, the iTSS in *copQ* was expressed more strongly than the pTSS in the CT condition, while the inverse was detected in the Cu condition. This iTSS could potentially lead to an alternative, shortened CDS, where the N-terminal signal peptide as well as one of the typical motifs is absent [340]. Whether this transcript is really translated and has a biological role needs to be further analyzed. Noteworthy, there are 21 *copQ* homologs in *C. metallidurans* CH34, and although this protein family is still poorly characterized, many of them are transcriptionally induced in *C. metallidurans* CH34 in response to different metals [115], and an interplay between different homologues appears to confer metal resistance [340]. Antisense TSSs were identified in *copA*$_1$, *copF*, *copH*, *copL,* and *copM*, but only the aTSS in *copL* was overexpressed in the Cu condition, and a motif resembling the 10-bp motif, detected with Improbizer and described above, was detected around the –80 position. The aTSS in *copL* was also validated by 5'/3' RACE, indicating a transcript size of ± 700 bp (Figure 3-13). The functional role of these putative identified sRNAs in copper resistance will be tested in future studies. In addition to these observations, it is possible that trans-acting sRNAs (see 3.3.2.7) interact with mRNAs from the *cop* cluster.

The third main Cu resistance mechanism on pMOL30 is the HME-RND tripartite efflux pump encoded by *silDCBA*. While none of the *sil* genes are upregulated after acute copper exposure, as discussed previously, we detected several interesting TSSs in this cluster (Figure 3-15). Two clearly defined TSSs with similar expression levels were found upstream of *silD*, coding for a conserved protein with unknown function. The upstream TSS was preceded by a motif similar to the putative *cop* motif shown in Figure 3-17, suggesting (partially) shared regulation between these systems. No pTSSs were detected for *silC*, *silB,* or *silA*, indicating that the four-gene *sil* cluster is transcribed as one polycistronic mRNA of over 6 kb in length. A strong iTSS was found at nt 165562, more or less halfway through the *silA* gene. In addition, we detected a differentially expressed aTSS (named *silY*) that could putatively interact with the *silDCBA* mRNA, partially overlapping the ORFs of both *silC* and *silB*. Interestingly, this aTSS was downregulated in the Cu condition, hinting at a role of the antisense transcript in the post-transcriptional regulation of either or both of these two genes. This aTSS was validated by 5'/3' RACE, indicating a transcript size of roughly 500 bp (Figure 3-13). These data could provide insights with regard to the regulation of the *sil* cluster, which has thus far not been elucidated, considering the cluster lacks

adjacent proteins with regulatory functions. The possible role of this aTSS will be elucidated in further research.

3.4 Conclusions

In an effort to map the transcriptomic profile and the regulatory features of *C. metallidurans* CH34 in response to acute Cu stress, we performed tagRNA-Seq on *C. metallidurans* CH34 cultures exposed to Cu^{2+} and analyzed both differential gene expression and transcription start sites. Most differentially expressed genes belonged to eggNOG classes representing either transport and metabolism of inorganic ions, transport and metabolism of amino acids, and posttranslational modification, protein turnover, and chaperoning. A considerable fraction of CH34's impressive HMR arsenal was overexpressed, not limited to Cu-specific detoxification clusters. The importance of the cysteine/sulfur metabolism was also highlighted, in agreement with similar studies. Finally, Cu toxicity via the production of reactive oxygen species (ROS) was detected by the upregulation of multiple clusters involved in cellular redox chemistry. Interestingly, several key differences with previous microarray data were found, likely owing to the lower dose and the longer exposure time used in those experiments. This comparison demonstrates the highly transient nature of the transcriptomic response to Cu stress. Analysis of transcription start sites enabled us to (re)annotate TSSs of over 35% of known CDSs. Many leaderless mRNAs were discovered, often with functions in transcription and replication, recombination, and repair. An unexpectedly high number of TSSs were found inside CDSs, both in sense and antisense. Antisense TSSs were enriched near the 5' and the 3' ends of sense transcripts, indicating a function in post-transcriptional regulation of these transcripts. In addition, several transcripts starting in intergenic regions were detected, of which 35 were likely sRNAs. We did not detect sRNAs found in related strains *Burkholderia cenocepacia* [398] and *Bordetella pertussis* [399]. An interesting consensus motif upstream of *cop₁* cluster pTSSs was detected, which could be a shared operator of many *cop₁* genes. In addition, a substantial number of internal and antisense TSSs were found in this cluster, indicating supplementary levels of regulation. In conclusion, our data not only present new insights in the response of *C. metallidurans* to Cu, they also reveal different regulatory aspects that still need to be clarified in order to fully comprehend, optimize, and control possible biotechnological applications of this strain.

This chapter builds on the phenotypic observations laid out in Chapter 2, and can be indirectly related to the study of Cu-based antimicrobials. While we opted for a more general experimental setup, which can be easily compared to similar studies, conclusions can be drawn regarding Cu ion toxicity, which constitutes an important part of the overall toxicity of Cu antimicrobials, especially in wet conditions (see Chapter 2). Here again, in the framework of the ESA BIOFILMS project, the confounding factors of the space environment have not yet been introduced. In Chapter 4, we will validate several of the non-coding RNAs detected in further laboratory experiments. The spotlight will be aimed at SilY, the antisense transcript located opposite the *silDCBA* cluster on the pMOL30 plasmid.

CHAPTER 4 Regulation of the *silDCBA* cluster: a role for antisense transcription?

4.1 Introduction

Bacterial copper and silver resistance is achieved in large part by efflux systems. Next to ATP-driven primary transporters, such as P-type ATPases, electrochemical gradient-driven secondary transport systems can contribute to overall metal resistance. In the case of Cu and Ag resistance, the *cusCFBA* system in *E. coli* [400] and the *silRSECBAP* system in *Salmonella enterica subsp. enterica* serovar Typhimurium [401] were the first discovered (secondary) HME-RND transporters. These complexes consist of three proteins: a resistance-nodulation-division (RND) protein located in the cytoplasmic membrane, a membrane fusion protein (MFP) in the periplasm, and an outer membrane protein (OMP) in the periplasmic membrane [102, 402]. The RND protein, consisting of 12 transmembrane helices and 2 large hydrophilic domains in the periplasm, is responsible for substrate recognition and specificity, and for the proton-substrate antiport [403].

Twelve potential HME-RND systems can be found in the genome of *C. metallidurans* CH34, spread over its four replicons [94]. This high number of HME-RND systems is exceptional, but not unexpected, as they assist survival in the harsh metal-contaminated environments where *Cupriavidus* species are often isolated. In fact, one of the most well-known HME-RND systems, the CzcCBA system, was originally described in *C. metallidurans* CH34 [404]. We will focus on the *silDCBA* system, which plays an important role in Cu and Ag resistance in many *Cupriavidus* and *Ralstonia* strains. In *C. metallidurans* CH34, the *silDCBA* genes are located on the pMOL30 megaplasmid, in close vicinity to the *cop* cluster, which is associated with Cu resistance [94, 125, 129]. While the HME-RND system is encoded by *silCBA*, the *silD* gene encodes a protein of unknown function. SilD does contain several putative metal binding residues (e.g. cysteines and histidines), and could be involved in metal coordination [94]. Heterologous expression of *silCBA* in *E. coli* induced a 2-fold

increase of the Cu^{2+} and Ag^{+} MIC. Interestingly, expression of *silA* alone also increased the MICs of both Cu^{2+} and Ag^{+} slightly, likely owing to cytoplasmic detoxification by the SilA protein, which was shown capable of metal ion transport over the cytoplasmic membrane [405].

Little is known about the regulation of the *silDCBA* cluster in *Cupriavidus*. Contrary to the partially homologous *silRSECBAP* cluster in *S.* Typhimurium, no adjacent regulatory systems are present. Likewise, the homologous *cusDCBAF* system on *C. metallidurans* CH34's chromid also lacks an adjacent regulator [91]. While transcriptomic studies have found upregulation of the *silDCBA* cluster under Cu^{2+} stress [115], this was refuted in a more recent study [116] (albeit under different experimental conditions). At the same time, a clear upregulation of several proteins in this cluster was noted after Cu^{2+} and Ag^{+} exposure [406] (again under slightly different conditions). While it is entirely possible that the *silDCBA* cluster is under the control of a regulator located elsewhere in the genome of CH34, these observations could also indicate regulation on a post-transcriptional level. In Chapter 3, we have shown the presence of an antisense transcript with a transcription start site on the opposite strand of the *silB* gene and from its 56^{th} nt onwards running antisense to the *silC* gene. The transcript could fulfill a role as a non-canonical regulator [116] (see also Chapter 3, Figure 3-15). Interestingly, the expression of this antisense transcript, coined here as *silY*, was downregulated after Cu^{2+} exposure. Recently, a similar antisense transcript was also detected in *C. metallidurans* NA4, a strain closely related to CH34 (unpublished data). In this chapter, we aim to elucidate the putative biological function of *silY*, by evaluating the interaction of the SilY sRNA with its putative cognate regulon, and the phenotypic result of this interaction.

4.2 Materials and methods

4.2.1 Bacterial strains, media and culture conditions

The bacterial strains and plasmids used in this study are listed in Table 4-1 and Table 4-2. *C. metallidurans* CH34 [93] and AE104 (plasmidless derivative of CH34) [92] were routinely grown in Tris-buffered mineral medium (MM284) [92] supplemented with 2 g/l gluconate at 30 °C. *E. coli* strains were routinely cultured at 37 °C in Lysogeny broth (LB). Liquid cultures were grown in the dark on a rotary shaker at 180 rpm. For culturing on agar plates, 2% (w/v) agar (Thermo Scientific, Oxoid) was added. When appropriate, the following chemicals (Sigma-Aldrich or Thermo Scientific) were

added to the growth medium at the indicated final concentrations: kanamycin (50 µg/mL for E. coli (Km^{50}) or 1500 µg/mL for C. metallidurans (Km^{1500})), tetracycline (20 µg/mL (Tc^{20})), 5-bromo-4-chloro-3-indolyl-β-galactopyranoside (X-Gal; 40 µg/mL). Ionic Cu was added to the medium as $CuSO_4$ (Sigma-Aldrich, Overijse, Belgium).

Table 4-1. Strains used in this study

Strain	Genotype/Relevant Characteristic[1]	Reference[2]
C. metallidurans		
CH34	pMOL28 pMOL30 (MIC Cu^{2+}: 3 mM in MM284)	[93]
$\Delta IGR_{3492\text{-}3493}$::*tet*	Intergenic region of Rmet_3492 and Rmet_3493 replaced by *tet,* Tc^R	This study
AE104	Plasmidless derivative of CH34 (MIC Cu^{2+}: 600 µM in MM284)	[92]
E. coli		
MFD*pir*	MG1655 RP4-2-Tc::[Δ*Mu1::aac(3)IV*-Δ*aphA*-Δ*nic35*-Δ*Mu2::zeo*] Δ*dapA*::(*erm-pir*) Δ*recA*	[407]
TOP10	F- *mcrA* Δ(*mrr-hsdRMS-mcrBC*) Φ80*lacZ*ΔM15 Δ*lacX74 recA1 araD139* Δ(*araleu*)7697 *galU galK rpsL* (Str^R) *endA1 nupG*	Thermo Fisher Scientific

[1]Str^R: streptomycin resistant, Tc^R: tetracycline resistant.

Table 4-2. Plasmids used in this study

Plasmid	Genotype/Relevant Characteristic[1]	Reference
pACYC184	p15A *ori*, Cm^R, Tc^R	Lab collection
pBBR1MCS-2	pBBR1 *ori*, Mob^+, *lacZ*, Tc^R	[408]
pBBR-*nluc-silC*	λ pR promoter-driven N-terminal translational fusion of NanoLuc to SilC (xx-AA, C-terminal), Tc^R	This study
pBBR-*nluc-silC+silY*	pBBR-*nluc-silC* + J23119 promoter-driven *silY*, Tc^R	This study
pBBR-*silDCBA*	λ pR promoter-driven *silDCBA*, Tc^R	This study
pGLR2	RK2 *ori*, *oriT*, GFP-*luxCDABE* reporter, Km^R	[409]
pGLR2-$P_{silDCBA}$	Promoter *silD*	This study
pGLR2-P_{silY}	Promoter *silY*	This study
pK18mob	pMB1 *ori*, Mob^+, *lacZ*, Km^R	[410]
pSCK108	IncQ, Mob^+, *lacZ*, Km^R	[340]
pSCK108-*silY*	J23119 promoter-driven *silY*, Km^R	This study

[1]Cm^R: chloramphenicol resistant, Km^R: kanamycin resistant Tc^R: tetracycline resistant.

4.2.2 Expression analysis with promoter probe vector

The promoter probe vector pGLR2 [409] was used to quantify expression of *silDCBA* and 5 selected putative sRNAs (Table 4-3) . In all cases, the 200-bp region upstream of each TSS was PCR-amplified with primers providing *Eco*RI/*Pst*I recognition sites (Table 4-4). These PCR fragments were then cloned as an *Eco*RI/*Pst*I fragment in pGLR2, fusing them with a bi-cistronic GFP-*luxCDABE* reporter cassette (see 4.5 Annex for cloning schemes). Next, these constructs, as well as an empty pGLR2 vector, were transformed to *C. metallidurans* CH34.

Table 4-3: Characteristics of the *silY* gene.

sRNA	Type	TSS location	Genomic context
silY, Rmet_R104	Antisense	pMOL30 plasmid, + strand, nt 168587	Antisense to *silB* (56 nt) and *silC*

For testing, cells were grown in triplicate to OD_{600} 0.4 in MM284 supplemented with 1500 µg/ml kanamycin. The resulting cultures were washed twice with 10 mM $MgSO_4$ solution, and adjusted to a final OD_{600} of 0.4 in MM284. This suspension was divided between the wells of a white-walled 96-well plate, where it was amended with various concentrations of $CuSO_4$ (0 µM, 100 µM, 400 µM, and 1000 µM). The 96-well plate was then incubated in a plate reader (Clariostar, BMG Labtech, Ortenberg, Germany) at 30 °C with intermittent shaking. Every 15 minutes, OD_{600} and bioluminescence (with four different gain settings) were measured.

4.2.3 Translational fusions with Nanoluc cassette

In order to quantify the effect of *silY* expression on Sil expression, we created a translational fusion of the proposed *silC* target with an ORF encoding the Nanoluc luciferase [411]. DNA fragments were synthesized (Twist Bioscience, South San Francisco, CA, USA), containing, from 5' to 3', the λ pR promoter, the *nluc* gene (513 bp, no stop codon) fused to 250 bp of the 3' end of *silC* (containing the TGA stop codon), 300 bp of *silB*, and both a *rrnB* T1 terminator and a T7Te terminator. This DNA fragment was flanked by *Pst*I and *Bsp*TI restriction sites, which were used to clone it into a linearized pBBR1MCS3 vector (reverse PCR-amplified with primers pBBR1_PstI_inv_FW and pBBR1_BspTI_inv_RV), resulting in pBBR-*silC-nluc* (see 4.5 Annex for cloning schemes). In parallel, a DNA fragment was synthesized containing, from 5' to 3', a J23119 promoter (BBa_J23119; Registry of Standard Biological Parts),

silY, and both a *rrnB* T1 terminator and a T7Te terminator. This DNA fragment was flanked by *Pst*I and *Bgl*II restriction sites, which were used to clone it into *Pst*I/*Bgl*II digested pBBR-*nluc-silC*, resulting in pBBR-*nluc-silC+silY* (see 4.5 Annex for cloning schemes). Both plasmids were transformed to competent *C. metallidurans* AE104 and *E. coli* TOP10.

For testing, 50 µl of both exponential phase and stationary phase cultures were used for the Nano-Glo® Luciferase Assay System (standard protocol; Promega Benelux, Leiden, Netherlands), absorbance at OD_{600} and luminescence was measured using a plate reader (Clariostar, BMG Labtech, Ortenberg, Germany).

4.2.4 Phenotypic effects of *silY* expression

A pBBR1MCS derivative carrying *silDCBA* under control of the λ pR promoter was constructed by PCR-amplifying the entire *silDCBA* cluster with primers silD_GA_FW and silD_GA_RV, and reverse PCR-ampifying the pBBR1MCS3 vector with primers lacZa_FW and lacZa_RV. The *sil* cluster was then cloned into the MCS of the pBBR1MCS3 vector by GeneArt™ cloning (Thermo Fisher Scientific). The latter was PCR-amplified (primers silD_aa2_FW and lacZ_RV; inverse PCR) and a λ pR promoter (PCR-amplified with primers lambda_lacZ_GA_FW and lambda_silD_GA_RV) was introduced by by GeneArt™ cloning, resulting in pBBR-*silDCBA* (see 4.5 Annex for cloning schemes). In addition, pSCK108 derivative with *silY* under control of the J23119 promoter was constructed by inserting a gBlock (Integrated DNA Technologies, Haasrode, Belgium) containing the J23119 promoter, *silY* and a T7Te terminator sequence flanked by *Eco*RI and *Pst*I sites, into EcoRI/PstI-digested pSCK108, resulting in pSCK108-*silY* (see 4.5 Annex for cloning schemes).

For testing, cultures of CH34 and AE104 carrying pBBR-*silDCBA* and pSCK108-*silY*, pBBR-*silDCBA* and pSCK108, or pBBR1MCS-3 and pSCK108-*silY* were grown in quadruplicate in MM284 medium until stationary phase. Cultures were then washed twice with MM284 and diluted to a final OD_{600} of 0.4. At this point, viable counts were made by spotting 10 µl of a 10-fold dilution series onto MM284 agar plates. Cultures were exposed to 1000 µM of $CuSO_4$ for 1 h (MIC of Cu^{2+} for AE104 is 600 µM). After 1 h, a dilution series was made and spotted on MM284 agar plates. All MM284 plates were grown for 4 days at 30 °C in the dark. Viable counts before and after Cu^{2+} exposure were compared.

For analyzing growth, cultures were grown in triplicate in MM284 until stationary phase, washed twice with a 10 mM $MgSO_4$ solution, and resuspended in fresh

MM284 at a final OD_{600} of 0.01. Next, these cultures were pipetted into a 96-well plate, and amended with appropriate concentrations of $CuSO_4$. Cultures were incubated in the dark in a plate reader (Clariostar, BMG Labtech, Ortenberg, Germany) at 30 °C, with intermittent shaking at 180 rpm. OD_{600} was measured for 4 days.

Table 4-4. Primers used in this study.

Primer	Sequence[1]
silY_EcoRI_FW	GATCGAATTCGCCGTCGGCATTTTCCTCT
silY_PstI_RV	GATCCTGCAGTGGCGCATATTACCTTGGACAACA
silD_GA_FW	TAACCCTCACTAAAGGGAACGGTGTCTTGATATTGTGGCG
silD_GA_RV	GGGCCCGGTACCCAGCTTTTTCGACGGCACAGAAAGGCG
lacZa_FW	GTTCCCTTTAGTGAGGGTTAATTGCG
lacZa_RV	AAAAGCTGGGTACCGGGC
lambda_lacZ_GA_FW	CGGTACCCAGCTTTTTACGTTAAATCTATCACCGCAAG
lambda_silD_GA_RV	GCGATAGGAGGCGTGCATATGTTTTTCCTCCTTATAAAGTTAATCT
silD_aa2_FW	CACGCCTCCTATCGC
pBBR1_PstI_inv_FW	GATCCTGCAGGCGCTCACTGCCCGCTTT
pBBR1_BspTI_inv_RV	GATCCTTAAGACCAATAGGCCGACTGCGATGAGT

[1]Restriction sites are underlined.

4.3 Results and discussion

4.3.1 Determining the transcript boundaries of *silY*

In a first experiment, we aimed to accurately determine the boundaries of *silY*, which is important for the search of its promotor region and the exact target mRNA it regulates. While the 5' end of *silY* was readily apparent from the tagRNA-Seq coverage profiles (Figure 3-15), and the transcript boundaries were roughly estimated by gel electrophoresis of 5' and 3' RACE PCR products, we performed a more accurate validation of the 5' and 3' boundaries by Sanger sequencing of these RACE-PCR products. In this way, the 5' of *silY* could be confirmed, although several tested samples showed slightly different 5' ends. This is likely due to the relatively low transcript abundancy of *silY.* The more abundant CopA mRNA, used as positive

control, yielded only 5' ends exactly as identified by tagRNA-Seq. Interestingly, the transcription start site of *silY* is preceded by a TAATAT sequence at the -10 position and a TTGCTG at the -38 position, closely resembling the consensus sequences for primary TSSs (see 3.3.2.2). Therefore, we hypothesize that expression of *silY* is under the control of a housekeeping sigma factor, such as $RpoD_1$ or $RpoD_2$ [94]. This hypothesis is putatively corroborated by the observation that *silY* expression decreased after Cu^{2+} exposure, which could bring a shift from housekeeping regulators to alternative regulators to face the imposed metal stress, with a concomitant decrease in *silY* expression. However, most housekeeping sigma factors in CH34 (e.g. $RpoD_1$ and $RpoD_2$) were not downregulated after Cu exposure.

We were not able to determine the 3' end of *silY* exactly, even with Sanger sequencing. Transcript lengths varied from ca. 100-1000 nt, and in addition no Rho-independent terminator sequence could be detected with the ARNold tool [412]. It is possible that *silY* transcription is terminated in a Rho-dependent manner, since this has been observed for other sRNAs [306], but even then a clearly defined 3' end should be visible. In any case, for the following experiments we selected the first 200 bp starting at the *silY* TSS as the practical sRNA length, since the tagRNA-Seq coverage shows a decrease after ca. 200 bp.

4.3.2 Differential expression of *silY*

A requirement for a functional role of *silY* in the regulation of the *silDCBA* cluster is a difference in abundance of the sRNA upon Cu^{2+} stress. To verify the tagRNA-Seq data, we cloned the promoter of *silY* (200 bp upstream of the TSS) in the pGLR2 promoter-probe vector [413, 414]. The resulting plasmid was transformed to *C. metallidurans* CH34, allowing for easy monitoring of *silY* expression by either fluorescence or luminescence. This approach was used as it is difficult to discriminate between sense and antisense transcripts via qPCR.

Exponential-phase cultures were exposed to sub-lethal Cu^{2+} concentrations in MM284 growth medium, and luminescence was measured. In CH34 pGLR2-P_{silY}, the measured luminescence was inversely correlated with Cu^{2+} concentration. This can be due to a decrease in the overall level of transcription and translation, as well as a decreased intracellular availability of reduced flavin mononucleotide and aldehyde substrate. While the decrease in expression of *silY* was more pronounced in the tagRNA-Seq coverage data, we did not take into account the rate of SilY degradation, which could impact the relation between expression and abundance of this transcript. The plasmid copy number, which is higher for pGLR2 than for pMOL30,

could also have an impact on SilY abundance. Interestingly, the expression immediately after Cu exposure of the empty control vector also decreased after addition of Cu^{2+}, indicating a general effect more so than an effect specific for *silY* expression. However, the quantitative difference between the control and Cu-stressed conditions increase with time only in the pGLR2-P_{silY}-*luxCDABE* vector, showing the expected (and stronger) effect on the regulation of SilY. In a similar experiment, the expression of *silDCBA* was measured, but luminescence levels did not exceed those of the empty pGLR2 vector control. However, this construct could not be timely validated.

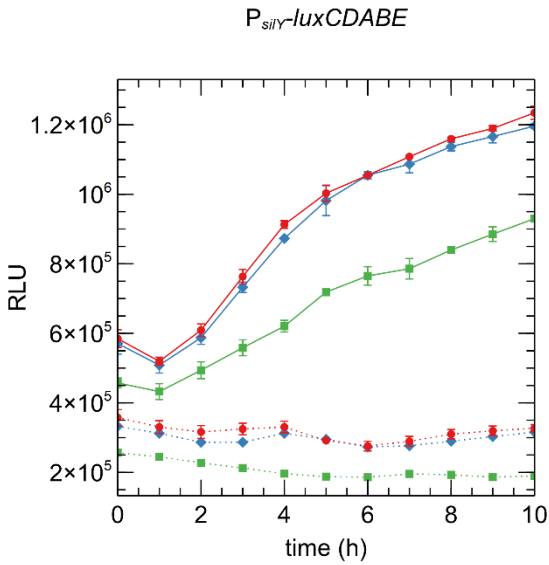

Figure 4-1. Expression of *silY* based on luminescence produced by the promoter probe vectors pGLR2-P_{silY} (full lines) and pGLR2 (dotted lines) in *C. metallidurans* CH34 grown for 10 h in MM284 containing 0, 100 and 400 µM Cu^{2+} (red, blue and green, respectively). n = 2.

4.3.3 SilY represses SilC translation

Repression of *silDCBA* translation by interaction with *silY* should lead to a measurable difference in Sil protein abundance. Therefore, we created a translational fusion of the nanoluc cassette to the 250-bp 3' end of *silC*, which overlaps with *silY*. This translation fusion enabled monitoring SilC translation in the absence and presence of SilY, driven by a strong constitutive promoter.

The expression of *silY* has a clear impact on the abundance of the NanoLuc-SilC fusion protein, with over 100-fold repression in both exponential as stationary phase, and in *E. coli* and *C. metallidurans* (all comparisons statistically significant with $p < 0.05$, Figure 4-2). This is a clear indication that SilY is capable of repressing the expression of its cognate region, likely by direct interaction. This interaction via hybridization putatively leads to the formation of an unstable dsRNA hybrid, prone to degradation mediated by RNases. It is unlikely that SilY can occlude the RBS located 5' of the *silC* start codon since this RBS is located quite far downstream of the *silY* TSS (and not present in the *nluc-silC* construct). However, occlusion of the *silB* RBS could occur, but post-transcriptional regulation of SilB has not yet been tested. Finally, these results hint at a repression mechanism on a post-transcriptional level rather than on a transcriptional level. While antisense transcription can have a regulatory effect on both transcription and translation, in this experiment *silY* was provided in trans, precluding mechanisms like transcriptional blocking (see section 1.1.4). In addition, repression of transcription would lead to lower *silDCBA* coverage in the tagRNA-Seq experiment, which was not observed. Curiously, repression was similar in exponential and stationary phase, indicating a growth-independent mechanism. In addition, there was also a strong similarity between repression in *E. coli* and *C. metallidurans*, hinting at a conserved functional mechanism. Thus, we conclude that *silY* impairs translation of the polycistronic *silDCBA* transcript.

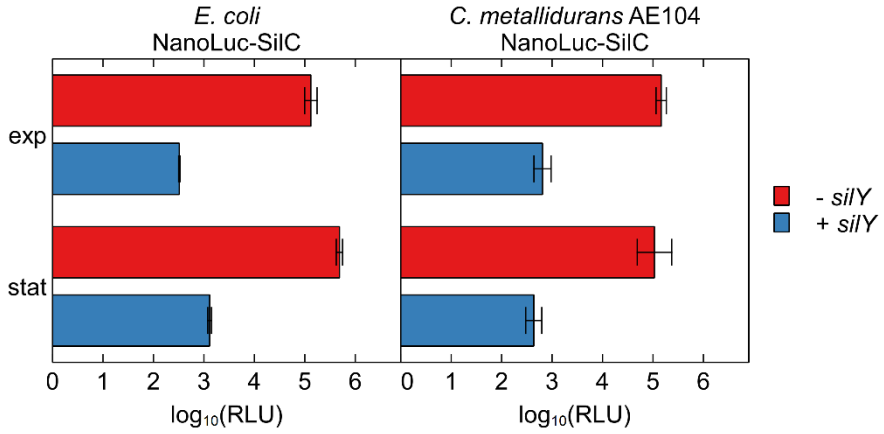

Figure 4-2. Nano-Glo® Luciferase assay on a translational NanoLuc-*silC* fusion in the absence (red) and presence (blue) of *silY* tested in *C. metallidurans* and *E. coli* background at exponential (exp) and stationary (stat) growth phase. n = 3.

4.3.4 Sil repression decreases Cu tolerance and resistance

If *silY* plays a functional role by repressing translation of the *sil* cluster, this should be measurable by a decreased tolerance and resistance to Cu^{2+}. In this context, tolerance is a measure of the ability of a bacterial population to withstand lethal concentrations of Cu^{2+}, whereas resistance is the ability of a population to actively divide and grow in medium containing sub-lethal concentrations of Cu^{2+}.

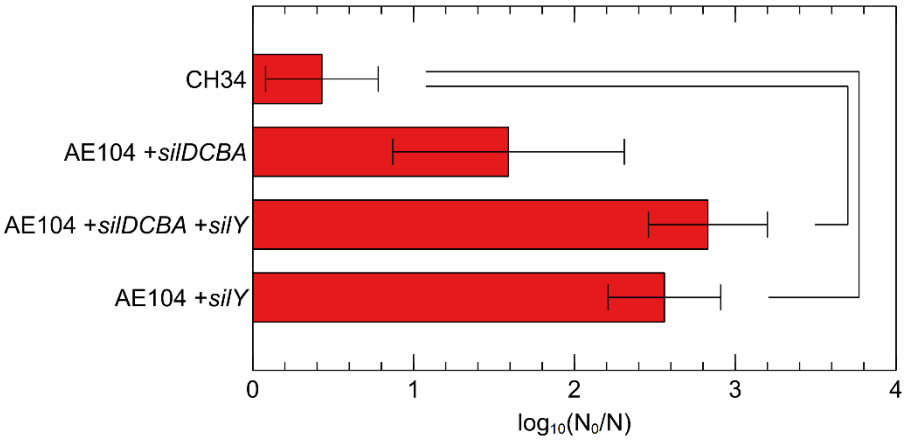

Figure 4-3. Inactivation ($\log(N_0/N)$) of stationary cultures of various *C. metallidurans* strains after exposure to 1000 µM of Cu^{2+} in MM284 for 1 h. Counts were assayed by spotting on MM284 agar plates. n = 4.

In a first experiment, *C. metallidurans* AE104 expressing *silDCBA* with or without expressing *silY* were subjected to a relatively short pulse of a lethal Cu^{2+} concentration. The viable count of AE104 strain expressing the *silDCBA* cluster, after exposure to 1 mM of Cu^{2+} for 1 h, decreased from ca. 10^9 CFU/ml to 10^7 CFU/ml, while a stronger decrease (to 10^6 CFU/ml) was observed in the presence of *silY* (Figure 4-3). This is coherent with the hypothesis that *silY* represses translation of the *silDCBA* cluster, leading to a decreased Cu^{2+} tolerance. Furthermore, AE104 expressing only *silY* but not the *silDCBA* cluster was on average as Cu^{2+}-tolerant as AE104 expressing both, indicating a high level of repression by *silY*. Noteworthy, AE104 expressing only the *silDCBA* cluster was not as tolerant as CH34, suggesting the role of additional Cu^{2+} tolerance-determining factors, including the *cop* cluster on pMOL30. However, due to the large variability of the results, no significant effects could be detected, other than the significant differences ($p < 0.05$) between CH34 and AE104+*silDCBA*+*silY*, and between CH34 and AE104+*silY*. Consequently, no

definitive conclusions could be drawn regarding the difference between e.g. AE104+*silDCBA* and AE104+*silDCBA*+*silY*.

In a next series of experiments, we tested if *silY* had a measurable effect on Cu^{2+} resistance. No difference in growth was observed in MM284 for AE104 expressing *silDCBA, silDCBA* and *silY*, or *silY* (Figure 4-4). When MM284 was supplemented with 500 µM Cu^{2+} (ca. 83% of the MIC for AE104), a noticeable, though not statistically significant, difference was observed between AE104 expressing *silDCBA* with or without *silY*, with a lower Cu^{2+} resistance when *silY* was expressed (Figure 4-4). This corroborates *silDCBA* repression by *silY*. However, AE104 expressing only *silY* was even less resistant, indicating that in this case repression was not as complete as observed in the tolerance measurement. Noteworthy, variability on these measurements was high, and consequently results must be interpreted with caution.

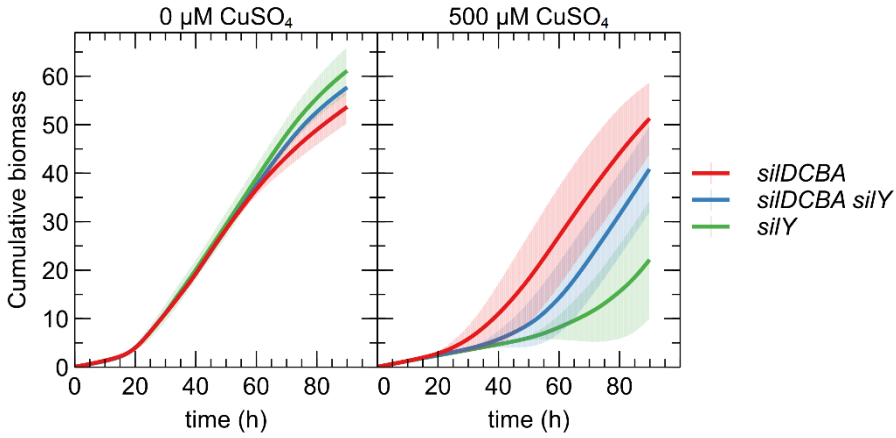

Figure 4-4. Cumulative biomass of AE104 carrying *silDCBA* (red), *silDCBA* and *silY* (blue),or *silY* (green), grown in MM284 with or without 500 µM Cu^{2+}. Cumulative biomass (time × OD_{660}) is the average empirical area under the growth curve for three biological replicates (n = 3).

4.4 Conclusions

In this chapter, we have studied the putative function of the noncoding transcript *silY*. While at present we have only been able to accurately define its 5' end, a transcript consisting of the first 200 nt was able to strongly repress translation of the *silDCBA* cluster, likely via hybridization with the polycistronic SilDCBA mRNA and subsequent RNase-mediated degradation. In addition, this post-transcriptional repression appears to affect Cu^{2+} sensitivity, as a decrease of Cu^{2+} tolerance and Cu^{2+}

resistance were observed (however not statistically significant). From these experiments, we conclude that *silY* has the potential to function as a repressor. This is especially interesting considering the lack of known regulators of the *silDCBA* cluster, but the apparent overexpression of SilB and SilC proteins after Cu^{2+} exposure [406]. It would be very interesting to further scout for putative transcriptional regulators of the *silDCBA* cluster, both at a computational and an experimental level. In addition, we do not know how the expression of *silY* is regulated. From the tagRNA-Seq study performed in Chapter 3, we noted that the RNA coverage level of *silY* relative to *silDCBA* is halved after acute Cu^{2+} exposure. While a decrease in *silY* expression was also noted after Cu^{2+} exposure via promoter-probe experiments, this was not as large as observed with RNA-Seq. As noted before, this could be due to the difference between transcript expression (as measured with the promoter-probe assay) and transcript abundance (as measured by tagRNA-Seq), which also depends on the stability and the degradation rate of SilY. Thus, based on our results we can draw the preliminary conclusion that SilY plays a functional role in the regulation of the *silDCBA* cluster. Finally, we provide a short overview of the putative mechanism of regulation: *silY* transcription is repressed by Cu exposure, while *silDCBA* transcription is constitutive. The SilY antisense transcript in turn represses translation of the polycistronic SilDCBA mRNA by hybridization and subsequent degradation via RNases. This degradation is thus less extensive during Cu exposure, leading to a stronger translation of SilDCBA mRNA, resulting in more SilDCBA proteins and a subsequent increase in Cu resistance. Overexpression of *silY* induces a Cu-sensitive phenotype, but an increased sensitivity to Cu antimicrobials has not yet been evaluated. In follow up experiments, it would be interesting to study the role of the *silDCBA* cluster and *silY* regulation in a setup similar to the one described in Chapter 2. In Chapter 5, we will focus on the role of environmental chemistry in the regulatory response to Cu exposure with *C. crescentus* as case study.

4.5 Annex (cloning schemes)

Construction of pBBR-*nluc-silC+silY*

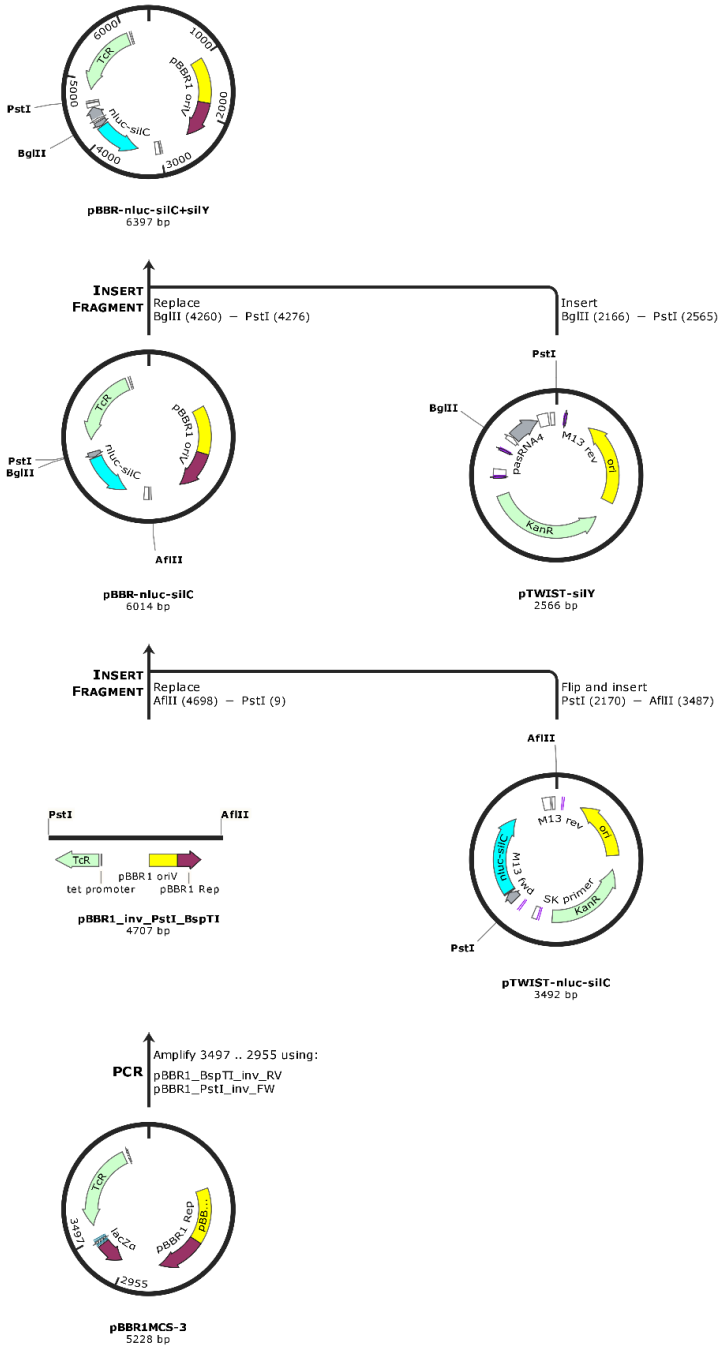

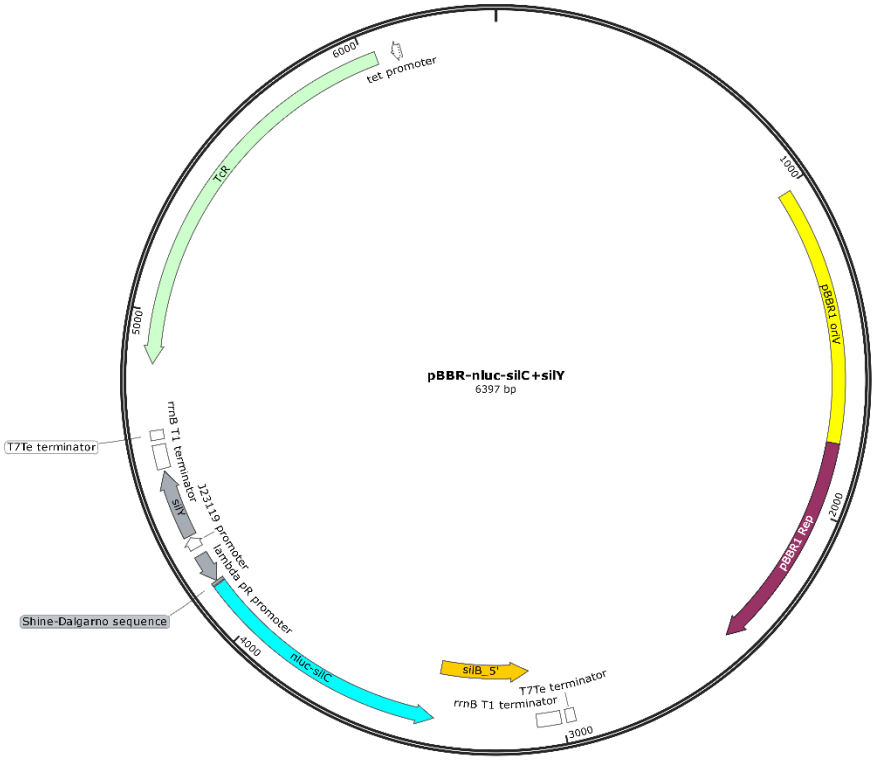
pBBR-nluc-silC+silY
6397 bp
6000
tet promoter
TetR
5000
1000
pBBR1 oriV
pBBR1 Rep
2000
T7Te terminator
rrnB T1 terminator
silY
J23119 promoter
lambda PR promoter
Shine-Dalgarno sequence
4000
nluc-silC
silB_5'
T7Te terminator
rrnB T1 terminator
3000

Construction of pBBR-*silDCBA*

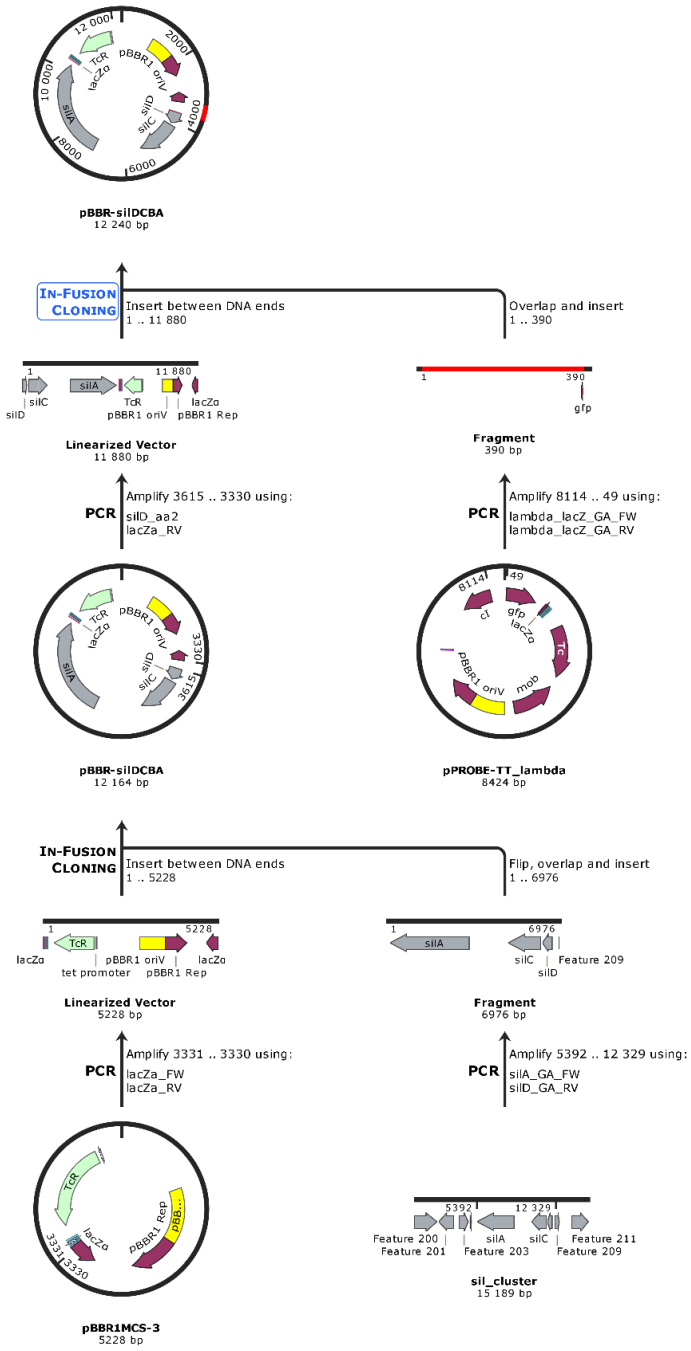

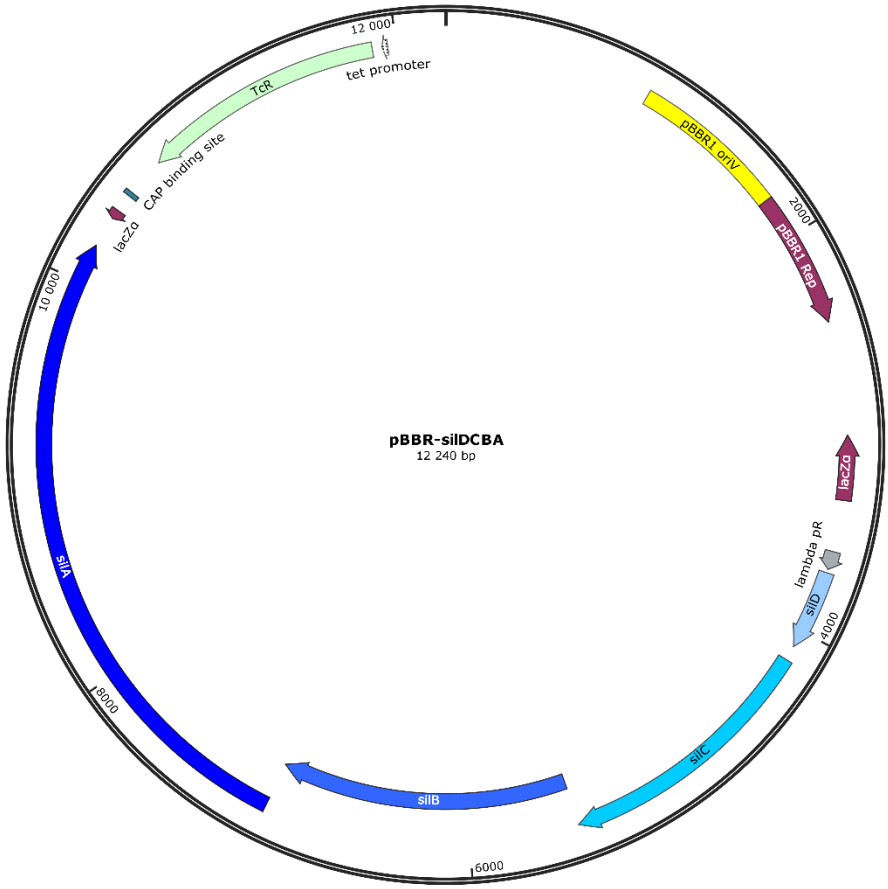
pBBR-silDCBA
12 240 bp
12 000
tet promoter
TcR
CAP binding site
lacZo
10 000
silA
8000
silB
6000
silC
4000
silD
lambda PR
lacZo
2000
pBBR1 Rep
pBBR1 oriV

Construction of pSCK108-*silY*

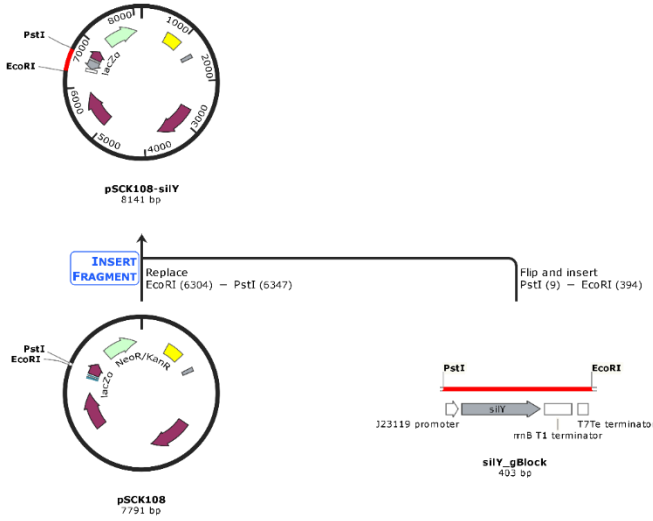

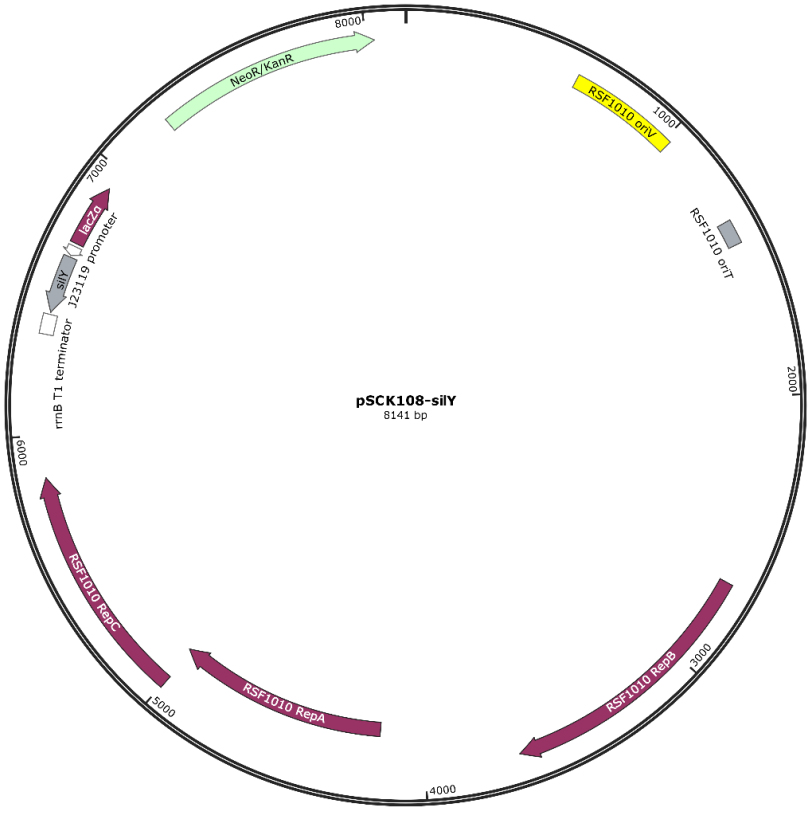

Construction of pGLR2-P*silY*

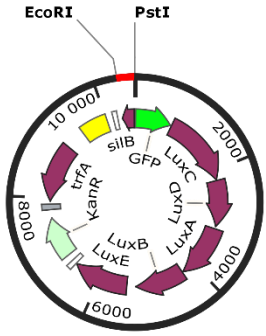

pGLR2-P_silY
10 557 bp

INSERT FRAGMENT

Replace
EcoRI (10 306) – PstI (10 349)

Insert
EcoRI (5) – PstI (250)

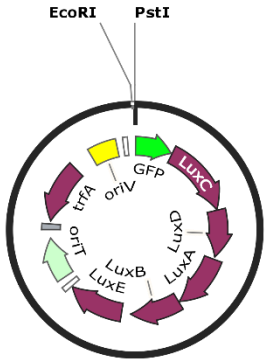

pGLR2
10 355 bp

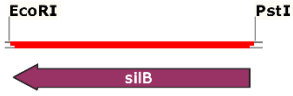

silY_upstream_region
255 bp

PCR

Amplify 4503 .. 4739 using:
pasRNA4_EcoRI_FW
pasRNA4_PstI_RV

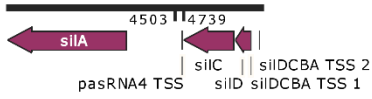

sil cluster
6830 bp

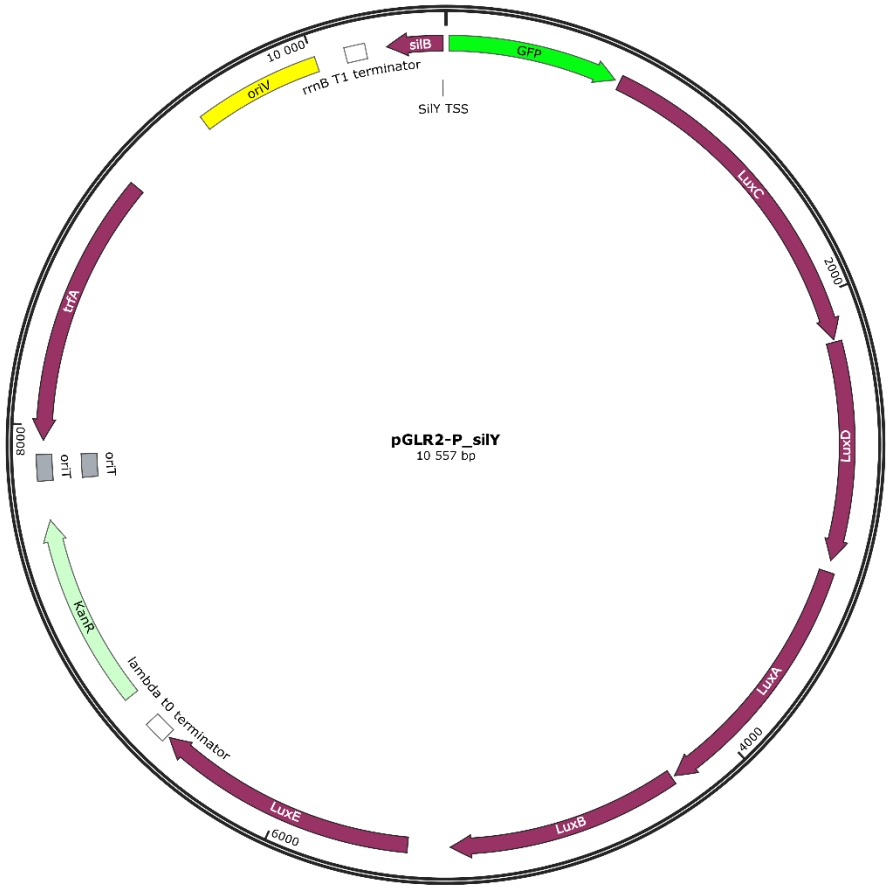
pGLR2-P_silY
10 557 bp
10 000
silB
GFP
rrnB T1 terminator
SilY TSS
oriV
LuxC
2000
LuxD
LuxA
4000
LuxB
LuxE
6000
lambda t0 terminator
KanR
oriT
oriT
8000
trfA

Construction of pK18mob-IGR$_{3492-3493}$::*tet*

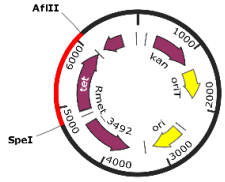

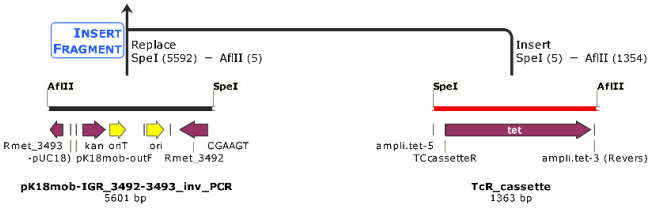

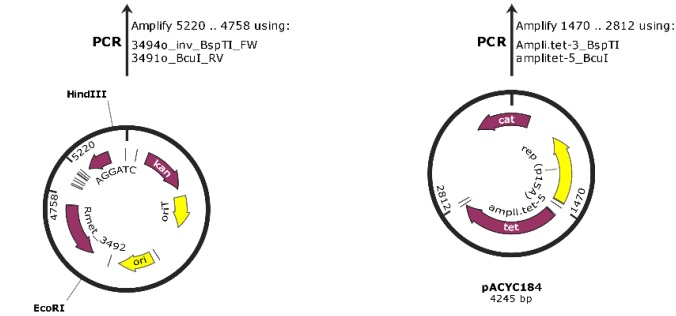

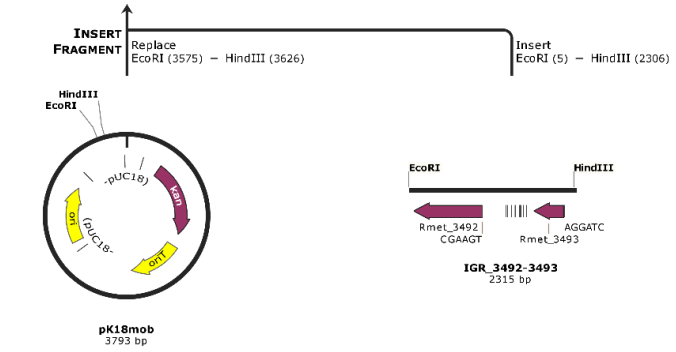

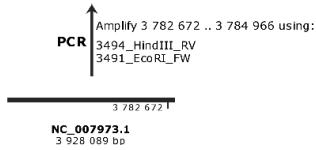

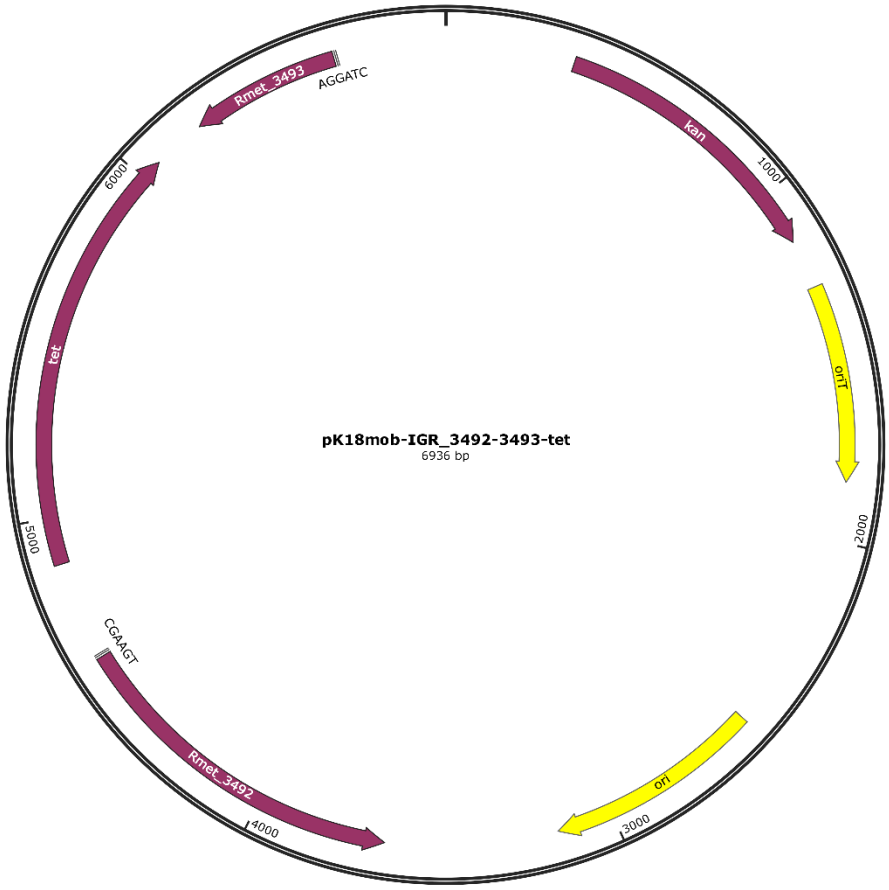
pK18mob-IGR_3492-3493-tet
6936 bp
Rmet_3493
AGGATC
kan
1000
oriT
2000
ori
3000
Rmet_3492
CGAAGT
4000
5000
tet
6000

CHAPTER 5 Case study in *Caulobacter crescentus*: impact of the environment on copper toxicity*

5.1 Introduction

Copper (Cu) is an essential micronutrient for all living organisms, but elevated intracellular concentrations can quickly lead to toxic effects. Thus, it is imperative to maintain a strictly controlled Cu ion homeostasis. Elevated Cu ion concentrations in the environment can originate from both natural and anthropogenic sources, with the latter including sources such as mining, smelting, domestic waste emission, and pesticide runoff [415]. Since Cu contamination in the environment is a growing issue, it is necessary to gain a thorough understanding of the biological response to this stressor. Microorganisms can also come into contact with toxic Cu ion concentrations in macrophages, which use the metal to combat invading microbes [416]. Finally, new Cu-based antimicrobial therapies are in development as alternatives for traditional organic antibiotics [30]. Overall, the influence of a variable environment on the microbial Cu stress response remains elusive.

Recent studies have asserted a large diversity of cellular targets of Cu toxicity. Giachino and Waldron [38] emphasized the impact on the cell envelope, where Cu ions interfere with peptidoglycan and lipoprotein maturation [43, 44]. In addition, Cu ions can displace other metals from binding sites in proteins [417, 418]. Especially solvent-exposed Fe-S clusters could be vulnerable to this aspect of toxicity [53]. Finally, Lemire et al. [42] highlighted the role of oxidative stress following the generation of reactive oxygen species (ROS) from the rapid intracellular cycling between Cu^{+} and Cu^{2+} [51, 52].

* This chapter is based on the following publication: Maertens, L., Cherry, P., Tilquin, F., Van Houdt R., and Matroule, J.Y. (2021). Environmental Conditions Modulate the Transcriptomic Response of Both *Caulobacter crescentus* Morphotypes to Cu Stress. Microorganisms 9: 6.

Bacteria have evolved several distinct defense systems against toxic Cu ion concentrations. Nies and Silver [419] distinguished six general metal resistance strategies, of which active ion export from the cytoplasm and periplasm, sequestration, and enzymatic alteration of the toxic ion are most prevalent. Indeed, these strategies have all been found to play their roles in bacterial Cu ion homeostasis, though not necessarily all in the same species. Cu^{+} export from the cytoplasm is achieved by P-type ATPases such as CopA [420]. In addition, heavy metal efflux-resistance nodulation cell division (HME-RND) systems such as CusCBA and SilCBA have been described to play a role in removing intracellular Cu^{+} ions [54, 421, 422]. Chaperones such as CopZ are involved in intracellular Cu^{+} sequestration, while multi-copper oxidases such as CueO oxidize Cu^{+} to the less toxic Cu^{2+} ion [105, 423, 424]. An overview of bacterial Cu ion resistance mechanisms can be found in Gillet et al. (2019) [425].

Caulobacter spp. have been isolated from highly diverse environments, such as metal-contaminated sites, including deep subsurface sediments and a gold mine [426-428]. *Caulobacter crescentus* has been studied intensively for its asymmetric cell division, controlled by four disparate regulators and comprising multiple morphotypes. Briefly, the stalked (ST) morphotype carries a polar stalk with a holdfast protein, enabling physical attachment to surfaces. This ST morphotype can initiate cell division, resulting in the generation of a daughter cell of the swarmer (SW) morphotype. The SW morphotype is motile by a polar flagellum and pili, and is itself unable to divide. It then matures into a ST cell, and cell division can start anew. In the laboratory strain *C. crescentus* NA1000, metal resistance mechanisms against Cd^{2+}, Cr^{6+}, U^{6+} and Cu^{2+} have been detected [429]. We showed before that *C. crescentus* NA1000 employs a bimodal response to Cu stress, where the ST morphotype relies strongly on the PcoAB system for detoxification, while the SW morphotype favors a negative chemotaxis to escape toxic Cu concentrations [117].

Prior studies have highlighted important features of the Cu stress response in *C. crescentus* NA1000, but a genome-wide response has not yet been examined. In addition, there is currently a lack of knowledge about the role of environmental conditions such as culture medium on the Cu stress response. This is especially relevant since *Caulobacter* species have been isolated from diverse environments, often with dissimilar chemical makeup. We opted to study *C. crescentus* to enable comparison to the much more Cu-resistant *C. metallidurans*. Both strains are routinely detected in oligotrophic conditions (and aboard the ISS). In addition, much

more transcriptomic data is available for *Caulobacter*, enabling validation of our newly developed analysis techniques. Here, we performed tagRNA-seq, which allows for differential gene expression analysis as well as the accurate delineation of transcription start sites, of synchronized SW and ST NA1000 cells stressed by sub-lethal Cu concentrations in a mineral medium (M2G) and a complex medium (PYE).

5.2 Materials and methods

5.2.1 Bacterial strains and growth conditions

C. crescentus NA1000 and a *sigF*::Tn*5* mutant (lab collection) were routinely cultured in either PYE medium or M2G medium at 30 °C on an orbital shaker at 180 rpm [430]. Growth in the presence of Cu was evaluated by diluting exponential growth phase cultures to a final optical density of 0.05 at 660 nm (OD_{660}) in either PYE or M2G medium containing different $CuSO_4.5H_2O$ concentrations and recording OD_{660} every 10 min for 24 h at 30 °C under continuous shaking in an Epoch 2 absorbance reader (BioTek Instruments Inc., Winooski, VT, USA).

5.2.2 Synchronization and RNA extraction

For experiments with PYE medium, NA1000 overnight cultures in PYE medium were diluted in fresh PYE medium to an OD_{660} of 0.1 and allowed to grow to an OD_{660} of 0.4. Bacterial cultures were synchronized in order to isolate the swarmer fraction of cells [431], which was verified by light microscopy. The isolated swarmer cell suspension was diluted to an OD_{660} of 0.4 with PYE medium, and divided into four equal volumes. To one volume, a $CuSO_4$ solution was added to a concentration of 175 µM, while to a second volume, an equivalent amount of H_2O was added. After 10 min at 30 °C, these suspensions were centrifuged for 3 min at 8000 g and the resulting cell pellets were flash frozen. The two remaining volumes were allowed to grow at 30 °C for 40 min to enable differentiation to the stalked cell type, which was verified by light microscopy. Then, to one volume a $CuSO_4$ solution was added to a concentration of 175 µM, while an equivalent amount of H_2O was added to the other volume. After 10 min at 30 °C, these stalked cell suspensions were pelleted and flash frozen as described above (Figure 5-1). For experiments with M2G, an identical protocol was followed, but $CuSO_4$ concentrations were decreased to 15 µM and swarmer cell differentiation time was increased to one hour. These adaptations were required to achieve similar phenotypic effects in both media (Figure 5-1).

The resulting cell pellets were flash frozen until resuspension in 40 µL of a 20 mg/mL proteinase K solution (Avantor®, Radnor, PA, USA) with 1 µL of undiluted Ready-Lyse Lysozyme solution (Lucigen®, Middlesex, UK), and lysis was allowed to proceed for 10 min in a shaking incubator at 37 °C and 600 rpm. Total RNA was retrieved from the cell suspensions using the *mir*Vana miRNA Isolation kit (Invitrogen™, Carlsbad, CA, USA). RNA integrity was verified by running the samples on an Agilent 2100 Bioanalyzer Nano chip (Agilent, Machelen, Belgium), and only samples with RIN values above 9 were accepted for sequencing.

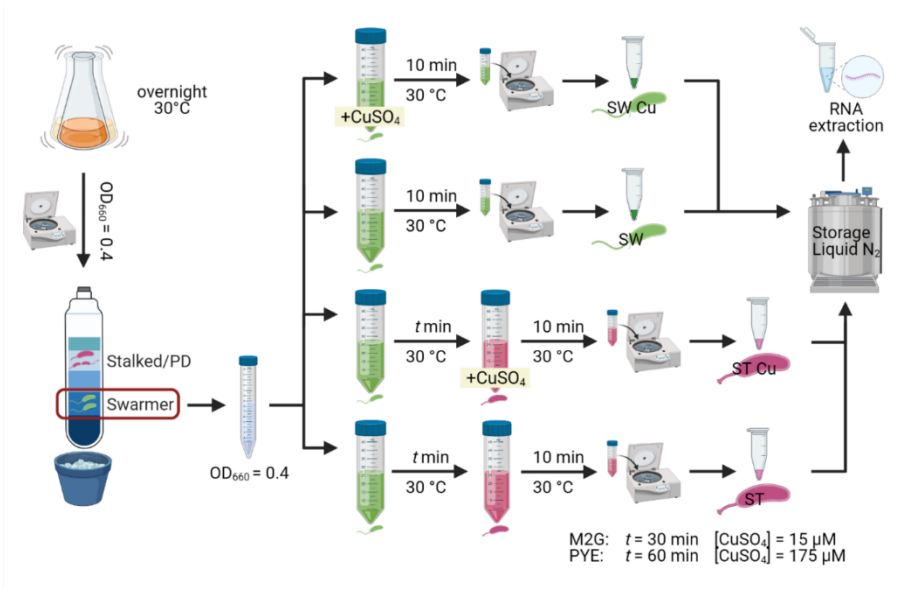

Figure 5-1. Overview of tagRNA-seq experimental setup.

5.2.3 Differential RNA sequencing and read mapping

A modified tagRNA-seq protocol was performed by Vertis Biotechnologie AG, Germany, as described in chapter 3 [116]. Because of the different sequencing adapters in combination with RNA fragmentation, 3 read libraries were acquired for every sample. One library contained all reads originating from the 5′ end of 5′ monophosphate group RNA molecules (processing start sites, PSS reads), a second library contained all reads originating from the 5′ end of 5′ triphosphate group RNA molecules (transcription start sites, TSS reads), and a third library contained all reads from non-tagged RNA (mostly resulting from RNA fragmentation after differential adapter tagging). Trimmomatic version 0.36 [327] was used to remove adapter sequences from all three read libraries, resulting in unpaired reads of 55–75 nt. Read

quality was evaluated with FastQC (version 0.10.0; https://www.bioinformatics.babraham.ac.uk/projects/fastqc/, accessed April 1, 2020). Trimmed reads were then aligned to the *C. crescentus* NA1000 reference genome (NCBI accession number CP001340) with bwa version 0.7.12 [432], using default parameters. Reads mapping to multiple loci were removed from their respective libraries. The RNA-seq datasets generated and analyzed for this study are available from the NCBI Sequence Read Archive (SRA) under accession number PRJNA721587.

5.2.4 Differential gene expression analysis

For every sample, reads from PSS, TSS, and unassigned libraries were compiled into one composite library. Read coverage counts were calculated with the featureCounts function of the Rsubread package for R [330], and subsequently normalized using the TMM method [433]. Options—isStrandSpecific was set to TRUE, and otherwise standard options were used. Differential expression was calculated using edgeR and limma [331-333], with the *treat* method used in addition (lfc = 1) [434]. Genes were found to be differentially expressed if they showed an FDR value lower than 0.05 and a $\log_2$ fold change (logFC) value either higher than 1 or lower than -1. TSSs were detected using a Python script, as previously described [116]. Principal component analysis was performed using the prcomp function in R, with options 'scale' and 'center' set to TRUE, and with the normalized read counts from featureCounts as input.

5.2.5 Reverse trancription quantitative real-time PCR

RNA (2 µg) isolated from synchronized *C. crescentus* was incubated with DNAse I (Thermo Scientific, Merelbeke, Belgium) for 30 min at 37 °C. DNAse I was then inactivated with 50 mM EDTA for 10 min at 65 °C. Subsequently, RNA was subjected to reverse transcription using MultiScribe Reverse Transcriptase (Applied Biosystems®, Foster City, CA, USA) with random primers (as described by the manufacturer). A total of 300 ng of cDNA was mixed with Takyon No Rox SYBR MasterMix dTTP Blue (Eurogentec, Seraing, Belgium) and the appropriate primer sets (Table 5-1) and used for qPCR in a LightCycler96 (Roche, Basel, Switzerland). Forty-five PCR cycles were performed (95 °C for 10 s, 60 °C for 10 s and 72 °C for 10 s). Primer specificity was checked by melting curves analysis. Relative gene expression levels between different samples were calculated with the $2^{-\Delta\Delta Ct}$ method, using the *mreB* gene as a reference. Three technical replicates were analysed for each sample.

Table 5-1. Primers used for qPCR.

Name	Sequence
mreB_F	CATCGAGGCCAAGCAGATGC
mreB_R	AGCCCTTGCGGTTGTGAACC
pcoB_F	CGCCCTATTGGTTCGAGCTG
pcoB_R	GTTGCAGGATCAGCCTCTGG
CCNA_00028_F	ATAGTTGGTGAACGCCCAGG
CCNA_00028_R	ACGATCGCTACGAGAGCAAG
CCNA_00140_F	GATGGATCCCATCCTGGGGA
CCNA_00140_R	AGAACCACAGCTTATGGCCC
CCNA_01010_F	CCAGGACCCCTACTGCCT
CCNA_01010_R	GAAGATCAGCGGATTGTCCGA

5.2.6 Data visualization

Figure 5-1 was created with biorender.com. Figure 5-2 was created with Veusz 3.3.1 based on data generated with the growthcurver package [435]. Figure 5-3 was created with Veusz 3.3.1 based on data generated with the prcomp function for the R project for statistical computing and the car package [436]. Figure 5-4 was created with the ComplexHeatmap package [437], using the internal k-means clustering method at row level. Figure 5-5 was generated with Inkscape v1.0.1. Figure 5-7 was created with Veusz 3.3.1 based on data generated with the growthcurver package [435]. Figure 5-8 was constructed with the STRING database output [438] that was color coded using Cytoscape 3.8.2 and combined using Inkscape 1.0.1.

5.3 Results and discussion

5.3.1 Growth of C. crescentus in the presence of Cu

The effect of Cu on the growth of *C. crescentus* in M2G and PYE medium was compared via biomass accumulation after 24 h (Figure 5-2). It is immediately clear that more $CuSO_4$ must be supplemented to the complex PYE medium to achieve similar deleterious effects. Interestingly, there seems to be a hormesis effect of $CuSO_4$ supplementation in M2G medium for 5 and 10 µM of Cu (p-value = 0.034 and 0.002, respectively). The Cu concentration for the subsequent transcriptome study were chosen to elicit a “moderate stress” in both media.

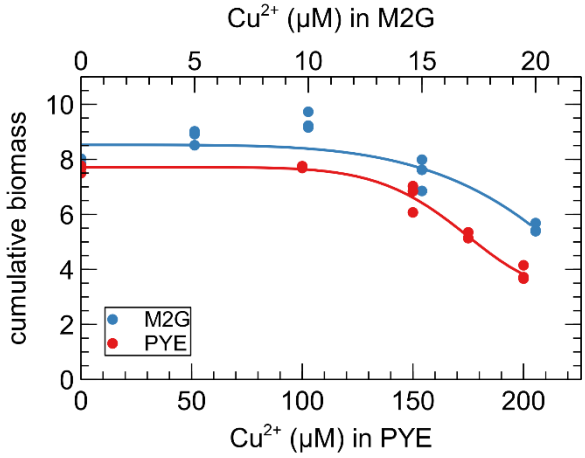

Figure 5-2. Effect of $CuSO_4$ concentration on the growth of *C. crescentus* in PYE (red) and M2G (blue) medium. Cumulative biomass (time x OD_{660}) is the empirical area under the growth curve (0–24 h) for three biological replicates. A four-parameter Weibull distribution was used for non-linear regression.

5.3.2 Read coverage analysis

In order to study the effects of growth conditions on the response of both morphotypes to sub-lethal Cu stress, we performed tagRNA-seq on Cu-exposed and unexposed SW and ST cells grown in M2G and PYE medium. On average, 11,289,879 reads were generated for every sample. Of these reads, ca. 14.7 % were derived from the 5′ end of primary transcripts (transcription start sites, TSS), 17.7 % from the 5′ end of processed transcripts (processing sites, PSS), and the remainder of reads from transcripts not derived from 5′ ends (unassigned) (Table 5-2). For most of the analyses, the different read libraries (TSS, PSS, and unassigned) were combined. This generated triplicates of eight data sets: two growth media (complex PYE medium and mineral M2G medium), two cell types (ST: stalked cells, SW: swarmer cells) and two conditions (Cu exposed and unexposed).

Table 5-2. Raw read counts of tagRNA-Seq libraries.

Sample				Unassigned	TSS	PSS	Total
M2G	St	Cu	1	7029956	941625	1996589	9968170
			2	6493672	772038	1343006	8608716
			3	5637679	804827	1432578	7875084
		Ct	1	6555009	742017	1496397	8793423
			2	7052540	800345	1684963	9537848
			3	6574748	801229	1740855	9116832
	Sw	Cu	1	8011110	1100154	2198595	11309859
			2	6211153	909899	1597453	8718505
			3	5336313	685777	1557530	7579620
		Ct	1	6221880	684872	1911990	8818742
			2	6651033	840671	1689593	9181297
			3	6777805	572727	1195243	8545775
PYE	St	Cu	1	7700765	2759732	1875608	12336105
			2	8225721	2959976	2319953	13505650
			3	8770754	2715491	2418996	13905241
		Ct	1	9130811	2447386	2087056	13665253
			2	8637565	2408231	2113804	13159600
			3	8409195	2472966	2020761	12902922
	Sw	Cu	1	8585751	3735415	2590338	14911504
			2	8272520	3076795	2754637	14103952
			3	8643418	2838859	2561540	14043817
		Ct	1	8530708	2490665	2371096	13392469
			2	7731070	2765604	2252039	12748712
			3	8850095	2783986	2593916	14227997

Principal component analysis (PCA) on all combined read libraries indicated, as expected, that the three main principal components correlated with culture medium, cell type and Cu stress, in decreasing order of explained variation (Figure 5-3). In addition, it is clear that the impact of Cu stress is more pronounced in M2G than in PYE, and for ST cells than SW cells. Nevertheless, the PCA indicates that a moderate Cu stress has a smaller impact on the transcriptome than cell differentiation or growth conditions.

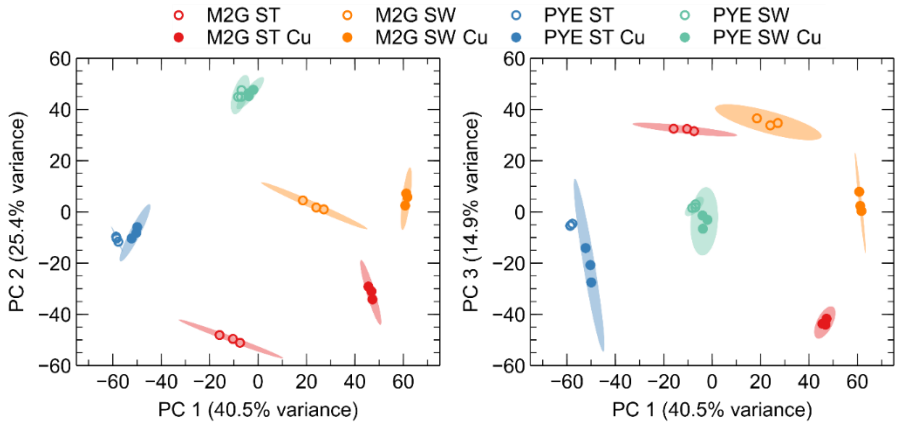

Figure 5-3. Principal component analysis (PCA) of the log2-transformed normalized gene expression values between the different control (open symbols) and Cu-treated (closed symbols) *C. crescentus* samples in M2G and PYE medium. PCA plots show the variance of the three biological replicates with 95% confidence level (colored ellipses). The percentages on each axis represent the percentages of variation explained by the principal components.

The top-2000 genes with the highest variability in read coverage between all conditions were selected (out of a total of 4085 genes) for K-means clustering (Figure 5-4). This analysis showed that clusters 2, 4, 5, 6, 7, and 8 correlated with cell type (987 genes total), while clusters 1, 3, 9, 10, and 11 correlated with medium (596 genes total). Clusters 12, 13, 14, and 15 correlated with Cu stress (417 genes total). While it would be possible to discern gene-enriched pathways from these Cu stress-correlated clusters, we have opted to analyze and compare functional enrichment from all Cu-CT contrasts separately in order to attain a comprehensive analysis.

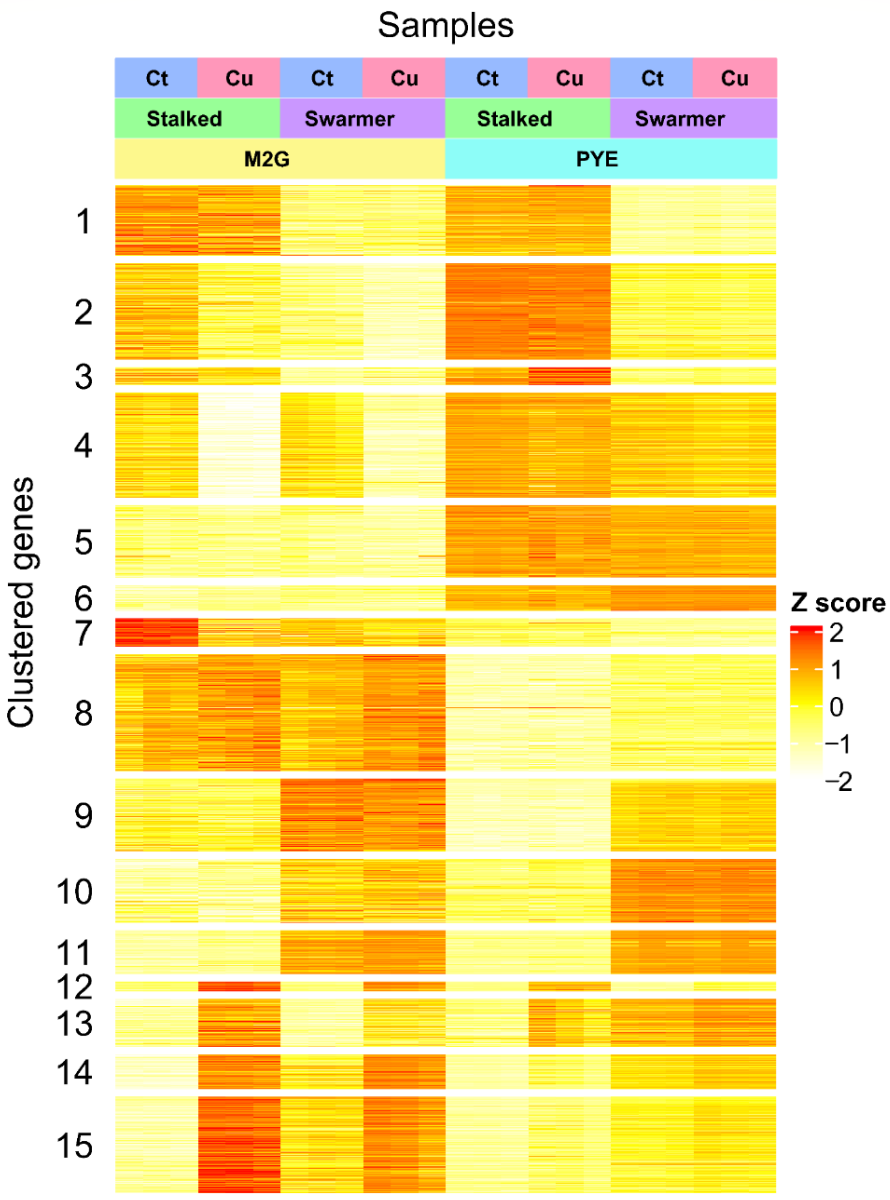

Figure 5-4. Read coverage heatmap of the 2000 most variable genes in 15 clusters. Z scores were calculated by subtracting row-average value from corresponding cell value and dividing by row standard deviation. Fifteen gene clusters were created by K-means clustering. Experimental conditions: Cu stress (blue), no Cu stress (red); cell type: stalked cells (green), swarmer cells (purple); medium: M2G medium (yellow), PYE medium (teal).

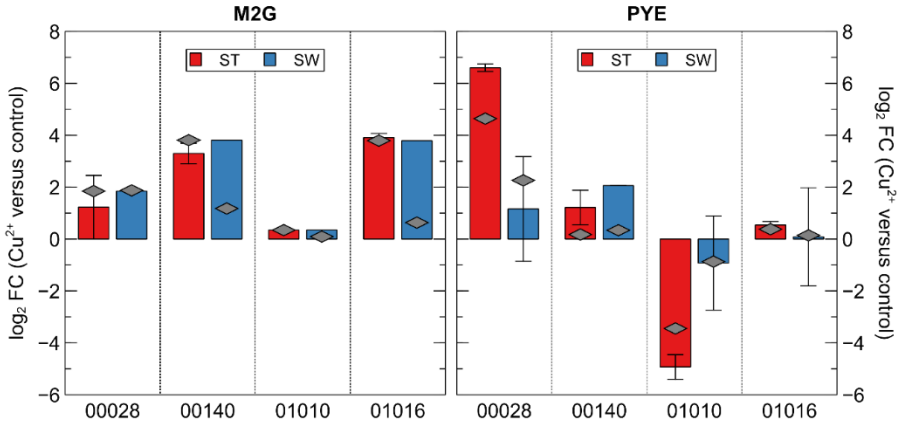

Figure 5-5. Differential expression of 4 selected genes, in stalked cells (ST) and swarmer cells (SW) in 2 culture media (M2G and PYE). Bars represent log2 fold change values from qRT-PCR data, with diamonds representing log2 fold changes calculated with tagRNA-seq. CCNA accession numbers are shown at the bottom.

5.3.3 Transcriptomic response of *C. crescentus* to Cu stress

Differentially expressed genes were calculated for all Cu-CT contrasts, several of which were validated with qRT-PCR (Figure 5-5). It is immediately clear that the transcriptomic response to Cu stress was more pronounced in mineral M2G than in the complex PYE medium, and in ST cells than in SW cells (Figure 5-5). ST cells in M2G medium showed the strongest transcriptional response to acute Cu stress. Out of 4085 genes, 1006 were differentially expressed and four (out of 20) eggNOG classes were enriched, i.e., class C (energy production and conversion), J (translation, ribosomal structure and biogenesis), O (posttranslational modification, protein turnover, chaperones) and V (defense mechanisms), with class O displaying the largest enrichment (Table 5-3). The transcriptome of the SW cells in M2G medium was less strongly affected by Cu stress than their ST counterparts, and 270 out of 382 (71%) of up- or downregulated genes were also up- or downregulated in the ST cells (Figure 5-6). In complex PYE medium, the number of upregulated genes in ST cells was much higher than the number of downregulated genes, in response to Cu stress (Figure 5-6). In this contrast, only eggNOG class P, related to inorganic ion transport and metabolism, was overrepresented. SW cells in PYE medium were affected the least by Cu stress, and only class U, related to intracellular trafficking, secretion, and

vesicular transport, was overrepresented. An overview of the functional roles of differentially expressed genes is shown in Table 5-4.

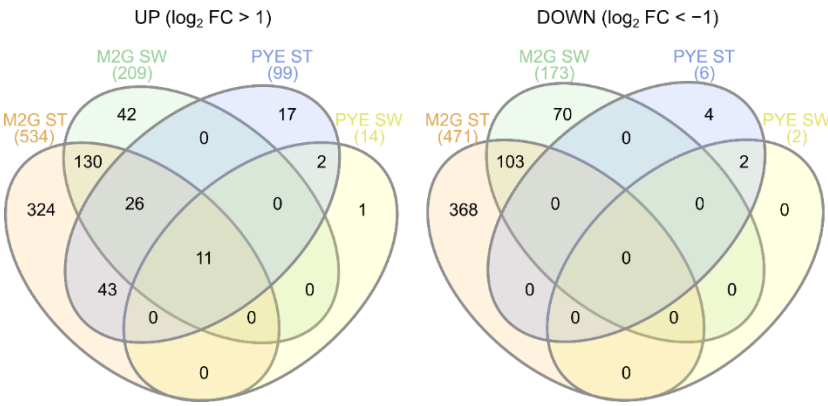

Figure 5-6. Venn diagrams showing overlap between upregulated (left) and downregulated (right) genes upon Cu stress in all experimental conditions.

Table 5-3. Overrepresented eggNOG classes calculated from the differential expression analysis of several tagRNA-seq contrasts.

Contrast	Overrepresented eggNOG class		p-value
MStCu-MStCt	O	Posttranslational modification, protein turnover, chaperones	$5.98*10^{-104}$
	J	Translation, ribosomal structure and biogenesis	$6.49*10^{-28}$
	C	Energy production and conversion	$7.26*10^{-5}$
	V	Defense mechanisms	$2.58*10^{-3}$
MSwCu-MSwCt	O	Posttranslational modification, protein turnover, chaperones	$3.29*10^{-3}$
	V	Defense mechanisms	$1.99*10^{-2}$
PStCu-PStCt	P	Inorganic ion transport and metabolism	$3.13*10^{-8}$
PSwCu-PSwCt	U	Intracellular trafficking, secretion, and vesicular transport	$6.11*10^{-3}$
MCt-PCt	E	Amino acid transport and metabolism	$9.84*10^{-36}$
	T	Signal transduction mechanisms	$7.33*10^{-14}$
	G	Carbohydrate transport and metabolism	$8.04*10^{-5}$
	N	Cell motility	$2.02*10^{-2}$
	P	Inorganic ion transport and metabolism	$3.65*10^{-2}$
	F	Nucleotide transport and metabolism	$4.77*10^{-2}$

Table 5-4. Overview of functional roles of differentially regulated genes in all Cu-CT contrasts.

Pathway or Functional Relation		M2G ST		M2G SW		PYE ST		PYE SW	
		↑	↓	↑	↓	↑	↓	↑	↓
Metal resistance mechanisms		19	0	5	0	6	1	0	0
Proteases and peptidases		32	9	13	6	4	0	0	0
Ribosome synthesis		2	78	0	24	0	0	0	0
ATP synthesis		0	10	0	6	0	0	0	0
sRNAs		16	0	3	1	5	1	0	0
Antibiotic resistance		12	3	5	1	0	0	0	0
Chaperons		13	2	5	2	0	0	0	0
Transporters	ABC transport	18	4	9	3	1	0	0	0
	TonB-dependent receptors	6	10	2	4	4	2	1	0
	Other	19	19	2	9	4	0	3	0
Regulators	Known function	19	19	6	13	6	2	1	0
	Other	33	16	11	3	4	0	1	0
Amino acid metabolism	Methionine biosynthesis	0	4	0	0	0	0	0	0
	Cysteine biosynthesis & S assimilation	8	2	0	0	1	3	0	0
	Arginine biosynthesis	1	7	1	5	0	0	0	0
	Serine biosynthesis	2	7	1	1	0	0	0	0
	Histidine	2	1	0	0	4	0	1	0
Redox and oxidative stress-related	Radical removal & antioxidants	16	2	11	0	4	0	2	0
	Glutathione cycle	7	2	2	1	0	0	0	0
	Other	37	39	14	5	7	0	2	0
Hypothetical proteins		73	33	48	23	22	2	2	0

5.3.3.1 A core gene-set in the response to Cu

Only 11 genes (9 of which are included in cluster 12; see Figure 5-4) were upregulated by Cu exposure irrespective of cell type or growth medium (Table 5-5). The CCNA_03273,03362-03366 cluster encodes uncharacterized cytoplasmic, membrane and periplasmic proteins regulated by the ECF sigma factor SigF (CCNA_03362) and the anti-sigma factor NrsF (CCNA_03273). In fact, the SigF

regulon includes, in addition to this cluster, the two other clusters that were commonly upregulated by Cu exposure [303] (Table 5-5). Transcription of this regulon has already been shown to be upregulated in response to chromate (CrO_4^{2-}) and cadmium (Cd), in an oxidative stress-independent manner [429]. However, a *sigF* mutant displayed a similar sensitivity profile to these metals [303], but showed a severely impaired resistance to oxidative stress during the stationary phase [439].

Table 5-5. List of genes upregulated by Cu stress in all tested conditions and cell types.

Locus Tag[1]	Gene Product	Log2 Fold Change			
		M2G		PYE	
		ST	SW	ST	SW
00028[$]	TonB-dependent receptor protein	1.85	1.87	4.64	2.26
02833	Sulfoxide reductase heme-binding subunit	5.32	4.18	3.13	1.84
02834	Sulfoxide reductase catalytic subunit	5.84	5.73	3.34	2.60
02999	DNA-binding domain-containing protein	5.03	4.32	3.24	2.04
03000	DUF692 domain-containing protein	5.94	5.77	3.63	2.80
03001	Hypothetical protein	5.67	6.21	3.17	2.00
03273	Anti-sigma factor NrsF	4.15	4.27	2.88	1.84 *
03362	ECF-family sigma factor SigF	4.44	4.70	2.78	2.17
03363	DUF2282 domain-containing protein	5.79	6.07	3.46	2.01
03364	DUF692 domain-containing protein	6.16	6.31	4.22	3.53
03365	Hypothetical protein	5.86	5.06	4.15	2.74
03366	DoxX-family protein	5.50	4.35	4.27	1.40 *
03372[$]	Bacterioferritin-associated ferredoxin	4.50	5.59	2.97	5.33

[1] Locus tag is preceded by CCNA_. [$] All genes except those marked with $ are under control of SigF. * Only significant ($p < 0.05$) on the basis of statistical testing without *treat* lfc cutoff (see Materials and Methods).

In contrast to CrO_4^{2-} and Cd^{2+}, *sigF* inactivation severely impacted the growth of *C. crescentus* in the presence of Cu, demonstrating a role of this regulon in Cu tolerance (Figure 5-7). Interestingly, this cluster has also been studied in *Cupriavidus metallidurans* CH34, a model organism for metal resistance, in which it was first named *dax* in Monsieurs et al. (2011) [115], and renamed *gig* for "gold-induced genes" in Wiesemann et al. (2013) [440]. The cluster is upregulated in the presence

of Au^{3+}, Ag^{+} and Cu^{2+} [116, 440]. In *C. metallidurans* CH34, it does not impact Cu resistance [440], but it should be noted that *C. metallidurans* CH34 carries multiple Cu resistance determinants that could mask its role.

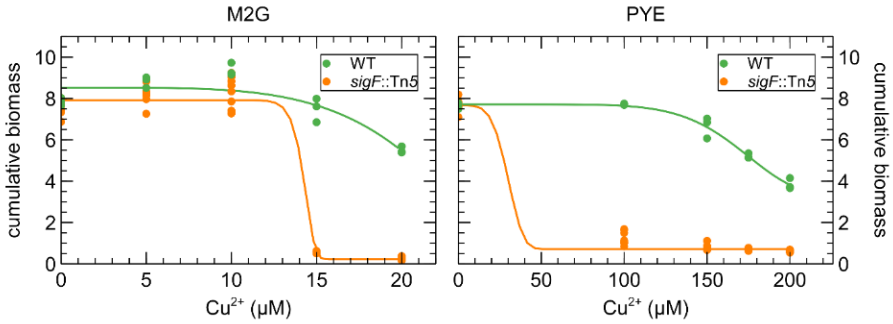

Figure 5-7. Effect of $CuSO_4$ concentration on the growth of *C. crescentus* (green) and a *sigF*::Tn5 mutant (orange) in M2G (left) and PYE (right) medium. Cumulative biomass (time x OD_{660}) is the empirical area under the growth curve (0–24 h) for three biological replicates. A four-parameter Weibull distribution was used for non-linear regression.

The SigF-regulated CCNA_02999-03001 cluster codes for uncharacterized proteins, but CCNA_03000 and CCNA_03001 share 44.5% and 38.5% protein similarity with CCNA_03364 and CCNA_003363, respectively. Finally, the SigF-regulated CCNA_02834-02833 cluster is homologous to the MrsPQ system, which is involved in the protection of proteins from oxidative stress by repairing oxidized periplasmic proteins containing methionine sulfoxide residues [441]. Although, the SigF regulon plays a central role in the Cu response, expression levels were not similar across the different conditions. When exposed to Cu, expression in ST cells was higher than in SW cells when grown in PYE but not in M2G, and expression in M2G was higher than in PYE for both ST and SW cells. In unexposed conditions, the expression level of the SigF regulon did not significantly differ between cell types and growth medium.

The CCNA_00028 gene, encoding a TonB-dependent receptor, and CCNA_03372, encoding a bacterioferritin-associated ferredoxin, are both also upregulated under iron (Fe)-limiting conditions and repressed by Fur under Fe sufficiency [442], but their actual role is currently under investigation. However, as Fur has an important role in oxidative stress tolerance [442-445], their increased expression could be elicited in response to and to cope with oxidative stress generated by Cu.

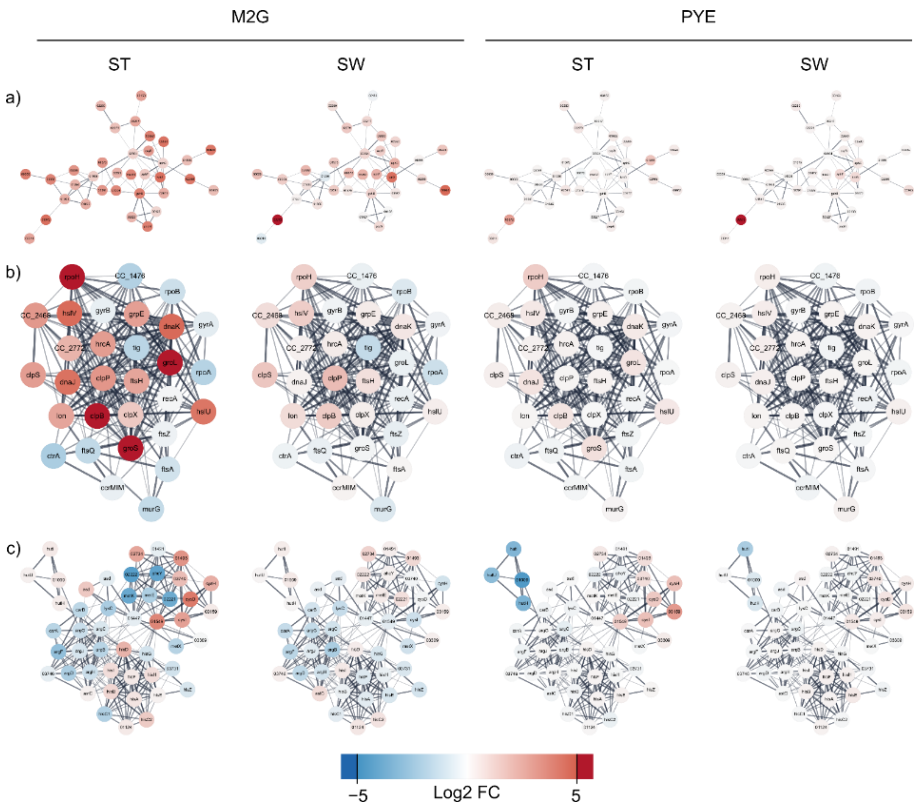

Figure 5-8. Analysis of interacting gene networks related to oxidative stress (**a**), protein misfolding, proteome rearrangement and chaperones (**b**), and the amino acid metabolism (**c**) of the *C. crescentus* differentially expressed gene dataset. Color coding is based on log2 fold change in Cu stress.

5.3.3.2 Oxidative stress

Next to this core gene set, many genes upregulated by Cu stress in mineral M2G medium are involved in oxidative stress relief, a response that was not observed in complex PYE medium (Figure 5-8). This impact of ROS toxicity is reflected in the upregulation of catalase, two superoxide dismutases, and several hydroperoxide reductases, thioredoxins and glutaredoxins. In addition, the biosynthesis pathway of glutathione, an important antioxidant with a central role in cellular ROS protection, was strongly upregulated. OxyR, a major regulator of the oxidative stress response, was upregulated in both SW and ST cells. In *C. crescentus*, OxyR has been shown to control the expression of the catalase KatG and the alkyl hydroperoxidase system AhpCF [442, 445]. Oxidative stress induction by Cu exposure has been described in

several bacteria [116, 200, 366, 367, 446-450]. Interestingly, Cu shock, but not adaptation, was linked to the oxidative stress response in *Pseudomonas aeruginosa* [451].

The origin of Cu-induced oxidative stress is still a matter of debate [38]. While the cycling of Cu^{+} and Cu^{2+} has been linked to ROS formation, it has also been posited that the Cu-mediated destruction of enzymatic Fe-S clusters could result in the release of free Fe ions to the cell [51, 52, 128], which can cycle between divalent and trivalent forms to generate ROS via the Fenton reaction [53]. This mechanism of toxicity can also be observed in the oxidative stress response to non-redox-active metals such as Cd^{2+} [429]. Conversely, Fe starvation has also been linked to oxidative stress [452]. In this study, Cu stress had a notable impact on the expression of many Fe-S cluster-containing, redox-active enzymes such as cytochromes, cytochrome oxidases, and NADH quinone oxidoreductase components. However, with the current data, it is difficult to determine whether these enzymes are differentially regulated due to direct toxic effects of Cu, or due to their involvement in ROS detoxification. We note, however, that expression of the bacterioferritin Dps, which plays a role in oxidative stress response by storing free Fe ions [453], was not induced by Cu stress in any of the tested media or cell types. In addition, the bacterioferritin Bfr was downregulated during Cu stress, but only in ST cells in M2G medium. Consequently, the measurable effects of free Fe ions on oxidative stress seem relatively small. A final aspect of Cu-induced oxidative stress is evidenced by the upregulation of glutathione biosynthesis. Glutathione can reduce oxidized glutaredoxins, which serve as antioxidants. Both glutathione and thioredoxin have been shown to play a role in cell cycle regulation, and their concentrations vary between different growth phases [454, 455]. However, Cu can also form a catalytic complex with glutathione, generating additional ROS instead of depleting them [456].

In PYE medium, no evidence of oxidative stress response was detected in either cell type, except for the upregulation of three sulfoxide reductase subunits in the ST cells, and two in the SW cells. We conclude that Cu exposure generates more oxidative stress in M2G than in PYE, despite comparable effects on growth. In addition, the oxidative stress response is more extensive in ST cells than in SW cells.

5.3.3.3 Protein misfolding and proteome rearrangement

A wide array of chaperones, such as DnaK, DnaJ and several of their homologs, were upregulated by Cu stress in M2G medium. Interestingly, while depletion of DnaK has

been linked to an increase in RpoH abundance, both were strongly upregulated by Cu stress, indicating additional factors in their regulation. RpoH in turn has been linked to the control of heat shock chaperones, the upregulation of repair and maintenance functions, and the downregulation of growth and DNA replication [457, 458]. The chaperones GroEL and GroES were upregulated by Cu exposure in M2G and have been associated with oxidative, saline, and osmotic stresses [459] (Figure 5-8). The dual-function holdase and thioredoxin oxidoreductase CnoX, which transfers unfolded proteins to DnaK/J and GroEL/ES, was also upregulated by Cu exposure in M2G [460]. In addition, general proteases such as the Clp, Hsl, and Lon complexes were upregulated. Cu and oxidative stress can lead to the production of toxic protein precursors and stress-denatured proteins [45, 461]. The response to protein misfolding was also observed after general metal stress in *C. crescentus* [462]. Since proteotoxic stress can induce cell-cycle arrest, it is vital for the cell to overcome [463]. In this sense, it is interesting to note that the proteases FtsH and ClpXP are involved in regulatory processes and cell cycle progression [439, 464-468]. In addition, the Lon protease allows *Caulobacter* cells undergoing proteolytic stress to maintain replicative ability [469]. It is also indirectly involved in cell cycle regulation since it can degrade the regulatory protein SciP [470]. Finally, we observed a general downregulation of translation, ribosomal structure and biosynthesis. This was evident from the observation that 79 genes out of 186 in eggNOG class J were downregulated, while only 7 were upregulated. Curiously, this observation was only made in ST cells in M2G medium, indicating again that this population is more responsive to Cu stress. In conclusion, these data illustrate a shift in the proteome and accumulation of misfolded proteins due to Cu stress.

In ST cells in PYE, several proteases were slightly overexpressed, indicating some level of proteome rearrangement. Two genes encoding homologs of the dual-function chaperone/protease DegP-family serine protease were upregulated, as well as a trypsin-like serine protease. No evidence for Cu stress-induced proteome rearrangement was detected in SW cells in PYE medium. As a whole, the proteome of *C. crescentus* cells was far less affected by Cu stress in PYE medium than in M2G medium.

5.3.3.4 Metal resistance and transport systems

Lawarée et al. (2016) [117] showed that the PcoAB system represents the main mechanism for Cu detoxification in *C. crescentus*. This system consists of the periplasmic Cu^{+} oxidase PcoA and the outer membrane Cu efflux pump PcoB. *pcoAB*

transcription was observed during the SW-to-ST cell transition and was hardly induced by Cu in HIGG medium [117]. Seemingly, the induction of this system depends on both medium and cell type, as it was only induced by Cu stress in ST cells in M2G, but not at all in PYE.

C. crescentus also encodes additional metal tolerance clusters, some of which were induced by Cu stress. We measured a strong overexpression of the arsenic (As) resistance determinant ArsH and the arsenate reductase CCNA_01571. A similar upregulation of *ars* genes was observed after Cu exposure in *Cupriavidus metallidurans* CH34, but this phenomenon was not further analyzed [116]. However, some aspects of toxicity, such as ROS generation, are shared between Cu^{2+} and As^{3+} [471]. Such commonalities might also link the transcriptomic response to these metals. Likewise, upregulation of the tellurium (Te) resistance genes *terB*, *terC*, and CCNA_00755 was observed. Much like Cu^{2+} and As^{3+}, Te^{4+} toxicity is characterized by oxidative stress [472]. While As and Te resistance determinants were induced in both cell types in M2G, the entire *czc*-like *nczCBA* cluster (CCNA_02471-02473) was induced by Cu stress only in ST cells in M2G. This gene cluster confers resistance to nickel and cobalt, and to a lesser degree to zinc (Zn) and Cd [473]. Likewise, the *czr* cluster (CCNA_02806-02811), consisting of an HME-RND export system and a P-type ATPase, was fully upregulated in ST cells in M2G. This cluster mainly confers resistance to Cd and Zn [473].

In agreement with Park et al. [474], the genes encoding the U/Zn/Cu responsive two-component regulatory UzcRS were induced by Cu stress in M2G. Although this regulatory system is responsive to U, Zn and Cu, it is not required for tolerance to these metals. Its regulon contains many genes involved in envelope stress response and several (antibiotic) transport systems, as well as a small regulatory RNA [474]. Indeed, 63 out of the 73 genes in the UzcRS regulon were differentially expressed in ST cells vs. 43 genes in SW cells. In addition, in M2G, transcription of the two-component system ChvGI, which is stimulated by starvation, prolonged DNA damage, acidic pH and cell wall stress, was also upregulated in response to Cu. ChvGI activates the ChvR sRNA (its expression was also upregulated with Cu), which in turn downregulates translation of the TonB-dependent receptor ChvT (its transcription was downregulated with Cu) [475]. Deletion of *chvT* has been shown to increase resistance to certain antibiotics (vancomycin and cefixime). Similarly, cross-regulation with many known and putative antimicrobial resistance mechanisms was observed in the Cu stress response. Toxicity mechanisms of organic antibiotics are

often characterized by the induction of the oxidative stress response, similar to As and Te toxicity [49].

Finally, transport systems of several classes were differentially regulated due to Cu stress. In M2G medium, a relatively high percentage of ABC-transporters were upregulated, but in contrast a small percentage of TonB-dependent receptor proteins was affected by Cu stress. However, the substrates of many of these systems are not known, and consequently it is difficult to discover functional relations between their differential expression and their possible role in the Cu stress response. However, a special mention must be made of the downregulation of two ATP synthase systems. While co-import of Cu ions with the proton gradient could be a possible mechanism of toxicity, the downregulation of ATP synthases could result in a breakdown of the proton motive force as reported for silver toxicity, which is similar to Cu toxicity [476].

Curiously, the Cu-specific PcoAB system was not induced by Cu stress in PYE medium. In ST cells, the *ncz* and *czr* clusters (described above) were induced, as well as 6 TonB-dependent receptor proteins. All of these receptor proteins transport unknown substrates, except the hemin utilization system HutA. Receptor proteins such as these have been shown to play a role in metal acquisition, and as such may also be important transporters involved in the Cu stress response [477, 478]. In SW cells in PYE, no metal resistance system was induced by Cu stress at all. This cell population displayed overexpression of the Type I secretion protein CdzB, which is part of a contact-dependent bacteriocin system [479], and a ferrous iron transport protein. The latter observation again highlights the role of Fe ion transport in the Cu stress response, apparently influential in both tested media.

5.3.3.5 Amino acid metabolism

Several amino acid biosynthesis pathways were differentially regulated by Cu exposure. In ST cells, L-cysteine biosynthesis was strongly upregulated in M2G, similar to observations made in *Cupriavidus* [116, 367]. In addition, both the pathway from 3-phosphoglycerate to serine and the assimilation of sulfate to hydrogen sulfide were upregulated, providing essential precursors for L-cysteine biosynthesis. At the same time, the cysteinyl-tRNA was downregulated and no significant change in the expression of cysteinyl-tRNA synthetase was observed, indicating a decreased consumption of cellular L-cysteine pools for protein synthesis. All the while, the synthesis pathways leading to methionine were downregulated. The essential role of thioether residues in Cu ion binding has been reviewed by Davis and O'Halloran

(2008) [480]. We conclude that cellular sulfur pools seem to be geared towards L-cysteine synthesis, but that this cysteine is not used in translation so much as in the synthesis of other cysteine-containing compounds such as glutathione and thioredoxins. Curiously, the disparate use of S and cysteine pools was not as strongly observed in SW cells or in both morphotypes in PYE medium.

The biosynthesis of arginine was downregulated in both morphotypes in M2G medium. Conversely, in *Mycobacterium tuberculosis*, arginine biosynthesis was upregulated by oxidative stress, and arginine deprivation was linked to antioxidant depletion [481]. In *Pseudomonas putida* KT2440, arginine-derived polyamines were shown to play a role in oxidative stress relief [482]. Finally, arginine exacerbated oxidative stress from hydrogen peroxide addition in *Streptococcus mutans* [483]. In this *S. mutans* study, a metal transporter was implicated in the observed behavior, among other genes. All in all, the role of arginine in Cu homeostasis seems to be complex, and we cannot provide a final explanation for the observed behavior without additional experiments.

In ST cells, grown in PYE medium, we observed an overall downregulation of the complete histidine degradation pathway, suggesting an increased need for L-histidine. Similar to cysteine, histidine residues have been implicated as a cellular Cu ligand [103, 480]. This property has been utilized to engineer *C. crescentus* strains for biosorption of Cd^{2+} ions, which have similar binding characteristics to Cu^{2+} [292]. While the specific role of histidine in the Cu stress response has not been studied in bacteria, in the fungal pathogen *Aspergillus fumigatus*, a strong relation between histidine biosynthesis and metal resistance has been shown [484]. Some overexpression of sulfate assimilation genes, possibly integrating into L-cysteine metabolism, was also noted.

5.3.3.6 Regulation by small regulatory RNAs

C. crescentus harbors many small regulatory RNAs (sRNAs) that can influence gene expression at the post-transcriptional level in a variety of ways, such as direct interaction with mRNAs [485, 486]. Differential expression of sRNAs in response to Cu was observed in all conditions, except for SW cells in PYE. The strongest evidence for sRNA regulation in response to Cu stress was detected in M2G medium (17 upregulated in ST cells, 3 up- and 1 downregulated in SW cells). In PYE medium, six sRNAs were upregulated in ST cells (Figure 5-9). The ChvR sRNA and its function have been described in section 5.3.3.4, but unfortunately the target genes have yet to be identified for most other sRNAs. Therefore, we predicted putative target genes for

all differentially expressed sRNAs for which no experimentally validated target has been reported (Table 5-6). Several of these sRNAs could be involved in the regulation of proteins relevant to the Cu stress response, such as transporters, regulators, and superoxide dismutases. In conclusion, while regulation via sRNAs is potentially extensive and far-reaching, there is a need for additional experiments to determine sRNA-target interactions. An overview of computational and experimental validation strategies can be found in Georg et al. (2020) [487].

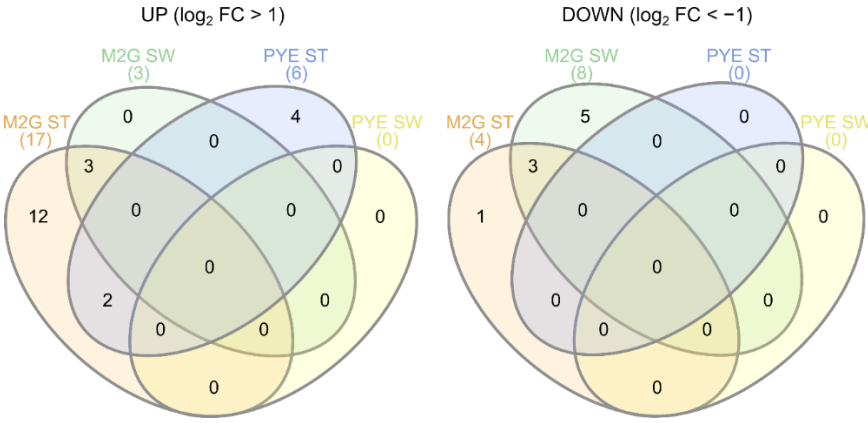

Figure 5-9. Venn diagrams showing overlap between sRNAs upregulated (left) and downregulated (right) by Cu stress in all experimental conditions.

*

Table 5-6. Differentially expressed small regulatory RNAs and their top 3 putative target genes, based on maximal binding free energy.

sRNA	Log2(FC) of Cu-Ct				Target[1]	Gene product	Binding site[2]
	M2G ST	M2G SW	PYE ST	PYE SW			
R0002	4.65	0.30	0.59	0.33	01301	NAD dependent formate dehydrogenase alpha subunit	2038><2108
					02875	Hypothetical protein	55><81
					02651	Drug/metabolite exporter	-188><-160
R0032					02892	Hypothetical protein	-15><3
					01081	Hypothetical protein	38><58
					03699	M16 falily peptidase	2538><2554
R0078					03523	Hypothetical protein	-153><-124
					00723	Glyoxalase family protein	138><159
					02370	TonB-dependent maltose transporter MalA	1822><1850
R0088	3.79	1.35	1.74	-0.10	03779	Cytosolic protein	-179><-150
					02816	Hypothetical protein	130><147
					02454	N-methylhydantoinase (ATP hydrolyzing)	3640><3657
R0092					02816	Hypothetical protein	121><144
					00664	C4 dicarboxylate transport protein	45><67
					02642	UDP-N-acetylmuramoylalanyl-D-glutamate-2,6-DAP ligase	196><211
R0095					00006	Enoyl-CoA hydratase	271><789
R0097	0.82	0.66	4.19	0.51	02483	Acyl-CoA synthetase	-34><-24
					00739	Hypothetical protein	55><65
					03872	tRNA modification GTPase TrmE	1053><1061
R0100[3]	3.12	1.21	0.22	0.37	03108	TonB-dependent receptor	-70><-59 & -20><-10
R0110	1.18	0.67	1.80	-0.01	00546	Hypothetical protein	-195><-166
					00545	Acetoacetyl-CoA reductase	651><680
					00817	L-sorbosone dehydrogenase	1299><1324
R0111					00593	Hypothetical protein	1177><1584
R0119	3.87	2.68	0.52	1.17	01083	Hypothetical protein	-110><-86
					00275	Transposase	-167><-146

Table 5-6. Differentially expressed small regulatory RNAs and their top 3 putative target genes, based on maximal binding free energy.

sRNA	Log2(FC) of Cu-Ct				Target[1]	Gene product	Binding site[2]
	M2G ST	M2G SW	PYE ST	PYE SW			
					01895	MFS superfamily transporter	1244><1258
R0128	1.37	0.78	2.74	-0.03	01034	TonB-dependent outer membrane receptor	-28><1
					00423	Phosphohydrolase	-110><-85
					03204	Alanine racemase	-96><-74
R0131					00697	Hypothetical protein	300><321
					02509	Glycosyltransferase HfsG	594><613
					02270	MarR-family transcriptional regulator	-20><-4
R0134	3.18	-0.88	1.56	0.59	01174	LysR family transcriptional regulator	-96><-68
					00181	Type II secretion pathway protein M	-158><-143
					00471	GDP L-fucose synthase	-188><-172
R0140	1.44	0.64	0.41	0.52	02329	Exodeoxyribonuclease VII large subunit	-110><-89
					00771	Hypothetical protein	89><118
					00798	CydC ATP-binding protein (ABC transport)	-68><-43
R0143					01584	Multimodular transglycosylase	-169><-142
					02235	Putative secreted protein	-75><-47
					00989	Acyl-esterase	11><26
R0158	1.39	-0.28	7.85	0.02	02221	Methionine synthase I MetH	496><507
					01382	Long chain fatty acid-CoA ligase	1432><1448
					00056	Ribosomal protein S18 acetyltransferase	410><426
R0161	3.26	0.17	3.01	0.38	03167	Hypothetical protein	469><492
					01215	Histidine triad protein	388><401
					03168	Hypothetical protein	517><537
R0162					02324	Hsp33-like chaperonin	-176><-148
					01651	DNA gyrase subunit A	-186><-161
					00105	MarC-family integral membrane protein	-151><-124
R0169	1.69	0.86	1.54	0.00	02606	Hybrid histidine kinase/receiver domain protein	842><871

Table 5-6. Differentially expressed small regulatory RNAs and their top 3 putative target genes, based on maximal binding free energy.

sRNA	Log2(FC) of Cu-Ct				Target[1]	Gene product	Binding site[2]
	M2G ST	M2G SW	PYE ST	PYE SW			
					01515	C4 dicarboxylate transporter large subunit	633><659
					01604	Hypothetical protein	52><73
R0182	2.85	3.32	0.48	0.15	02949	Hypothetical protein	-167><-140
					03128	Drug/metabolite exporter	-53><-25
					00276	Hypothetical protein	274><298
R0199	4.93	1.27	1.81	0.04	02024	NADH dehydrogenase I subunit F	-83><-58
					02172	Transporter	1323><1350
					01650	Cu/Zn superoxide dismutase	8><24

[1]CCNA_ gene annotation. [2]Nucleotide range (nt) of the target CDS putatively binding with the sRNA.

5.3.4 Role of environmental conditions in the Cu stress response

It is clear that the Cu stress response of SW cells in PYE is more closely related to that of ST cells in PYE than to that of SW cells in M2G medium (Figure 5-4). Similarly, the response of SW cells in M2G medium aligns more closely to that of ST cells in M2G than to that of SW cells in PYE medium. The differences in the response to Cu stress in the mineral medium M2G and the complex medium PYE can at least be partially ascribed to the speciation of Cu ions in these media. While a modelling approach might provide insights into approximate speciation at chemical equilibrium, the addition of highly complex, living bacterial cells would generate a large degree of uncertainty. The important role of medium composition on the free metal ion concentration, which lies at the basis of metal toxicity [488], has been shown in several studies [489, 490]. To illustrate, there can be a difference of at least 3 orders of magnitude in measured free Cu ion concentrations between complex and defined media, at relevant levels of Cu supplementation [490]. Here, we will provide a brief overview of the main chemical species suspected to sequester Cu ions. Nies (2016) compared the main chelating agents of transition metals in mineral and complex media [491]. M2G medium contains ca. 20 mM of phosphate anions, as well as 8 µM of EDTA. These compounds are the most likely to sequester supplemented Cu. However, Fe^{3+} will outcompete Cu^{2+} for EDTA binding, since the stability constant of Fe^{3+}-EDTA (logK = 25 [492]) is higher than that of Cu^{2+}-EDTA (logK = 18.46 [493]). Even though 15 µM of $CuSO_4$ was added to the medium, which contains only 10 µM Fe^{3+}, it is unlikely that EDTA is able to sequester much of the Cu ions present. Consequently, the extant phosphate moieties are the most likely Cu ligands. It should be noted that a far-reaching impact of Cu addition on the cells' phosphate metabolism is not expected due to the high PO_4^{3-} concentration relative to Cu in the medium. The sulfate and chloride anions are fairly 'hard' ions, and are thus unlikely to sequester the relatively 'soft' Cu^{2+} ions. PYE medium contains 2 g of peptone and 1 g of yeast extract per liter of medium. Adapting the calculations of Nies (2016) [491] and Sezonov et al. (2007) [494], this leads to final concentrations of 44 µM cysteine and 396 µM histidine from peptone, as well as 23 µM glutathione (containing one cysteine residue per molecule) from yeast extract. Cysteine and histidine represent the main transition metal-sequestering amino acids in this composition [491]. Since we added 175 µM Cu, enough binding capacity exists in the form of cysteine and histidine residues alone for the complexation of essentially all

added Cu. However, we must be cautious in the interpretation of these results, since we do observe moderate toxicity after the addition of $CuSO_4$ to PYE medium. First, other amino acid residues may also sequester Cu, albeit with lower stability constants. As the sum of these residues is present in higher concentrations than cysteine and histidine, they may still play important parts in the final equation [494]. In addition, casein hydrolysates from different sources can be quite different in composition, which has been shown to affect the oxidative stress response [495]. Finally, we have not taken the intrinsic Cu-binding capacity of the bacterial cell population into account. At an inoculum density of 4×10^8 cells per ml, it is likely that a relevant fraction of available Cu is associated with the bacterial cell surface.

As mentioned above, it is difficult to assess the total Cu-binding capacity in the presence of living cells. However, it is clear that more $CuSO_4$ must be added to PYE medium than M2G medium to achieve a similar deleterious effect on *C. crescentus* growth (Figure 5-2). Even with a higher Cu concentration in PYE, the transcriptomic response of SW and ST cells to Cu stress in PYE was markedly weaker than that of their counterparts in M2G medium. In addition, these disparate responses showed clear differences. No oxidative stress response was observed in PYE medium, while it was highly evident in M2G medium. This could be due to the presence of readily available glutathione and other antioxidants derived from the yeast extract in PYE [496]. The proteomic reconfiguration, which was also only observed in M2G medium, would then be a consequence of the oxidative stress in this medium. Interestingly, we detected changes in amino acid metabolism regulation in both media. In M2G medium, cysteine and arginine anabolism was overexpressed. As M2G does not contain amino acids and they must all be biosynthesized by the cell, we conclude that cysteine and arginine actually play a role in the Cu stress response. In contrast, in PYE medium, a need for histidine was observed after Cu stress. While histidine has been implicated in metal resistance, it could be the case that Cu-ligated histidine in the medium cannot (easily) interact with its cognate cellular importer, thus creating an apparent need for this amino acid. In other words, histidine could be 'titrated away' from cellular uptake by interaction with Cu. We did not find any indication of a similar phenomenon regarding cysteine, but then the cellular requirement for cysteine relative to its environmental concentration might be lower than is the case for histidine. However, to our knowledge, no such indirect toxicity mechanism has been described in literature.

We conclude that the mechanisms of Cu toxicity show extensive differences between the mineral medium M2G and the complex medium PYE. This is likely in large part due to the chemical speciation of Cu ions in these media. In addition, both cell types display intrinsic differences between their transcriptomes in M2G and PYE, mostly evident in their amino acid and carbohydrate metabolisms (as further shown in section 5.3.5). Since cells must import either mineral compounds and glucose (in M2G) or complex organic compounds such as amino acids (in PYE), the constitutive transportomes of cells in these media could play a crucial part in their intrinsic ability to handle the sudden addition of $CuSO_4$. In addition, both phosphates and peptone components can alter the cell surface affinity for metal ions [497]. However, other than on the transcriptomic level, little study has gone into the phenotypes of *C. crescentus* in disparate culture media [498]. Finally, the diverse real-world environments where *Caulobacter* species are isolated are not perfectly mirrored by either M2G or PYE medium, so aspects from the Cu stress responses from either medium could be relevant in these diverse situations. For example, in the oligotrophic freshwater streams and lakes where *Caulobacter* species are commonly isolated [499], an oxidative stress response would be a likely consequence of Cu stress (as seen in the mineral M2G medium). Conversely, for *Caulobacter* species found in soil habitats [500], where the concentration of complexing compounds is higher, the Cu stress response could align more closely with the reorganization of the transportome observed in the complex PYE medium.

5.3.5 Cu stress perception by stalked and swarmer cells

Overall, the differentially expressed genes in the swarmer cell population belonged to the same functional groups as in the ST cell population. However, fewer genes in each SW cell population were differentially expressed (Figure 5-6). Generally, the genes more strongly up- or downregulated between the Cu-stressed and control ST cell populations are those detected to be up- or downregulated in the SW cell population. The few systems exclusively altered by Cu stress in SW cells point to a slightly altered use of sulfate, phosphate and nitrogen sources, but a link to Cu detoxification is not clear. The question then remains: why are SW cells impacted to a lesser extent than ST cells? While it is evident that the number of genes upregulated due to Cu stress is larger in ST cells than in SW cells, many of the detoxification systems induced in ST cells could have already been active in SW cells. The constitutive expression of such systems becomes apparent when comparing the control conditions of ST and SW cells. In M2G medium, it is striking that of the 734

genes differentially expressed by Cu stress in ST cells but not differentially expressed in SW cells, 268 were differentially expressed between the control conditions of ST and SW cells. Of these 268 genes, 196 were overexpressed in control-condition SW cells. Among these genes were many relevant cell defense systems, including chaperones such as GroES/EL and DnaK/J, parts of cysteine and glutathione metabolism, the catalase KatG, and metal resistance mechanisms such as PcoAB. In previous studies, it has been shown that the intracellular redox state is dependent on the growth phase in *C. crescentus*, with a more reducing state in SW cells and a more oxidizing state in ST cells [455, 501]. This relatively reducing state in SW cells could be linked to the upregulation of cell protection systems, but the causality of this relationship is unclear. We note that oxidative stress represents but one aspect of Cu stress, and little information has been gathered on the cell cycle dependency of other aspects such as the accumulation of toxic protein precursors or shifts in amino acid requirements. Finally, we have previously shown that SW cells accumulate more Cu than ST cells in order to sustain a negative chemotaxis to flee from the Cu stress [117]. This is consistent with the less extensive induction of cell defense mechanisms observed in the current study. In SW cells in PYE medium, a similar high basal expression level was noted for several systems induced by Cu stress in ST cells, including several transport systems. We conclude that in both media, the SW morphotype is less responsive to Cu stress, which might be due to the inherently higher level of mRNAs encoding cell protection systems.

We must mention that 112 genes were differentially regulated by Cu stress solely in the SW cells in M2G medium. Downregulation of the regulatory proteins of the nitrogen metabolism, such GlnB, GlnK, and NtrC, might indicate a different use, need, or level of assimilation of N sources under Cu stress. Genes encoding the phosphate transporters PstA and PstC as well as the P-starvation inducible protein PhoH were downregulated. In addition, several genes involved in S transport were downregulated. We also observed a slightly altered expression of genes involved in flagellar biosynthesis and motility, such as *fliQ*, *flbT*, and *cheW*. In addition, genes involved in stalk biogenesis *cpaA* and *hfaE* were differentially regulated. However, these observations were more diffuse than the overall tendency towards an oxidative stress response and other systems similarly induced in the ST cells.

5.3.6 Transcription start site analysis

The tagRNA-seq protocol used in this study allowed us to accurately detect 5’ ends of primary RNAs [116]. Several previous studies have performed genome-wide

transcription site (TSS) analyses, leading to a high degree of accurately defined TSSs in standard growth conditions [119, 379, 502, 503]. Consequently, we have opted to focus on the detection of new TSSs in the Cu stress conditions (Figure 5-10 and Table 5-7). In addition, several genes induced by Cu stress seem to be transcribed from multiple TSSs, indicating complex stress-dependent regulation (Table 5-8 and Figure 5-11).

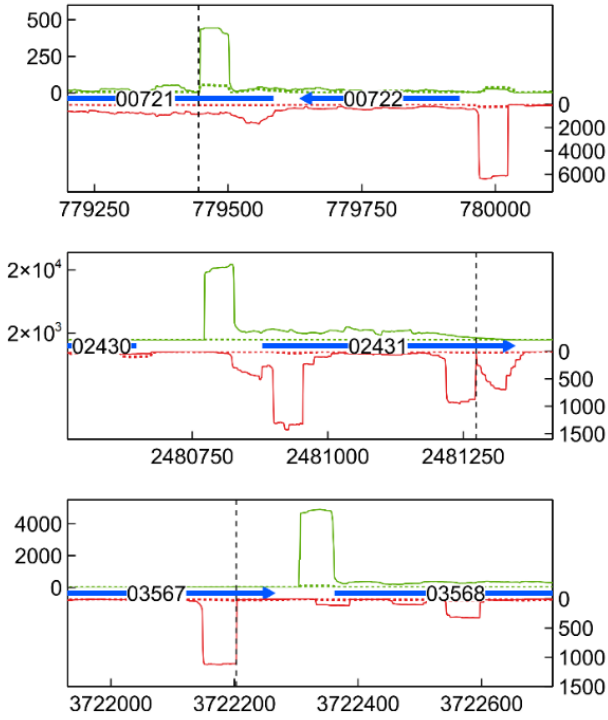

Figure 5-10. Transcription profile of identified aTSSs for selected genes. Combined TSS read counts of the three biological replicates of Cu-exposed (solid line) and unexposed (dotted line) stalked cells in M2G medium are shown for the positive (green) and negative (red) strand. Coding sequences are represented by a horizontal blue arrow (number is CCNA_ locus tag, x axis positions being the genomic location). Detected aTSSs are indicated with a vertical dashed line.

Table 5-7. Positions of Cu^{2+} stress-induced intragenic and antisense TSSs. Log2-fold change due to Cu^{2+} stress in disparate experimental conditions, as well as genomic context are shown for each TSS. Previously known TSSs are shown in bold.

5' end pos	strand	M2G ST	M2G SW	PYE ST	PYE SW	Genomic context[1]
779445	+	3.34	-0.27	0.60	0.06	aTSS of 00721
1160259	+	2.58	1.80	-0.20	0.04	iTSS of 01059
1868809	+	3.54	0.06	0.00	2.06	aTSS of 01738
2481274	-	4.91	-0.27	0.00	0.57	aTSS of 02341
3198577	+	3.66	-1.12	-0.12	-0.09	aTSS of 03043
3294538	-	1.12	0.28	0.30	0.34	Long 5'UTR of 03142
3328034	-	2.35	0.51	1.96	2.69	aTSS of 03169
3579018	-	5.11	1.83	2.50	0.59	aTSS of 03906
3579126	-	4.69	1.36	2.07	0.68	aTSS of 03906
3579259	-	4.81	1.33	1.90	0.54	aTSS of 03906
3722203	-	5.26	0.69	0.00	1.04	aTSS of 03567
3946388	+	3.19	-1.25	3.63	-0.12	iTSS of R0092

[1]CCNA_ gene annotation

Table 5-8. Genes putatively transcribed from multiple TSSs and their corresponding alternative TSS positions. Previously known TSSs are shown in bold.

CCNA_	Gene	Strand	Start codon position	TSS 1	TSS 2	TSS 3
00011	*dnaJ*	+	10223	10178	10092	10075
00721	*groEL*	-	779585	779585	779608	779703
01261		+	1388006	1387963	1387950	
01341		+	1454414	1454394	1454375	1454280
02039	*clpX*	-	2185128	2185230	2185325	
02552	*clpS*	+	2699457	2699418	2699367	2699283
02845	*uzcR*	-	2998187	2998223	2998266	
02846		-	3000222	3000341	3000364	
02860		-	3013060	3013083	3013098	
03299		+	3472717	3472677	3472603	
03362	*sigF*	-	3541812	3541814	3542003	
03483		-	3646517	3646553	3646572	
03706		+	3874686	3874440	3874475	3874612
R0095		-	4950	5035	5053	5188

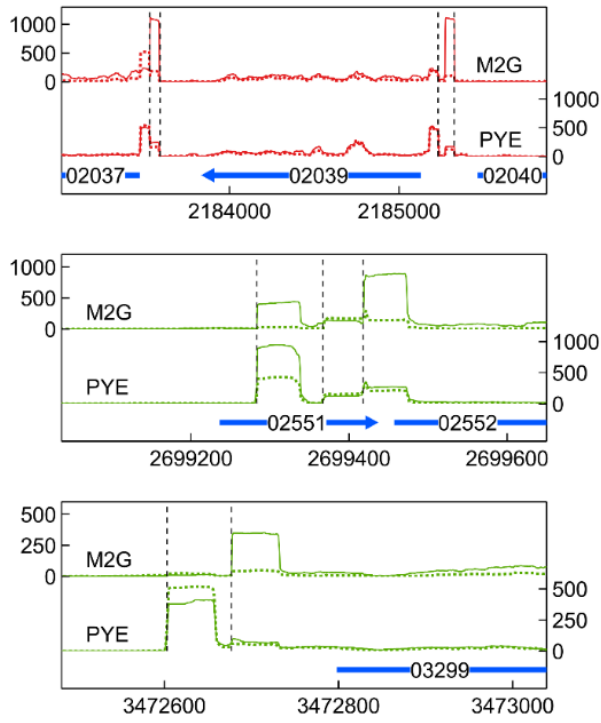

Figure 5-11. Transcription profile of identified alternative TSSs for selected genes. Combined TSS read counts of the three biological replicates of Cu-exposed (solid line) and unexposed (dotted line) stalked cells in M2G (upper) and PYE (lower) medium are shown for the positive (green) and negative (red) strand. Coding sequences are represented by a horizontal blue arrow (number is CCNA_ locus tag, x axis positions being the genomic location). Detected TSSs are indicated with a vertical dashed line.

Newly detected TSSs were often associated with known CDSs, with transcription proceeding either in the same sense (intragenic, iTSS) or in the antisense direction (aTSS). iTSSs, located inside coding regions, can mark the start of alternative mRNAs encoding shortened proteins. Alternatively, they can indicate trans-acting, non-coding RNA. Such iTSSs were found in the genes encoding the S-layer structural protein RsaA (not to be confused with the sRNA RsaA in *Staphylococcus aureus* [504]), and the sRNA CCNA_R0092. While expression of the *rsaA* gene itself was not induced by Cu stress, increased expression of its iTSS was detected after Cu exposure in M2G medium. Sorption of metals onto S-layer proteins has been shown in other bacteria [505, 506], and it is possible that an alternate, shorter RsaA protein has disparate Cu-binding characteristics, putatively playing a part in the Cu stress

response. Since the role of the sRNA CCNA_R0092 is not known, we cannot comment on a possible role of its iTSS.

Antisense TSSs are found on the antisense strand of a coding region, and usually denote the start of cis-acting sRNAs, which can form an important part of post-transcriptional regulation [172]. Some of these aTSSs were found in CDSs induced by Cu stress, such as GroEL (CCNA_00721), the Hsp20-family gene CCNA_02341 (3 distinct aTSSs), the TonB-dependent receptor protein CCNA_001738 (unknown substrate), and the acyl-CoA dehydrogenase CCNA_03567 (Figure 5-10 and Table 5-7). All aTSSs linked to these CDSs were induced by Cu stress. Finally, several aTSSs were induced by Cu stress, while their corresponding CDSs were not. The PilA mRNA, encoding a Type IV pilin, was present at higher levels in SW cells than in ST cells, but was not induced by Cu stress. However, a Cu stress-inducible aTSS was detected on its antisense strand. The PilA protein was recently shown to couple mechanical cell-surface contact with initiation of the cell cycle [507]. Expression of *pilA* is regulated by the cell-cycle regulator CtrA [508]; nonetheless, non-canonical factors governing its expression seem to be present.

Finally, several genes seemed to be transcribed from multiple TSSs, indicating complex regulation with multiple regulators. Such alternative TSSs were found for genes encoding transport systems, such as the TolC-family outer membrane protein CCNA_03299 and the ABC transport ATP-binding cassette CCNA_03483. In the case of CCNA_03299, a clearly medium-dependent alternative TSS was detected. Unfortunately, the substrates of these systems are not known, but both systems are induced by Cu stress in M2G. In addition, alternative TSSs were linked to genes encoding proteases and chaperones such as *lon* (CCNA_02037), *clpX* (CCNA_02039), *clpS* (CCNA_02552), and the gene encoding the Hsp20-family protein CCNA_03706 (Figure 5-11 and Table 5-8). For all of these genes, at least one TSS was previously detected (i.e., Zhou et al., 2015 [117]). It is likely that additional TSSs, often preferred during Cu stress, can give rise to mRNA isoforms. The biological relevance of these isoforms remains to be studied. In any case, the clear dependency of transcription start site selection on environmental conditions shows that the response to Cu stress is governed by different regulators in these conditions.

5.3.7 Correspondence with previous transcriptomic studies

Although cross-study transcriptome results are difficult to compare due to variability in, e.g., experimental setup, measurement sensitivity, and statistical methods, we examined the correlation of our results with existing datasets.

Hottes et al. [498] used a microarray analysis to investigate the transcriptome of unsynchronized *C. crescentus* populations in PYE and M2G medium. Both datasets can only be partly compared, because of limited data and data analysis availability. Nevertheless, based on eggNOG class overrepresentation (amino acid metabolism, signal transduction, carbohydrate metabolism, motility, inorganic ion transport and metabolism, and nucleotide metabolism), both studies correspond well (Table 5-3).

The transcriptomes of synchronized *C. crescentus* populations at several points along the cell cycle were studied by Fang et al. (2013) [509]. We compared their and our (without $CuSO_4$) dataset, and for SW cells, 96 of their top 100 upregulated genes in SW cells were also upregulated in our data, in both M2G and PYE medium. Similarly, of the top 100 upregulated genes in ST cells, 99 were upregulated in ST cells in our data, again in both tested media. Thus, we conclude that the results of our cell synchronization corresponded very closely to those reported in literature.

To validate the detection of transcription start sites (TSSs), we compared the list of detected TSSs to those of a similar study. In Zhou et al. (2015) [119], TSSs were detected from RNA extracted at several points along the cell cycle of *C. crescentus*, in M2G medium, with an RNA-Seq-based method. We examined the overlap for both SW cells and ST cells in M2G medium. Around 35% of the 2728 TSSs reported in Zhou et al. were also detected in our study, for both cell types. The discrepancy can largely be attributed to differences in RNA treatment and processing, as well as the software used to handle sequencing reads and TSS identification. This is evident from the fact that we detect higher percentages of TSSs experimentally validated by, e.g., β-galactosidase reporter assays in both cell types (56.3 % in SW cells, 49.4 % in ST cells). Finally, Zhou et al. considered TSSs from RNAs expressed at eight time points in the cell cycle, while we only have data from two time points. In conclusion, our results correlate fairly closely to those reported previously.

5.4 Conclusions

We studied the transcriptomes of Cu-stressed *C. crescentus* SW and ST cell morphotypes in a defined mineral (M2G) and a complex (PYE) medium, in order to examine the influence of disparate cellular environments on the genome-wide Cu stress response. While the level of Cu supplementation achieved similar deleterious effects in both media, a far larger impact on the bacterial transcriptome was observed in M2G. In parallel, more extensive changes to the transcriptome of ST cells, relative to SW cells, were found in both media. The ECF sigma factor SigF and

its regulon, containing several genes of unknown function, were induced by Cu stress in all tested conditions. In addition, disruption of *sigF* induced a Cu-sensitive phenotype, highlighting the importance of this regulon in the Cu stress response. In M2G, both morphotypes displayed a strong oxidative stress response, as well as a proteome rearrangement likely because, in part, of the accumulation of toxic pre-proteins. Several metal resistance mechanisms were induced in both media, but the PcoAB system, which confers resistance to Cu, was only upregulated in stalked cells in M2G. While a role for cysteine and arginine metabolisms could be discerned in the stress response in M2G, there was an apparent need for histidine in PYE. In general, the response to Cu exposure depended greatly on the environment. While neither of the tested media necessarily directly represent natural environments, it is clear that we must be careful in generalizing data from one environment to the other. Further validation of the role of specific resistance mechanisms is largely out of the scope of this manuscript, but these results emphasize the importance of tailoring the experimental conditions to the biological question at hand. Several questions remain open, such as the precise interactions between cell (surface), medium components and Cu ions, which could be further unraveled by a combinatory approach, including transcriptomics, proteomics, a direct assessment of the chemical speciation and dynamic modelling. In addition, it would be interesting to modulate the cell phenotype before applying Cu stress, e.g., by pre-inducing Cu resistance mechanisms, or applying stress to cells in stationary phase or encapsulated in biofilms, which are often more relevant than the exponential-phase populations used in this study. Finally, neither M2G nor PYE are especially oligotrophic, and consequently the response to Cu stress in freshwater or relevant soil extracts could be the object of further study. To a lesser extent, the Cu stress response was dependent on the morphotype, and we found that many relevant resistance systems were constitutively expressed in SW cells, indicating a higher level of inherent metal tolerance. Further study of the role of the morphotype could reveal the ecological significance of the more resistant SW cells. Nevertheless, it is clear that the response to Cu stress varies strongly between culture media and cell type, which shows the variety of ways in which a population of cells with the same genome can handle such a stress. In this chapter, we pivoted away from the study of *C. metallidurans* CH34, to *C. crescentus* NA1000. The similar experimental setups in Chapters 3 and 5 allowed us to compare results, with e.g. the common SigF/RpoQ regulons being overexpressed in both strains. However, we did not explicitly focus on the discovery

of novel non-coding RNAs in the NA1000 strain, since many have already been described in previous work.

General discussion and future perspectives

The worldwide rise in bacterial antimicrobial resistance drives the need for the development of novel or rediscovered antimicrobial therapies, with ubiquitous use cases e.g. in healthcare, agriculture and food production, and even in the space industry. Effective antimicrobials in the latter are especially relevant in the face of persistent contaminations observed inside spacecraft, posing risks to material integrity as well as astronaut health. *C. metallidurans* CH34, a model organism for bacterial metal resistance and survival in harsh oligotrophic environments, is of interest as a test organism for novel Cu-based antimicrobials, because of its high Cu resistance and the prevalence of the species (and closely related ones) in spacecraft and assembly cleanrooms.

We studied the phenotypic effects of Cu metal exposure under wet conditions in *C. metallidurans* CH34. Cu metal was able to kill ca. 95% of the cell population within 48 hours, as evidenced by a decrease in culturability and an increase in the cell fraction with propidium iodide-permeable cell envelopes. Our results are in line with previous works on less metal-resistant strains [510]. In this sense, Cu metal indeed seems like a promising antimicrobial at least in the short term, especially with recently developments in additional surface functionalization resulting in higher lethality, e.g. via pattern etching [36]. Furthermore, in contrast with some other biocide-releasing surfaces, Cu surfaces have the advantage of being easy to shape, relatively sturdy, and retaining long-lasting antimicrobial activity [511]. However, some inherent issues must be overcome to achieve lasting antimicrobial efficacy. Bare Cu surfaces in ambient conditions are prone to fairly rapid oxidation, which can reduce killing rates [510, 512]. This problem could be overcome by the use of more electrochemically stable Cu alloys, with the challenge of not decreasing the antimicrobial behavior too strongly [513]. Another issue is the deposition of dust and debris [514], which can impede direct cell-to-metal contact, and similar concerns exist for e.g. biofilm formation (e.g. via the creation of organic (microbial) layers impeding contact killing) [515]. While the release of free Cu ions to the medium is an important cause of cellular toxicity, this direct contact is still particularly paramount

to achieve a sufficient killing efficacy [30, 46, 510]. Thorough cleaning protocols therefore seem a necessity for prolonged antimicrobial activity. Finally, the surface charge of the (ungrounded) metallic antimicrobial might play a role in its inactivation efficiency, especially in atmospherically dry conditions. For example, a positive charge was associated with increased antimicrobial activity for polymethacrylate surfaces [516]. However, to our knowledge this parameter has not yet been studied for Cu antimicrobials.

An important observation in our first study was the apparent conversion of a fraction of *C. metallidurans* CH34 cells to the viable-but-non-culturable (VBNC) state 48 hours after Cu metal exposure. In the following days, up to ca. 25% of these VBNC cells regained culturability. While the precise timing and extent of these phenomena likely vary with environmental conditions, we showed that a small fraction of cells can escape the VBNC state (resuscitation) without altering the conditions, indicating that the outcome of culture-based monitoring methods needs to be critically interpreted. For instance, microbial monitoring onboard the ISS is currently based on culturing methods [72]. These methods are time and resource intensive, and the culturing of microbes increases the number of cells, which in itself increases the risk of exposure to potentially pathogenic strains. Air, water and surface contaminations are scored by aerobic and heterotrophic culturing on a rich agar [72]. For instance, if the CFU count for drinking water samples exceeds 100 CFU/100 ml, which occurred in 60% of measurements from 2000-2004 [73], fresh drinking water must be sourced from Earth and onboard reserves must be disinfected. Both procedures are costly. Consequently, there is a clear need for the accurate estimation of the total microbial load, instead of only the culturable fraction. If VBNC cells remain undetectable, quality assessment might underestimate this total load. In addition pathogenic strains often regain virulence upon resuscitation [517], and so it could easily be imagined that such strains, residing in a temporary VBNC state and thus unmeasurable in a practical sense, could later pose increased risks to spacecraft crew. The question then is whether such a scenario poses a high enough risk to warrant an increased level of biocontrol, taking into account the technical challenges of analysis aboard operational spacecraft. To date, microbial infections or health issues of space crew have been rarely reported, while at the same time spacecraft conditions are selective for microbial persistence and virulence [66, 70]. This would indicate that the microbiological threat, at least as far as pathogenic strains are concerned, is more or less curbed with the existing protocols. However,

extrapolating to future missions with longer durations and concomitant greater health risk (e.g. to Mars) could open a window for additional point-of-use control protocols able to detect VBNC cells, such as semi-quantitative PCR [518]. Ideally, such techniques would also be able to detect difficult-to-culture strains that also evade current detection by culturing. In this sense, new microbiological quality standards should follow newly validated protocols, instead of (solely) relying on e.g. a quantification of colony forming units per unit of volume or surface [72].

In addition to a conversion to the VBNC state, the role of Cu resistance mechanisms (CRM) was identified as a major contributor to long-term survival in the presence of metallic Cu. This role was confirmed both by the higher inactivation of *C. metallidurans* AE104, which lacks many active CRMs compared to CH34, and by the lower inactivation of CH34 cells pre-conditioned by $CuSO_4$. While few known bacterial strains encode a network of metal resistance determinants as extensive as CH34, these determinants are often present on mobile genetic elements (MGEs) [94, 125, 519]. In the case of CH34, it has been hypothesized that many metal resistance determinants had been acquired fairly recently at the time of isolation [115]. The presence of CRM on MGEs could allow their spread through horizontal gene transfer, resulting in overall lower killing rates of Cu antimicrobials. At the same time, antimicrobial resistance (AMR) determinants are often co-selected with metal resistance determinants, exacerbating this threat. In any case, it is clear that for *C. metallidurans* CH34, extremely high levels of Cu resistance are not necessary for survival in wet contact with a Cu surface, since even strain AE104 was capable of irregular resuscitation form the VBNC state after several days. If the Cu surface is allowed to oxidize and gather a passive layer of dust, its antimicrobial function could decrease to such an extent that there is a timeframe for initially sensitive microbes to develop or become part of an existing biofilm and exchange CRM determinants [520], and as such survive or even proliferate on the surface. This will depend again on the implemented cleaning method and regime, but also on environmental factors that influence contact killing rates, such as temperature, humidity and surface wetness, and the Cu-content of the antimicrobial surface [30].

It is clear that additional research is needed, especially on Cu surface toxicity in longer timeframes. We have provided new data on this case, but many questions remain open. It has become apparent that Cu surface toxicity leads to an array of complex microbial behaviors, such as the induction of metal resistance determinants (which ones?) and the rise of subpopulations with distinct survival strategies

(culturable cells vs. VBNC cells), which are variable in time. On a fundamental level, there is a clear need for the characterization of VBNC cells. We have developed a robust strategy to induce a Cu^{2+} ion-mediated VBNC state in 99.99% of the cell population (at least in CH34), allowing for bulk analysis strategies like transcriptomics and proteomics, and measurement of intracellular Cu and ATP content. Thus far, only a single study on the proteome of Cu-induced VBNC cells has been performed [216], with a complete lack of transcriptomic data. In addition, valuable insights could be gained from analysis on a single cell level, since we have little information about the intra-population variability of the observed phenomena. Finally, a comparison of culturable cells before VBNC state induction and after resuscitation could be made, to analyze any changes in e.g. stress resistance, virulence, biofilm formation etc. On a more applied level, the relationship between Cu surface toxicity and microbial load could be studied as in Hahn *et al.* [510], with mixed communities, relevant environmental variations (e.g. microgravity for space-related ones), and organic matter as additional variables.

In the second chapter, we performed a detailed analysis of the transcriptome of Cu^{2+}-stressed *C. metallidurans* CH34 cells. The regulatory response consisted in large part of the activation of a broad array of metal resistance mechanisms, not limited to Cu-detoxification mechanisms alone. This broad response to a single specific transition metal has been reported before, and evidences extensive cross-regulation [115]. Strain CH34 was originally isolated from an environment contaminated with various metals such as Ni, Zn and Co, where cross-regulation of metal resistance determinants might provide an evolutionary advantage. However, it could be imagined that the Cu-specific response could be further streamlined upon continuous Cu exposure, leading to increased resistance levels. For instance, Cu-conditioning decreased the inactivation efficiency of Cu metal on the CH34 strain. Furthermore, in a separate preliminary experiment, we observed a 3-fold increase of the Cu^{2+} MIC (to 8 mM) after five successive passages in mineral medium supplemented with increasing Cu^{2+} concentrations (Figure A). Noteworthy, sequencing of the genomes of these Cu-conditioned CH34 strains did not show any mutations. This gradual adaptation to Cu exposure might provide a drawback to the long-term use of Cu antimicrobials, in addition to the ones listed above. At the same time, however, the intracellular need for Cu ions as a micronutrient might preclude the further evolution of resistance mechanisms. In other words, there will always be

a pool of Cu ions *not* to be removed to the cellular exterior. Further experiments could provide insight into the evolution of CRM with conservation of intracellular Cu homeostasis.

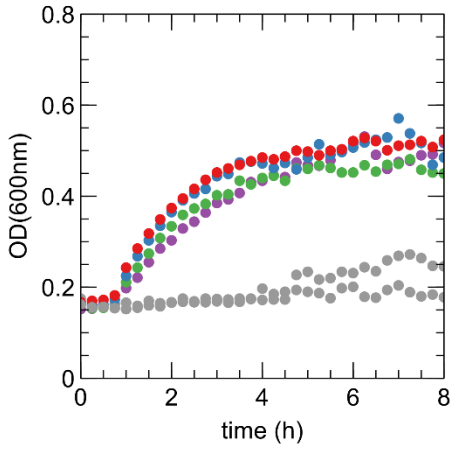

Figure A. Growth of parental (grey; two replicates) and Cu-preconditioned (colored; four independent lines) *C. metallidurans* CH34 in MM284 medium supplemented with 8 mM $CuSO_4$.

In addition to the induction of resistance mechanisms, the regulatory response to acute Cu^{2+} exposure provided an insight into the tolerance mechanisms of strain CH34. Cu tolerance was characterized mostly by the induction of an oxidative stress response and a proteomic reconfiguration, similar to comparable studies [367]. The characterization of these tolerance mechanisms could be exploited to enhance the toxicity of Cu antimicrobials, e.g. by combinatory approaches with complementary disinfection technologies. Even sporadic treatment of biofilms on a Cu metal surface could putatively improve biocontrol. Optimal results would likely be achieved if there is little overlap between the mechanisms of toxicity of the Cu antimicrobial and the complementary disinfection technology, in order to avoid occurrences where the bacterial response to the one also increases tolerance towards the other. In that sense, ROS-generating technologies like the application of UV-C light and hydrogen peroxide might show too great an overlap with the contact killing mechanism of Cu antimicrobials [521, 522]. In contrast, the use of e.g. quaternary ammonium compounds or even sodium chloride might be more appropriate, as studied by Steinhauer *et al.* [523] and Luo *et al.* [524].

On a more immediate level, the regulatory overview we provided for *C. metallidurans* CH34 allows for the development of biotechnological applications.

Especially the information regarding transcription start sites provides a novelty, and can be exploited e.g. in the search for promoter sequences for future (constitutive and Cu-inducible) expression constructs. Currently, there is a lack of well-characterized promoter sequences that ensure reliable gene expression in *C. metallidurans* in the mineral MM284 medium.

Finally, some notes must be made about the putative sRNAs detected in this study. From the relatively large pool of orphan TSSs, fairly few transcripts were identified as likely intergenic sRNAs, in contrast to the many antisense RNAs. With adapted protocols and further wet-lab validation, it could be possible to pinpoint additional intergenic sRNAs. Furthermore, it is likely that some sTSSs were wrongly annotated and actually represent the 5' of sRNAs. In addition, there is an abundance of data regarding RNA processing sites, that has been gathered but not yet analyzed. It seems unlikely that the short length of some sRNAs would cause them to evade detection, since the RNA extraction kit was optimized for transcript lengths down to 17 nt, and since tRNAs were detected with ample coverage.

In our experimental tagRNA-Seq setup, we opted for a more general, practically achievable approach at the expense of some contextual relevance. We laid a baseline of the regulatory response to acute moderate Cu^{2+} stress, which can now be easily compared to other (similar) studies and used to design further studies more tailored to the use of Cu antimicrobials. In the design of such studies, additional variables could be the physiology of the bacterial population (e.g. exponential phase vs. stationary phase, or VBNC cells), the medium used (e.g. water, saline solution or various growth media), and the formulation, dosage and timing of Cu antimicrobial (e.g. ionic, nanoparticle or metal surface). Challenges might be faced mainly in the experimental design phase, and in the recovery of sufficient RNA of good quality from physiologically distinct subpopulations. In the context of the ESA BIOFILMS experiment, a successor experiment might provide important data on the molecular mechanisms and the cellular regulation that are active in Cu-exposed cells in space. Furthermore, RNA-Seq studies on samples gathered in a space context have already been performed, by freezing at -80 °C or the use of fixatives like RNAlater [525, 526].

Several of the non-coding RNAs identified in the tagRNA-Seq study (Chapter 3) were studied in more detail, focusing on an antisense transcript of the *silDCBA* cluster, coined *silY*. Interestingly, previous experiments have shown that post-transcriptional regulation by non-coding RNAs is especially critical in bacteria exposed to spaceflight

conditions [186, 187]. These observations also triggered our interest in non-coding RNA regulators in *C. metallidurans* CH34, specifically those involved in the regulation of Cu^{2+} resistance mechanisms. We found that *silY* was capable of regulating translation of the *silDCBA* cluster via a post-translational repressive mechanism. This repression resulted in a more Cu^{2+} sensitive phenotype. While several open questions remain, this regulatory mechanism would be one of the first of its kind reported for bacterial Cu resistance [180]. Metal resistance in *C. metallidurans* CH34 relies mostly on several families of one or two-component transcriptional regulators [91], but no such system was known to regulate the *silDCBA* cluster, contrary to partially homologous *sil* clusters in e.g. *Salmonella* species [401]. Regulation by *silY* might be relevant for the acute response to Cu antimicrobials, since regulation via non-coding RNAs can be faster and more resource-efficient than canonical regulation systems [175, 176]. While it is impractical to generate a *silY* deletion strain, this hypothesis can be tested via a (shortened) variation of the metallic Cu exposure experiments described in Chapter 2, using the constructed AE104 pBBR-*silDCBA* pSCK108-*silY* (see section 4.2.4). Still, more fundamental knowledge gaps are left with insufficient attention. Questions about e.g. the precise transcript length (if there is one), the exact mechanism of interaction with the polycistronic *silDCBA* mRNA, and the regulation of *silY* itself await answering, in order to definitively pinpoint its functional role in bacterial Cu biology. Transcript length could be further analyzed by repeated RACE PCR, or alternatively an estimation could be made by Northern blotting. The mechanism of repression could be studied via electrophoretic mobility shift assay (EMSA) [527, 528]. Insights into the regulation of *silY* itself could be gained by evaluating its expression in variable environments, or by inserting point mutations into its supposed regulatory regions. Additional non-coding RNAs detected in the tagRNA-Seq study and confirmed by 5'RACE still require further work. As an example, one of these was located antisense to the *copL* gene located in the *cop* cluster on the pMOL30 plasmid. While the function of CopL has not been characterized in detail, its antisense transcript might also play a role in Cu resistance regulation. All in all, generating a deeper understanding of these non-canonical regulation mechanisms will likely not be directly applicable to the design of more effective Cu antimicrobials, but it could aid in forming a more complete picture of the intricate bacterial response and adaptation to such antimicrobials. In addition, it could lead to the development of bio-engineered regulation mechanisms for e.g. bioremediation, biosensing, biomining and bioproduction.

In the final chapter, we made a case study of the transcriptomic Cu stress response in *C. crescentus* NA1000, with the same tagRNA-Seq protocol as described before (Chapter 3). As additional variables, experiments were performed on both the swarmer and the stalked cell morphotypes, and in both a defined medium and a complex medium. We chose to study the Cu stress response in *C. crescentus* NA1000 to provide a comparison to the data acquired for *C. metallidurans* CH34. Contrary to CH34, NA1000 only contains a single active CRM, resulting in a much lower Cu resistance [117]. In addition, transcriptomic data is more abundant for *C. crescentus* NA1000, and more TSSs and sRNAs have been detected and studied in this strain. This wealth of available data provided a valuable set of validation points for our newly developed methods. Both *C. crescentus* and *C. metallidurans* species can thrive expertly in oligotrophic environments, and interestingly, both have been isolated from spacecraft [66, 236]. Due to this resilience, both species can pose risks for extended spaceflight, e.g. by contamination of onboard drinking water reserves. However, a direct hazard to astronaut health is unlikely to be presented by either of these species, as they are opportunistic pathogens at worst [529, 530]. At the same time, valuable resources could be wasted on attempts to control existing populations, which would be detected with current CFU-based protocols. [117]

We showed in a short series of experiments that *C. crescentus* NA1000 is much more sensitive to metallic Cu surfaces, with efficient inactivation and a lack of apparent VBNC cell resuscitation (Figure B). The inactivation efficiency was notably lower for a NA1000 strain constitutively expressing the *pcoAB* system. This data again highlights the impact of CRM on the antimicrobial efficacy of metallic Cu. However, even in a basic formulation of the Cu antimicrobial, efficient inactivation was achieved. In the case of *C. crescentus* it would be interesting to study the environmental factors that decrease this antimicrobial efficacy or even permit long term survival, such as the accumulation of dust and debris, the presence of a biofilm, or the acquisition of more extensive Cu resistance and tolerance mechanisms.

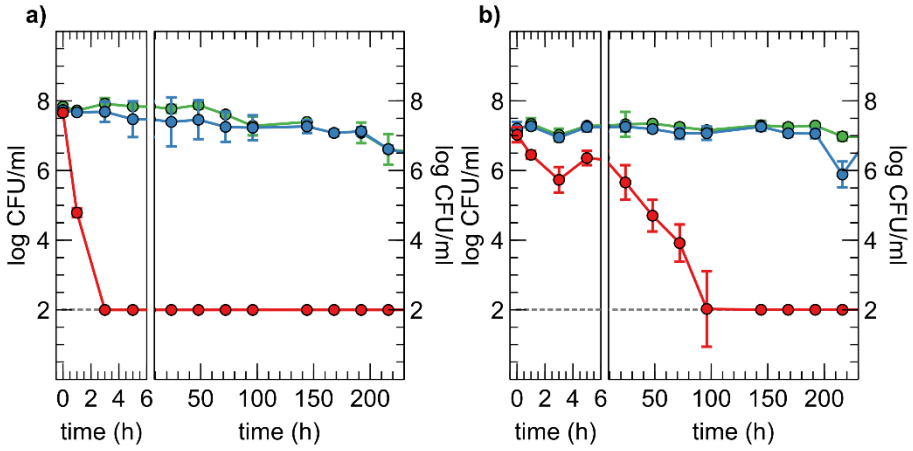

Figure B. Viable counts of *C. crescentus* NA1000 (a) and NA1000 pMR-*pcoAB* providing constitutive *pcoAB* expression (b) suspended in mineral water in the presence of metallic Cu (red), stainless steel (blue) and control condition (green). All experiments were independently performed with *n* = 3 (see also 2.2.2 and 2.2.3).

On a transcriptomic level, the response to Cu stress was much stronger in the defined mineral medium M2G, even though at the relevant Cu^{2+} concentrations, growth impairment was slightly more pronounced in the complex PYE medium. For this reason, the induction of resistance mechanisms as well as the toxic effects of the Cu^{2+} exposure were much clearer in M2G. In PYE, these mechanisms were much more obscured, with only several transport systems induced. In addition, the mechanism of Cu^{2+} toxicity in PYE was not evident, other than an apparent cellular need for histidine. We do mention the importance of the SigF regulon, which seems to play a role in Cu resistance in both media. Follow up research would be needed to provide deeper insights into Cu resistance and tolerance in the complex medium PYE, but a direct use case seems elusive. The higher capacity for Cu-chelation could perhaps be useful to mimic some soil extracts, however more accurate media have been developed to that purpose [531]. Overall, we note that the results acquired for this growth medium mostly highlight importance of characterizing the studied environment in order to understand the bacterial Cu response and adaptation to Cu exposure.

In M2G medium, results were quite similar to the Cu^{2+} exposure study performed on *C. metallidurans* CH43 (also in a mineral medium, see Chapter 3). We observed a broad upregulation of metal resistance determinants, not limited to Cu-specific mechanisms. The response to Cu toxicity was manifested mostly by the induction of

an extensive oxidative stress response and a proteome reconfiguration. As in PYE, the SigF regulon was strongly differentially regulated upon Cu exposure. Many of the genes in this regulon have been poorly characterized, but their importance seems evident, and similarities with the RpoQ regulon of *C. metallidurans* CH34 were found despite the phylogenetic distance between these strains (see section 5.3.3.1). It would be very interesting to study this regulon further, its role in Cu resistance and tolerance, and its phylogeny. We were able to confirm the role of the PcoAB system in Cu resistance, but some uncertainties about its regulation persist. It has previously been demonstrated that this system is constitutively expressed as a ready-to-use resistance mechanism against Cu, with extensive experiments performed in HIGG medium [117]. In M2G medium however, we found a strong induction of *pcoAB* transcription, but curiously no induction was detected in PYE medium. This could be due to a difference in Cu sensing in cells growing in these media, with more extensive Cu chelation by PYE (and HIGG) medium components. Further research should provide insights at the protein level, but at present it is unclear which conclusions can be extrapolated to the oligotrophic freshwater environments where *Caulobacter* species are often isolated (or to specific environments in a spaceflight context).

Similarly to *C. metallidurans*, tagRNA-Seq experiments were performed in commonly used growth media in order to maintain a practically feasible setup, with results that could be easily compared to similar studies. As we have shown in 0, the chemical makeup of these media can fundamentally alter the bacterial response to similar stresses due to the presence of metal-binding ligands that preclude toxic effects to varying degrees [489, 490]. For this reason, the free ion activity model was developed to rationalize experimental behaviors of trace cations (such as Cu^{+}, Cu^{2+}) in complex environments [488]. Variations of this model are being used to design growth media more suited to the study of metal resistance [490]. On the other hand, in-depth metal resistance studies in directly relevant environments that do not necessarily allow for bacterial growth, such as drinking water, are needed.

References

1. WHO, *Global action plan on antimicrobial resistance*. 2015: Geneva, Switzerland. p. 28.
2. Cook, M., E. Molto, and C. Anderson, *Fluorochrome labelling in Roman period skeletons from Dakhleh Oasis, Egypt.* Am J Phys Anthropol, 1989. **80**: p. 137-143.
3. Nelson, M.L., et al., *Brief communication: Mass spectroscopic characterization of tetracycline in the skeletal remains of an ancient population from Sudanese Nubia 350-550 CE.* Am J Phys Anthropol, 2010. **143**(1): p. 151-4.
4. Aminov, R.I., *A brief history of the antibiotic era: lessons learned and challenges for the future.* Front Microbiol, 2010. **1**: p. 134.
5. Cassini, A., et al., *Attributable deaths and disability-adjusted life-years caused by infections with antibiotic-resistant bacteria in the EU and the European Economic Area in 2015: a population-level modelling analysis.* Lancet Infect Dis, 2019. **19**(1): p. 56-66.
6. Oldenkamp, R., et al., *Filling the gaps in the global prevalence map of clinical antimicrobial resistance.* Proc Natl Acad Sci U S A, 2021. **118**(1).
7. O'Neill, J., *Tackling drug-resistant infections globally: final report and recommendations*. 2016.
8. Micoli, F., et al., *The role of vaccines in combatting antimicrobial resistance.* Nat Rev Microbiol, 2021. **19**(5): p. 287-302.
9. Lin, D.M., B. Koskella, and H.C. Lin, *Phage therapy: An alternative to antibiotics in the age of multi-drug resistance.* World J Gastrointest Pharmacol Ther, 2017. **8**(3): p. 162-173.
10. Harrison, F., et al., *A 1,000-year-old antimicrobial remedy with antistaphylococcal activity.* mBio, 2015. **6**(4): p. e01129.
11. Jaishankar, M., et al., *Toxicity, mechanism and health effects of some heavy metals.* Interdiscip Toxicol, 2014. **7**(2): p. 60-72.
12. Politano, A.D., et al., *Use of silver in the prevention and treatment of infections: silver review.* Surg Infect (Larchmt), 2013. **14**(1): p. 8-20.
13. Gaetke, L., *Copper toxicity, oxidative stress, and antioxidant nutrients.* Toxicology, 2003. **189**(1-2): p. 147-163.
14. de Romana, D.L., et al., *Risks and benefits of copper in light of new insights of copper homeostasis.* J Trace Elem Med Biol, 2011. **25**(1): p. 3-13.
15. Breasted, J.H., *The Edwin Smith Surgical Papyrus*. The University of Chicago Oriental Institute Publications. Vol. 1. 1930, Chicago: The University of Chicago Press.
16. Dollwet, H.H.A. and J.R.J. Sorenson, *Historic uses of copper compounds in medicine.* Trace elem med, 1985. **2**(2): p. 80-87.
17. Borkow, G., *Using copper to fight microorganisms.* Curr Chem Biol, 2012. **6**.
18. Wang, Q.Y., et al., *Integration of chemical and toxicological tools to assess the bioavailability of copper derived from different copper-based fungicides in soil.* Ecotoxicol Environ Saf, 2018. **161**: p. 662-668.
19. Shen, X., et al., *Evaluating the treatment effectiveness of copper-based algaecides on toxic algae Microcystis aeruginosa using single cell-inductively coupled plasma-mass spectrometry.* Anal Bioanal Chem, 2019. **411**(21): p. 5531-5543.
20. Fanta, F.T., et al., *Copper doped zeolite composite for antimicrobial activity and heavy metal removal from waste water.* BMC Chem, 2019. **13**(1): p. 44.
21. Clewell, A., et al., *Efficacy and tolerability assessment of a topical formulation containing copper sulfate and Hypericum perforatum on patients with herpes skin lesions: a comparative, randomized controlled trial.* J Drugs Dermatol, 2012. **11**(2): p. 209-215.
22. Chen, M.X., K.S. Alexander, and G. Baki, *Formulation and evaluation of antibacterial creams and gels containing metal ions for topical application.* J Pharm (Cairo), 2016. **2016**: p. 5754349.

23. Abbott, C.L. and D.C. Abbott, *Topical copper ion treatments and methods of making topical copper ion treatments for use in various anatomical areas of the body*, I.B. World Intellectual Property Organization, Editor. 2014: USA.
24. Styczynski, A.R., et al., *In vitro antiretroviral activity and in vivo toxicity of the potential topical microbicide copper phthalocyanine sulfate.* Virol J, 2015. **12**: p. 132.
25. Tamayo, L., et al., *Copper-polymer nanocomposites: An excellent and cost-effective biocide for use on antibacterial surfaces.* Mater Sci Eng C Mater Biol Appl, 2016. **69**: p. 1391-409.
26. Borkow, G., *Using copper to improve the well-being of the skin.* Curr Chem Biol, 2014. **8**: p. 89-102.
27. Anita, S., et al., *A study of the antimicrobial property of encapsulated copper oxide nanoparticles on cotton fabric.* Text Res J, 2011. **81**(10): p. 1081-1088.
28. Perelshtein, I., et al., *CuO–cotton nanocomposite: Formation, morphology, and antibacterial activity.* Surf Coat Technol, 2009. **204**(1-2): p. 54-57.
29. Teli, M.D. and J. Sheikh, *Modified bamboo rayon-copper nanoparticle composites as antibacterial textiles.* Int J Biol Macromol, 2013. **61**: p. 302-7.
30. Vincent, M., et al., *Contact killing and antimicrobial properties of copper.* J Appl Microbiol, 2018. **124**(5): p. 1032-1046.
31. Wilks, S.A., H. Michels, and C.W. Keevil, *The survival of Escherichia coli O157 on a range of metal surfaces.* Int J Food Microbiol, 2005. **105**(3): p. 445-54.
32. Noyce, J.O., H. Michels, and C.W. Keevil, *Use of copper cast alloys to control Escherichia coli O157 cross-contamination during food processing.* Appl Environ Microbiol, 2006. **72**(6): p. 4239-44.
33. Dwidjosiswojo, Z., et al., *Influence of copper ions on the viability and cytotoxicity of Pseudomonas aeruginosa under conditions relevant to drinking water environments.* Int J Hyg Environ Health, 2011. **214**: p. 485-492.
34. Maertens, L., et al., *Copper resistance mediates long-term survival of Cupriavidus metallidurans in wet contact with metallic copper.* Front Microbiol, 2020. **11**(1208).
35. Vincent, M., P. Hartemann, and M. Engels-Deutsch, *Antimicrobial applications of copper.* Int J Hyg Environ Health, 2016. **219**(7 Pt A): p. 585-591.
36. Müller, D.W., et al., *Increasing antibacterial efficiency of Cu surfaces by targeted surface functionalization via ultrashort pulsed direct laser interference patternings.* Adv Mater Interfaces, 2020. **8**(5).
37. Dupont, C.L., G. Grass, and C. Rensing, *Copper toxicity and the origin of bacterial resistance--new insights and applications.* Metallomics, 2011. **3**(11): p. 1109-18.
38. Giachino, A. and K.J. Waldron, *Copper tolerance in bacteria requires the activation of multiple accessory pathways.* Mol Microbiol, 2020. **114**(3): p. 377-390.
39. Rensing, C. and G. Grass, *Escherichia coli: mechanisms of copper homeostasis in a changing environment.* FEMS Microbiol Rev, 2003. **27**(2-3): p. 197-213.
40. Imlay, K.A. and J.A. Imlay, *Cloning and analysis of sodC, encoding the copper-zinc superoxide dismutase of Escherichia coli.* J Bacteriol, 1996. **178**(9): p. 2564-2571.
41. Steinman, H.M., *Function of periplasmic copper-zinc superoxide dismutase in Caulobacter crescentus.* J Bacteriol, 1993. **175**(4): p. 1998-1202.
42. Lemire, J.A., J.J. Harrison, and R.J. Turner, *Antimicrobial activity of metals: mechanisms, molecular targets and applications.* Nat Rev Microbiol, 2013. **11**(6): p. 371-84.
43. May, K.L., et al., *A stress response monitoring lipoprotein trafficking to the outer membrane.* mBio, 2019. **10**(3).
44. Peters, K., et al., *Copper inhibits peptidoglycan LD-transpeptidases suppressing beta-lactam resistance due to bypass of penicillin-binding proteins.* Proc Natl Acad Sci U S A, 2018. **115**(42): p. 10786-10791.
45. Ito, K. and K. Inaba, *The disulfide bond formation (Dsb) system.* Curr Opin Struct Biol, 2008. **18**(4): p. 450-8.
46. Mathews, S., et al., *Contact killing of bacteria on copper is suppressed if bacterial-metal contact is prevented and is induced on iron by copper ions.* Appl Environ Microbiol, 2013. **79**(8): p. 2605-11.
47. Hong, R., et al., *Membrane lipid peroxidation in copper alloy-mediated contact killing of Escherichia coli.* Appl Environ Microbiol, 2012. **78**(6): p. 1776-84.
48. Grass, G., C. Rensing, and M. Solioz, *Metallic copper as an antimicrobial surface.* Appl Environ Microbiol, 2011. **77**(5): p. 1541-7.
49. Van Acker, H. and T. Coenye, *The role of reactive oxygen species in antibiotic-mediated killing of bacteria.* Trends Microbiol, 2017. **25**(6): p. 456-466.

50. Macomber, L., C. Rensing, and J.A. Imlay, *Intracellular copper does not catalyze the formation of oxidative DNA damage in Escherichia coli.* J Bacteriol, 2007. **189**(5): p. 1616-26.
51. Valko, M., H. Morris, and M.T.D. Cronin, *Metals, toxicity and oxidative stress.* Curr Med Chem, 2005. **12**: p. 1161-1208.
52. Stohs, S.J. and D. Bagchi, *Oxidative mechanisms in the toxicity of metal ions.* Free Radical Bio Med, 1995. **18**(2): p. 321-336.
53. Macomber, L. and J.A. Imlay, *The iron-sulfur clusters of dehydratases are primary intracellular targets of copper toxicity.* PNAS, 2009. **106**(20): p. 8344-8349.
54. Arguello, J.M., D. Raimunda, and T. Padilla-Benavides, *Mechanisms of copper homeostasis in bacteria.* Front Cell Infect Microbiol, 2013. **3**: p. 73.
55. Lasseur, C., et al., *MELiSSA: The European project of closed life support system.* Grav Space Biol, 2010. **23**(2).
56. Checinska, A., et al., *Microbiomes of the dust particles collected from the International Space Station and Spacecraft Assembly Facilities.* Microbiome, 2015. **3**: p. 50.
57. Mora, M., et al., *Resilient microorganisms in dust samples of the International Space Station-survival of the adaptation specialists.* Microbiome, 2016. **4**(65): p. 1-21.
58. Venkateswaran, K., et al., *International Space Station environmental microbiome - microbial inventories of ISS filter debris.* Appl Microbiol Biotechnol, 2014. **98**(14): p. 6453-66.
59. Be, N.A., et al., *Whole metagenome profiles of particulates collected from the International Space Station.* Microbiome, 2017. **5**(1).
60. Lang, J.M., et al., *A microbial survey of the International Space Station (ISS).* PeerJ, 2017. **5**: p. e4029.
61. Singh, N. and J.T. Wade, *Identification of regulatory RNA in bacterial genomes by genome-scale mapping of transcription start sites.* Methods Mol Biol, 2014. **1103**: p. 1-10.
62. Romsdahl, J., et al., *Characterization of Aspergillus niger Isolated from the International Space Station.* mSystems, 2018. **3**(5).
63. Seuylemezian, A., et al., *Draft genome sequences of Acinetobacter and Bacillus strains isolated from spacecraft-associated surfaces.* Genome Announc, 2017. **6**.
64. Mijnendonckx, K., et al., *Characterization of the survival ability of Cupriavidus metallidurans and Ralstonia pickettii from space-related environments.* Microb Ecol, 2013. **65**(2): p. 347-60.
65. Urbaniak, C., et al., *Detection of antimicrobial resistance genes associated with the International Space Station environmental surfaces.* Sci Rep, 2018. **8**(1): p. 814.
66. Singh, N.K., et al., *Succession and persistence of microbial communities and antimicrobial resistance genes associated with International Space Station environmental surfaces.* Microbiome, 2018. **6**(1): p. 204.
67. Sonnenfeld, G., J.S. Butel, and W.T. Shearer, *Effects of the space flight environment on the immune system.* Rev Environ Health, 2003. **18**(1).
68. Sonnenfeld, G. and W.T. Shearer, *Immune Function During Space Flight.* Nutrition, 2002. **18**: p. 899-903.
69. Aponte, V.M., D.S. Finch, and D.M. Klaus, *Considerations for non-invasive in-flight monitoring of astronaut immune status with potential use of MEMS and NEMS devices.* Life Sci, 2006. **79**(14): p. 1317-33.
70. Mora, M., et al., *Space Station conditions are selective but do not alter microbial characteristics relevant to human health.* Nat Commun, 2019. **10**(1): p. 3990.
71. Crucian, B., et al., *Incidence of clinical symptoms during long-duration orbital spaceflight.* International Journal of General Medicine, 2016. **Volume 9**: p. 383-391.
72. Van Houdt, R., K. Mijnendonckx, and N. Leys, *Microbial contamination monitoring and control during human space missions.* Planetary and Space Science, 2012. **60**(1): p. 115-120.
73. Bruce, R.J., et al., *Microbial surveillance of potable water sources of the International Space Station.* 2005.
74. Davey, H.M., *Life, death, and in-between: Meanings and methods in microbiology.* Appl Environ Microbiol, 2011. **77**(16): p. 5571-6.
75. Schottroff, F., et al., *Sublethal injury and viable but non-culturable (VBNC) state in microorganisms during preservation of food and biological materials by non-thermal processes.* Front Microbiol, 2018. **9**: p. 2773.
76. Flemming, H.C., et al., *Biofilms: an emergent form of bacterial life.* Nat Rev Microbiol, 2016. **14**(9): p. 563-75.

77. Koo, H., et al., *Targeting microbial biofilms: current and prospective therapeutic strategies.* Nat Rev Microbiol, 2017. **15**(12): p. 740-755.
78. Singh, S., et al., *Understanding the mechanism of bacterial biofilms resistance to antimicrobial agents.* Open Microbiol J, 2017. **11**: p. 53-62.
79. Perrin, E., et al., *Furnishing spaceship environment: evaluation of bacterial biofilms on different materials used inside International Space Station.* Res Microbiol, 2018. **169**(6): p. 289-295.
80. Novikova, N., et al., *Survey of environmental biocontamination on board the International Space Station.* Res Microbiol, 2006. **157**(1): p. 5-12.
81. Klintworth, R., et al., *Biological induced corrosion of materials II: new test methods and experiences from Mir station.* Acta Astronaut, 1999. **44**(7-12): p. 569-578.
82. Ilyin, V.K., *Microbiological status of cosmonauts during orbital spaceflights on Salyut and Mir orbital stations.* Acta Astronaut, 2005. **56**(9-12): p. 839-50.
83. Horneck, G., D.M. Klaus, and R.L. Mancinelli, *Space microbiology.* Microbiol Mol Biol Rev, 2010. **74**(1): p. 121-56.
84. Zea, L., et al., *Design of a spaceflight biofilm experiment.* Acta Astronaut, 2018. **148**: p. 294-300.
85. Kim, W., et al., *Spaceflight promotes biofilm formation by Pseudomonas aeruginosa.* PLoS One, 2013. **8**(4): p. e62437.
86. Santomartino, R., et al., *No effect of microgravity and simulated mars gravity on final bacterial cell concentrations on the international space station: Applications to space bioproduction.* Frontiers in Microbiology, 2020. **11**.
87. Zea, L., et al., *Phenotypic changes exhibited by E. coli cultured in space.* Front Microbiol, 2017. **8**: p. 1598.
88. Li, Y.H. and X. Tian, *Quorum sensing and bacterial social interactions in biofilms.* Sensors (Basel), 2012. **12**(3): p. 2519-38.
89. Mastroleo, F., et al., *Modelled microgravity cultivation modulates N-acylhomoserine lactone production in Rhodospirillum rubrum S1H independently of cell density.* Microbiology, 2013. **159**(Pt 12): p. 2456-2466.
90. Wong, W.C., et al., *Efficacy of various chemical disinfectants on biofilms formed in spacecraft potable water system components.* Biofouling, 2010. **26**(5): p. 583-6.
91. Mergeay, M. and R. Van Houdt, *Metal response in Cupriavidus metallidurans volume I: From habitats to genes and proteins*. SpringerBriefs in Molecular Science, SpringerBriefs in Biometals. Vol. 1. 2015: Springer.
92. Mergeay, M., et al., *Alcaligenes eutrophus CH34 is a facultative chemolithotroph with plasmid-bound resistance to heavy metals.* J Bacteriol, 1985. **162**(1): p. 328-334.
93. Mergeay, M., C. Houba, and J. Gerits, *Extrachromosomal inheritance controlling resistance to cobalt, cadmium, copper, and zinc ions: Evidence from curing in a Pseudomonas.* Arch Int Physiol Biochim 1978. **86**(2): p. 440-441.
94. Janssen, P.J., et al., *The complete genome sequence of Cupriavidus metallidurans strain CH34, a master survivalist in harsh and anthropogenic environments.* PLoS One, 2010. **5**(5): p. e10433.
95. Vandenbussche, G., R. Van Houdt, and M. Mergeay, *Metal response in Cupriavidus metallidurans volume II: Insights into the structure-function relationship of proteins*. 2015.
96. Bruins, M.R., S. Kapil, and F.W. Oehme, *Microbial resistance to metals in the environment.* Ecotoxicol Environ Saf, 2000. **45**(3): p. 198-207.
97. Wheaton, G., et al., *The confluence of heavy metal biooxidation and heavy metal resistance: Implications for bioleaching by extreme thermoacidophiles.* Minerals, 2015. **5**(3): p. 397-451.
98. Brauner, A., et al., *An experimental framework for quantifying bacterial tolerance.* Biophys J, 2017. **112**(12): p. 2664-2671.
99. Egler, M., et al., *Role of the extracytoplasmic function protein family sigma factor RpoE in metal resistance of Escherichia coli.* J Bacteriol, 2005. **187**(7): p. 2297-307.
100. Andreini, C., et al., *Occurrence of copper proteins through the three domains of life: A bioinformatic approach.* J Proteome Res, 2008. **7**: p. 209-216.
101. Franke, S., et al., *Molecular analysis of the copper-transporting efflux system CusCFBA of Escherichia coli.* Journal of Bacteriology, 2003. **185**(13): p. 3804-3812.
102. Nies, D.H., *Efflux-mediated heavy metal resistance in prokaryotes.* FEMS Microbiology Reviews, 2003. **27**(2-3): p. 313-339.
103. Xue, Y., et al., *Cu(I) recognition via cation-pi and methionine interactions in CusF.* Nat Chem Biol, 2008. **4**(2): p. 107-9.

104. Mealman, T.D., N.J. Blackburn, and M.M. McEvoy, *Metal export by CusCFBA, the periplasmic Cu(I)/Ag(I) transport system of Escherichia coli.* Curr Top Membr, 2012. **69**: p. 163-96.
105. Singh, S.K., et al., *Cuprous oxidase activity of CueO from Escherichia coli.* J Bacteriol, 2004. **186**(22): p. 7815-7.
106. Hobman, J.L. and L.C. Crossman, *Bacterial antimicrobial metal ion resistance.* J Med Microbiol, 2015. **64**(Pt 5): p. 471-497.
107. Staehlin, B.M., et al., *Evolution of a heavy metal homeostasis/resistance island reflects increasing copper stress in Enterobacteria.* Genome Biol Evol, 2016. **8**(3): p. 811-26.
108. Pontel, L.B. and F.C. Soncini, *Alternative periplasmic copper-resistance mechanisms in Gram negative bacteria.* Mol Microbiol, 2009. **73**(2): p. 212-225.
109. Chaturvedi, K.S. and J.P. Henderson, *Pathogenic adaptations to host-derived antibacterial copper.* Front Cell Infect Microbiol, 2014. **4**: p. 3.
110. Djoko, K.Y., Z. Xiao, and A.G. Wedd, *Copper resistance in E. coli: the multicopper oxidase PcoA catalyzes oxidation of copper(I) in Cu(I)Cu(II)-PcoC.* Chembiochem, 2008. **9**(10): p. 1579-82.
111. Zimmermann, M., et al., *PcoE--a metal sponge expressed to the periplasm of copper resistance Escherichia coli. Implication of its function role in copper resistance.* J Inorg Biochem, 2012. **115**: p. 186-97.
112. Lee, S.M., et al., *The Pco proteins are involved in periplasmic copper handling in Escherichia coli.* Biochem Biophys Res Comm, 2002. **295**: p. 616-620.
113. Rouch, D.A. and N.L. Brown, *Copper-inducible transcriptional regulation at two promoters in the Escherichia coli copper resistance determinant pco.* Microbiology, 1997. **143**: p. 1191-1202.
114. Colombi, E., et al., *Evolution of copper resistance in the kiwifruit pathogen Pseudomonas syringae pv. actinidiae through acquisition of integrative conjugative elements and plasmids.* Env Microbiol, 2017. **19**(2): p. 819-832.
115. Monsieurs, P., et al., *Heavy metal resistance in Cupriavidus metallidurans CH34 is governed by an intricate transcriptional network.* Biometals, 2011. **24**(6): p. 1133-51.
116. Maertens, L., et al., *The transcriptomic landscape of Cupriavidus metallidurans CH34 acutely exposed to copper.* Genes, 2020. **11**(9).
117. Lawaree, E., et al., *Caulobacter crescentus intrinsic dimorphism provides a prompt bimodal response to copper stress.* Nat Microbiol, 2016. **1**(9): p. 16098.
118. Schrader, J.M., et al., *Dynamic translation regulation in Caulobacter cell cycle control.* Proc Natl Acad Sci U S A, 2016. **113**(44): p. E6859-E6867.
119. Zhou, B., et al., *The global regulatory architecture of transcription during the Caulobacter cell cycle.* PLoS Genet, 2015. **11**(1): p. e1004831.
120. Schrader, J.M. and L. Shapiro, *Synchronization of Caulobacter crescentus for investigation of the bacterial cell cycle.* J Vis Exp, 2015(98).
121. Jacob, F. and J. Monod, *Genetic regulatory mechanisms in the synthesis of proteins.* J Mol Biol, 1961. **3**: p. 318-356.
122. Lewis, M., *A tale of two repressors.* J Mol Biol, 2011. **409**(1): p. 14-27.
123. Hobman, J.L., J. Wilkie, and N.L. Brown, *A design for life: prokaryotic metal-binding MerR family regulators.* Biometals, 2005. **18**(4): p. 429-36.
124. Zhang, Y.B., et al., *ArsR arsenic-resistance regulatory protein from Cupriavidus metallidurans CH34.* Antonie Van Leeuwenhoek, 2009. **96**(2): p. 161-70.
125. Monchy, S., et al., *Plasmids pMOL28 and pMOL30 of Cupriavidus metallidurans are specialized in the maximal viable response to heavy metals.* J Bacteriol, 2007. **189**(20): p. 7417-25.
126. Grosse, C., et al., *The third pillar of metal homeostasis in Cupriavidus metallidurans CH34: preferences are controlled by extracytoplasmic function sigma factors.* Metallomics, 2019. **11**(2): p. 291-316.
127. Nies, D.H., *Essential and toxic effects of elements on microorganisms*, in *Metals and their compounds in the environment*, K. Anke, M. Ihnat, and M. Stoeppler, Editors. 2004, Wiley-VCH: Weinheim.
128. Rensing, C. and S.F. McDevitt, *The copper metallome in prokaryotic cells.* Met Ions Life Sci, 2013. **12**: p. 417-50.
129. Monchy, S., et al., *Transcriptomic and proteomic analyses of the pMOL30-encoded copper resistance in Cupriavidus metallidurans strain CH34.* Microbiology, 2006. **152**(Pt 6): p. 1765-1776.
130. Jagodnik, J., et al., *Mechanistic study of base-pairing small regulatory RNAs in bacteria.* Methods, 2017. **117**: p. 67-76.

131. Papenfort, K. and J. Vogel, *Multiple target regulation by small noncoding RNAs rewires gene expression at the post-transcriptional level.* Res Microbiol, 2009. **160**(4): p. 278-87.
132. Storz, G., J. Vogel, and K.M. Wassarman, *Regulation by small RNAs in bacteria: expanding frontiers.* Mol Cell, 2011. **43**(6): p. 880-91.
133. Miyakoshi, M., Y. Chao, and J. Vogel, *Regulatory small RNAs from the 3' regions of bacterial mRNAs.* Curr Opin Microbiol, 2015. **24**: p. 132-9.
134. Dar, D. and R. Sorek, *Bacterial noncoding RNAs excised from within protein-coding transcripts.* mBio, 2018. **9**(5).
135. Bossi, L. and N. Figueroa-Bossi, *Competing endogenous RNAs: a target-centric view of small RNA regulation in bacteria.* Nat Rev Microbiol, 2016. **14**(12): p. 775-784.
136. Gottesman, S. and G. Storz, *RNA reflections: converging on Hfq.* RNA, 2015. **21**(4): p. 511-2.
137. Wagner, E.G., *Cycling of RNAs on Hfq.* RNA Biol, 2013. **10**(4): p. 619-26.
138. Olejniczak, M. and G. Storz, *ProQ/FinO-domain proteins: another ubiquitous family of RNA matchmakers?* Mol Microbiol, 2017. **104**(6): p. 905-915.
139. Masse, E., F.E. Escorcia, and S. Gottesman, *Coupled degradation of a small regulatory RNA and its mRNA targets in Escherichia coli.* Genes Dev, 2003. **17**(19): p. 2374-83.
140. Brantl, S., *Regulatory mechanisms employed by cis-encoded antisense RNAs.* Current Opinion in Microbiology, 2007. **10**(2): p. 102-109.
141. Adams, P.P. and G. Storz, *Prevalence of small base-pairing RNAs derived from diverse genomic loci.* Biochim Biophys Acta Gene Regul Mech, 2020. **1863**(7): p. 194524.
142. Dutta, T. and S. Srivastava, *Small RNA-mediated regulation in bacteria: A growing palette of diverse mechanisms.* Gene, 2018. **656**: p. 60-72.
143. Jorgensen, M.G., J.S. Pettersen, and B.H. Kallipolitis, *sRNA-mediated control in bacteria: An increasing diversity of regulatory mechanisms.* Biochim Biophys Acta Gene Regul Mech, 2020. **1863**(5): p. 194504.
144. Babitzke, P. and T. Romeo, *CsrB sRNA family: sequestration of RNA-binding regulatory proteins.* Curr Opin Microbiol, 2007. **10**(2): p. 156-63.
145. Nitzan, M., R. Rehani, and H. Margalit, *Integration of bacterial small RNAs in regulatory networks.* Annu Rev Biophys, 2017. **46**: p. 131-148.
146. Brophy, J.A. and C.A. Voigt, *Antisense transcription as a tool to tune gene expression.* Mol Syst Biol, 2016. **12**(1): p. 854.
147. Georg, J. and W.R. Hess, *Cis-antisense RNA, another level of gene regulation in bacteria.* Microbiol Mol Biol Rev, 2011. **75**(2): p. 286-300.
148. Raghavan, R., D.B. Sloan, and H. Ochman, *Antisense transcription is pervasive but rarely conserved in enteric bacteria.* mBio, 2012. **3**(4).
149. He, Y., et al., *The antisense transcriptomes of human cells.* Science, 2008. **322**(5909): p. 1855-7.
150. Li, J., et al., *Global mapping transcriptional start sites revealed both transcriptional and post-transcriptional regulation of cold adaptation in the methanogenic archaeon Methanolobus psychrophilus.* Sci Rep, 2015. **5**: p. 9209.
151. Wurtzel, O., et al., *A single-base resolution map of an archaeal transcriptome.* Genome Res, 2010. **20**(1): p. 133-41.
152. Passalacqua, K.D., et al., *Strand-specific RNA-seq reveals ordered patterns of sense and antisense transcription in Bacillus anthracis.* PLoS One, 2012. **7**(8): p. e43350.
153. Sharma, C.M., et al., *The primary transcriptome of the major human pathogen Helicobacter pylori.* Nature, 2010. **464**(7286): p. 250-5.
154. Wade, J.T. and D.C. Grainger, *Pervasive transcription: illuminating the dark matter of bacterial transcriptomes.* Nat Rev Microbiol, 2014. **12**(9): p. 647-53.
155. Beaume, M., et al., *Cartography of methicillin-resistant S. aureus transcripts: detection, orientation and temporal expression during growth phase and stress conditions.* PLoS One, 2010. **5**(5): p. e10725.
156. Nicolas, P., et al., *Condition-dependent transcriptome reveals high-level regulatory architecture in Bacillus subtilis.* Science, 2012. **335**(6072): p. 1103-6.
157. Lloréns-Rico, V., et al., *Bacterial antisense RNAs are mainly the product of transcriptional noise.* Sci Adv, 2018. **2**.
158. Singh, S.S., et al., *Widespread suppression of intragenic transcription initiation by H-NS.* Genes & Development, 2014. **28**(3): p. 214-219.
159. Dühring, U., et al., *An internal antisense RNA regulates expression of the photosynthesis gene isiA.* PNAS, 2006. **103**(18): p. 7054-7058.

160. Legewie, S., et al., *Small RNAs establish delays and temporal thresholds in gene expression.* Biophys J, 2008. **95**: p. 3232-3238.
161. Mackie, G.A., *Ribonuclease E is a 5'-end-dependent endonuclease.* Nat Letters, 1998. **395**: p. 720-723.
162. Stazic, D., D. Lindell, and C. Steglich, *Antisense RNA protects mRNA from RNase E degradation by RNA-RNA duplex formation during phage infection.* Nucleic Acids Res, 2011. **39**(11): p. 4890-9.
163. Kawano, M., L. Aravind, and G. Storz, *An antisense RNA controls synthesis of an SOS-induced toxin evolved from an antitoxin.* Mol Microbiol, 2007. **64**(3): p. 738-54.
164. Bouvier, M., et al., *Small RNA binding to 5' mRNA coding region inhibits translational initiation.* Mol Cell, 2008. **32**(6): p. 827-37.
165. Darfeuille, F., et al., *An antisense RNA inhibits translation by competing with standby ribosomes.* Mol Cell, 2007. **26**(3): p. 381-92.
166. Majdalani, N., et al., *DsrA RNA regulates translation of RpoS message by an anti-antisense mechanism, independent of its action as an antisilencer of transcription.* PNAS, 1998. **95**(21): p. 12462-12467.
167. Giangrossi, M., et al., *A novel antisense RNA regulates at transcriptional level the virulence gene icsA of Shigella flexneri.* Nucleic Acids Res, 2010. **38**(10): p. 3362-75.
168. Stork, M., et al., *Transcription termination within the iron transport-biosynthesis operon of Vibrio anguillarum requires an antisense RNA.* J Bacteriol, 2007. **189**(9): p. 3479-88.
169. Sneppen, K., et al., *A mathematical model for transcriptional interference by RNA polymerase traffic in Escherichia coli.* J Mol Biol, 2005. **346**(2): p. 399-409.
170. Crampton, N., et al., *Collision events between RNA polymerases in convergent transcription studied by atomic force microscopy.* Nucleic Acids Res, 2006. **34**(19): p. 5416-25.
171. Prescott, E.M. and N.J. Proudfoot, *Transcriptional collision between convergent genes in budding yeast.* PNAS, 2002. **99**(13): p. 8796-8801.
172. Saberi, F., et al., *Natural antisense RNAs as mRNA regulatory elements in bacteria: a review on function and applications.* Cell Mol Biol Lett, 2016. **21**: p. 6.
173. Bordoy, A.E. and A. Chatterjee, *Cis-antisense transcription gives rise to tunable genetic switch behavior: A mathematical modeling approach.* PLoS One, 2015. **10**(7): p. e0133873.
174. Villegas, V.E. and P.G. Zaphiropoulos, *Neighboring gene regulation by antisense long non-coding RNAs.* Int J Mol Sci, 2015. **16**(2): p. 3251-66.
175. Beisel, C.L. and G. Storz, *Base pairing small RNAs and their roles in global regulatory networks.* FEMS Microbiol Rev, 2010. **34**(5): p. 866-82.
176. Shimoni, Y., et al., *Regulation of gene expression by small non-coding RNAs: a quantitative view.* Mol Syst Biol, 2007. **3**: p. 138.
177. Holmqvist, E. and E.G.H. Wagner, *Impact of bacterial sRNAs in stress responses.* Biochem Soc Trans, 2017. **45**(6): p. 1203-1212.
178. Chareyre, S. and P. Mandin, *Bacterial iron homeostasis regulation by sRNAs.* Microbiol Spectrum, 2018. **6**(2).
179. Lalaouna, D., et al., *RsaC sRNA modulates the oxidative stress response of Staphylococcus aureus during manganese starvation.* Nucleic Acids Res, 2019. **47**(18): p. 9871-9887.
180. de Freitas, E.C., et al., *The copper-inducible copAB operon in Xanthomonas citri subsp. citri is regulated at transcriptional and translational levels.* Microbiology, 2019. **165**(3): p. 355-365.
181. Chen, Y., et al., *sRNA OsiA stabilizes catalase mRNA during oxidative stress response of Deinococcus radiodurans R1.* Microorganisms, 2019. **7**(10).
182. Fröhlich, K.S. and S. Gottesman, *Small regulatory RNAs in the Enterobacterial response to envelope damage and oxidative stress.* Microbiol Spectr, 2018.
183. Peng, T., et al., *Identification of novel sRNAs involved in oxidative stress response in the fish pathogen Vibrio alginolyticus by transcriptome analysis.* J Fish Dis, 2019. **42**(2): p. 277-291.
184. Schachterle, J.K., D.M. Onsay, and G.W. Sundin, *Small RNA ArcZ regulates oxidative stress response genes and regulons in Erwinia amylovora.* Front Microbiol, 2019. **10**: p. 2775.
185. Gelsinger, D.R. and J. DiRuggiero, *Transcriptional landscape and regulatory roles of small noncoding RNAs in the oxidative stress response of the haloarchaeon Haloferax volcanii.* J Bacteriol, 2018. **200**(9).
186. Wilson, J.W., et al., *Space flight alters bacterial gene expression and virulence and reveals a role for global regulator Hfq.* PNAS, 2007. **104**(41): p. 16299-16304.

187. Crabbe, A., et al., *Transcriptional and proteomic responses of Pseudomonas aeruginosa PAO1 to spaceflight conditions involve Hfq regulation and reveal a role for oxygen.* Appl Environ Microbiol, 2011. **77**(4): p. 1221-30.
188. Pinto, D., M.A. Santos, and L. Chambel, *Thirty years of viable but nonculturable state research: unsolved molecular mechanisms.* Crit Rev Microbiol, 2015. **41**(1): p. 61-76.
189. Rittershaus, E.S., S.H. Baek, and C.M. Sassetti, *The normalcy of dormancy: common themes in microbial quiescence.* Cell Host Microbe, 2013. **13**(6): p. 643-51.
190. Betts, J., et al., *Evaluation of a nutrient starvation model of Mycobacterium tuberculosis persistence by gene and protein expression profiling.* Mol Microbiol, 2002. **43**(3): p. 717-731.
191. Bogosian, G. and E.V. Bourneuf, *A matter of bacterial life and death.* EMBO rep, 2001. **2**(9): p. 770-774.
192. Fisher, R.A., B. Gollan, and S. Helaine, *Persistent bacterial infections and persister cells.* Nat Rev Microbiol, 2017. **15**(8): p. 453-464.
193. Kim, J.S., et al., *Viable but non-culturable and persistence describe the same bacterial stress state.* Environ Microbiol, 2018. **20**(6): p. 2038-2048.
194. Ayrapetyan, M., T. Williams, and J.D. Oliver, *Relationship between the viable but nonculturable state and antibiotic persister cells.* J Bacteriol, 2018. **200**(20).
195. Whitesides, M.D. and J.D. Oliver, *Resuscitation of Vibrio vulnificus from the viable but nonculturable state.* Appl Environ Microbiol, 1997. **63**(3): p. 1002-1005.
196. Grey, B. and T.R. Steck, *Concentrations of copper thought to be toxic to Escherichia coli can induce the viable but nonculturable condition.* Appl Environ Microbiol, 2001. **67**(11): p. 5325-7.
197. Aurass, P., R. Prager, and A. Flieger, *EHEC/EAEC O104:H4 strain linked with the 2011 German outbreak of haemolytic uremic syndrome enters into the viable but non-culturable state in response to various stresses and resuscitates upon stress relief.* Environ Microbiol, 2011. **13**(12): p. 3139-48.
198. Bedard, E., et al., *Recovery of Pseudomonas aeruginosa culturability following copper- and chlorine-induced stress.* FEMS Microbiol Lett, 2014. **356**(2): p. 226-34.
199. Grey, B.E. and T.R. Steck, *The viable but nonculturable state of Ralstonia solanacearum may be involved in long-term survival and plant infection.* Appl Environ Microbiol, 2001. **67**(9): p. 3866-72.
200. Um, H.Y., et al., *Altered gene expression and intracellular changes of the viable but nonculturable state in Ralstonia solanacearum by copper treatment.* Plant Pathol J, 2013. **29**(4): p. 374-85.
201. Ordax, M., et al., *Survival strategy of Erwinia amylovora against copper: induction of the viable-but-nonculturable state.* Appl Environ Microbiol, 2006. **72**(5): p. 3482-8.
202. Alexander, E., D. Pham, and T.R. Steck, *The viable-but-nonculturable condition is induced by copper in Agrobacterium tumefaciens and Rhizobium leguminosarum.* Appl Environ Microbiol, 1999. **65**(8): p. 3754-3756.
203. Jiang, N., et al., *Induction of the viable but nonculturable state in Clavibacter michiganensis subsp.michiganensis and in planta resuscitation of the cells on tomato seedlings* Plant Pathol, 2016. **65**(5): p. 826-836.
204. Kan, Y., et al., *Induction and resuscitation of the viable but non-culturable (VBNC) state in Acidovorax citrulli, the causal agent of bacterial fruit blotch of cucurbitaceous crops.* Front Microbiol, 2019. **10**: p. 1081.
205. del Campo, R., et al., *Xanthomonas axonopodis pv. citri enters the VBNC state after copper treatment and retains its virulence.* FEMS Microbiol Lett, 2009. **298**(2): p. 143-8.
206. Zhao, X., et al., *Current perspectives on viable but non-culturable state in foodborne pathogens.* Front Microbiol, 2017. **8**: p. 580.
207. Cuny, C., et al., *Investigation of the first events leading to loss of culturability during Escherichia coli starvation: future nonculturable bacteria form a subpopulation.* J Bacteriol, 2005. **187**(7): p. 2244-8.
208. Liao, X., D. Liu, and T. Ding, *Nonthermal plasma induces the viable-but-nonculturable state in Staphylococcus aureus via metabolic suppression and the oxidative stress response.* Appl Environ Microbiol, 2020. **86**(5): p. e02216-19.
209. Li, L., et al., *The importance of the viable but non-culturable state in human bacterial pathogens.* Front Microbiol, 2014. **5**.
210. Longkumer, T., et al., *OxyR-dependent expression of a novel glutathione S-transferase (Abgst01) gene in Acinetobacter baumannii DS002 and its role in biotransformation of organophosphate insecticides.* Microbiology (Reading), 2014. **160**(Pt 1): p. 102-112.
211. Abe, A., et al., *Isolation and characterization of a cold-induced nonculturable suppression mutant of Vibrio vulnificus.* Microbiol Res, 2007. **162**(2): p. 130-8.

212. Wang, H.W., et al., *Roles of alkyl hydroperoxide reductase subunit C (AhpC) in viable but nonculturable Vibrio parahaemolyticus.* Appl Environ Microbiol, 2013. **79**(12): p. 3734-43.
213. Franca, M.B., A.D. Panek, and E.C. Eleutherio, *Oxidative stress and its effects during dehydration.* Comp Biochem Physiol A Mol Integr Physiol, 2007. **146**(4): p. 621-31.
214. McDougald, D., et al., *Defences against oxidative stress during starvation in bacteria.* Antonie Van Leeuwenhoek, 2002. **81**: p. 3-13.
215. da Cruz Nizer, W.S., V. Inkovskiy, and J. Overhage, *Surviving reactive chlorine stress: Responses of gram-negative bacteria to hypochlorous acid.* Microorganisms, 2020. **8**(8).
216. Kan, Y., et al., *iTRAQ-based proteomic analyses of the plant-pathogenic bacterium Acidovorax citrulli during entrance into and resuscitation from the viable but nonculturable state.* J Proteomics, 2020. **211**: p. 103547.
217. Chen, Y., et al., *Biostimulants application for bacterial metabolic activity promotion and sodium dodecyl sulfate degradation under copper stress.* Chemosphere, 2019. **226**: p. 736-743.
218. Feng, S., et al., *Metabolic transcriptional analysis on copper tolerance in moderate thermophilic bioleaching microorganism Acidithiobacillus caldus.* J Ind Microbiol Biotechnol, 2020. **47**(1): p. 21-33.
219. Reyes, V.C., et al., *Copper status of exposed microorganisms influences susceptibility to metallic nanoparticles.* Environ Toxicol Chem, 2016. **35**(5): p. 1148-58.
220. Bai, H., et al., *Citric acid can force Staphylococcus aureus into viable but nonculturable state and its characteristics.* Int J Food Microbiol, 2019. **305**: p. 108254.
221. Kim, J.C., et al., *Non-selective regulation of peroxide and superoxide resistance genes by PerR in Campylobacter jejuni.* Front Microbiol, 2015. **6**: p. 126.
222. Parry, B.R. and D.H. Shain, *Manipulations of AMP metabolic genes increase growth rate and cold tolerance in Escherichia coli: implications for psychrophilic evolution.* Mol Biol Evol, 2011. **28**(7): p. 2139-45.
223. Ramamurthy, T., et al., *Current perspectives on viable but non-culturable (VBNC) pathogenic bacteria.* Front Public Health, 2014. **2**: p. 103.
224. Nandakumar, R., et al., *Quantitative proteomic profiling of the Escherichia coli response to metallic copper surfaces.* BioMetals, 2011. **24**(3): p. 429-444.
225. Ding, T., et al., *Significance of viable but nonculturable Escherichia coli: induction, detection, and control.* J Microbiol Biotechnol, 2017. **27**(3): p. 417-428.
226. Ott, C.M., R.J. Bruce, and D.L. Pierson, *Microbial characterization of free floating condensate aboard the Mir space station.* Microb Ecol, 2004. **47**(2): p. 133-6.
227. Baker, P.W. and L. Leff, *The effect of simulated microgravity on bacteria from the Mir space station.* Micrograv Sci Tech, 2004. **15**(1): p. 35-41.
228. Pierson, D.L., *Microbial contamination of spacecraft.* Grav Space Biol Bull, 2001. **14**(2).
229. Newcombe, D.A., et al., *Impact of assembly, testing and launch operations on the airborne bacterial diversity within a spacecraft assembly facility clean-room.* International Journal of Astrobiology, 2008. **7**(3-4): p. 223-236.
230. La Duc, M.T., et al., *Microbial characterization of the Mars Odyssey spacecraft and its encapsulation facility.* Environ Microbiol, 2003. **5**(10): p. 977-85.
231. La Duc, M.T., R. Kern, and K. Venkateswaran, *Microbial monitoring of spacecraft and associated environments.* Microb Ecol, 2004. **47**(2): p. 150-8.
232. Loudon, C.-M., et al., *BioRock: new experiments and hardware to investigate microbe–mineral interactions in space.* International Journal of Astrobiology, 2017. **17**(4): p. 303-313.
233. Leys, N., et al., *The response of Cupriavidus metallidurans CH34 to spaceflight in the International Space Station.* Antonie Van Leeuwenhoek, 2009. **96**(2): p. 227-45.
234. Byloos, B., et al., *The impact of space flight on survival and interaction of Cupriavidus metallidurans CH34 with basalt, a volcanic moon analog rock.* Front Microbiol, 2017. **8**: p. 671.
235. Cockell, C.S., et al., *Space station biomining experiment demonstrates rare earth element extraction in microgravity and Mars gravity.* Nat Commun, 2020. **11**(1): p. 5523.
236. La Duc, M.T., et al., *Characterization and monitoring of microbes in the International Space Station drinking water.* SAE Technical Papers Series, 2003. **2003-01-2404**: p. 1-8.
237. Pehkonen, S.O., A. Palit, and X. Zhang, *Effect of specific water quality parameters on copper corrosion.* Corrosion, 2002. **58**(2): p. 156-165.
238. Karczewska, A. and K. Milko, *Effects of chelating agents on copper, lead, and zinc solubility in polluted soils and tailings produced by copper industry.* Ecol Chem Eng, 2010. **17**(4-5): p. 395-403.

239. Lin, Y.-S., et al., *Individual and combined effects of copper and silver ions on inactivation of Legionella pneumophila.* Water Res, 1996. **30**(8): p. 1905-1913.
240. Cervantes, H.I., et al., *Antimicrobial activity of copper against organisms in aqueous solution: a case for copper-based water pipelines in hospitals?* Am J Infect Control, 2013. **41**(12): p. e115-8.
241. Faúndez, G., et al., *Antimicrobial activity of copper surfaces against suspensions of Salmonella enterica and Campylobacter jejuni.* BMC Microbiol, 2004. **4**(19).
242. Michels, H.T., J.O. Noyce, and C.W. Keevil, *Effects of temperature and humidity on the efficacy of methicillin-resistant Staphylococcus aureus challenged antimicrobial materials containing silver and copper.* Lett Appl Microbiol, 2009. **49**(2): p. 191-5.
243. Molteni, C., H.K. Abicht, and M. Solioz, *Killing of bacteria by copper surfaces involves dissolved copper.* Appl Environ Microbiol, 2010. **76**(12): p. 4099-101.
244. Tian, W.X., et al., *Copper as an antimicrobial agent against opportunistic pathogenic and multidrug resistant Enterobacter bacteria.* J Microbiol, 2012. **50**(4): p. 586-93.
245. Cui, Z., et al., *Susceptibility of opportunistic Burkholderia glumae to copper surfaces following wet or dry surface contact.* Molecules, 2014. **19**(7): p. 9975-85.
246. San, K., et al., *Antimicrobial copper alloy surfaces are effective against vegetative but not sporulated cells of gram-positive Bacillus subtilis.* MicrobiologyOpen, 2015. **4**(5): p. 753-63.
247. Warnes, S.L., V. Caves, and C.W. Keevil, *Mechanism of copper surface toxicity in Escherichia coli O157:H7 and Salmonella involves immediate membrane depolarization followed by slower rate of DNA destruction which differs from that observed for Gram-positive bacteria.* Environ Microbiol, 2012. **14**(7): p. 1730-43.
248. Espirito Santo, C., et al., *Bacterial killing by dry metallic copper surfaces.* Appl Environ Microbiol, 2011. **77**(3): p. 794-802.
249. Santo, C.E., D. Quaranta, and G. Grass, *Antimicrobial metallic copper surfaces kill Staphylococcus haemolyticus via membrane damage.* MicrobiologyOpen, 2012. **1**(1): p. 46-52.
250. Orman, M.A. and M.P. Brynildsen, *Establishment of a method to rapidly assay bacterial persister metabolism.* Antimicrob Agents Chemother, 2013. **57**(9): p. 4398-409.
251. Nowakowska, J. and J.D. Oliver, *Resistance to environmental stresses by Vibrio vulnificus in the viable but nonculturable state.* FEMS Microbiol Ecol, 2013. **84**(1): p. 213-22.
252. Dopp, E., et al., *Influence of the copper-induced viable but non-culturable state on the toxicity of Pseudomonas aeruginosa towards human bronchial epithelial cells in vitro.* Int J Hyg Environ Health, 2017. **220**(8): p. 1363-1369.
253. Ye, C., et al., *Characterization and potential mechanisms of highly antibiotic tolerant VBNC Escherichia coli induced by low level chlorination.* Sci Rep, 2020. **10**(1): p. 1957.
254. Lee, D.-G., S.J. Park, and S.-J. Kim, *Influence of pipe materials and VBNC cells on culturable bacteria in a chlorinated drinking water model system.* J Microbiol Biotech, 2007. **17**(9): p. 1558-1562.
255. Lutkenhaus, J.F., *Role of a major outer membrane protein in Escherichia coli.* J Bacteriol, 1977. **131**(2): p. 631-637.
256. Balasubramanian, R., G.E. Kenney, and A.C. Rosenzweig, *Dual pathways for copper uptake by methanotrophic bacteria.* J Biol Chem, 2011. **286**(43): p. 37313-9.
257. Ekici, S., et al., *Novel transporter required for biogenesis of cbb3-type cytochrome c oxidase in Rhodobacter capsulatus.* mBio, 2012. **3**(1): p. 1-11.
258. Espirito Santo, C., et al., *Contribution of copper ion resistance to survival of Escherichia coli on metallic copper surfaces.* Appl Environ Microbiol, 2008. **74**(4): p. 977-86.
259. Elguindi, J., J. Wagner, and C. Rensing, *Genes involved in copper resistance influence survival of Pseudomonas aeruginosa on copper surfaces.* J Appl Microbiol, 2009. **106**(5): p. 1448-55.
260. Collard, J.M., et al., *Plasmids for heavy metal resistance in Alcaligenes eutrophus CH34: Mechanisms and applications.* FEMS Microbiol Rev, 1994. **14**: p. 405-414.
261. Props, R., et al., *Measuring the biodiversity of microbial communities by flow cytometry.* Methods Ecol Evol, 2016. **7**(11): p. 1376-1385.
262. Kanellis, V.G., *Sensitivity limits of biosensors used for the detection of metals in drinking water.* Biophys Rev, 2018. **10**(5): p. 1415-1426.
263. Strauber, H. and S. Muller, *Viability states of bacteria - specific mechanisms of selected probes.* Cytometry Part A, 2010. **77**(7): p. 623-34.
264. Shi, L., et al., *Limits of propidium iodide as a cell viability indicator for environmental bacteria.* Cytometry A, 2007. **71**(8): p. 592-8.
265. Yang, Y., Y. Xiang, and M. Xu, *From red to green: the propidium iodide-permeable membrane of Shewanella decolorationis S12 is repairable.* Sci Rep, 2015. **5**: p. 18583.

266. Berney, M., et al., *Assessment and interpretation of bacterial viability by using the LIVE/DEAD BacLight Kit in combination with flow cytometry.* Appl Environ Microbiol, 2007. **73**(10): p. 3283-90.
267. Vandecraen, J., et al., *Zinc-induced transposition of insertion sequence elements contributes to increased adaptability of Cupriavidus metallidurans.* Front Microbiol, 2016. **7**.
268. Cuppett, J.D., S.E. Duncan, and A.M. Dietrich, *Evaluation of copper speciation and water quality factors that affect aqueous copper tasting response.* Chem Senses, 2006. **31**(7): p. 689-97.
269. Lehtola, M.J., et al., *Microbiology, chemistry and biofilm development in a pilot drinking water distribution system with copper and plastic pipes.* Water Res, 2004. **38**(17): p. 3769-79.
270. Jungfer, C., et al., *Drinking water biofilms on copper and stainless steel exhibit specific molecular responses towards different disinfection regimes at waterworks.* Biofouling, 2013. **29**(8): p. 891-907.
271. Yu, J., D. Kim, and T. Lee, *Microbial diversity in biofilms on water distribution pipes of different materials.* Water Sci Technol, 2010. **61**(1): p. 163-71.
272. Sarandan, M., et al., *Biofilm formation on materials commonly used in household drinking water systems.* Water Supply, 2011. **11**(2): p. 252-257.
273. Nguyen, C.C., et al., *Association between heavy metals and antibiotic-resistant human pathogens in environmental reservoirs: A review.* Front Env Sci Eng, 2019. **13**(3).
274. Stepanauskas, R., et al., *Coselection for microbial resistance to metals and antibiotics in freshwater microcosms.* Environ Microbiol, 2006. **8**(9): p. 1510-4.
275. Dickinson, A.W., et al., *Heavy metal pollution and co-selection for antibiotic resistance: A microbial palaeontology approach.* Environ Int, 2019. **132**: p. 105117.
276. Baker-Austin, C., et al., *Co-selection of antibiotic and metal resistance.* Trends Microbiol, 2006. **14**(4): p. 176-82.
277. Manaia, C.M., et al., *Heterotrophic plate counts and the isolation of bacteria from mineral waters on selective and enrichment media.* J Appl Bacteriol, 1990. **69**: p. 871-876.
278. Berthiaume, C., et al., *Identification of dichloroacetic acid degrading Cupriavidus bacteria in a drinking water distribution network model.* J Appl Microbiol, 2014. **116**(1): p. 208-21.
279. Pindi, P.K., P.R. Yadav, and A.S. Shanker, *Identification of opportunistic pathogenic bacteria in drinking water samples of different rural health centers and their clinical impacts on humans.* Biomed Res Int, 2013. **2013**: p. 348250.
280. Valette-Silver, N.J., *The use of sediment cores to reconstruct historical trends in contamination of estuarine and coastal sediments.* Estuaries, 1993. **16**(3B): p. 577-588.
281. Nicholson, F.A., et al., *An inventory of heavy metals inputs to agricultural soils in England and Wales.* Sci Total Environ, 2003. **311**(1-3): p. 205-219.
282. Francois, F., et al., *Isolation and characterization of environmental bacteria capable of extracellular biosorption of mercury.* Appl Environ Microbiol, 2012. **78**(4): p. 1097-106.
283. Samanta, A., et al., *An investigation on heavy metal tolerance and antibiotic resistance properties of bacterial strain Bacillus sp. isolated from municipal waste.* J Microbiol Biotech Res, 2012. **2**(1): p. 178-189.
284. Sobolev, D. and M.F.T. Begonia, *Effects of heavy metal contamination upon soil microbes: Lead-induced changes in general and denitrifying microbial communities as evidenced by molecular markers.* Int J Env Res Public Health, 2008. **5**(5): p. 450-456.
285. Hoostal, M.J., M.G. Bidart-Bouzat, and J.L. Bouzat, *Local adaptation of microbial communities to heavy metal stress in polluted sediments of Lake Erie.* FEMS Microbiol Ecol, 2008. **65**(1): p. 156-68.
286. Igiri, B.E., et al., *Toxicity and bioremediation of heavy metals contaminated ecosystem from tannery wastewater: A review.* J Toxicol, 2018. **2018**: p. 2568038.
287. Köhler, S., S. Belkin, and R.D. Schmid, *Reporter gene bioassays in environmental analysis.* Fresenius J Anal Chem, 2000. **366**: p. 769-779.
288. Tauriainen, S.M., M.P.J. Virta, and M.T. Karp, *Detecting bioavailable toxic metals and metalloids from natural water samples using luminescent sensor bacteria.* Wat Res, 2000. **34**(10): p. 2661-2666.
289. Flynn, H.C., et al., *Antimony bioavailability in mine soils.* Env Pollut, 2003. **124**(1): p. 93-100.
290. Magrisso, S., Y. Erel, and S. Belkin, *Microbial reporters of metal bioavailability.* Microb Biotechnol, 2008. **1**(4): p. 320-30.
291. Meliani, A. and A. Bensoltane, *Biofilm-mediated heavy metals bioremediation in PGPR Pseudomonas.* J Bioremediat Biodegrad, 2016. **7**(5).
292. Xu, Z., Y. Lei, and J. Patel, *Bioremediation of soluble heavy metals with recombinant Caulobacter crescentus.* Bioeng Bugs, 2010. **1**(3): p. 207-12.

293. Tabak, H.H., et al., *Developments in bioremediation of soils and sediments polluted with metals and radionuclides – 1. Microbial processes and mechanisms affecting bioremediation of metal contamination and influencing metal toxicity and transport.* Rev Environ Sci Biotechnol, 2005. **4**(3): p. 115-156.
294. Akcil, A., et al., *A review of approaches and techniques used in aquatic contaminated sediments: metal removal and stabilization by chemical and biotechnological processes.* J Clean Prod, 2015. **86**: p. 24-36.
295. Nies, D.H., *Microbial heavy-metal resistance.* Appl Microbiol Biotechnol, 1999. **51**: p. 730-750.
296. Diels, L., et al., *From industrial sites to environmental applications with Cupriavidus metallidurans.* Antonie Van Leeuwenhoek, 2009. **96**(2): p. 247-58.
297. Corbisier, P., E. Thiry, and L. Diels, *Bacterial biosensors for the toxicity assessment of solid wastes.* Environ Tox Water Qual: Int J, 1996. **11**: p. 171-177.
298. Tibazarwa, C., et al., *A microbial biosensor to predict bioavailable nickel in soil and its transfer to plants.* Env Pollut, 2001. **113**: p. 19-26.
299. Corbisier, P., et al., *Whole cell- and protein-based biosensors for the detection of bioavailable heavy metals in environmental samples.* Anal Chim Act, 1999. **387**: p. 235-244.
300. Diels, L., et al., *Heavy metals bioremediation of soil.* Mol Biotechnol, 1999. **12**: p. 149-158.
301. Berezina, N., B. Yada, and R. Lefebvre, *From organic pollutants to bioplastics: insights into the bioremediation of aromatic compounds by Cupriavidus necator.* New Biotechnol, 2015. **32**(1): p. 47-53.
302. Lee, K.-Y., J. Bosch, and R.U. Meckenstock, *Use of metal-reducing bacteria for bioremediation of soil contaminated with mixed organic and inorganic pollutants.* Environ Geochem Hlth, 2011. **34**(S1): p. 135-142.
303. Kohler, C., et al., *Extracytoplasmic function (ECF) sigma factor σF is involved in Caulobacter crescentus response to heavy metal stress.* BMC Microbiol, 2012. **12**(210).
304. Osman, D. and J.S. Cavet, *Copper homeostasis in bacteria*. 2008. p. 217-247.
305. Hor, J. and J. Vogel, *Global snapshots of bacterial RNA networks.* EMBO J, 2017. **36**(3): p. 245-247.
306. Chen, J., T. Morita, and S. Gottesman, *Regulation of transcription termination of small RNAs and by small RNAs: Molecular mechanisms and biological functions.* Front Cell Infect Microbiol, 2019. **9**: p. 201.
307. Dietrich, M., et al., *The effect of hfq on global gene expression and virulence in Neisseria gonorrhoeae.* FEBS J, 2009. **276**(19): p. 5507-20.
308. Sousa, S.A., et al., *The hfq gene is required for stress resistance and full virulence of Burkholderia cepacia to the nematode Caenorhabditis elegans.* Microbiology, 2010. **156**(Pt 3): p. 896-908.
309. Feliciano, J.R., et al., *Hfq: a multifaceted RNA chaperone involved in virulence.* Future Microbiol, 2016. **11**(1): p. 137-151.
310. Kakoschke, T.K., et al., *The RNA chaperone Hfq is essential for virulence and modulates the expression of four adhesins in Yersinia enterocolitica.* Sci Rep, 2016. **6**: p. 29275.
311. Fantappie, L., et al., *The RNA chaperone Hfq is involved in stress response and virulence in Neisseria meningitidis and is a pleiotropic regulator of protein expression.* Infect Immun, 2009. **77**(5): p. 1842-53.
312. Eshghi, A., et al., *A putative regulatory genetic locus modulates virulence in the pathogen Leptospira interrogans.* Infect Immun, 2014. **82**(6): p. 2542-52.
313. Geng, J., et al., *Involvement of the post-transcriptional regulator Hfq in Yersinia pestis virulence.* PLoS One, 2009. **4**(7): p. e6213.
314. Molina-Santiago, C., et al., *Differential transcriptional response to antibiotics by Pseudomonas putida DOT-T1E.* Environ Microbiol, 2015. **17**(9): p. 3251-62.
315. Chen, Y., et al., *Small RNAs in the genus Clostridium.* mBio, 2011. **2**(1): p. e00340-10.
316. Yu, J. and T. Schneiders, *Tigecycline challenge triggers sRNA production in Salmonella enterica serovar Typhimurium.* BMC Microbiol, 2012. **12**(195).
317. Howden, B.P., et al., *Analysis of the small RNA transcriptional response in multidrug-resistant Staphylococcus aureus after antimicrobial exposure.* Antimicrob Agents Chemother, 2013. **57**(8): p. 3864-74.
318. Fröhlich, K.S. and K. Papenfort, *Interplay of regulatory RNAs and mobile genetic elements in enteric pathogens.* Mol Microbiol, 2016. **101**(5): p. 701-713.
319. Oglesby-Sherrouse, A.G. and E.R. Murphy, *Iron-responsive bacterial small RNAs: variations on a theme.* Metallomics, 2013. **5**(4): p. 276-86.

320. Sridhar, J. and M. Gayathri, *Transcriptome-based identification of silver stress responsive sRNAs from Bacillus cereus ATCC14579.* Bioinformation, 2019. **15**(7): p. 474-479.
321. Olaya-Abril, A., et al., *Putative small RNAs controlling detoxification of industrial cyanide-containing wastewaters by Pseudomonas pseudoalcaligenes CECT5344.* PLoS One, 2019. **14**(2): p. e0212032.
322. Innocenti, N., et al., *Whole-genome mapping of 5' RNA ends in bacteria by tagged sequencing: a comprehensive view in Enterococcus faecalis.* RNA, 2015. **21**(5): p. 1018-30.
323. Sharma, C.M. and J. Vogel, *Differential RNA-seq: the approach behind and the biological insight gained.* Curr Opin Microbiol, 2014. **19**: p. 97-105.
324. Maes, A., et al., *Landscape of RNA polyadenylation in E. coli.* Nucleic Acids Res, 2017. **45**(5): p. 2746-2756.
325. Innocenti, N., F. Repoila, and E. Aurell, *Detection and quantitative estimation of spurious double stranded DNA formation during reverse transcription in bacteria using tagRNA-seq.* RNA Biol, 2015. **12**(9): p. 1067-9.
326. Qi, L., et al., *Genome-wide mRNA processing in methanogenic archaea reveals post-transcriptional regulation of ribosomal protein synthesis.* Nucleic Acids Res, 2017. **45**(12): p. 7285-7298.
327. Bolger, A.M., M. Lohse, and B. Usadel, *Trimmomatic: a flexible trimmer for Illumina sequence data.* Bioinformatics, 2014. **30**(15): p. 2114-20.
328. Langmead, B. and S.L. Salzberg, *Fast gapped-read alignment with Bowtie 2.* Nat Methods, 2012. **9**(4): p. 357-9.
329. Li, H., et al., *The Sequence Alignment/Map format and SAMtools.* Bioinformatics, 2009. **25**(16): p. 2078-9.
330. Liao, Y., G.K. Smyth, and W. Shi, *featureCounts: an efficient general-purpose program for assigning sequence reads to genomic features.* Bioinformatics, 2014. **30**: p. 923-930.
331. McCarthy, D.J., Y. Chen, and G.K. Smyth, *Differential expression analysis of multifactor RNA-Seq experiments with respect to biological variation.* Nucleic Acids Res, 2012. **40**(10): p. 4288-97.
332. Robinson, M.D., D.J. McCarthy, and G.K. Smyth, *edgeR: a Bioconductor package for differential expression analysis of digital gene expression data.* Bioinformatics, 2010. **26**(1): p. 139-40.
333. Ritchie, M.E., et al., *limma powers differential expression analyses for RNA-sequencing and microarray studies.* Nucleic Acids Res, 2015. **43**(7): p. e47.
334. Benjamini, Y. and Y. Hochberg, *Controlling the false discovery rate: A practical and powerful approach to multiple testing.* J R Stat Soc, 1995.
335. Jensen, L.J., et al., *eggNOG: automated construction and annotation of orthologous groups of genes.* Nucleic Acids Res, 2008. **36**: p. D250-4.
336. Vallenet, D., et al., *MicroScope--an integrated microbial resource for the curation and comparative analysis of genomic and metabolic data.* Nucleic Acids Res, 2013. **41**: p. D636-47.
337. Quinlan, A.R. and I.M. Hall, *BEDTools: a flexible suite of utilities for comparing genomic features.* Bioinformatics, 2010. **26**(6): p. 841-2.
338. Dieppois, G., et al., *The transcriptional regulator CzcR modulates antibiotic resistance and quorum sensing in Pseudomonas aeruginosa.* PLoS One, 2012. **7**(5): p. e38148.
339. Urano, H., et al., *Cross-regulation between two common ancestral response regulators, HprR and CusR, in Escherichia coli.* Microbiology, 2017. **163**(2): p. 243-252.
340. Mijnendonckx, K., et al., *Spontaneous mutation in the AgrRS two-component regulatory system of Cupriavidus metallidurans results in enhanced silver resistance.* Metallomics, 2019. **11**(11): p. 1912-1924.
341. Caille, O., C. Rossier, and K. Perron, *A copper-activated two-component system interacts with zinc and imipenem resistance in Pseudomonas aeruginosa.* J Bacteriol, 2007. **189**(13): p. 4561-8.
342. Reith, F., et al., *Mechanisms of gold biomineralization in the bacterium Cupriavidus metallidurans.* PNAS, 2009. **109**(42): p. 17757-17762.
343. Huang, N., et al., *Multiple transcriptional mechanisms collectively mediate copper resistance in Cupriavidus gilardii CR3.* Environ Sci Technol, 2019. **53**(8): p. 4609-4618.
344. Kim, S.O., et al., *OxyR: A molecular code for redox-related signaling.* Cell, 2002. **109**: p. 383-396.
345. Koo, M.-S., et al., *A reducing system of the superoxide sensor SoxR in Escherichia coli.* EMBO J, 2003. **22**(11): p. 2614-2622.
346. Lesniak, J., W.A. Barton, and D.B. Nikolov, *Structural and functional characterization of the Pseudomonas hydroperoxide resistance protein Ohr.* EMBO J, 2002. **21**(24): p. 6649-6659.
347. Sukchawalit, R., et al., *Complex regulation of the organic hydroperoxide resistance gene (ohr) from Xanthomonas involves OhrR, a novel organic peroxide-inducible negative regulator, and posttranscriptional modifications.* J Bacteriol, 2001. **183**(15): p. 4405-4412.

348. Scarpa, M., et al., *Activated oxygen species in the oxidation of glutathione: A kinetic study.* Biophysical Chemistry, 1996. **60**: p. 53-61.
349. Romsang, A., et al., *The iron-sulphur cluster biosynthesis regulator IscR contributes to iron homeostasis and resistance to oxidants in Pseudomonas aeruginosa.* PLoS One, 2014. **9**(1): p. e86763.
350. Chillappagari, S., et al., *Copper stress affects iron homeostasis by destabilizing iron-sulfur cluster formation in Bacillus subtilis.* J Bacteriol, 2010. **192**(10): p. 2512-2524.
351. Fang, Z. and P.C. Dos Santos, *Protective role of bacillithiol in superoxide stress and Fe-S metabolism in Bacillus subtilis.* Microbiologyopen, 2015. **4**(4): p. 616-31.
352. Fung, D.K., et al., *Copper efflux is induced during anaerobic amino acid limitation in Escherichia coli to protect iron-sulfur cluster enzymes and biogenesis.* J Bacteriol, 2013. **195**(20): p. 4556-68.
353. Sticht, H. and P. Rösch, *The structure of iron-sulfur proteins.* Prog Biophys Mol Biol, 1998. **70**: p. 95-136.
354. Beinert, H., *Iron-sulfur proteins: ancient structures, still full of surprises*, in *9th International Conference on Biological Inorganic Chemistry*. 2000: Minneapolis, US. p. 2-15.
355. Woo, K.M., et al., *The heat-shock protein ClpB in Escherichia coli is a protein-activated ATPase.* J Biol Chem, 1992. **267**(28): p. 20429-20434.
356. Skowyra, D., C. Georgopoulos, and M. Zylicz, *The E. coli dnaK gene product, the hsp70 homolog, can reactivate heat-inactivated RNA polymerase in an ATP hydrolysis-independent manner.* Cell, 1990. **62**: p. 939-944.
357. Rohrwild, M., et al., *HslV-HslU: A novel ATP-dependent protease complex in Escherichia coli related to the eukaryotic proteasome.* Proc Natl Acad Sci U S A, 1996. **93**: p. 5808-5813.
358. Gutsche, J., U. Remminghorst, and B.H. Rehm, *Biochemical analysis of alginate biosynthesis protein AlgX from Pseudomonas aeruginosa: purification of an AlgX-MucD (AlgY) protein complex.* Biochimie, 2006. **88**(3-4): p. 245-51.
359. Irisawa, T., et al., *Effect of trans-4-guanidinomethylcyclohexanecarboxylic acid 4-tert-butylphenyl ester, a trypsin inhibitor, on the growth of various strains of Escherichia coli.* Biol Pharm Bull, 1993. **16**(7): p. 621-626.
360. Bieniossek, C., et al., *The molecular architecture of the metalloprotease FtsH.* PNAS, 2006. **103**(9): p. 3066-3071.
361. Tomoyasu, T., et al., *Escherichia coli FtsH is a membrane-bound, ATPdependent protease which degrades the heat-shock transcription factor sigma 32.* EMBO J, 1995. **14**(11): p. 2251-2260.
362. Lu, Z.H. and M. Solioz, *Copper-induced proteolysis of the CopZ copper chaperone of Enterococcus hirae.* J Biol Chem, 2001. **276**(51): p. 47822-7.
363. Solioz, M., *Role of proteolysis in copper homoeostasis.* Biochem Soc Trans, 2002. **30**: p. 688-691.
364. Van der Ploeg, J.R., E. Eichhorn, and T. Leisinger, *Sulfonate-sulfur metabolism and its regulation in Escherichia coli.* Arch Microbiol, 2001. **176**(1-2): p. 1-8.
365. Salazar, C.N., et al., *Analysis of Gene Expression in Response to Copper Stress in Acidithiobacillus ferrooxidans Strain D2, Isolated from a Copper Bioleaching Operation.* Adv Mat Res, 2013. **825**: p. 157-161.
366. Wheaton, G.H., A. Mukherjee, and R.M. Kelly, *Transcriptomes of the extremely thermoacidophilic archaeon Metallosphaera sedula exposed to metal "shock" reveal generic and specific metal responses.* Appl Environ Microbiol, 2016. **82**(15): p. 4613-4627.
367. Huang, N., et al., *Responses to copper stress in the metal-resistant bacterium Cupriavidus gilardii CR3: a whole-transcriptome analysis.* J Basic Microbiol, 2019. **59**(5): p. 446-457.
368. Rigo, A., et al., *Interaction of copper with cysteine: stability of cuprous complexes and catalytic role of cupric ions in anaerobic thiol oxidation.* J Inorg Biochem, 2004. **98**(9): p. 1495-501.
369. Heidrich, N., et al., *The primary transcriptome of Neisseria meningitidis and its interaction with the RNA chaperone Hfq.* Nucleic Acids Res, 2017. **45**(10): p. 6147-6167.
370. Borremans, B., et al., *Cloning and functional analysis of the pbr lead resistance determinant of Ralstonia metallidurans CH34.* J Bacteriol, 2001. **183**(19): p. 5651-8.
371. Große, C., et al., *Transcriptional organization of the czc heavy-metal homeostasis determinant from Alcaligenes eutrophus.* J Bacteriol, 1999. **181**(8): p. 2385-2393.
372. Lomsadze, A., et al., *Modeling leaderless transcription and atypical genes results in more accurate gene prediction in prokaryotes.* Genome Res, 2018. **28**(7): p. 1079-1089.
373. Schmidt, T. and H.G. Schlegel, *Combined nickel-cobalt-cadmium resistance encoded by the ncc locus of Alcaligenes xylosoxidans 31A.* J Bacteriol, 1994. **176**(22): p. 7045-7054.

374. Hynninen, A., et al., *An efflux transporter PbrA and a phosphatase PbrB cooperate in a lead-resistance mechanism in bacteria.* Mol Microbiol, 2009. **74**(2): p. 384-94.
375. Keshav, V., et al., *Recombinant expression and purification of a functional bacterial metallo-chaperone PbrD-fusion construct as a potential biosorbent for Pb(II).* Protein Expr Purif, 2019. **158**: p. 27-35.
376. Sass, A.M., et al., *Genome-wide transcription start site profiling in biofilm-grown Burkholderia cenocepacia J2315.* BMC Genomics, 2015. **16**: p. 775.
377. Vockenhuber, M.P., et al., *Deep sequencing-based identification of small non-coding RNAs in Streptomyces coelicolor.* RNA Biol, 2011. **8**(3): p. 468-77.
378. Kroger, C., et al., *The transcriptional landscape and small RNAs of Salmonella enterica serovar Typhimurium.* Proc Natl Acad Sci U S A, 2012. **109**(20): p. E1277-86.
379. Schrader, J.M., et al., *The coding and noncoding architecture of the Caulobacter crescentus genome.* PLoS Genet, 2014. **10**(7): p. e1004463.
380. Bischler, T., et al., *Differential RNA-seq (dRNA-seq) for annotation of transcriptional start sites and small RNAs in Helicobacter pylori.* Methods, 2015. **86**: p. 89-101.
381. Zheng, X., et al., *Leaderless genes in bacteria: clue to the evolution of translation initiation mechanisms in prokaryotes.* BMC Genomics, 2011. **12**(361).
382. Beck, H.J. and I. Moll, *Leaderless mRNAs in the spotlight: Ancient but not outdated!* Microbiol Spectr, 2018. **6**(4).
383. Ao, W., et al., *Environmentally induced foregut remodeling by PHA-4/FoxA and DAF-12/NHR.* Science, 2004. **305**: p. 1743-1746.
384. Mitschke, J., et al., *Dynamics of transcriptional start site selection during nitrogen stress-induced cell differentiation in Anabaena sp. PCC7120.* PNAS, 2011. **108**(50): p. 20130-20135.
385. Thomason, M.K., et al., *Global transcriptional start site mapping using differential RNA sequencing reveals novel antisense RNAs in Escherichia coli.* J Bacteriol, 2015. **197**(1): p. 18-28.
386. Ko, J.H., et al., *Differential promoter usage of infA in response to cold shock in Escherichia coli.* FEBS Lett, 2006. **580**(2): p. 539-44.
387. Güell, M., et al., *Bacterial transcriptomics: what is beyond the RNA horiz-ome?* Nat Rev Microbiol, 2011. **9**(9): p. 658-669.
388. Thomason, M.K. and G. Storz, *Bacterial antisense RNAs: how many are there, and what are they doing?* Annu Rev Genet, 2010. **44**: p. 167-88.
389. Eckweiler, D. and S. Haussler, *Antisense transcription in Pseudomonas aeruginosa.* Microbiology, 2018. **164**(6): p. 889-895.
390. Eiamphungporn, W. and J.D. Helmann, *Extracytoplasmic function sigma factors regulate expression of the Bacillus subtilis yabE gene via a cis-acting antisense RNA.* J Bacteriol, 2009. **191**(3): p. 1101-5.
391. Friedman, R.C., et al., *Common and phylogenetically widespread coding for peptides by bacterial small RNAs.* BMC Genomics, 2017. **18**(1): p. 553.
392. Tsai, C.H., et al., *Genome-wide analyses in bacteria show small-RNA enrichment for long and conserved intergenic regions.* J Bacteriol, 2015. **197**(1): p. 40-50.
393. Sobrero, P. and C. Valverde, *The bacterial protein Hfq: much more than a mere RNA-binding factor.* Crit Rev Microbiol, 2012. **38**(4): p. 276-99.
394. Bailey, T.L. and C. Elkan. *Fitting a mixture model by expectation maximization to discover motifs in biopolymers*. in *Second International Conference on Intelligent Systems for Molecular Biology*. 1994. AAAI Press.
395. Galperin, M.Y., *Structural classification of bacterial response regulators: diversity of output domains and domain combinations.* J Bacteriol, 2006. **188**(12): p. 4169-82.
396. Ali, M.M., et al., *DNA-binding and transcription activation by unphosphorylated response regulator AgrR from Cupriavidus metallidurans involved in silver resistance.* Front Microbiol, 2020. **11**.
397. Grant, C.E., T.L. Bailey, and W.S. Noble, *FIMO: scanning for occurrences of a given motif.* Bioinformatics, 2011. **27**(7): p. 1017-8.
398. Sass, A., S. Kiekens, and T. Coenye, *Identification of small RNAs abundant in Burkholderia cenocepacia biofilms reveal putative regulators with a potential role in carbon and iron metabolism.* Sci Rep, 2017. **7**(1): p. 15665.
399. Hot, D., et al., *Detection of small RNAs in Bordetella pertussis and identification of a novel repeated genetic element.* BMC Genomics, 2011. **12**(207).
400. Franke, S., G. Grass, and D.H. Nies, *The product of the ybdE gene of the Escherichia coli chromosome is involved in detoxification of silver ions.* Microbiology, 2001. **147**: p. 965-972.

401. Gupta, A., et al., *Molecular basis for resistance to silver cations in Salmonella.* Nat Med, 1999. **5**(2): p. 183-188.
402. Saier, M.H.J., et al., *Two novel families of bacterial membrane proteins concerned with nodulation, cell division and transport.* Mol Microbiol, 1994. **11**(5): p. 841-847.
403. Murakami, S., et al., *Crystal structure of bacterial multidrug efflux transporter AcrB.* Nature, 2002. **419**: p. 587-593.
404. Nies, D.H., et al., *Expression and nucleotide sequence of a plasmid-determined divalent cation efflux system from Alcaligenes eutrophus.* PNAS, 1989. **86**: p. 7351-7355.
405. Ekendé, E.C.N., *Towards a better understanding of bacterial resistance to heavy metal ions: the case of the sil and zne systems from Cupriavidus metallidurans CH43*, in *Centre de Biologie Structurale et de Bioinformatique*

Service de Structure et Fonction des Membranes Biologiques. 2012, Université Libre de Bruxelles: Bruxelles, Belgium. p. 252.
406. Auquier, V., *Identification et caractérisation de protéines membranaires impliquées dans les systèmes de résistance aux métaux lourds chez Cupriavidus metallidurans CH34*, in *Faculté des Sciences*. 2006, Université Libre de Bruxelles: Bruxelles, Belgium. p. 230.
407. Ferrieres, L., et al., *Silent mischief: bacteriophage Mu insertions contaminate products of Escherichia coli random mutagenesis performed using suicidal transposon delivery plasmids mobilized by broad-host-range RP4 conjugative machinery.* J Bacteriol, 2010. **192**(24): p. 6418-27.
408. Kovach, M.E., et al., *Four new derivatives of the broad-host-range cloning vector pBBRMCS, carrying different antibiotic-resistance cassettes.* Gene, 1995. **166**: p. 175-176.
409. Benedetti, I.M., V. de Lorenzo, and R. Silva-Rocha, *Quantitative, non-disruptive monitoring of transcription in single cells with a broad-host range GFP-luxCDABE dual reporter system.* PLoS One, 2012. **7**(12): p. e52000.
410. Schäfer, A., et al., *Small mobilizable multi-purpose cloning vectors derived from the Escherichia coli plasmids pK18 and pK19: selection of defined deletions in the chromosome of Corynebacterium glutamicum.* Gene, 1994. **145**: p. 69-73.
411. Hall, M.P., et al., *Engineered luciferase reporter from a deep sea shrimp utilizing a novel imidazopyrazinone substrate.* ACS Chem Biol, 2012. **7**(11): p. 1848-57.
412. Gautheret, D. and A. Lambert, *Direct RNA motif definition and identification from multiple sequence alignments using secondary structure profiles.* J Mol Biol, 2001. **313**(5): p. 1003-11.
413. Hastings, J.W., *Chemistries and colors of bioluminescent reactions: a review.* Gene, 1996. **173**: p. 5-11.
414. Demidova, T.N., et al., *Monitoring photodynamic therapy of localized infections by bioluminescence imaging of genetically engineered bacteria.* J Photoch Photobio B, 2005. **81**(1): p. 15-25.
415. Flemming, C.A. and J.T. Trevors, *Copper toxicity and chemistry in the environment: a review.* Water Air Soil Pollut, 1989. **44**: p. 143-158.
416. Besold, A.N., E.M. Culbertson, and V.C. Culotta, *The Yin and Yang of copper during infection.* J Biol Inorg Chem, 2016. **21**(2): p. 137-44.
417. Tan, G., et al., *Anaerobic copper toxicity and iron-sulfur cluster biogenesis in Escherichia coli.* Appl Environ Microbiol, 2017. **83**(16).
418. Djoko, K.Y., et al., *Interplay between tolerance mechanisms to copper and acid stress in Escherichia coli.* Proc Natl Acad Sci U S A, 2017. **114**(26): p. 6818-6823.
419. Nies, D.H. and S. Silver, *Molecular microbiology of heavy metals*. Microbiol Monogr, ed. A. Steinbüchel. 2007: Springer.
420. Arguello, J.M., M. Gonzalez-Guerrero, and D. Raimunda, *Bacterial transition metal P(1B)-ATPases: transport mechanism and roles in virulence.* Biochem, 2011. **50**(46): p. 9940-9.
421. Kim, E.H., et al., *Switch or funnel: how RND-type transport systems control periplasmic metal homeostasis.* J Bacteriol, 2011. **193**(10): p. 2381-7.
422. Su, C.C., et al., *Crystal structure of the membrane fusion protein CusB from Escherichia coli.* J Mol Biol, 2009. **393**(2): p. 342-55.
423. Boal, A.K. and A.C. Rosenzweig, *Structural biology of copper trafficking.* Chem Rev, 2009. **106**: p. 4760-4779.
424. Roberts, S.A., et al., *Crystal structure and electron transfer kinetics of CueO, a multicopper oxidase required for copper homeostasis in Escherichia coli.* PNAS, 2002. **99**(5): p. 2766-2771.

425. Gillet, S., E. Lawarée, and J.-Y. Matroule, *Functional diversity of bacterial strategies to cope with metal toxicity*, in *Microbial Diversity in the Genomic Era*. 2019. p. 409-426.
426. North, N.N., et al., *Change in bacterial community structure during in situ biostimulation of subsurface sediment cocontaminated with uranium and nitrate.* Appl Environ Microbiol, 2004. **70**(8): p. 4911-20.
427. Benyehuda, G., et al., *Metal resistance among aerobic chemoheterotrophic bacteria from the deep terrestrial subsurface.* Can J Microbiol, 2003. **49**(2): p. 151-6.
428. Inagaki, F., et al., *Distribution and phylogenetic diversity of the subsurface microbial community in a Japanese epithermal gold mine.* Extremophiles, 2003. **7**(4): p. 307-17.
429. Hu, P., et al., *Whole-genome transcriptional analysis of heavy metal stresses in Caulobacter crescentus.* J Bacteriol, 2005. **187**(24): p. 8437-49.
430. Ely, B., *Genetics of Caulobacter crescentus.* Methods Enzymol, 1991. **204**: p. 372-384.
431. Evinger, M. and N. Agabian, *Envelope-associated nucleoid from Caulobacter crescentus stalked and swarmer cells.* J Bacteriol, 1977. **132**(1): p. 294-301.
432. Li, H. and R. Durbin, *Fast and accurate short read alignment with Burrows-Wheeler transform.* Bioinformatics, 2009. **25**(14): p. 1754-1760.
433. Robinson, M.D. and A. Oshlack, *A scaling normalization method for differential expression analysis of RNA-seq data.* Genome Biol, 2010. **11**(R25).
434. McCarthy, D.J. and G.K. Smyth, *Testing significance relative to a fold-change threshold is a TREAT.* Bioinformatics, 2009. **25**(6): p. 765-71.
435. Sprouffske, K. and A. Wagner, *Growthcurver: an R package for obtaining interpretable metrics from microbial growth curves.* BMC Bioinformatics, 2016. **17**: p. 172.
436. Fox, J. and S. Weisberg, *An R companion to applied regression*. Third Edition ed. 2019, Thousand Oaks, CA: Sage.
437. Gu, Z., R. Eils, and M. Schlesner, *Complex heatmaps reveal patterns and correlations in multidimensional genomic data.* Bioinformatics, 2016. **32**(18): p. 2847-9.
438. Szklarczyk, D., et al., *STRING v11: protein-protein association networks with increased coverage, supporting functional discovery in genome-wide experimental datasets.* Nucleic Acids Res, 2019. **47**(D1): p. D607-D613.
439. Alvarez-Martinez, C.E., R.L. Baldini, and S.L. Gomes, *A Caulobacter crescentus extracytoplasmic function sigma factor mediating the response to oxidative stress in stationary phase.* J Bacteriol, 2006. **188**(5): p. 1835-46.
440. Wiesemann, N., et al., *Influence of copper resistance determinants on gold transformation by Cupriavidus metallidurans strain CH34.* J Bacteriol, 2013. **195**(10): p. 2298-308.
441. Gennaris, A., et al., *Repairing oxidized proteins in the bacterial envelope using respiratory chain electrons.* Nature, 2015. **528**(7582): p. 409-412.
442. Silva, L.G., et al., *OxyR and the hydrogen peroxide stress response in Caulobacter crescentus.* Gene, 2019. **700**: p. 70-84.
443. da Silva Neto, J.F., R.F. Lourenço, and M.V. Marques, *Global transcriptional response of Caulobacter crescentus to iron availability.* BMC Genomics, 2013. **14**(549).
444. da Silva Neto, J.F., et al., *Fur controls iron homeostasis and oxidative stress defense in the oligotrophic alpha-proteobacterium Caulobacter crescentus.* Nucleic Acids Res, 2009. **37**(14): p. 4812-25.
445. Italiani, V.C., et al., *Regulation of catalase-peroxidase KatG is OxyR dependent and Fur independent in Caulobacter crescentus.* J Bacteriol, 2011. **193**(7): p. 1734-44.
446. Baker, J., et al., *Copper stress induces a global stress response in Staphylococcus aureus and represses sae and agr expression and biofilm formation.* Appl Environ Microbiol, 2010. **76**(1): p. 150-60.
447. López, C., S.K. Checa, and F.C. Soncini, *CpxR/CpxA controls scsABCD transcription to counteract copper and oxidative stress in Salmonella enterica serovar Typhimurium.* J Bacteriol, 2018. **200**(16).
448. Svenningsen, N.B., et al., *Cupriavidus pinatubonensis AEO106 deals with copper-induced oxidative stress before engaging in biodegradation of the herbicide 4-chloro-2-methylphenoxyacetic acid.* BMC Microbiol, 2017. **17**(1): p. 211.
449. Qian, H., et al., *Effects of copper sulfate, hydrogen peroxide and N-phenyl-2-naphthylamine on oxidative stress and the expression of genes involved photosynthesis and microcystin disposition in Microcystis aeruginosa.* Aquat Toxicol, 2010. **99**(3): p. 405-12.
450. Bagwell, C.E., et al., *Proteomic and physiological responses of Kineococcus radiotolerans to copper.* PLoS One, 2010. **5**(8): p. e12427.

451. Teitzel, G.M., et al., *Survival and growth in the presence of elevated copper: transcriptional profiling of copper-stressed Pseudomonas aeruginosa.* J Bacteriol, 2006. **188**(20): p. 7242-56.
452. Leaden, L., et al., *Iron deficiency generates oxidative stress and activation of the SOS response in Caulobacter crescentus.* Front Microbiol, 2018. **9**: p. 2014.
453. de Castro Ferreira, I.G., et al., *Role and regulation of ferritin-like proteins in iron homeostasis and oxidative stress survival of Caulobacter crescentus.* Biometals, 2016. **29**(5): p. 851-62.
454. Hartl, J., et al., *Untargeted metabolomics links glutathione to bacterial cell cycle progression.* Nat Metab, 2020. **2**(2): p. 153-166.
455. Goemans, C.V., et al., *An essential thioredoxin is involved in the control of the cell cycle in the bacterium Caulobacter crescentus.* J Biol Chem, 2018. **293**(10): p. 3839-3848.
456. Kachur, A.V., C.J. Koch, and J.E. Biaglow, *Mechanism of copper-catalyzed oxidation of glutathione.* Free Rad Res, 1998. **28**: p. 259-269.
457. da Silva, A.C., et al., *Downregulation of the heat shock response is independent of DnaK and sigma32 levels in Caulobacter crescentus.* Mol Microbiol, 2003. **49**(2): p. 541-53.
458. Schramm, F.D., et al., *An essential regulatory function of the DnaK chaperone dictates the decision between proliferation and maintenance in Caulobacter crescentus.* PLoS Genet, 2017. **13**(12): p. e1007148.
459. Susin, M.F., et al., *GroES/GroEL and DnaK/DnaJ have distinct roles in stress responses and during cell cycle progression in Caulobacter crescentus.* J Bacteriol, 2006. **188**(23): p. 8044-53.
460. Goemans, C.V., et al., *The chaperone and redox properties of CnoX chaperedoxins are tailored to the proteostatic needs of bacterial species.* mBio, 2018. **9**(6).
461. Subedi, P., et al., *The Scs disulfide reductase system cooperates with the metallochaperone CueP in Salmonella copper resistance.* J Biol Chem, 2019. **294**(44): p. 15876-15888.
462. Yung, M.C., et al., *Shotgun proteomic analysis unveils survival and detoxification strategies by Caulobacter crescentus during exposure to uranium, chromium, and cadmium.* J Proteome Res, 2014. **13**(4): p. 1833-47.
463. Jonas, K., et al., *Proteotoxic stress induces a cell-cycle arrest by stimulating Lon to degrade the replication initiator DnaA.* Cell, 2013. **154**(3): p. 623-36.
464. Fischer, B., et al., *The FtsH protease is involved in development, stress response and heat shock control in Caulobacter crescentus.* Mol Microbiol, 2002. **44**(2): p. 461-478.
465. Simao, R.C., et al., *Cells lacking ClpB display a prolonged shutoff phase of the heat shock response in Caulobacter crescentus.* Mol Microbiol, 2005. **57**(2): p. 592-603.
466. Bhat, N.H., et al., *Identification of ClpP substrates in Caulobacter crescentus reveals a role for regulated proteolysis in bacterial development.* Mol Microbiol, 2013. **88**(6): p. 1083-92.
467. Liu, J., et al., *ClpAP is an auxiliary protease for DnaA degradation in Caulobacter crescentus.* Mol Microbiol, 2016. **102**(6): p. 1075-1085.
468. Vass, R.H., R.D. Zeinert, and P. Chien, *Protease regulation and capacity during Caulobacter growth.* Curr Opin Microbiol, 2016. **34**: p. 75-81.
469. Zeinert, R.D., et al., *The Lon protease links nucleotide metabolism with proteotoxic stress.* Mol Cell, 2020. **79**(5): p. 758-767 e6.
470. Gora, K.G., et al., *Regulated proteolysis of a transcription factor complex is critical to cell cycle progression in Caulobacter crescentus.* Mol Microbiol, 2013. **87**(6): p. 1277-89.
471. Parvatiyar, K., et al., *Global analysis of cellular factors and responses involved in Pseudomonas aeruginosa resistance to arsenite.* J Bacteriol, 2005. **187**(14): p. 4853-64.
472. Perez, J.M., et al., *Bacterial toxicity of potassium tellurite: unveiling an ancient enigma.* PLoS One, 2007. **2**(2): p. e211.
473. Valencia, E.Y., et al., *Two RND proteins involved in heavy metal efflux in Caulobacter crescentus belong to separate clusters within proteobacteria.* BMC Microbiol, 2013. **13**(79).
474. Park, D.M., et al., *Identification of a U/Zn/Cu responsive global regulatory two-component system in Caulobacter crescentus.* Mol Microbiol, 2017. **104**(1): p. 46-64.
475. Frohlich, K.S., K.U. Forstner, and Z. Gitai, *Post-transcriptional gene regulation by an Hfq-independent small RNA in Caulobacter crescentus.* Nucleic Acids Res, 2018. **46**(20): p. 10969-10982.
476. Dibrov, P., et al., *Chemiosmotic mechanism of antimicrobial activity of Ag(+) in Vibrio cholerae.* Antimicrob Agents Chemother, 2002. **46**(8): p. 2668-70.
477. Balhesteros, H., et al., *TonB-dependent heme/hemoglobin utilization by Caulobacter crescentus HutA.* J Bacteriol, 2017. **199**(6).
478. Mazzon, R.R., et al., *Analysis of the Caulobacter crescentus Zur regulon reveals novel insights in zinc acquisition by TonB-dependent outer membrane proteins.* BMC Genomics, 2014. **15**(734).

479. Garcia-Bayona, L., M.S. Guo, and M.T. Laub, *Contact-dependent killing by Caulobacter crescentus via cell surface-associated, glycine zipper proteins.* Elife, 2017. **6**.
480. Davis, A.V. and T.V. O'Halloran, *A place for thioether chemistry in cellular copper ion recognition and trafficking.* Nat Chem Biol, 2008. **4**(3): p. 148-151.
481. Tiwari, S., et al., *Arginine-deprivation-induced oxidative damage sterilizes Mycobacterium tuberculosis.* Proc Natl Acad Sci U S A, 2018. **115**(39): p. 9779-9784.
482. Barrientos-Moreno, L., et al., *Arginine biosynthesis modulates pyoverdine production and release in Pseudomonas putida as part of the mechanism of adaptation to oxidative stress.* J Bacteriol, 2019. **201**(22).
483. Chakraborty, B. and R.A. Burne, *Effects of arginine on Streptococcus mutans growth, virulence gene expression, and stress tolerance.* Appl Environ Microbiol, 2017. **83**(15).
484. Dietl, A.-M., et al., *Histidine biosynthesis plays a crucial role in metal homeostasis and virulence of Aspergillus fumigatus.* Virulence, 2016. **7**(4): p. 465-476.
485. Hor, J., S.A. Gorski, and J. Vogel, *Bacterial RNA Biology on a Genome Scale.* Mol Cell, 2018. **70**(5): p. 785-799.
486. Assis, N.G., et al., *Identification of Hfq-binding RNAs in Caulobacter crescentus.* RNA Biol, 2019. **16**(6): p. 719-726.
487. Georg, J., et al., *The power of cooperation: Experimental and computational approaches in the functional characterization of bacterial sRNAs.* Mol Microbiol, 2020. **113**(3): p. 603-612.
488. Brown, P.L. and S.J. Markich, *Evaluation of the free ion activity model of metal-organism interaction: extension of the conceptual model.* Aquat Toxicol, 2000. **51**: p. 177-194.
489. Hoffman, D.R., J.L. Okon, and T.R. Sandrin, *Medium composition affects the degree and pattern of cadmium inhibition of naphthalene biodegradation.* Chemosphere, 2005. **59**(7): p. 919-27.
490. Rathnayake, I.V., et al., *Heavy metal toxicity to bacteria - are the existing growth media accurate enough to determine heavy metal toxicity?* Chemosphere, 2013. **90**(3): p. 1195-200.
491. Nies, D.H., *The biological chemistry of the transition metal "transportome" of Cupriavidus metallidurans.* Metallomics, 2016. **8**(5): p. 481-507.
492. Smith, R.M. and A.E. Martell, *Critical stability constants*. 1989, Plenum Press, New York. p. 173-174.
493. Hiroshi, O., *The stability constants of ethylenediaminetetraacetato, trimethylenediaminetetraacetato and propylenediaminetetraacetato complexes of some divalent metal ions.* BCSJ, 1965. **38**(5): p. 771-777.
494. Sezonov, G., D. Joseleau-Petit, and R. D'Ari, *Escherichia coli physiology in Luria-Bertani broth.* J Bacteriol, 2007. **189**(23): p. 8746-9.
495. De Spiegeleer, P., et al., *Source of tryptone in growth medium affects oxidative stress resistance in Escherichia coli.* J Appl Microbiol, 2004. **97**(1): p. 124-33.
496. Mosser, M., et al., *Fractionation of yeast extract by nanofiltration process to assess key compounds involved in CHO cell culture improvement.* Biotechnol Prog, 2015. **31**(4): p. 875-82.
497. El-Helow, E.R., S.A. Sabry, and R.M. Amer, *Cadmium biosorption by a cadmium resistant strain of Bacillus thuringiensis: regulation and optimization of cell surface affinity for metal cations.* Biometals, 2000. **13**: p. 273-280.
498. Hottes, A.K., et al., *Transcriptional profiling of Caulobacter crescentus during growth on complex and minimal media.* J Bacteriol, 2004. **186**(5): p. 1448-61.
499. Laub, M.T., L. Shapiro, and H.H. McAdams, *Systems biology of Caulobacter.* Annu Rev Genet, 2007. **41**: p. 429-41.
500. Yang, E., et al., *Complete genome sequence of Caulobacter flavus RHGG3(T), a type species of the genus Caulobacter with plant growth-promoting traits and heavy metal resistance.* 3 Biotech, 2019. **9**(2): p. 42.
501. Narayanan, S., et al., *A cell cycle-controlled redox switch regulates the topoisomerase IV activity.* Genes Dev, 2015. **29**(11): p. 1175-87.
502. Landt, S.G., et al., *Small non-coding RNAs in Caulobacter crescentus.* Mol Microbiol, 2008. **68**(3): p. 600-14.
503. McGrath, P.T., et al., *High-throughput identification of transcription start sites, conserved promoter motifs and predicted regulons.* Nat Biotechnol, 2007. **25**(5): p. 584-92.
504. Romilly, C., et al., *Current knowledge on regulatory RNAs and their machineries in Staphylococcus aureus.* RNA Biol, 2012. **9**(4): p. 402-13.
505. Makarova, A.A., et al., *Insight into bio-metal interface formation in vacuo: interplay of S-layer protein with copper and iron.* Sci Rep, 2015. **5**: p. 8710.

506. Kawasaki, Y., et al., *Identification and characterization of the S-layer formed on the sheath of Thiothrix nivea.* Arch Microbiol, 2018. **200**(8): p. 1257-1265.
507. Del Medico, L., et al., *The type IV pilin PilA couples surface attachment and cell-cycle initiation in Caulobacter crescentus.* PNAS, 2020. **117**(17): p. 9546-9553.
508. Skerker, J.M. and L. Shapiro, *Identification and cell cycle control of a novel pilus system in Caulobacter crescentus.* EMBO J, 2000. **19**(13): p. 3223-3234.
509. Fang, G., et al., *Transcriptomic and phylogenetic analysis of a bacterial cell cycle reveals strong associations between co-expression and evolution.* BMC Genomics, 2013. **14**(450).
510. Hahn, C., et al., *Pure and oxidized copper materials as potential antimicrobial surfaces for spaceflight activities.* Astrobiology, 2017. **17**(12): p. 1183-1191.
511. Adlhart, C., et al., *Surface modifications for antimicrobial effects in the healthcare setting: a critical overview.* J Hosp Infect, 2018. **99**(3): p. 239-249.
512. Gattinoni, C. and A. Michaelides, *Atomistic details of oxide surfaces and surface oxidation: the example of copper and its oxides.* Surface Science Reports, 2015. **70**(3): p. 424-447.
513. Li, J., J.W. Mayer, and E.G. Colgan, *Oxidation and protection in copper and copper alloy thin films.* Journal of Applied Physics, 1991. **70**(5): p. 2820-2827.
514. Lemelle, L., et al., *Towards a passive limitation of particle surface contamination in the Columbus module (ISS) during the MATISS experiment of the Proxima Mission.* npj Microgravity, 2020. **6**(1).
515. Landry, K.S., et al., *Biofilms—Impacts on human health and its relevance to space travel.* Microorganisms, 2020. **8**(7).
516. Gottenbos, B., et al., *Antimicrobial effects of positively charged surfaces on adhering Gram-positive and Gram-negative bacteria.* J Antimicrob Chemother, 2001. **48**: p. 7-13.
517. Maertens, L., J.Y. Matroule, and R. Van Houdt, *Characteristics of the copper-induced viable-but-non-culturable state in bacteria.* World J Microbiol Biotechnol, 2021. **37**(3): p. 37.
518. Khodadad, C.L.M., et al., *A microbial monitoring system demonstrated on the International Space Station provides a successful platform for detection of targeted microorganisms.* Life, 2021. **11**(6).
519. Li, L.G., Y. Xia, and T. Zhang, *Co-occurrence of antibiotic and metal resistance genes revealed in complete genome collection.* ISME J, 2017. **11**(3): p. 651-662.
520. Madsen, J.S., et al., *The interconnection between biofilm formation and horizontal gene transfer.* FEMS Immunol Med Microbiol, 2012. **65**(2): p. 183-95.
521. Zea, L., et al., *Potential biofilm control strategies for extended spaceflight missions.* Biofilm, 2020. **2**.
522. Weber, D.J., et al., *Continuous room decontamination technologies.* Am J Infect Control, 2019. **47S**: p. A72-A78.
523. Steinhauer, K., et al., *Antimicrobial efficacy and compatibility of solid copper alloys with chemical disinfectants.* PLoS One, 2018. **13**(8): p. e0200748.
524. Luo, J., et al., *Sodium chloride assists copper release, enhances antibacterial efficiency, and introduces atmospheric corrosion on copper surface.* Surfaces and Interfaces, 2020. **20**.
525. Morrison, M.D., P. Fajardo-Cavazos, and W.L. Nicholson, *Comparison of Bacillus subtilis transcriptome profiles from two separate missions to the International Space Station.* NPJ Microgravity, 2019. **5**: p. 1.
526. Aunins, T.R., et al., *Spaceflight modifies Escherichia coli gene expression in response to antibiotic exposure and reveals role of oxidative stress response.* Front Microbiol, 2018. **9**: p. 310.
527. Jager, D., et al., *An archaeal sRNA targeting cis- and trans-encoded mRNAs via two distinct domains.* Nucleic Acids Res, 2012. **40**(21): p. 10964-79.
528. Morita, T., K. Maki, and H. Aiba, *Detection of sRNA-mRNA interactions by electrophoretic mobility shift assay.* Methods Mol Biol, 2012. **905**: p. 235-44.
529. Langevin, S., et al., *First case of invasive human infection caused by Cupriavidus metallidurans.* J Clin Microbiol, 2011. **49**(2): p. 744-5.
530. Penner, F., et al., *Caulobacter spp: A rare pathogen responsible for paucisintomatic persisitant meningitis in a glioblastoma patient.* World Neurosurg, 2016. **96**: p. 611 e11-611 e13.
531. Liebeke, M., et al., *Chemical characterization of soil extract as growth media for the ecophysiological study of bacteria.* Appl Microbiol Biotechnol, 2009. **83**(1): p. 161-73.

Scientific output

Peer-reviewed publications

Ali M. M., Provoost A., **Maertens L.**, Leys N., Monsieurs P., Charlier D. (2019). "Genomic and transcriptomic changes that mediate increased platinum resistance in *Cupriavidus metallidurans*." Genes **10**(1).

Maertens L., Conincx I., Claesen J., Leys N., Matroule J.-Y., Van Houdt R. (2020). "Copper resistance mediates long-term survival of *Cupriavidus metallidurans* in wet contact with metallic copper." Frontiers in Microbiology **11**(1208).

Maertens L., Leys N., Matroule J.-Y., Van Houdt R. (2020). "The transcriptomic landscape of *Cupriavidus metallidurans* CH34 acutely exposed to copper." Genes **11**(9).

Maertens L., Matroule J.-Y., Van Houdt R. (2021). "Characteristics of the copper-induced viable-but-non-culturable state in bacteria." World J Microbiol Biotechnol **37**(3): 37.

Maertens L., Cherry P., Tilquin F., Van Houdt R., Matroule J.-Y. (2021). "Environmental conditions modulate the transcriptomic response of both *Caulobacter crescentus* morphotypes to copper stress." Microorganisms **9**(6).

Yadav A., **Maertens L.**, Meese T., Van Nieuwerburgh F., Mysara M., Leys N., Cuypers A., Janssen P. J. (2021). "Genetic responses of metabolically active *Limnospira indica* strain PCC 8005 exposed to γ-radiation during its lifecycle." Microorganisms **9**(8).

Louis G., Cherry P., Michaux C., Dieu M., Tilquin F., **Maertens L.**, Renard P., Van Houdt R., Perpete E., Matroule, J.-Y. (2021). "Reactive oxygen species-based

sensing by a single chemoreceptor controls copper chemotaxis in *Caulobacter crescentus*. *In preparation.*

Siems K., Müller D., **Maertens L.**, Ahmed A., Van Houdt R., Mancinelli R., Caplin N., Krause J., Demets R., Vukich M., Tortora A., Rösch C., Holland G., Laue M., Mücklich F., Hellweg C. E., Moeller R. (2021). Designing the spaceflight experiment BIOFILMS: testing laser-patterned metal surfaces for prevention of bacterial biofilm formation in microgravity. *In preparation.*

Oral presentations

Maertens L., Monsieurs P., Leys N., Matroule J.-Y., Van Houdt R. (2018, October 19th). Understanding copper and silver antimicrobials and their potential for space applications. BSM Meeting, Brussels, Belgium.

Maertens L., Leys N., Matroule J.-Y., Van Houdt R. (2019, April 24th). The bacterial transcriptome under copper stress. SCK CEN PhD Day, Mol, Belgium.

Maertens L., Coninx I., Claesen J., Leys N., Matroule J.-Y., Van Houdt R. (2019, November 18th-19th). Metallic copper rapidly inactivates the metal-resistant *Cupriavidus metallidurans*. H2020 DelNAM workshop, Ghent, Belgium.

Maertens L., Coninx I., Claesen J., Leys N., Matroule J.-Y., Van Houdt R. (2020, March 24th). Metallic copper rapidly inactivates the metal-resistant *Cupriavidus metallidurans*. DLR webinar, online.

Maertens L., Coninx I., Claesen J., Leys N., Matroule J.-Y., Van Houdt R. (2020, November 3rd-5th). Metallic copper rapidly inactivates the metal-resistant *Cupriavidus metallidurans*. MELiSSA conference, online.

Maertens L., Matroule J.-Y., Van Houdt R. (2021, June 21st). Investigating the role of small regulatory RNAs in copper resistance in *Cupriavidus metallidurans* CH34. World Microbe Forum, online.

Poster presentations

Maertens L., Monsieurs P., Leys N., Matroule J.-Y., Van Houdt R. (2018, September 19th). Understanding copper and silver antimicrobials and their potential for space applications. SCK CEN PhD Day, Mol, Belgium.

Maertens L., Matroule J.-Y., Van Houdt R. (2019, July 7th-11th). The regulatory landscapes of copper-exposed *Cupriavidus metallidurans* CH34 and *Caulobacter crescentus* NA1000. FEMS Congress, Glasgow, Scotland.

Maertens L., Coninx I., Claesen J., Leys N., Matroule J.-Y., Van Houdt R. (2019, October 18th). Metallic copper rapidly inactivates the metal-resistant *Cupriavidus metallidurans*. BSM meeting, Brussels, Belgium. Agar art award.

Students supervised

Michelle Billen (02/2018-06/2018)

Master in de Industriële wetenschappen: biochemie (UHasselt, Belgium)

Master thesis: "The influence of copper and silver ions on *Cupriavidus metallidurans* biofilm formation and development"

Michael Stolk (02/2018-06/2018)

Bachelor in Biomedical Engineering (TU Eindhoven, The Netherlands)

Internship: "Scanning electron microscopy studies of CH34 biofilm formation"

Andra Marissen (02/2019-06/2019)

Master in Biochemistry and Biotechnology (KU Leuven, Belgium)

Internship: "*Cupriavidus metallidurans* CH34 is moderately sensitive to metallic copper"

Valerie Maes (02/2019-06/2019)

Master in Biochemistry and Biotechnology (KU Leuven, Belgium)

Internship: "Unravelling the molecular mechanisms behind copper resistance of *Cupriavidus metallidurans*"

Julie Boonen (02/2020-06/2020)

Master in de Industriële wetenschappen: biochemie (UHasselt, Belgium)

Master thesis: “De rol van kleine regulatorische RNA’s in de respons van *Cupriavidus metallidurans* CH34 op koperstress”

Nissem Abdeljelil (02/2020-04/2020)

PhD candidate (CNSTN, Tunisia)

Internship: “Understanding copper- and silver-based antimicrobials and their potential in space applications”